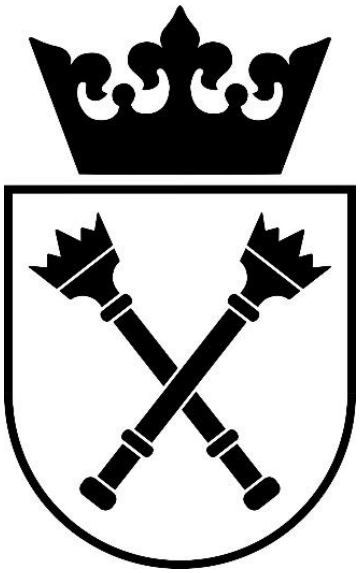

Studies of interaction of pentapeptide repeat proteins with *Escherichia coli* DNA gyrase

Łukasz Mazurek

Doctoral Thesis prepared in the Bionanoscience and Biochemistry Laboratory
under the supervision of prof. dr hab. Jonathan Heddle

Malopolska Centre of Biotechnology,
Jagiellonian University
Krakow, 2023

This project was supported by the:

National Science Centre (NCN, Poland) grant no. 2015/19/P/NZ1/03137 (POLONEZ1), 2019/35/D/NZ1/01770 (SONATA15) and 2020/39/B/NZ1/02898 (OPUS20)

Acknowledgments

Firstly, I would like to thank Professor Jonathan Heddle for accepting me as PhD student in Bionanoscience and Biochemistry. I would like to thank all the members of the Laboratory for the great atmosphere of work.

Dr Dmitry Ghilarov for being a gyrase giant. Спасибо.

I would like to also thank who helped me to finalise the research for the PhD thesis:

Elizabeth Michalczyk for being best technician ever

Zuzanna Pakosz-Stępień for her positive attitude, patience and help.

Piotr Stępień for his musical approach to science.

Wojciech Czyszczoń for very fruitful cooperation on the crosslinking project.

Joanni Markiewicz and Arkadiusz Dobosz for their critical comments.

Kindze dziękuję za góry i uśmiech.

Tomkowi dziękuję za to, że nie przestał stawiać pytań.

Rodzicom za wszelkie wsparcie i pomoc.

CZEŚĆ GÓROM, GÓROM CZEŚĆ!

Table of contents

List of publications

The major part of PhD thesis is published in:

Mazurek Ł, Ghilarov D, Michalczyk E, Pakosz Z, Metelev M, Czyszczoń W, Wawro K, Behroz I, Dubiley S, Süssmuth RD, Heddle JG. (2021). Pentapeptide repeat protein QnrB1 requires ATP hydrolysis to rejuvenate poisoned gyrase complexes. Nucleic Acids Res 49:1581–1596. DOI: 10.1093/nar/gkaa1266

Other publications:

Michalczyk, E., Hommernick, K., Behroz, I., Kulike, M., Pakosz-Stępień, Z., **Mazurek, Ł**., Seidel, M., Kunert, M., Santos, K., von Moeller, H., Loll, B., Weston, J. B., Mainz, A., Heddle, J. G., Süssmuth, R. D., & Ghilarov, D. (2023). Molecular mechanism of topoisomerase poisoning by the peptide antibiotic albicidin. Nature Catalysis. https://doi.org/10.1038/s41929-022-00904-1

Wladyka,B., Piejko,M., Bzowska,M., Pieta,P., Krzysik,M., **Mazurek,Ł**., Guevara-Lora,I., Bukowski,M., Sabat,A.J., Friedrich,A.W., *et al.* (2015) A peptide factor secreted by Staphylococcus pseudintermedius exhibits properties of both bacteriocins and virulence factors. *Sci. Rep.*, **5**, 14569

Abstract in English

Gyrase, as a bacterial topoisomerase II, is essential for maintenance of DNA topology during replication and transcription. The gyrase heterotetramer consists of two GyrA and two GyrB subunits. The enzyme is unique in being able to negatively supercoil DNA and is an appealing antibiotic target because of the fact that during the reaction cycle gyrase must pass through an intermediate stage at which the DNA is cleaved across both strands. Drugs that inhibit religation of the cleaved strands result in production of double-strand breaks in the cell, which are lethal. Drugs that target gyrase bind to different sites across enzyme and include the widely used and most clinically important fluoroquinolone antibiotics introduced in the mid-1980s. Unfortunately, resistance to fluoroquinolone has spread and anti- fluoroquinolone binding mutations in DNA gyrase have been widely described.

In last 15 years, plasmid-borne quinolone resistance (qnr) has also emerged. The most common *qnr* gene encodes a pentapeptide repeat protein (PRP). The *qnr* plasmid provides only moderate level of protection against fluoroquinolone action. The low-level resistance favours further selection for more specific and effective mechanisms of resistance. This enables the development of full resistance thanks to acquirement of additional chromosomal mutations or efflux pumps.

The PRP proteins that interact with quinolone target i.e., topoisomerases have been termed of Topoisomerase acting PRPs (TA-PRPs). There are three basic models of TA-PRPs action. After the solving the first structure of the TA-PRP, MfpA from *Mycobacterium tuberculosis* it was suggested that MfpA competes with dsDNA for binding to the region of the enzyme where DNA is bound and then cleaved. In this model PRPs mimic the G-segment and bind to the G-segment binding and cleavage site across the GyrA saddle. A different mechanism was proposed for PRPs to explain how protection against the action of FQ can be achieved without affecting supercoiling. It is suggested that rather than mimicking the initial bound state of DNA and competing for its binding site, the PRPs recognize the quinolone-stabilized cleaved complex and interact with it. Interaction causes destabilization whereby the loss of quinolone from the binding site occurs. That allows the supercoiling reaction to proceed. There is another alternative model for gyrase-targeting PRPs. In this model TA-PRPs also acts as a DNA mimic

however it mimics the T-segment. TTPRP is captured by gyrase-DNA complex in which the G-segment is already bound.

The aim of the thesis is to provide structural and biochemical information about the interactions between pentapeptide repeat proteins and *E. coli* DNA gyrase. The obtained data were used to try to explain the observed specificity of the inhibitory and protective action mediated by different PRPs A new model for pentapeptide repeat protein-mediated topoisomerase interaction with their targets was built based on the obtained results.

During the studies, activities of three different PRP were analysed. QnrB1 from *Klebsiella pneumoniae* responsible for resistance to fluoroquinolones, AlbG from *Xanthomonas albilineans* responsible for protection against albicidin and McbG from *E. coli* responsible for protection against microcin B17. Albicidin and microcin b17 are natural gyrase toxins that, analogously, to quinolones converts gyrase into a poison by stabilising the cleavage complex.

QnrB1 has been purified and analysed biochemically and structurally. During a gyrase assay the specificity of the protein towards fluoroquinolones has been confirmed. The protein has been shown to efficiently destabilise the cleavage complex in the presence of nucleotide hydrolysis. It has been established that hydrolysis is necessary for the protective effect of the QnrB1 protein. The addition of QnrB1 was stimulating the ATPase activity of DNA gyrase. Those are novel observations that were never previously reported for qnr proteins. During the course of biochemical studies, it has been found that gyrase B is the main interaction partner of QnrB1 protein. Crosslinking reactions with QnrB1 bearing orthogonal UV-crosslinkable amino acid identified the interaction sites within the QnrB1 protein. A structural model of QnrB1:DNA:gyrase:moxifloxacin has been built based on Cryo-EM data. The structural data buttressed the biochemical observations for QnrB1 interaction with gyrase B. Obtained data for QnrB1 allowed us to propose a new model of PRP interaction with gyrase. It seems that the correct mechanism incorporates some elements of T-segment mimicry and cleavage complex recognition. QnrB1 seems to follow the route of the T-segment and the protective action is mediated by the recognition of specific features of structure of cleavage complex.

The AlbG protein has been analysed similarly to QnrB1 it also shown the ability to disrupt cleavage complex and specificity towards its cognate toxin albicidin. In contrast to QnrB1, it shown interaction with both gyrase subunits during the crosslinking experiments. AlbG did not stimulate the ATPase activity of gyrase. A loop deletion mutant of AlbG shown no protective activity against albicidin: results that could be correlated with the data presented for loop lacking QnrB1. The activity of chimeric proteins AlbG with QnrB1 loop and QnrB1 with AlbG loop did not show any activity suggesting that the loop itself is not the only determinant factor of PRP specificity.

Successful purification of the McbG protein studied in the thesis has never previously been reported. Also, the structure of this PRP has never been established, in contrast to QnrB1 and AlbG. Several expression and purification approaches were used to obtain higher amounts of protein for crystallisation. Despite these efforts the expression was not efficient and the crystallographic data were not successfully collected. Biochemical experiments shown protective activity of McbG towards microcin B17. Unfortunately, the low amount and instability of purified protein allowed only for limited biochemical analysis.

Overall, the findings of the thesis allowed the formulation of a new model of PRP mechanism of action. Gathered data can be used as a guide to design new gyrase poisons molecules using structure activity relationships which can pave the way for overcoming the problem of gyrase targeting antimicrobials resistance.

Streszczenie w języku polskim

Tytuł w języku polskim: Badania interakcji między białkami z motywem pentapeptydu a gyrazą z *Escherichia coli*

Gyraza będąca bakteryjną topoizomerazą II jest enzymem niezbędnym do zmiany topologii DNA podczas procesów replikacji i transkrypcji. Heterotetramer gyrazy składa się z dwóch podjednostek GyrA i dwóch podjednostek GyrB. Enzym jest wyjątkowy, ponieważ jako jedyna topoizomerazą jest w stanie generować ujemnie superskręty DNA. Gyraza jest atrakcyjnym celem dla antybiotyków ze względu na fakt, że podczas cyklu reakcji enzym musi przejść przez etap pośredni, w którym DNA jest przecięte na obu niciach. Antybiotyki hamujące ligację przeciętych nici powodują nagromadzenie dwuniciowych przerw w DNA komórkowym, które są letalne dla komórki. Antybiotyki, których molekularnym celem jest gyraza, wiążą się do różnych miejsc enzymu. Przykładem takich klinicznie istotnych antybiotyków są fluorochinolony, wprowadzone do użytku w połowie lat 80. Niestety oporność na fluorochinolony stała się powszechna. Mutacje odpowiedzialne za obniżenie wiązania fluorochinolonów do gyrazy DNA zostały szeroko opisane.

W ciągu ostatnich 15 lat pojawiła się również plazmidowo przenoszona oporność na fluorochinolony. Najpopularniejszy gen *qnr* koduje białko zawierające motyw powtórzeń pentapeptydowych (PRP). Plazmid *qnr* zapewnia jedynie umiarkowany poziom ochrony przed działaniem fluorochinolonów. Jednak częściowa oporność umożliwia rozwój pełnej oporności dzięki nabyciu dodatkowych mutacji chromosomalnych lub pomp błonowych.

Istnieją trzy podstawowe modele białek PRP oddziałujących z gyrazą DNA. Po rozwiązaniu pierwszej struktury białka PRP oddziałującego z topoizomerazą MfpA z *Mycobacterium tuberculosis* zasugerowano, że MfpA konkuruje z dwuniciowym DNA o wiązanie się z regionem enzymu, w którym dochodzi do rozcinania i ligacji DNA. W tym modelu białka PRP naśladują segment G DNA i wiążą się z miejscem wiązania segmentu G w podjednostce GyrA. Zaproponowano również inny mechanizm wyjaśniający w jaki sposób białka PRP dają ochronę przed działaniem fluorochinolonów bez wpływu na superskręcanie, które byłoby obserwowane w pierwszym modelu na skutek kompetycji wiązania DNA. Sugeruje się, że zamiast naśladować początkowy stan związania DNA i

konkurować o jego miejsce wiązania, PRP rozpoznają kompleks enzymu, który jest stabilizowany przez wiązanie fluorochinolonu. Interakcja ta powoduje destabilizację kompleksu, w wyniku której dochodzi do dysocjacji fluorochinolonu z miejsca wiązania i uwolnienia enzymu. Pozwala to na kontynuowanie reakcji przez gyrazę. Istnieje jeszcze inny, alternatywny model działania PRP. W tym modelu PRP naśladuje segment T który jest transportowany podczas reakcji superskręcania PRP jest wychwytywany przez kompleks gyraza-DNA, w którym segment G jest już związany.

Celem niniejszej pracy było dostarczenie informacji strukturalnych i biochemicznych na temat interakcji między białkami PRP a gyrazą DNA z *Escherichia coli.* Uzyskane dane wykorzystano do próby wyjaśnienia obserwowanej specyficzności działania hamującego i ochronnego, w którym pośredniczą różne białka PRP. Na podstawie uzyskanych wyników zbudowano nowy model interakcji gyrazy z białkami PRP.

Podczas badań analizowano działania trzech różnych PRP. QnrB1 z *Klebsiella pneumoniae* odpowiedzialny za oporność na fluorochinolony, AlbG z *Xanthomonas albilineans* odpowiedzialny za ochronę przed albicydyną oraz McbG z *Escherichia coli* odpowiedzialny za ochronę przed mikrocyną B17. Albicydyna i mikrocyna B17 są naturalnie syntetyzowanymi toksynami wiążącymi gyrazę, które podobnie jak fluorochinolony oddziałują z gyrazą poprzez stabilizację kompleksu gyraza: DNA: fluorochinolon.

Białko QnrB1 zostało oczyszczone i przeanalizowane biochemicznie oraz strukturalnie. W trakcie analiz potwierdzono specyficzność protekcji w stosunku do fluorochinolonów. Wykazano, że białko skutecznie destabilizuje kompleks gyraza: DNA: fluorochinolon w obecności hydrolizy ATP. Ustalono, że hydroliza jest niezbędna do ochronnego działania białka QnrB1. Dodatek QnrB1 stymulował aktywność ATPazową gyrazy DNA. W trakcie analiz biochemicznych stwierdzono, że gyraza B jest głównym celem interakcji białka QnrB1. Reakcja sieciowania indukowana UV z ortogonalnym aminokwasem inkorporowanym do QnrB1 wykazała miejsca interakcji z enzymem w białku QnrB1.

Model strukturalny QnrB1: DNA: gyraza: moxifloxacyna został zbudowany w oparciu o dane Cryo-EM. Dane strukturalne potwierdziły obserwacje biochemiczne interakcji QnrB1 z gyrazą B. Uzyskane dane dla QnrB1 pozwoliły zaproponować nowy model

interakcji PRP z gyrazą. Wydaje się, że prawidłowy mechanizm zawiera w sobie pewne elementy mimikry segmentu T i rozpoznawania kompleksu gyraza: DNA. QnrB1 wydaje się obierać drogę segmentu T podczas wiązania do enzymu, a działanie ochronne ma miejsce za pośrednictwem rozpoznania specyficznych cech struktury kompleksu gyraza: DNA: fluorochinolon.

Białko AlbG analizowano podobnie jak QnrB1. Wykazano jego zdolność do destabilizacji kompleksu gyraza: DNA; albicydyna i specyficzność wobec albicydyny. W przeciwieństwie do QnrB1, wykazano interakcję AlbG z obiema podjednostkami gyrazy podczas eksperymentów sieciowania. AlbG nie stymulował aktywności ATPazy gyrazy. Mutacja AlbG z delecją pętli, nie wykazała aktywności ochronnej przeciwko albicydynie, Wyniki, te mogą korelować z danymi przedstawionymi dla białka QnrB1 pozbawionego pętli. Białka chimeryczne: AlbG z pętlą QnrB1 i QnrB1 z pętlą AlbG nie wykazały żadnej aktywności, co sugeruje, że sama pętla obecna w strukturze niektórych białek PRP nie jest jedynym czynnikiem determinującym swoistość PRP.

Struktura białka McbG badanego w pracy, w przeciwieństwie do QnrB1 i AlbG, nie jest znana. W pracy zastosowano kilka metod ekspresji w celu uzyskania większej ilości białka do krystalizacji. Pomimo wysiłków ekspresja nie była skuteczna i dane krystalograficzne nie zostały pomyślnie zebrane. Eksperymenty biochemiczne wykazały ochronną aktywność McbG wobec mikrocyny B17. Niestety, mała ilość i niestabilność oczyszczonego białka pozwoliła jedynie na ograniczoną analizę biochemiczną.

Wyniki uzyskane w pracy pozwoliły sformułować nowy model działania PRP oddziałujących z gyrazą. Zebrane dane można wykorzystać do projektowania nowych cząsteczek inhibitorów gyrazy przy użyciu badań strukturalnych, które mogą utorować drogę do przezwyciężenia problemu oporności gyrazy na środki przeciwdrobnoustrojowe.

1. List of abbreviations

Abbreviation	Meaning
6xHis-tag	6x histidine protein tag
ALB	Albicidin
Ara	Arabinose
ATP	Adenosine 5'-triphosphate
ATPase	Adenosine 5'-triphosphatase
CFX	Ciprofloxacin
CTD	C-terminal domain
CV	Column volume
EC_{50}	Half maximal effective concentration
EDTA	Ethylenediaminetetraacetic acid
EtBr	Ethidium bromide
FLAG-tag	a peptide protein tag with the sequence DYKDDDDK
For	Forward primer
FQ	Fluoroquinolone
GHKL	(Gyrase, Hsp90, Histidine Kinase, MutL) domain
GyrA	Gyrase A subunit
GyrA59	*E. coli* gyrase A subunit truncation consisting of Winged-helix, Tower and Coiled-Coil domains
GyrB	Gyrase B subunit
GyrB24	*E. coli* gyrase B ATPase domain
GyrB43	*E. coli* gyrase B subunit truncation consisting of GHKL and transducer domains
GyrB47	*E. coli* gyrase B Toprim domain
IC_{50}	Half maximal inhibitory concentration
IPTG	Isopropyl β-D-1-thiogalactopyranoside
LB	Luria Broth
Lk	DNA linking number
MccB17	Microcin B17
MFX	Moxifloxacin
MHA	Mueller Hinton agar
MHB	Mueller Hinton broth
MIC	Minimal inhibitory concentration
Novo	Novobiocin
NTD	N-terminal domain
OD_{600}	Optical density value at 600 nm wavelength

PAGE	Polyacrylamide gel electrophoresis
pBpa	p-benzoyl-L-phenylalanine
PBS	Phosphate-buffered saline
PDB	Protein Data Bank
PEP	2-phosphoenolpyruvate
PRP	Pentapeptide repeat protein
PVDF	Polyvinylidene difluoride
RCF (g)	Relative centrifugal force (gravitational acceleration)
Rev	Reverse primer
RPM	Revolutions per minute
SDS	Sodium dodecyl sulphate
SDS-PAGE	Sodium dodecyl sulphate polyacrylamide gel electrophoresis
SEC	Size exclusion chromatography
SPA-tag	Sequential Peptide Affinity tag
TAE	Tris(hydroxymethyl)aminomethane, acetic acid, ethylenediaminetetraacetic acid
TBE	Tris-borate-EDTA
TEMED	Tetramethylethylenediamine
Toprim	Topoisomerase-primase domain
TPRPs	Topoisomerase-targeting pentapeptide repeat proteins
WHD	winged helix domain
wt	wild-type

2. Introduction

2.1. Antimicrobial resistance

Bacterial antimicrobial resistance (AMR) has arisen as a one of the biggest threats to public health in the 21st century. The biggest study of global burden of antibiotic resistance shows that around 1.27 million deaths in 2019 were directly caused by antibiotic resistant bacterial infections. The study shows that the antibiotic resistance is not a future threat. It is already one of the leading cause of global mortality (Murray *et al.*, 2022). During Recent COVID-19 pandemic the emergence and transmission of AMR has increased, especially in the case of Gram-negative bacterial infections in hospital settings (Langford *et al.*, 2023). There are few main causes of AMR. Overuse, inappropriate prescribing and extensive agricultural use of antibiotics contributes to emerging of drug resistance bacteria. The low availability of new antibiotics which is observed in recent years is also promoting the spread of resistance bacteria (Ventola, 2015).

The main biological causes of AMR are: selective pressure, mutations and horizontal gene transfer. Selective pressure is observed when the survivors of antimicrobial exposure replicate and become dominant throughout population. Resistance mutations can emerge spontaneously and it the presence of drug the resistance bearing bacteria survive leading to emerging resistance population. Horizontal gene transfer (HGT) allows bacteria to exchange their genetic materials including resistance genes. “Superbugs” describes bacteria that carry a number of HGT-transferred antimicrobial resistance genes on plasmids (Mathers, Peirano and Pitout, 2015; Wang and Sun, 2015).

Clearly, the AMR is multithreaded issue that has a great influence on public health. Estimates made by The World Bank predict that yearly expense of AMR will reach 1.2 trillion $ by 2050 (The World Bank, 2017). The 2021 WHO report shows that since 2017 only 12 antibiotics have been approved and by 2021 only 21 were under clinical trials (WHO, 2021). The low amount of new antibiotics produced by pharmaceutical companies requires commitment of academic to solve the AMR problem.

Tackling the molecular causes of antibiotic resistance allows us to challenge the AMR issue at the very root of the problem. Recent development of structural biology methods such as Cryo-EM allows for more accurate studies of the molecular background of AMR.

There are various molecular mechanisms of AMR. Reduced permeability of bacterial cell prevents the enter of the antibiotics preventing its activity inside. That can be achieved by the reduced expression of porins leading to lower uptake of the drug. Another mechanism is based on increased efflux of the antibiotic induced by efflux pumps that allows the drug to be removed from the cell. Resistance could be also achieved through changes in antibiotic target by mutations and physical protection before antibiotic interaction with its target, preventing the appropriate binding of the drug. Lastly the drug could be inactivated by the enzymes present in bacterial cell. (Blair *et al.*, 2015).

2.2. Quinolones

One of most commonly clinically used antimicrobials affected by AMR are fluoroquinolones**.** Quinolones are synthetic antimicrobials with 4-quinolone skeleton (**Figure 1**). The first discovered quinolone drug was nalidixic acid – a by-product of chloroquine synthesis. Nalidixic acid has moderate antimicrobial activity against Gram-negative species. It was introduced to clinical use to treat urinary tract infections (Lesher *et al.*, 1962) and was followed by oxolinic acid (Guyer and Whitford, 1975; Emmerson and Jones, 2003). It was established that oxolinic and nalidixic acid impair chromosomal replication in bacteria inhibiting both gyrase and topoisomerase IV (Crumplin and Smith, 1976). Addition of a fluorine atom onto carbon 6 (C-6) of the quinolone scaffold produced – norfloxacin the first fluoroquinolone which significantly improved potency – it was the first member of the second generation of quinolone drugs. It was shown to have a broader scope of activity, better bioavailability, as well as improved pharmacokinetic and pharmacodynamic properties (Wolfson and Hooper, 1988). Addition of a cyclopropyl group at position N-1 have led to synthesis of ciprofloxacin. The molecule was created by Bayer during a long term study of the effects of very minor changes to the norfloxacin structure (Wise, Andrews and Edwards, 1983). Ciprofloxacin was the first fluoroquinolone to show effective systemic activity (Schacht *et al.*, 1988; Segev *et al.*, 1999). The drug became widely used as a treatment of variety of bacterial infections (Emmerson and Jones, 2003). The World Health Organization has placed ciprofloxacin on the list of "Critically Important Antimicrobials for Human Medicine"(WHO, 2017).

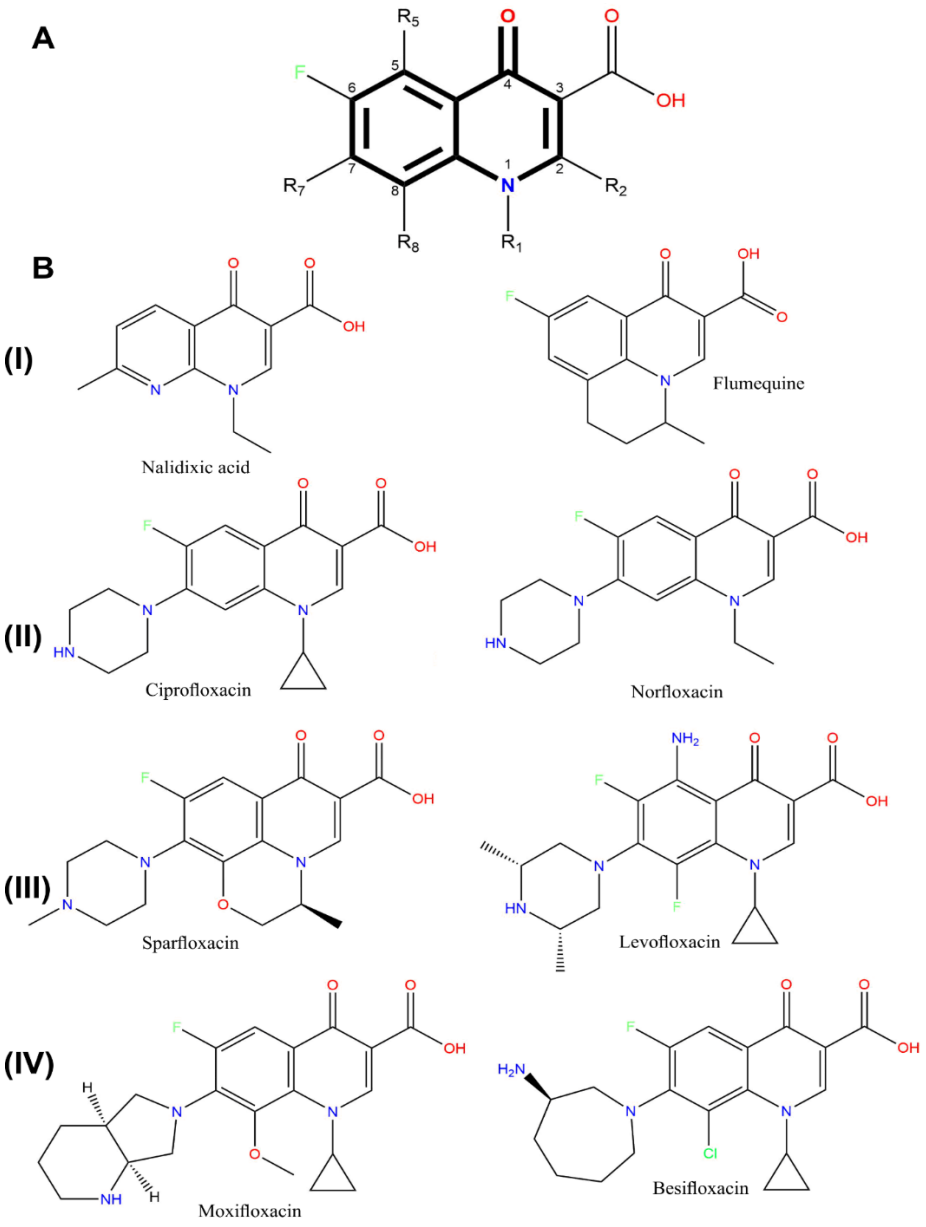

Figure 1 A. General structure of fluoroquinolones. 4-Quinolone backbone is presented as bolded. **B**. Examples of quinolone drugs. Roman numerals represent generation of the drug in the row.

Due to success of ciprofloxacin the optimisation of a fluoroquinolone molecule was further explored. Those efforts resulted in third and fourth generations of fluoroquinolone. Sparfloxacin and moxifloxacin are the most studied representatives of the third and fourth generations, respectively. These drugs have even broader spectra of activity and higher efficacy (Mitscher, 2005) and show a high potency against Gram-positive bacteria (Goa, Bryson and Markham, 1997; Wise, 1999). Together with levofloxacin, moxifloxacin is the most commonly used drug to treat multidrug-resistant tuberculosis infections (Ahuja *et al.*, 2012).

The mechanism of action of quinolones is strictly connected with the activity of bacterial topoisomerases, the enzymes responsible for maintaining the DNA topology inside the bacterial cell.

2.3. DNA topoisomerases

Maintaining DNA topology in cells is necessary in all organisms. *Escherichia coli* chromosome consists of approximately 4.7 x 10^6 base pairs which, if stretched in a line, would be 1.6 mm long. An *E. coli* cell, however, is only around 0.002 mm long (Bakshi *et al.*, 2012) . Consequently, DNA must be "packed" in order to fit to the cell. It must be also "unpacked" during processes that require protein - DNA interaction.

The geometrical description of DNA's topological state of DNA is simple and can be described with a formula:

$$Lk = Tw + Wr$$

where *Lk* is linking number, *Tw* - twisting number, *Wr* - writhing number.

Tw is the total number of base pairs in a DNA molecule divided by the number of bases per turn of the double helix and *Wr* is the is a measure of the coiling of the axis of the double helix. A Positive sign is assigned to right-handed turns whereas negative for left-handed. For a covalently closed DNA molecule (such as plasmid or a circular bacterial chromosome) *Lk* is constant. Any change in twist must be compensated by a change in writhe. For linear form DNA we can define the hypothetical linking number Lk^0 as $\frac{N}{h}$ where *N* is the number of base pairs and *h* equals the number of base pairs per turn of the helix (10.5 for B form DNA). As mentioned for covalently closed DNA molecule, if writhe is introduced to DNA without changing the number of twists (i.e., without unwinding the double helix), the linking number changes. The difference between actual *Lk* value and Lk^0 is called linking difference ΔLk. If the value is different from zero, we say that the DNA molecule is supercoiled. The sign of the value differs between negative and positive supercoiling (Bates *et al.*, 2005) (**Figure 2**).

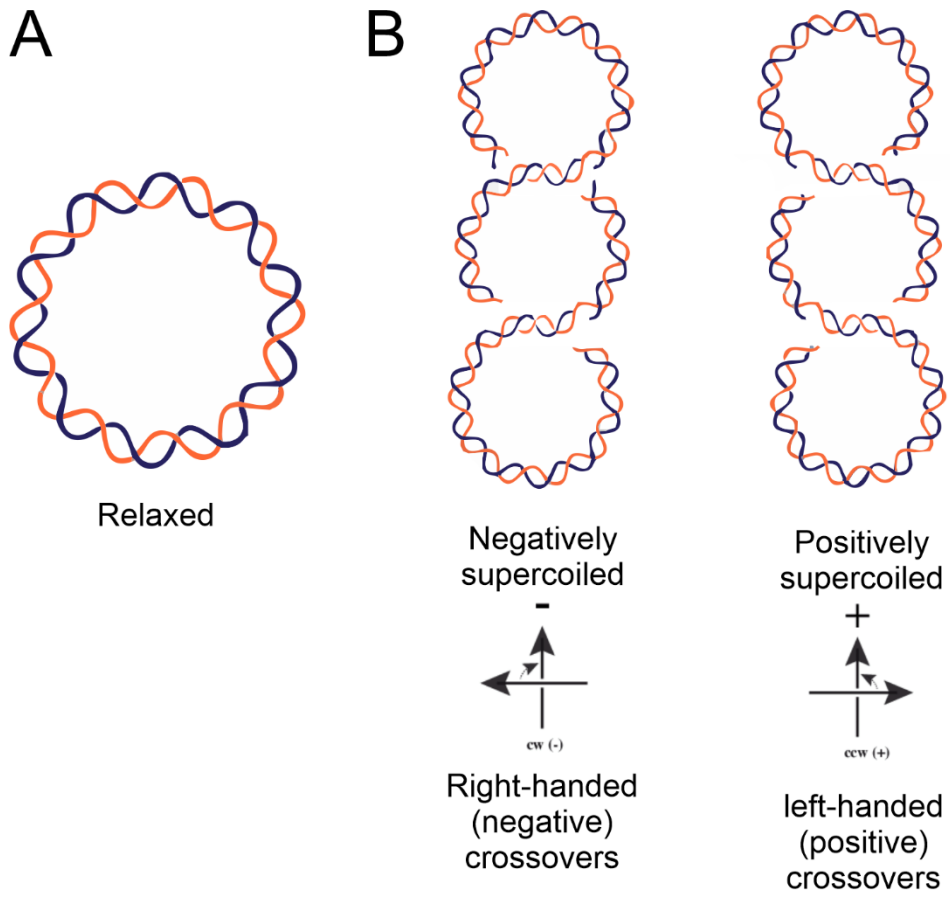

Figure 2. DNA topology. (**A**) Relaxed form of plasmid (**B**) supercoiled DNA plasmids where additional twisting is introduced into the double helix. The difference of negatively and positively supercoiling is explained on arrow diagram.

DNA topoisomerases are specialised enzymes responsible for maintaining DNA topology in the cell. Topoisomerases can cut and re-ligate the DNA which allows them to add or remove supercoil in a DNA strand and to disentangle DNA strands. DNA cutting across both strands (cleavage) is achieved by formation of transient, phosphodiester bond formed between the catalytic tyrosine of the enzyme and the 5′end of DNA.

Apart from DNA compaction, topoisomerases are responsible for management of DNA replication and for developmental processes depending on replication. (Vos *et al.*, 2011) The process of replication can be divided into several stages: initiation, elongation and termination. The DNA present in cells is usually in a negatively supercoiled state, this is due to conservation of its topology by topoisomerases or interaction with nucleoid-associated proteins. Negative supercoils ensure easier strand separation because of the fact that its separation is energetically less costly. Negative supercoiling aids such processes as DNA replication initiation (Witz and Stasiak, 2010). The elongation of replication requires the helix to separate, allowing the active replisome access to

nucleotides. The separation of the duplex leads to the accumulation of positive DNA supercoils ahead of the replicating fork and precatenanes behind it (Vos *et al.*, 2011) (**Figure 3**). The accumulation of positive supercoils would eventually physically inhibit the progression of the replication fork resulting in premature termination of replication. Unresolved positive supercoils would lead to DNA entanglements, catenation and improper segregation. The problem of removing positive supercoils is maintained by DNA topoisomerases making them vital enzymes playing a role in cellular processes.

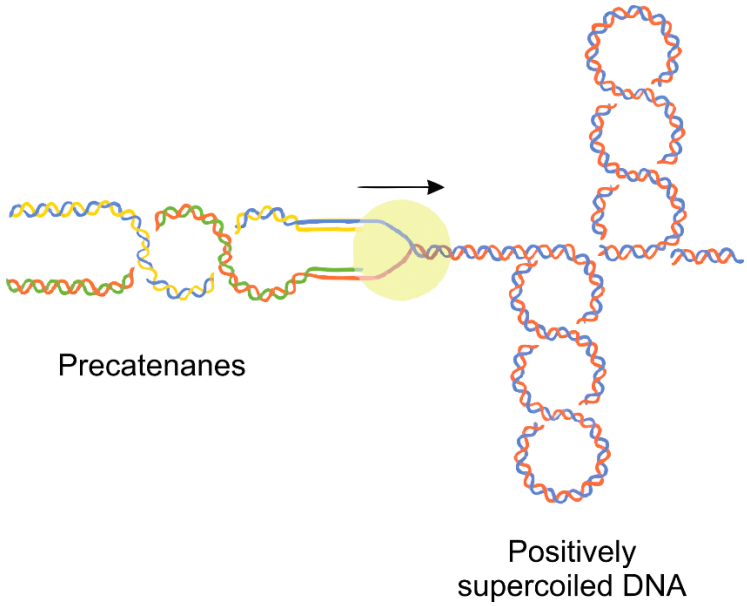

Figure 3. DNA topology problem during replication. During the progression of DNA polymerase accumulation of positive supercoils occurs in front of replication forks. Behind the polymerase newly synthetised double strands wrap and form precatenanes.

Topoisomerases are grouped in two types, depending on the number of DNA strands cut during their action. Type I topoisomerases cut only one DNA strand during catalysis, while Type II topoisomerases cut both DNA strands. Further classification to subtypes (A,B or C) of topoisomerases is based on distinct amino acid sequence or protein structure (Champoux, 2001). A summary of topoisomerases discussed in this chapter is presented in **Table 1**.

Table 1 Summary of topoisomerase classifications and characteristics.

Topoisomerase Type					
Type	Type I			Type II	
Subtype	Type I A	Type I B	Type I C	Type II A	Type II B
Mechanism	Single strand passage	Controlled rotation		Double strand passage	
Metal dependency	Yes (Mg^{2+})	No		Yes (Mg^{2+})	
ATP dependency	No (reverse gyrase -yes)	No		Yes	
DNA cleavage	Single strand			Double strand	
Δ Lk	+1	± n		± 2	
Main function	– Relaxation of SC DNA – Catenation – Decatenation – Positive supercoiling (reverse gyrase)	– Relaxation of +SC DNA – Relaxation of -SC DNA	– Relaxation of +SC DNA – Relaxation of -SC DNA	– Negative supercoiling – Relaxation of +SC DNA	– Relaxation of + SC DNA – Relaxation of -SC DNA – Catenation – Decatenation
Examples	– Topo IA – Topo III – Reverse gyrase	– Topo IB	– Topo V	– DNA gyrase – Topo IV – Topo II	– Topo VI

2.3.1. Type I topoisomerases

The proteins belonging to this subtype were found in organisms representing all cellular domains of life (archaea, bacteria and eukarya). These proteins are bacterial topo I (later called topo IA), bacterial and eukaryotic topo III, and reverse gyrase found in bacteria and archaea (Forterre *et al.*, 2007).

Topoisomerases from the IA subtype rely on a 'strand passage' mechanism where a single DNA strand is cleaved by the catalytic tyrosine, and a second DNA strand is transported through the break. After the passage the second DNA strand is released (Tse, Kirkegaard and Wang, 1980). The main function of these enzymes is to relax negatively supercoiled DNA in ATP-independent manner (Wang, 1971; Hiasa, DiGate and Marians, 1994). However, topoisomerase III acts preferentially on single-stranded DNA to solve topological problems during DNA replication and repair (DiGate and Marians, 1988; Wallis *et al.*, 1989; Hiasa, DiGate and Marians, 1994; Harmon, DiGate and Kowalczykowski, 1999). A distinct member of the topoisomerases IA subtype is reverse gyrase**:** an enzyme uniquely found in thermophilic archaea and bacteria, which is capable

of positively supercoiling DNA in an ATP dependent manner. It was shown that the enzyme is able to renature melted DNA strands (Kikuchi and Asai, 1984; Hsieh and Plank, 2006).

The mechanism and structure of type IB DNA topoisomerases is entirely different (Redinbo *et al.*, 1998). These enzymes nick double-stranded DNA and allow its rotation around the opposite strand (Koster *et al.*, 2005). The control over the rotation is achieved by friction between DNA and enzyme. The friction also aids in the alignment of the broken ends and resealing of the DNA (Champoux and Dulbecco, 1972; Koster *et al.*, 2005). Type IB topoisomerases preferentially bind to positively or negatively supercoiled DNA (Madden, Stewart and Champoux, 1995; Frohlich *et al.*, 2007). Some variants of type IB topoisomerases were shown to exhibit faster relaxation rates for positively supercoiled DNA (Frohlich *et al.*, 2007). The proteins belonging to type IB DNA topoisomerases were found in all eukarya, poxviruses and mimiviral families of eukaryotic viruses and in a plethora of bacterial genera (Forterre *et al.*, 2007).

Archaeal topo V is the only known member of type IC topoisomerases. It has been found in the archaeal genus *Methanopyrus* (Forterre, 2006). Type IC topoisomerases have a similar mechanism to its type IB counterparts and is also responsible for relaxing of positively and negatively supercoiled DNA in ATP and Mg^{2+} dependent manner (Slesarev *et al.*, 1993; Taneja *et al.*, 2007). The active site of topoisomerases IC has little similarity to active site of topoisomerases IB which suggests a different evolutionary origin of these two types of enzymes (Forterre, 2006; Taneja *et al.*, 2006). (Slesarev *et al.*, 1993).

The summary of reactions performed by type II topoisomerases are shown on **Figure 4**.

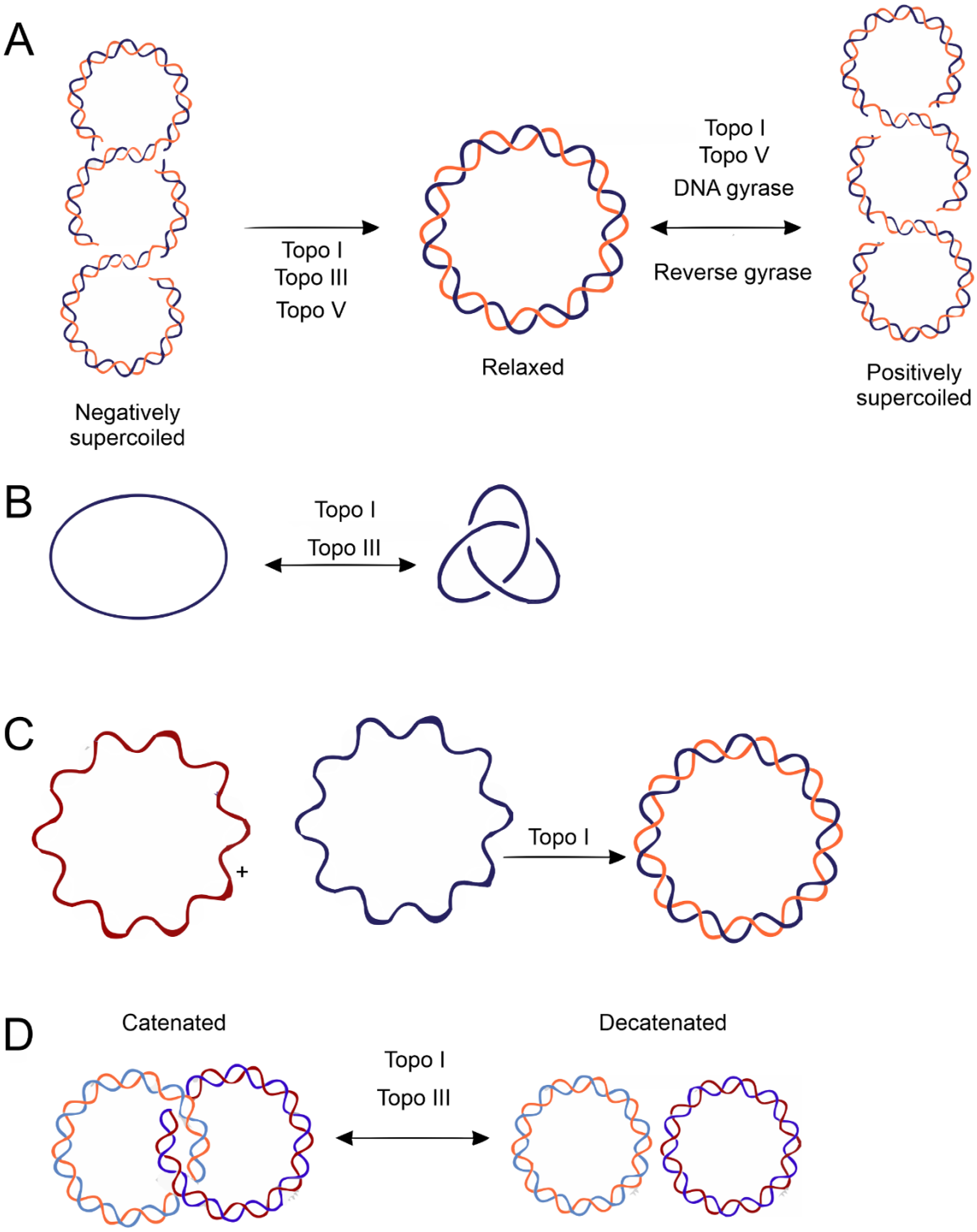

Figure 4. Summary of reactions performed by type I topoisomerases.

2.3.2. Type II topoisomerases

Within type II topoisomerases there are two subtypes – type IIA and type IIB. Similarly, to type IA topoisomerases, type IIA enzymes use an active strand passage mechanism to alter DNA topology. Type IA and IIA have similarities in catalytic domains important for DNA cleavage (Aravind, Leipe and Koonin, 1998; Berger *et al.*, 1998). However, unlike

Type IA enzymes, type II topoisomerases cleave both DNA strands of DNA helix and an intact DNA fragment is passed through transient break (Liu, Liu and Alberts, 1980). All of the enzymes conduct ATP-dependent reactions (Bates, Berger and Maxwell, 2011). Type IIA topoisomerases are able to resolve both positive and negative DNA supercoils and decatenate intertwined chromosomes and DNA catenates (Hsieh and Brutlag, 1980; Mizuuchi *et al.*, 1980). Type IIA topoisomerases are found in all cellular organisms and also in some viruses and organelles for example plastids. Type IIA topoisomerases can be classified into a few subfamilies: DNA gyrase, eukaryotic topoisomerase II (topo II), bacterial topoisomerase IV (topo IV).

Eukaryotic top II is expressed in two different isoforms (α and β) in vertebrates while lower eukaryotes like yeasts produces only one form of topo II. *A* isoform has been shown to be active in regions of active genes and is associated with highly transcribed loci (Yu *et al.*, 2017). The beta isoform is expressed constantly in all cell types and is referred to as "housekeeping topoisomerase " (Sandri *et al.*, 1996).

Topoisomerase IV is responsible for resolving topologically linked daughter chromosomes produced during DNA replication. The enzyme is able to relax supercoiled DNA in an ATP-dependent manner and knot and unknot DNA (Peng and Marians, 1993; Deibler, Rahmati and Zechiedrich, 2001). The active enzyme is a heterotetramer build from ParC and ParE proteins homologous to GyrA and GyrB (Kato *et al.*, 1990; Peng and Marians, 1993). Structurally the enzyme core resembles that of gyrase. An Important functional difference between the two enzymes is the fact that topo IV cannot actively introduce negative supercoils. This is due to the fact that topo IV ParE C-terminal domain lacks one of the β-pinwheel domains and the GyrA-box which was shown to be essential for gyrase supercoiling activity (Corbett *et al.*, 2005).

Similarly to their type IIA counterparts, Type IIB topoisomerases use a strand passage mechanism to relax both negative and positive supercoils (Bergerat, Gadelle and Forterre, 1994). These topoisomerases also consist of ATPase and DNA-cleavage domains, however there is substantial difference in their overall structure and sequence (Bergerat, Gadelle and Forterre, 1994; Corbett and Berger, 2003; Corbett, Benedetti and Berger, 2007). The DNA-binding subunit of type IIB enzymes is evolutionarily linked to SPO11 which is the factor responsible for creation of DNA double-strand breaks that initiate meiotic recombination (Bergerat *et al.*, 1997; Keeney, Giroux and Kleckner, 1997).

Archaeal topo VI was the first discovered member of type IIB topoisomerases (Bergerat *et al.*, 1997). Later plant topo VI was identified in *Arabidopsis thaliana* (Sugimoto-Shirasu *et al.*, 2002), Very recently Plasmodium topo VI has also been discovered (Chalapareddy *et al.*, 2016). Bacterial and archaeal topoisomerase VIII is another member of type IIB topoisomerase group (Gadelle *et al.*, 2014). The reactions performed by type II topoisomerases are shown in **Figure 5**.

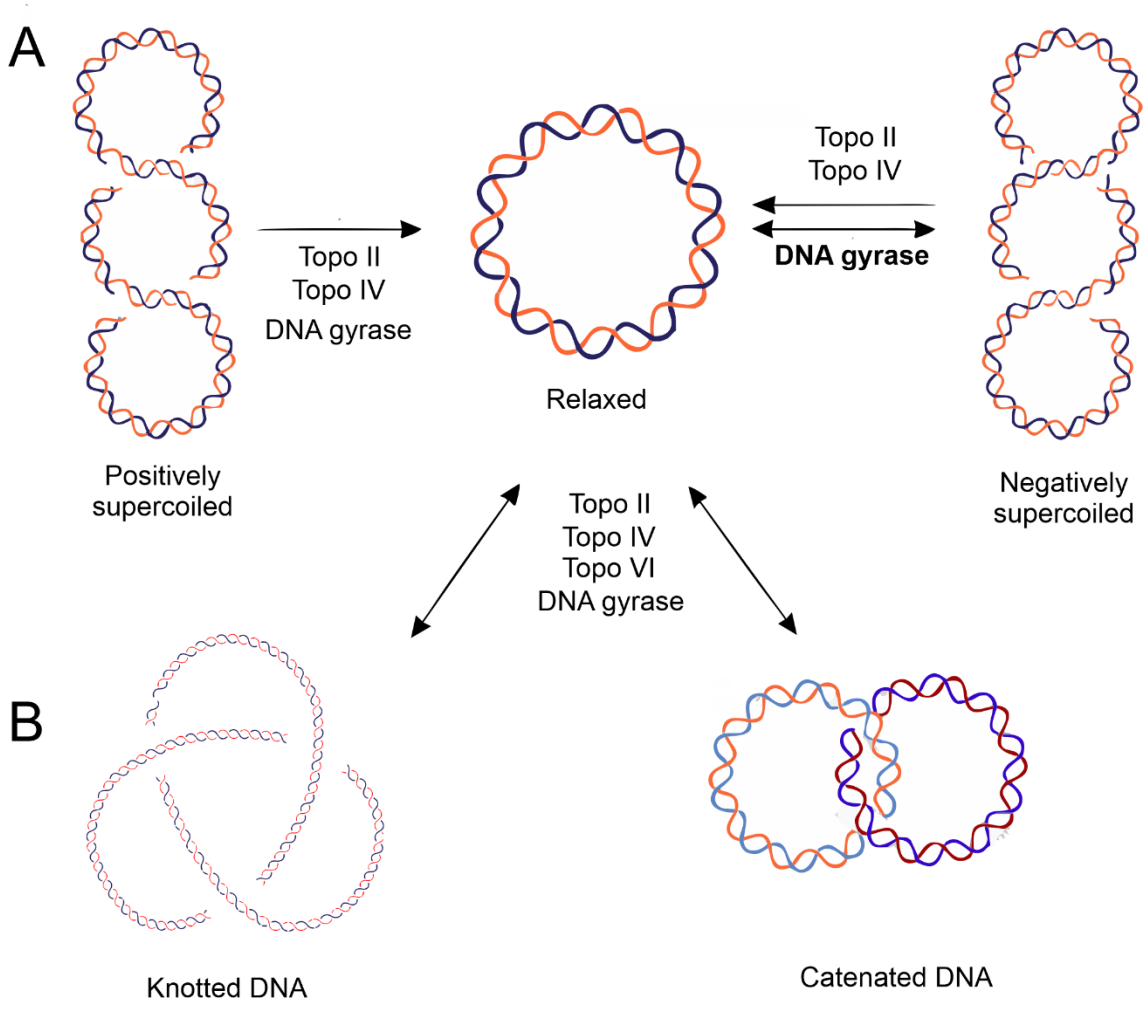

Figure 5. Summary of reaction performed by Type II topoisomerase. DNA gyrase is highlighted as only enzyme being able to perform negative supercoiling.

Structurally, Archaeal and bacterial types IIA and IIB topoisomerases are composed of two different subunits, A and B. In the case of type IIA enzymes from eukaryotic origin they are homodimers where A and B subunits are fused by a short linker. The B subunits are homologous among Type IIA and IIB families and contain similar ATP-binding sites with a characteristic fold for GHKL (**G**yrase, **H**sp90, **h**istidine **K**inase, Mut**L**) superfamily proteins (Bergerat *et al.*, 1997; Dutta and Inouye, 2000). The enzymes share

two other functional domains: the Toprim domain and the Winged Helix Domain (WHD) that contains the active site tyrosine. The significant difference between type II A and B topoisomerases is the fact that the Toprim domain of type IIA topoisomerases is located within the B subunit, whereas in the IIB family, this domain is located within the A subunit. What is more the A subunits of types IIA and IIB topoisomerases do not share sequence or structural similarity. This discrepancy suggests that both families originated independently via the association of homologous B subunits with non-homologous A subunits (Gadelle *et al.*, 2003).

2.4. DNA Gyrase

DNA gyrase is type IIA topoisomerase present in bacteria and archaea (Gellert *et al.*, 1976; Yamashiro and Yamagishi, 2005). It is also found in plant chloroplasts and the *Apicomplexa* apicoplast (Dar *et al.*, 2007; Evans-Roberts *et al.*, 2016) Gyrase is a unique topoisomerase thanks to its ability to introduce negative supercoils into DNA. Its supercoiling activity is ATP and Mg^{2+} dependent. Its supercoiling activity was the first to be discovered (by Gellert and co-workers in 1976 (Gellert *et al.*, 1976)). Gyrase is capable of performing ATP-coupled reactions such as: relaxation of positive supercoils, decatenation and unknotting (Kreuzer and Cozzarelli, 1980; Liu, Liu and Alberts, 1980; Marians, 1987). Gyrase can also relax negatively supercoiled DNA in the absence of ATP (Gellert, Fisher and O'Dea, 1979; Bates, O'Dea and Gellert, 1996).

E. coli gyrase is encoded by *gyrA* and *gyrB* genes. The encoded proteins GyrA and GyrB are 97-kDa and 90-kDa respectively. The active enzyme is formed from two GyrA and two GyrB subunits which forms an A_2B_2 heterotetramer (Adachi *et al.*, 1987). On a domain level GyrA contains winged-helix domain (WHD) a tower domain (Tower), a coiled-coil and C-terminal domain that adopts a DNA-bending beta-pinwheel fold. GyrB is divided into GHKL domain, transducer domain and TOPRIM domain.

Limited proteolysis assays shown that GyrB could be also divided into two domains: a 43-kDa N-terminal domain that is responsible for binding and hydrolysis of ATP (consisting of GHKL domain and transducer domain - GyrB43) and a 47- kDa C-terminal domain that interacts with DNA and GyrA (remaining TOPRIM domain) (Brown, Peebles and Cozzarelli, 1979; Wigley *et al.*, 1991; Chatterji *et al.*, 2000). Similarly the GyrA subunit can be divided into a 59-kDa N-terminal domain involved in DNA cleavage (WHD, Tower and Coiled coil domains) (Horowitz and Wang, 1987) and a 35-

kDa C-terminal domain involved in DNA wrapping (remaining CTD domain) (Reece and Maxwell, 1989). The domain architecture of DNA gyrase is presented on **Figure 6 A**.

While there has been a long history of structural studies of gyrase, X-ray crystallography has only been able to provide the structural data for individual domains of the protein, subunits, their truncated versions or the DNA binding and cleavage core consisting of GyrB TOPRIM domain fused to GyrA N-terminal part lacking CTD. The initial low-resolution (23 Å) structure of full-length gyrase was obtained for the thermophilic bacterium Thermus *Thermophilus gyrase* fusion (C-terminal of GyrB and N-termina of GyrA fused by three amino acid linker) using cryo-electron microscopy. Recent advances in cryo-electron microscopy have resulted in an improved resolution and allowed determination of the 6.6 Å structure of the *E. coli* gyrase holoenzyme complex with 180 bp DNA and an inhibitor gepotidacin with local resolution going 3.0 Å The Structure confirmed previous findings obtained using X-ray crystallography and complemented previously mentioned low resolution cryo-EM model (Vanden Broeck *et al.*, 2019) (**Figure 6 B**).

The enzyme forms an A_2B_2 complex with two-fold symmetry and protein - protein interfaces termed gates. The first gate (N-gate or ATP gate) is formed by two adjacent GyrB43 domains (Wigley *et al.*, 1991; Classen, Olland and Berger, 2003; Bellon *et al.*, 2004). The transducer domain contains two helices that translate the structural changes between the GHKL domain and the TOPRIM domain (Bjergbaek *et al.*, 2000). The TOPRIM domain is a structurally conserved topoisomerase-primase domain found in found in bacterial DnaG-type primases, small primase-like proteins from bacteria and archaea, type IA and type II topoisomerases, bacterial and archaeal nucleases of the OLD family and bacterial DNA repair proteins of the RecR/M family. The domain is responsible for DNA binding and chelation of metal ion in the active site. In the case of gyrase a magnesium ion is coordinated via the DxD motif (Aravind, Leipe and Koonin, 1998). It is still discussed how many ions are required for cleavage of DNA. The consensus leans toward the two ions mechanism (Sissi and Palumbo, 2009).

The interactions between TOPRIM and GyrA WHD domain forms the second gate termed the DNA -gate. Within the WHD domain the active site tyrosine (*E. coli* Y 122) is located (Gajiwala and Burley, 2000). The contiguous GyrA domain (Tower) is involved in the binding of DNA by electrostatic interactions (Cabral *et al.*, 1997). TOPRIM domain

from GyrB and WHD domain from GyrA are responsible for forming DNA-gate. The joint action of TOPRIM,WHD and tower domains facilitate the DNA-gate in performing its role of binding the DNA and cleaving each strand of the DNA duplex (Sander and Hsieh, 1983). The last dimerisation interface of gyrase, the C-gate is formed by a well conserved coiled-coil domain at the bottom of the heterotetramer (Berger *et al.*, 1996; Cabral *et al.*, 1997). The C-gate extends into the 35 kDa CTD being a β-pinwheel domain fold with a cylindrical shape composed of 6 β-sheet "blades". The DNA processed by the enzyme is wrapped around the outer rim of this domain. The domain is essential for the negative supercoiling activity of gyrase (Richard J. Reece and Maxwell, 1991; Kampranis and Maxwell, 1996). It has been shown that the deletion of this domain turns the enzyme into a conventional DNA relaxing topoisomerase. This domain contains the GyrA-box, a 7 amino-acid motif (QRRGGKG) which is essential for the supercoiling activity of gyrase (Kramlinger and Hiasa, 2006). The acidic tail at the very end of the extreme C-terminus of the GyrA CTD in *E. coli* is responsible for regulation of DNA wrapping and the rate of ATPase, making it responsible for control of the supercoiling (Tretter and Berger, 2012a, 2012b).

The GyrA domains (WHD, tower and coiled coil) together with TOPRIM form the catalytic core of the enzyme which has been shown to be a minimal part of the enzyme to be able to introduce DNA cleavage.

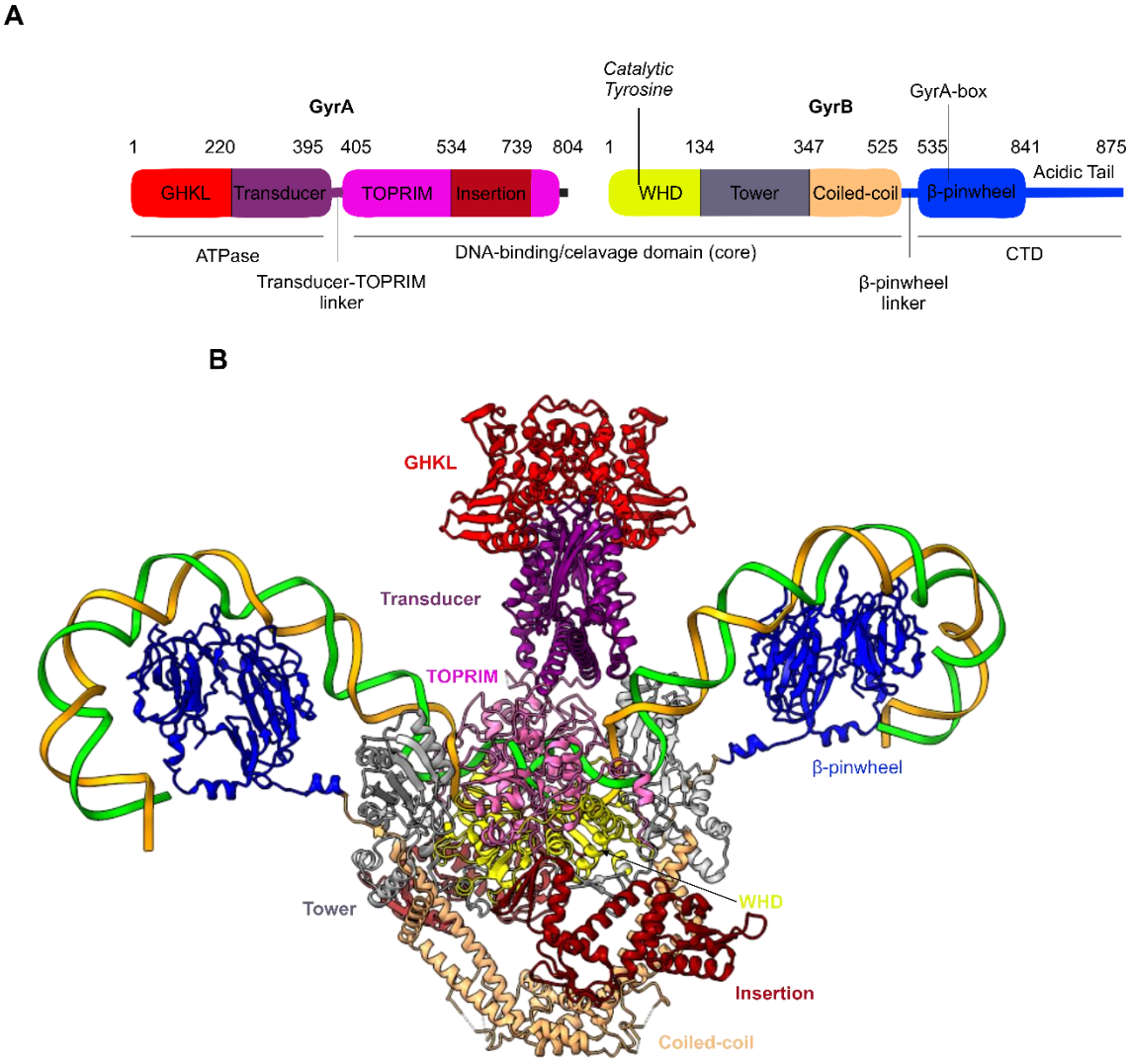

Figure 6. (**A**) Primary domain arrangement of *E. coli* gyrase (**B**) Cryo-EM structure of full-length *E. coli* gyrase complexed with 130 bp DNA (yellow-green) (PDB: 6RKW). Domain colours in B as in A.

2.4.1. DNA gyrase mechanism of action

The primary gyrase function is catalysing the ATP-dependent negative super-coiling of double stranded closed-circular DNA. The reaction is performed using a two gate mechanism (Mizuuchi *et al.*, 1980). The supercoiling reaction is started with the binding of a part of DNA termed G-segment (gate – segment), into the groove between the GyrA WHD domain and GyrB Toprim domain (DNA-gate). The bounding of DNA leads to twisting of the G-segment. Upon the G-segment binding the CTD domain of GyrA moves upwards allowing the section of DNA adjacent to G-segment to be wrapped around the β-pinwheel fold with a positive writhe (Orphanides and Maxwell, 1994; Heddle *et al.*, 2004; Lanz and Klostermeier, 2011). The wrapping of DNA around the CTDs is positioning the other part of DNA the T-segment (transport segment) across the bound

G-segment at an angle of about 60° (Papillon et al. 2013) The T-segment enters inside the enzyme through the N-gate formed by a GyrB43 dimers. The binding of DNA and the wrapping induces and narrowing of the N-gate which promotes the capture of the T-segment inside. Next, the ATP is bound by the GHKL domains by the each GyrB subunit which leads to dimerization of GyrB subunits and trapping T-segment and closure of the ATP operated clamp (Wigley *et al.*, 1991; Kampranis, Bates and Maxwell, 1999).

The hydrolysis of one of the ATP molecules induces cleavage of the G-segment by the active site tyrosine (*E. coli* GyrA Y122) located in WHD domain and the T-segment strand passage through cleaved G-segment and DNA gate. The cleaved DNA is re-ligated and the T-segment of DNA exits the enzyme through the C-gate. The enzyme is reset by ATP hydrolysis and the DNA is released upon releasing Pi and ADP. One full cycle of DNA gyrase changes the *Lk* number of DNA by -2. The schematic representation of the gyrase cycle is presented on **Figure 7**.

Importantly, the steps described up to the point of closure of the ATP operated clamp do not require energy form ATP hydrolysis and are possible also with binding of a non-hydrolysable analogue of ATP, Adenosine 5′-(β,γ-imido)triphosphate (ADPNP). (Roca and Wang, 1992). The reaction with ADPNP can perform a single strand-passage reaction, after which, the enzyme is stranded in an inactive state (Sugino *et al.*, 1978). To carry out the further catalytic cycle, the enzyme needs to be reset to its initial state which requires hydrolysis of ATP.

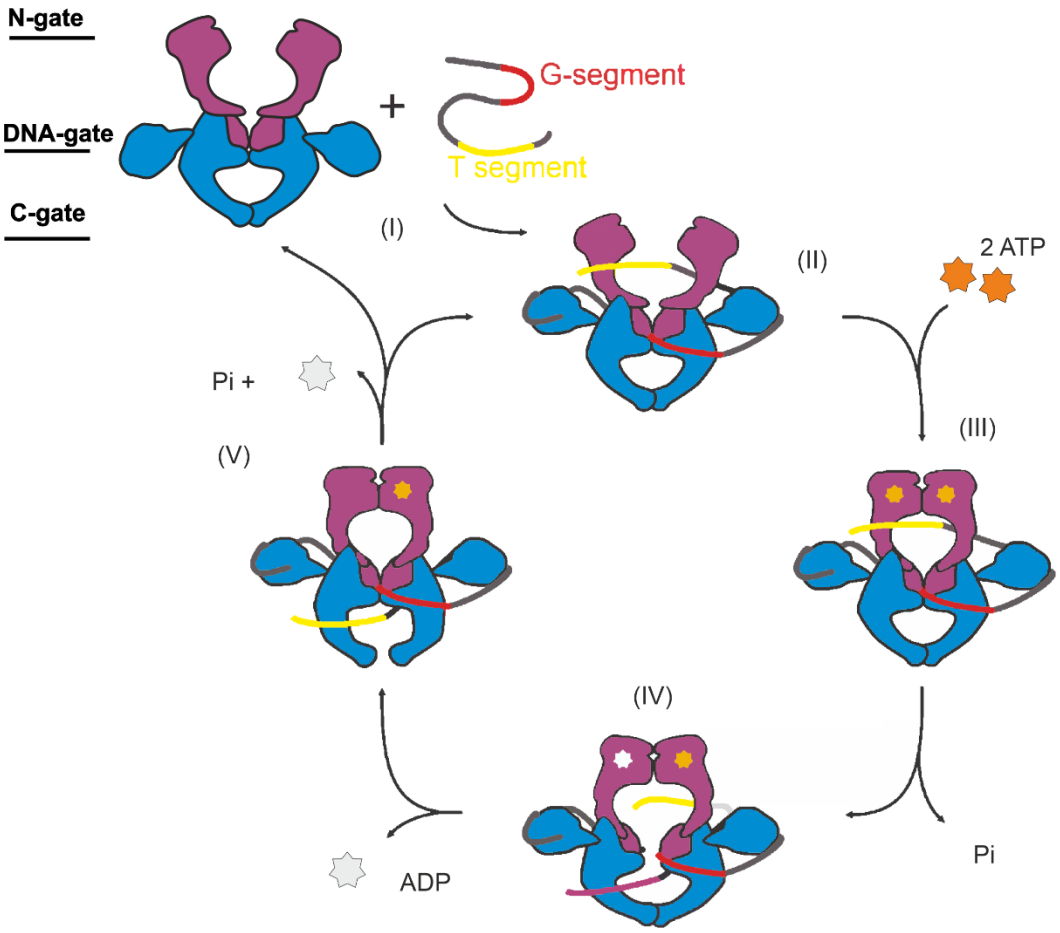

Figure 7. **Schematic representation of gyrase cycle**. (**I**) The G-segment DNA is bound at the DNA-gate and the contiguous DNA is wrapped (positive crossover) around the GyrA CTD; positioning the T-segment over the G-segment (**II**). (**III**) ATP binds at the GyrB NTDs, leading to dimerization of the domains, capture of the T-segment. (**IV**) Hydrolysis of one ATP molecule promotes the cleavage of the G-segment by the active tyrosine present in GyrA WHD domain and the T-segment strand passage through the DNA-gate (across cleaved G-segment DNA). (**V**) The G-segment is re-ligated. The process leads to the introduction of two negative supercoils into the DNA. The T-segment exits the DNA via the last dimer interface, the C-gate. The remaining ATP is hydrolysed to reset the enzyme.

The cleavage (DNA hydrolysis) that is performed by DNA gyrase is maintained by formation of the two phosphodiester bonds with catalytic tyrosines with two DNA bases form two DNA strands. That leads to formation of double strand break. The gyrase conformation when cleaved DNA is bound to DNA gyrase is termed “gyrase cleavage complex”

Gyrase uses the similar reaction to the one described above to perform ATP-independent relaxation of negatively supercoiled DNA. However, the reaction believed to be performed in reverse - T-segment passes through the enzyme in the opposite direction – through the C-gate first in the mechanism called “reverse strand passage” (Williams and Maxwell, 1999). The relaxation of positively supercoiled DNA requires ATP even though

the process is energetically favourable. This reaction utilises the same mechanism as the one described for introducing negative supercoils (Fisher *et al.*, 1992).

Gyrase activity could be tracked and analysed using agarose gel electrophoresis. Gel electrophoresis separates the DNA molecules on the basis of size and shape. Smaller more, compact molecules migrate faster through the gel pores due to the electric field during electrophoresis. Most commonly used DNA molecules during gyrase assays are bacterial plasmids of ~ 4000 base pairs for example *E. coli* pBR322 (Bates *et al.*, 2005). After the electrophoresis reaction the DNA is stained using ethidium bromide solution and visualised using UV lamp. A gel presents bands corresponding to different topological conformations of resolved DNA (**Figure 8**). The addition of ethidium bromide to the electrophoresis gel before electrophoresis is used to track the DNA cleavage amount. It is due the fact that the ethidium bromide binding to DNA results is unwinding of the DNA helix which forms a positive supercoiled which then run as a supercoiled band. In this way, all relaxed topological forms of uncleaved plasmid are "removed" from the area of the gels where linear DNA runs. This allows for easier visualisation of linear DNA which mobility would not be affected by EtBr binding.

For negatively supercoiled DNA, If the DNA is resolved in the presence of ethidium bromide during the electrophoresis the binding of the ethidium bromide to DNA would result in unwinding of the negatively supercoiled DNA helix. The initially negatively supercoiled DNA becomes more relaxed

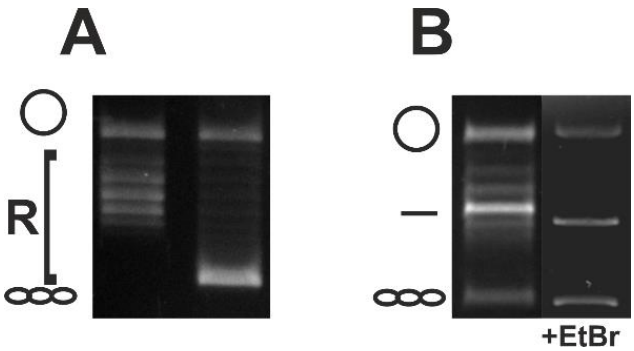

Figure 8. **Different topological states on agarose gel.** (A) DNA supercoiling, left line – migration pattern of relaxed DNA, right lane – migration pattern of supercoiled DNA (B) DNA cleavage, left line sample of cleaved DNA ran without intercalators, right line – same sample of DNA ran in the presence of ethidium bromide, the relaxed DNA topoisomers are turned into supercoiled molecules. Symbols describing DNA topoisomers – circle – open circular DNA, R – relaxed DNA, three connected circles – supercoiled DNA, dash – cleaved DNA.

Inside the bacterial cell the gyrase is responsible for negative supercoiling during the process of chromosome condensation, recombination, and replication initiation (Bates *et*

al., 2005; Dorman and Dorman, 2016). Gyrase is responsible for the resolution of positive supercoils that accumulate ahead of the replication fork. *In vivo* gyrase is antagonistic to topoisomerase I in the process of controlling DNA supercoiling levels (Drlica, 1992). If the cell is unable to remove positive supercoils ahead of the replication fork, the stalling of replication is induced and the lethal double-stranded DNA breaks that are lethal to the cell (Liu and Wang, 1987) are produced. This is one of the features that makes DNA gyrase a good antibacterial target.

2.4.2. DNA gyrase inhibitors

2.4.2.1. DNA gyrase as a quinolone target

Due to its housekeeping role and the fact that the gyrase is not present in eukaryotes gyrase is a good drug target. Its complex cycle allows the inhibitors to act on different stages of the cycle. Having introduced the concept of DNA topology, fluoroquinolones can now be considered in the context of gyrase activity. The fluoroquinolones inhibit DNA supercoiling and relaxation by binding to the DNA gyrase cleavage complex and stabilising it. The inhibitory activity is also observed for Topo IV. The preference of binding is often related to the fluoroquinolone and some of the molecules have been shown to bind equally to both enzymes.

Quinolones bind non-covalently to DNA gyrase near the cleavage active site via stacking interactions with DNA bases on either side of the cleavage site. This binding stabilizes the gyrase-drug cleavage complex and leads to inhibition of re-ligation of DNA. The stabilised DNA-quinolone-gyrase complex stalls the replication forks and inhibits the transcription machinery due to the fact that the enzyme cannot perform its topology resolving activity. The molecules are "hijacking" gyrase cleavage activity and turn gyrase into toxin. Due to this fact the fluoroquinolones are also termed gyrase "poisons" (Kreuzer and Cozzarelli, 1979; Spencer and Panda, 2023). Quinolone induced cleavage does not generally require ATP, and DNA substrates of ∼20 bp can be cleaved (Cove, Tingey and Maxwell, 1997; Gmünder, Kuratli and Keck, 1997)

Quinolone binding has been shown to be mediated through the metal ion bridge in the A subunit of DNA gyrase (Carter *et al.*, 2023). The C-3/C-4 region of the molecule is by noncatalytic Mg^{2+} ion that is coordinated by four water molecules. The waters form the hydrogen bonds between GyrA S83 and D87 for *E. coli* gyrase. The C-7 ring of the

quinolone extends into the GyrB subunit (Blower *et al.*, 2016). The binding of ciprofloxacin by a well characterised cleavage complex of *Mycobacterium tuberculosis* gyrase is depicted on **Figure 9**.

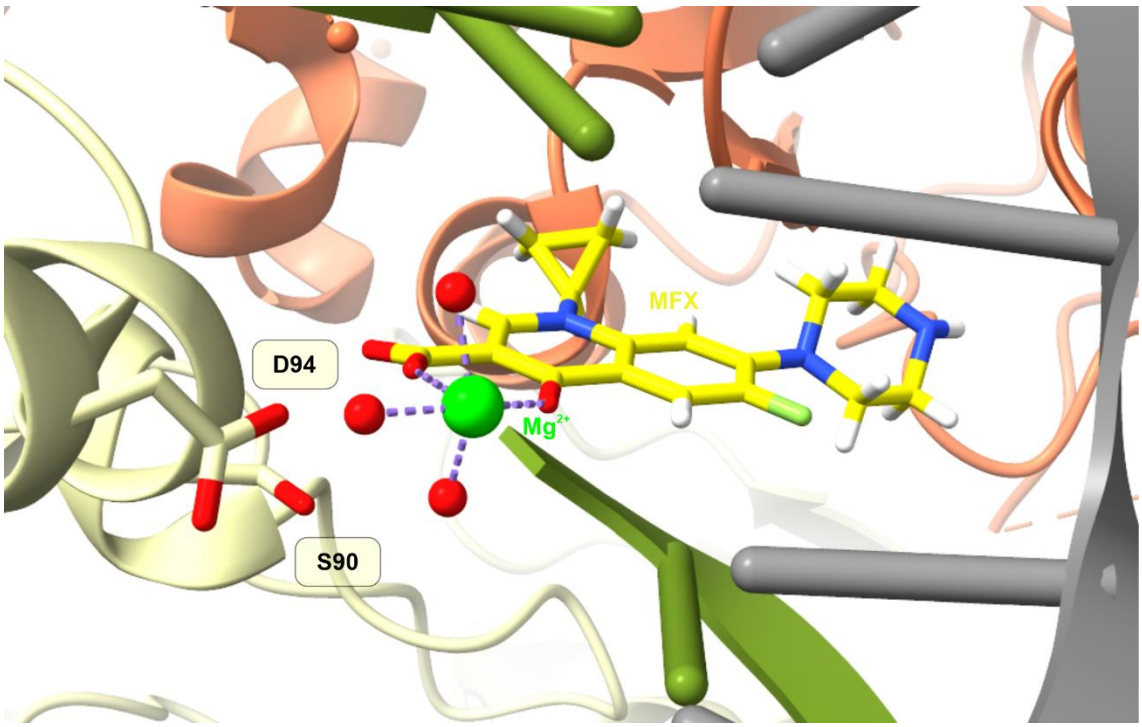

Figure 9. Binding of ciprofloxacin molecule by *Mycobacterium tuberculosis* gyrase (PDB: 5BTC). DNA gyrase amino S90 and D94 shown as sticks. S90 corresponds with S83 and D94 with D87 in *E. coli* gyrase GyrA shown as light beige cartoon, GyrB shown as coral cartoon, ciprofloxacin shown as a yellow molecule. Red spheres represent water. Magnesium ion is shown as a green sphere. DNA is depicted as grey and green ladder.

Quinolone induced cell killing at the first stage is connected to stalling the cleavage complex. The cleaved DNA cannot be re-ligated by the same enzyme molecule if the antibacterial is present. If the cleavage complex is not removed DNA replication and transcription are blocked leading to slow bacteria death.

The quinolone induced DNA damage can be repaired. It is not yet fully understood. It is possible that bacteria first remove the topoisomerase trapped on DNA by nuclease SbcCD or the helicase RuvAB. If the cleavage complex is removed by nuclease proteins or due to gyrase subunit dissociation and the broken DNA is not repaired, chromosome fragmentation occurs, leading to rapid bacterial death. The rate of bacterial death correlates with the MIC value for the molecules, Slow death occurs at concentrations around twice the MIC at higher amounts of antibacterial (5-10 x MIC) (Carret, Flandrois and Lobry, 1991). The release of double-strand breaks and would activate stress responses

such as the SOS response. The SOS response is a cellular response to DNA damage that is controlled by the auto-repressor LexA and the activator RecA (Kreuzer, 2013). This stress response leads to inducing the DNA repair involved genes. The DNA repair could be error – free like homologous recombination or error prone like translesion synthesis. The error prone repair generated mutations could lead to appearance of mutations that cause quinolone antimicrobial resistance.

If the cleavage complex is removed by nuclease proteins or due to gyrase subunit dissociation and the broken DNA is not repaired, chromosome fragmentation occurs, leading to rapid bacterial death. The rate of bacterial death correlates with the MIC value for the molecules, Slow death occurs at concentrations around twice the MIC at higher amount of antibacterial (5-10 x MIC) (Carret, Flandrois and Lobry, 1991),

2.4.2.2. Natural borne gyrase poisons microcin B17 and albicidin

2.4.2.2.1. Albicidin

Albicidin is an antibiotic produced by the plant pathogen *Xanthomonas albilineans* (Birch and Patil, 1985). It was shown that albicidin induces chlorosis in plants in co-culture with Xanthomonas albilineans strains (Birch and Patil, 1987). The Albicidin biosynthesis gene cluster encodes mixed PKS–NRPS (polyketide synthases - nonribosomal peptide synthases) genes (Royer *et al.*, 2004). Albicidin molecule consists of p-aminobenzoic acids and cyanoalanine (Birch and Patil, 1985; Cociancich *et al.*, 2015) (**Figure 10**).

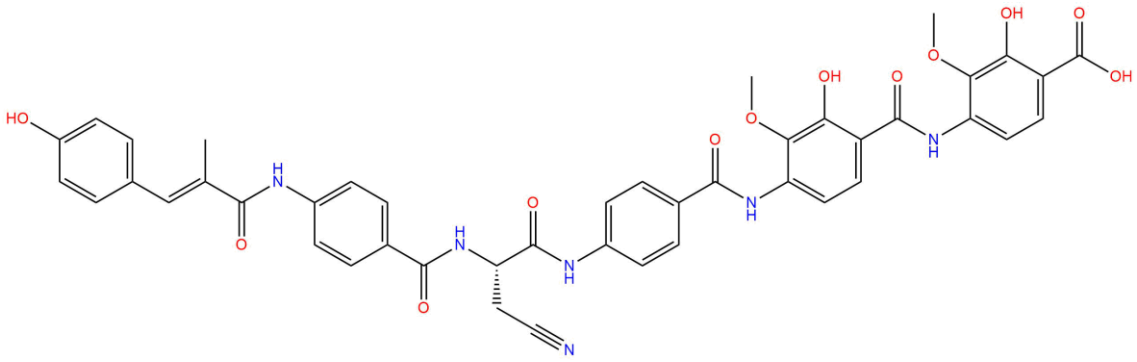

Figure 10. Albicidin molecule

Albicidin is bactericidal at nanomolar concentrations against a variety of Gram-positive and Gram-negative bacteria (Kretz *et al.*, 2015; Kerwat *et al.*, 2016). The drug does not show cytotoxicity to cultured mammalian cells (Hashimi *et al.*, 2007). Albicidin has been

shown to inhibit *E. coli* and *Arabidopsis thaliana* DNA gyrase by stabilising the cleavage complex in the presence of ATP and ADPNP (Hashimi *et al.*, 2007). The precise mode of action of albicidin was unknown. It was established that the hybrid enzyme comprising the *X. albilineans* gyrase A subunit and the *E. coli* gyrase B has activity and is resistant to albicidin. Those data suggested that the GyrA subunit is a target for albicidin (Hashimi *et al.*, 2008). The recently established structure of albicidin bound *E. coli* gyrase by Cryo-EM methodology shown that the albicidin binds with the "hybrid mode". One end of the molecule intercalates with the DNA and the other is located between two opposing helices (residues 66–76), forming the GyrA/GyrA′ dimer interface of the DNA gate. The structure shows a previously unreported catalytic state of gyrase that could be placed between the partially open pre-cleavage gepotidacin structure (PDB: 6RKV) and the fully open state (topo IIα structure, PDB: 5ZEN46). Albicidin in contrast to quinolones does not bind to the enzyme symmetrically and only DNA intercalating part of the albicidin is partially overlapping with the position where FQ molecule is located (Michalczyk *et al.*, 2023). The binding of albicidin is depicted on **Figure 11**.

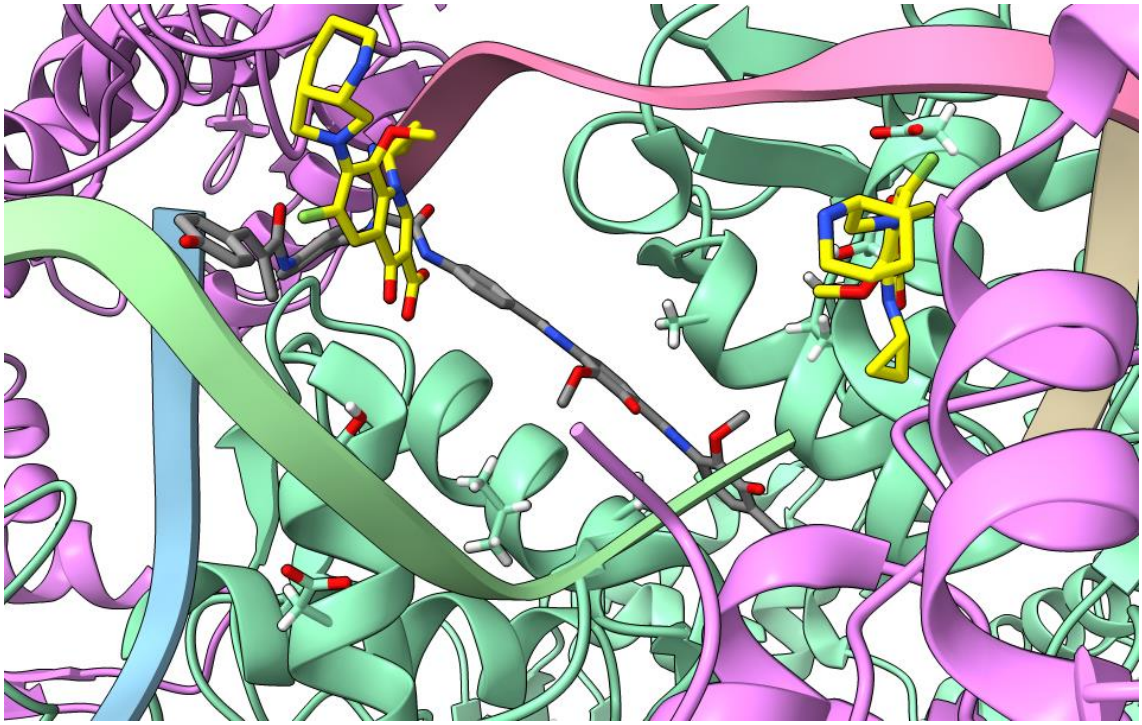

Figure 11. Comparison of binding of moxifloxacin and albicidin to *E. coli* gyrase. Albicidin molecule is depicted as grey sticks, moxifloxacin molecules are depicted as yellow sticks. GyrA is presented as green cartoon and GyrB is presented as pin cartoon. DNA strands are presented as ping and green sheets. The *E. coli* structure with bounded albicidin (PDB:7Z9C) has been superposed with moxifloxacin binding site of *E. coli* gyrase obtained in this thesis.

2.4.2.2.2. Mccb17

Microcins are low molecular antibacterial peptides (>10 kDa) produced by members of the *Enterobacteriaceae* family (Baquero and Moreno, 1984). Microcin B17 (MccB17) is a member of large group of ribosomally synthesised and post-translationally modified peptides (RiPP) and classified as a member of the linear azole-modified peptides (LAPs) - ribosomally synthesized peptides containing azole heterocycles (**Figure 12**). (Melby, Nard and Mitchell, 2011). The peptide is produced by bacteria carrying the pMccB17 plasmid (Davagnino *et al.*, 1986). The microcin B17 biosynthesis cluster consists of seven genes *mcbABCDEFG* (Genilloud, Moreno and Kolter, 1989). Genes mcb*ABCD* are responsible for microcin B17 production while mcb*EFG* genes confer resistance. (Garrido *et al.*, 1988; Kurepina *et al.*, 1993). *McbA* is a structural gene which encodes a 69 amino acid, glycine-rich precursor peptide. $McbA_{1-26}$ is a recognition element for the binding of the synthetase complex (Roy *et al.*, 1998, 1999). 4-5 of the serine residues and all cysteines are converted to oxazole and thiazole rings by the McbBCD complex. The modified peptide is cleaved by TldD/TldE protease removing the first N-terminal 26 amino acids The mature MccB17 is 3094-Da peptide containing 4 oxazole and 4 thiazole heterocycles (Yorgey, Lee and Kördel, 1994; Roy, Allen and Walsh, 1999; Allali *et al.*, 2002). An over-modified form of MccB17 containing an additional oxazole cycle (MccB17 Δ9) is also detected (Ghilarov *et al.*, 2011).

Microcin B17 is active against many bacteria from Enterobacteriaceae (Asensio *et al.*, 1976). It has been shown to block DNA replication and induce the SOS response in *E. coli* (Herrero and Moreno, 1986). The toxin has been shown to slow down the supercoiling and relaxation reaction of gyrase threefold by inducing the *E. coli* gyrase-mediated double-strand cleavage of DNA (Vizan *et al.*, 1991). Effects of MccB17 on the DNA cleavage reaction is topology dependent, when relaxed substrate is used MccB17 weakly stabilises the cleavage complex in the absence of ATP, however, in the presence of nucleotide more efficient cleavage stabilisation is observed. When negatively supercoiled DNA is used as a substrate, McbB17 efficiently stabilises the cleavage complex in the absence of ATP (Heddle *et al.*, 2001; Pierrat and Maxwell, 2003). It has also been shown that the action of MccB17 does not require the DNA-wrapping (CTD) domain of gyrase A or ATPase (B43) domain of gyrase B (Pierrat and Maxwell, 2005). Those observations taken together with the fact that the only known MccB17-resistant mutation is at position 751 of GyrB (W751R) prompted the hypothesis of MccB17

mechanism of action – microcin B71 binds to the C-terminal domain of gyrase B and prevents T-segment passage by trapping transient enzyme intermediate. (Vizan *et al.*, 1991; Pierrat and Maxwell, 2005). There are no structures of MccB17 with DNA gyrase so far, however an architecture of McbBCD-pro-MccB17 has been characterised (Ghilarov *et al.*, 2019).

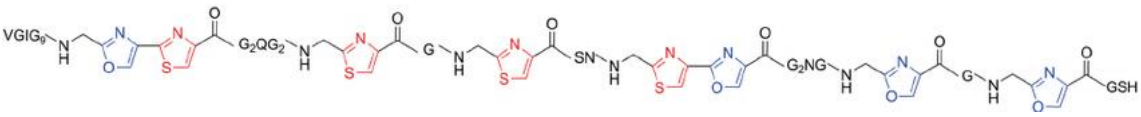

Figure 12. Microcin B17 molecule. The 3.1 kDa peptide contains four Thiazole (red) and four oxazole rings (blue)

2.4.2.3. Simocyclinones

Even though having some similarities to classical aminocoumarins mentioned above, simocyclinones does not have a similar binding site and inhibition mechanism. Simocyclinone D8 binds to GyrA subunit at a DNA-binding site and prevents interaction of enzyme with DNA (**Figure 13**) (Edwards *et al.*, 2009; Hearnshaw *et al.*, 2014). Its inhibition activities due to reduction of the binding of gyrase substrate.

Those hybrid molecules were first isolated from the mycelium extract of *Streptomyces antibioticus* Tü 6040 (Schimana *et al.*, 2000). Simocyclinone D8 was shown to be the main variant of antibiotic to be produced during fermentation (Theobald, Schimana and Fiedler, 2000; Schimana *et al.*, 2001; Trefzer *et al.*, 2002). It was shown to have weak antibacterial properties mostly against Gram-positive bacteria (Schimana *et al.*, 2000). It was shown that most laboratory Gram-negative strains are resistant to Simocyclinone D8. However clinical isolates of Gram-negative strains were susceptible for its antibacterial activity (Richter *et al.*, 2010). Simocyclinone D8 was shown to inhibit both *E. coli* and *S. aureus* gyrases, being not effective in inhibiting topoisomerase IV (Oppegard *et al.*, 2009). It was also demonstrated that simocyclinone D8 has cytotoxic effect on human cells and human topoisomerase II was shown to be its target (Sadiq *et al.*, 2010).

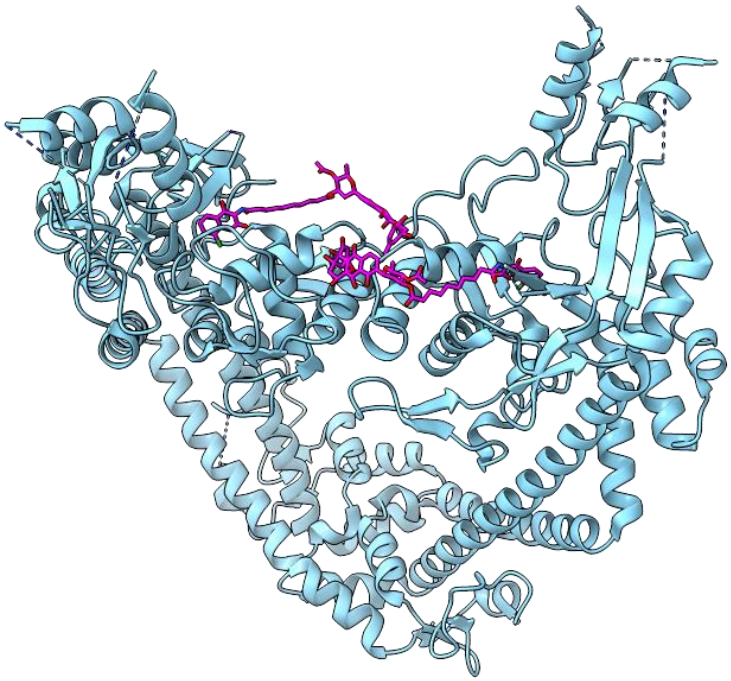

Figure 13. Binding of simocyclinone D8 to N-terminal domain of *E. coli* DNA gyrase A subunit dimer (PDB:4CKL). The simocyclinone D8 molecule is coloured violet. GyrA subunits are blue.

2.4.2.4. Aminocoumarins

Aminocoumarins inhibition activity is due to competitive inhibition of the ATPase reaction performed by the GyrB subunit (Mizuuchi, O'Dea and Gellert, 1978; Sugino and Cozzarelli, 1980). DNA gyrase has been shown to be the main target of aminocoumarin antibiotics. The GyrB GHKL binding site of novobiocin, a representative of aminocoumarins, has been structurally characterised. The molecule's binding site overlaps with the ATP binding site. The aminocoumarins have not been successful in clinical use due to their low solubility and issues if toxicity to eukaryotic cells.

2.4.2.5. Novel bacterial type II topoisomerase inhibitors

The rapid increase of resistance towards known type II topoisomerase inhibitors such as fluoroquinolones has resulted in a need for new antibacterials. As a result, the novel bacterial type II topoisomerase inhibitors (NBTIs) have been developed (**Figure 14 A**). NBTIs were discovered in SmithKline Beecham during trails to produce gepotidacin (O'riordan *et al.*, 2017). Those drugs do not have a single chemical scaffold however they have some features in common. (Surivet *et al.*, 2013).

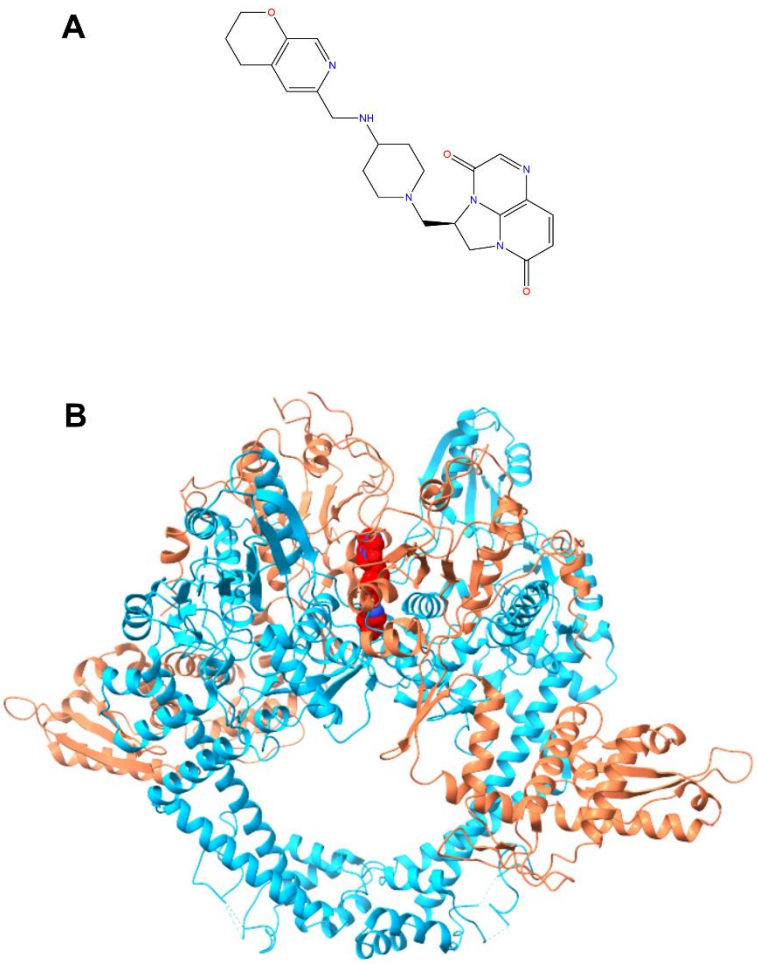

Figure 14. (A) Structure of gepotidacin molecule. (B) Binding of gepotidacin to *E. coli* gyrase (PDB:6RKW). gepotidacin molecule is presented as red spheres. GyrA is coloured light blue, GyrB is coloured coral

Gepotidacin is the first representative of triazaacenaphthylene NBTIs (Gibson *et al.*, 2019). The drug successfully went through phase II trials for the treatment of acute bacterial skin/skin structure infections and for the treatment of uncomplicated urogenital gonorrhoea (O'riordan *et al.*, 2017; Taylor *et al.*, 2018). Gepotidacin shows high activity against methicillin resistant *Staphylococcus aureus* and fluoroquinolone-resistant bacteria (Biedenbach *et al.*, 2016). It was shown that the compound is a potent inhibitor of Staphylococcus *aureus* gyrase supercoiling activity *in vitro* ($IC_{50} \approx 0.047$ μM). It was also able to inhibit gyrase mediated relaxation of supercoiled substrates. (IC50 ≈ 0.6 μM). Gepotidacin can be termed as gyrase poison because of the fact that it stabilises the cleavage complex. In contrast to fluoroquinolones, gepotidacin induced high levels of gyrase-mediated single-stranded breaks. Surprisingly gepotidacin was shown to supress the formation of double-stranded breaks. Structural data for *S. aureus* core fusion gyrase shows that gepotidacin bounds half-way between the two scissile DNA bonds and in a

pocket between the two GyrA subunits (**Figure 14 B**) (Gibson *et al.*, 2019). It is worth to mention that gepotidacin was used to obtain first-ever cryo-EM structure of gyrase complex (Vanden Broeck *et al.*, 2019).

2.4.2.6. CcdB

CcdB is a proteinaceous gyrase inhibitor which is a part of (CcdA/CcdB) Type II toxin-antitoxin system. The system controls the copy number of F plasmid (Miki, Chang and Horiuchi, 1984; Miki *et al.*, 1992). CcdB is a gyrase targeting toxin inactivated by CcdA. CcdB kills bacteria by a similar mechanism to quinolones (i.e., cleavage complex stabilisation). However, the interaction of CcdB with gyrase is different. CcdB binds in the dimer cavity of GyrA between the subunits. The role of R462 of GyrA (*E. coli*) in CcdB has been proved for the binding of the toxin for the enzyme by structural and biochemical experiments. CcdB dimer is able to bind DNA gyrase when the enzyme is in the DNA gate-open conformation (Smith and Maxwell, 2006). The protein requires nucleotide for its activity making its mechanism of action different to quinolone where the nucleotide is not necessary for binding.

2.5. Gyrase resistance mechanisms

As shown above, DNA gyrase is a target of many molecules that can disturb the enzyme activity. Bacterial cells have developed various mechanisms to prevent gyrase from the toxic action of the molecules. The resistance mechanisms of DNA gyrase include all of the AMR resistance types mentioned in section 2.2. The resistance mechanisms against gyrase targeting compounds mentioned in the previous section will be presented in this section. Schematic representation of resistance mechanism is shown on **Figure 15**.

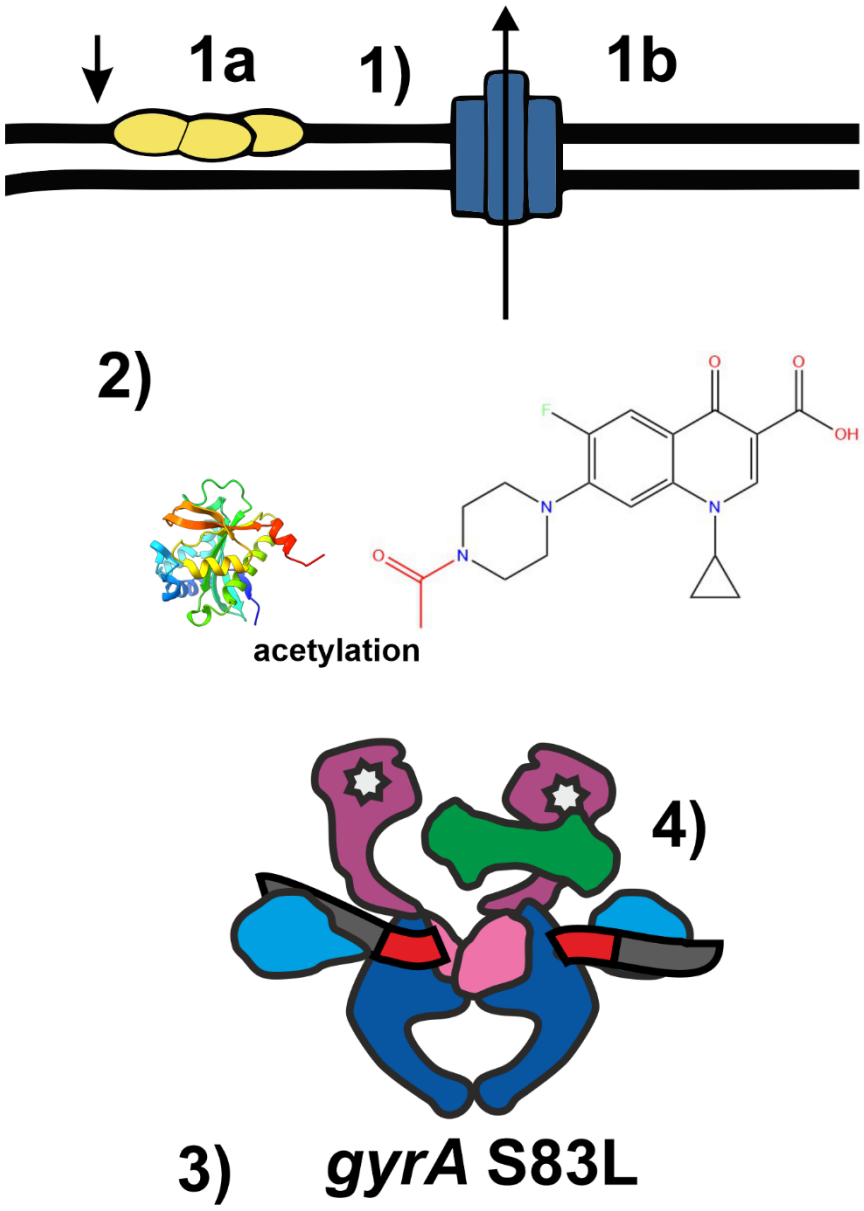

Figure 15. Schematic representation of gyrase targeting drugs resistance mechanisms. 1). Prevention of drug accumulation inside cell: 1a: down expression of porins, 1b: expression of efflux pumps. 2) Enzymatic inactivation of drug – acetylation of ciprofloxacin by aac (6′)-Ib. 3). Mutations of drug target -gyrase. 4) Interaction with drug target – gyrase interacting proteins.

2.5.1. Prevention of the drug entry and drug removal from the cell

The MarA gene (transcriptional activator found in gram negative bacteria) has been shown to block the translation of the OmpF gene and activates the expression of the porin down regulator OmpX which leads to reduced expression of porins OmpC, OmpD, OmpF, LamB and Tsx which has been linked to increased resistance to quinolones. The quinolone entrance to the cell can also be blocked by the changes in the structure and composition of LPS of the bacterial membrane (Correia *et al.*, 2017). The uptake of the drug can also be regulated by the mutations in porin genes. Tsx porin single amino acid

mutation has been shown to confer albicidin resistance in *E. coli* cells (Birch, Pemberton and Basnayake, 1990). Recently it was shown that inner membrane transporter SbmA mutations influence the uptake of the Microcin B17 conferring resistance on the cells (Ghilarov *et al.*, 2021).

Efflux pumps plays a significant role in gyrase targeting toxin resistance. The increased expression of those leads to removal of drug from the cell conferring to resistance. The *E. coli* AcrAB-TolC pump is major efflux pump conferring to resistance to various antimicrobials including ciprofloxacin. Quinolone resistance mutations often results in overexpression of AcrAB-TolC pump together with down-regulation of expression of above mentioned porin genes. Other pumps responsible for quinolone resistance are OqxAB and QepA. They are both plasmid mediated quinolone resistance factors (PMQR). QepA is responsible for resistance of ciprofloxacin and norfloxacin and often found on plasmids together with genes responsible for resistance for other antimicrobials such as aminoglycosides (Yamane *et al.*, 2007). OqxAB pump has wider substrate specificity. It is able to interact with chloramphenicol, trimethoprim, and quinolones such as ciprofloxacin, norfloxacin, and nalidixic acid. *OqxAB* gene was found in 39 % precent of isolates bearing resistance transmittable plasmids. The gene encoding the pump is very often found on chromosomal DNA of *K. pneumoniae* isolates which shows that resistance genes are mobile. Since the gene is usually flanked by insertion sequences it has been suggested that the mobilisation was achieved through a composite transposon (Hong *et al.*, 2009).

The efflux pump A DHA14 found in albicidin biosynthesis gene cluster is responsible for conferring specific resistance towards albicidin. It is for the self-protection mechanism of the albicidin producer *Xanthomonas albilineans* This pump is not similar to the multidrug resistance pumps, being specific towards polyketide containing antibiotics (Bostock *et al.*, 2006). Similarly, genes *mcbE* and *mcbF* encoded in the microcin b17 synthesis cluster also encodes the efflux pump responsible for MccB17 resistance. McbE has been suggested to be an integral membrane protein that associates with McbF, which is thought to be a nucleotide-binding protein. The McbE/F complex serves as a self-immunity mechanism for MccB17 producing cells (Garrido *et al.*, 1988).

The Simocyclinone D8 synthesis cluster also contains two genes that encode the efflux pump *simX*. The expression of simX is under the control of SimR, a member of the TetR

family of transcriptional regulators. *SimR* represses *simX* transcription. The expression of simX is regulated by Simocyclinone D8. Simocyclinone abolishes DNA binding by *SimR*, inducing expression of the SimX efflux pump which removes the drug from the producer cell providing the immunity (Le *et al.*, 2009).

2.5.2. Inactivation of the drug

Aminoglycoside acetyltransferase, aac (6′)-Ib is an enzyme which is responsible for acetylation of different antibiotics including quinolones. Enzymatic acetylation of antibiotics leads to its inactivation. It is another example of PMQR. It confers only modest resistance for quinolones but similarly to the abovementioned quinolone efflux pumps can give evolutionary advantage to gain further resistance (Robicsek *et al.*, 2006).

The albicidin resistance factor AlbD from gram negative bacterium *Pantoea dispersa* is a hydrolase that confers resistance to albicidin. The protein is an endopeptidase that cleaves the albicidin molecule at the central amide bond of the molecule. (Vieweg *et al.*, 2015).

Another mechanism of albicidin resistance is based on physical inactivation of the drug inside the cell. AlbA is a MerR-like (Mercury Resistance) albicidin binding protein. AlbA shows nanomolar activity of binding of albicidin and is able to bind different structural variations of the compound. Its expression confers high resistance to albicidin in various bacterial species. The protein binds the compound preventing its interaction with DNA gyrase (Rostock *et al.*, 2018).

2.5.3. Resistance mutations of gyrase

Quinolones because of their spectrum of activity, bioavailability, potency and safety profile were extensively used in clinical applications. Unfortunately, widespread usage of antibiotics very often goes hand in hand with the rise of resistance. Rapid growth of quinolone resistance clinical isolates was observed in the 2001-2006 period. In some countries a five-fold increase was observed (Kim and Hooper, 2014). In Poland 65% of invasive *Klebsiella pneumoniae* isolates of inpatients collected in 2020 were resistant to all clinically used quinolones (*OneHealthTrust. ResistanceMap: Antibiotic Resistance of Klebsiella pneumoniae in Poland*, 2021).

Target-associated resistance mutations for quinolones are often found in regions known as the quinolone resistance-determining region (QRDR located between positions 67-106 in GyrA and 63-102 in ParC (Yoshida *et al.*, 1990). The most common site of mutation in GyrA of *E. coli* is at S83 followed by D87. The alterations S83L and D87G/N/Y are most frequently found in resistant mutants (Bhatnagar and Wong, 2019). Those mutations disrupt the binding of quinolone molecules since residues S83 and D87 are key residues responsible for binding the drug. The mutation to hydrophobic residue prevents the formation of the water ion bridge important for quinolone binding.

There is also QRDR located in GyrB and ParE is located between positions 426-447 and 420-441 respectively (Yoshida *et al.*, 1991; Gensberg, Jin and Piddock, 1995; Heddle and Maxwell, 2002; Avalos *et al.*, 2015). However, GyrA mutations are more often responsible for quinolone resistance. Mutations outside QRDR has also been reported (Friedman, Lu and Drlica, 2001)

Point mutation W751R in *E. coli gyrB* was shown to be responsible for microcin resistance in microcin producing *E. coli*. (Vizan *et al.*, 1991). The position was further studied for different substitutions. Replacement with histidine or arginine resulted in only low resistance to MccB17 whereas substitution by glutamic acid or glycine shown a level of resistance comparable to W751R. Interestingly, substitution with lysine offered higher protection than W751R. Those mutations alter DNA gyrase activity. Only substitutions with arginine and phenylalanine offered protection without hampering gyrase activity. Deletion of W751 results in an inactive gyrase complex (Del Castillo, Del Castillo and Moreno, 2001). What is also important: GyrB W751R variant shows no resistance to quinolones (Metelev *et al.*, 2013).

Because of similarity between MccB17 and quinolone action it was hypothesised that quinolone resistant strains will also be resistant to microcin. It was shown that quinolone-resistant gyrase mutants GyrB K447E and GyrA S83W confers resistance to MccB17-induced gyrase cleavage *in vitro* (Heddle *et al.*, 2001).

Simocyclinones have slightly different mode of binding compared to aminocoumarins. Resistance mutations are also located in different positions. Structural studies revealed specific mutations in the aminocoumarin-binding pocket and polyketide- binding pocket. Due to the proximity of the quinolone binding site, some mutations that offer quinolone resistance are also responsible for simocyclinone susceptibility (Edwards *et al.*, 2009).

The Aminocoumarin-binding site overlaps with the ATP binding site. Due to this fact point mutations which offer resistance are limited to positions that do not significantly affect the activity of the enzyme. Several mutations of *E. coli* DNA gyrase have been shown to offer a resistance to aminocoumarin activity. The most common naturally occurring is Arg136. This residue contacts the aminocoumarin ring and is essential for drug binding (Confreres and Maxwell, 1992). Also, several resistant mutants of ParE and GyrB of *Staphyloccocus aureus* have been isolated. All of the positions are located in the Aminocoumarin-binding site (Fujimoto-Nakamura *et al.*, 2005).

D83 and M121 positions in S. aureus GyrA are the most commonly found NBTI resistance mutations. The amino acids are located in NBTIs binding site and their mutations impair binding of the molecule to the enzyme. S84 which is a residue responsible for quinolone resistance was also shown to confer resistance to NBTIs. It is worth mentioning that the speed of accumulation of NBTI resistance mutations by clinical strains is significantly slower compared to quinolone resistance mutations (Lahiri *et al.*, 2015).

2.5.4. Interaction with the antimicrobial target – gyrase interacting proteins

The resistance mechanism could be also based on the interaction with the antimicrobial target. Many molecules stabilise the DNA gyrase cleavage complex. To overcome this toxicity bacteria developed proteins that interact with the toxic conformation leading to resistance for cleavage stabilising agents.

The first representative of a gene encoding this type of resistance was isolated from *K. pneumoniae strain* bearing pMG252 plasmid. The strain was showing increased resistance towards quinolones. The effect was also observed when the plasmid was transferred to *E. coli*. The 657 bp gene responsible for quinolone resistance phenotype was isolated and termed *qnr* (quinolone resistance) (Martínez-martínez, Pascual and Jacoby, 1998). Later the protein was termed QnrA (Tran and Jacoby, 2002). Different variants of QnrA proteins were later reported (QnrA2, QnrA3, QnrA4, QnrA5). The proteins differ from each other by a few amino acids and confer a similar level of resistance (Poirel, Rodriguez-Martinez, *et al.*, 2005). Further search for plasmids responsible for transmissible quinolone resistance have led to discovery of four additional proteins QnrS (Hata *et al.*, 2005) ,QnrB (Jacoby *et al.*, 2006), QnrC (Wang *et al.*, 2009),

and QnrD (Cavaco *et al.*, 2009). *Qnr* genes are the third member of PMQR factors after the efflux pumps and inactivation enzymes mentioned above.

Qnr plasmids provide only a moderate level of protection against quinolones. But this partial resistance can allow the development of full resistance to quinolone drugs via acquirement of subsequent chromosomal mutations or efflux pumps (Strahilevitz *et al.*, 2009). Together with the fact that *qnr* genes are mobile makes them a serious clinical problem in hospital environment.

Due to contribution to increase of MIC, *qnr* genes may lead to decreased therapeutic efficacy of quinolones (Drlica and Zhao, 2007). It has been demonstrated that clinical strain of *K. pneumoniae* carrying *qnrA* plasmid that was lacking porins OmpK35 and OmpK36 had an active efflux system for quinolones and carried a resistance mutation in *gyrA*. Those factors have strengthened the effect of qnrA1 gene to the maximum (Rodríguez-Martínez, Pichardo, *et al.*, 2008).

Genes homologous to qnr are found in γ-*Proteobacteria*, *Firmicutes*, and *Actinomycetales*, including species of *Bacillus, Enterococcus, Listeria,* and *Mycobacteria and* anaerobes such as *Clostridium difficile* and *C. perfringens* (Arsène and Leclercq, 2007; Rodríguez-Martínez, Velasco, *et al.*, 2008; Sánchez *et al.*, 2008; Jacoby and Hooper, 2013). The presence of qnr homologous genes are strongly manifested in Aquatic bacteria species like *Aeromonas, Photobacterium, Shewanella,* and *Vibrio* (Poirel, Liard, *et al.*, 2005; Poirel, Rodriguez-Martinez, *et al.*, 2005; Poirel, Cattoir and Nordmann, 2012). The ubiquitous presence of qnr suggests that the origin of the gene is not correlated with quinolone introduction. The *qnrB* genes and pseudogenes have been identified in samples of *Citrobacter freundii* collected in the 1930s (Saga *et al.*, 2013). This fact clearly shows that the origin of *qnr* genes could not be linked to introduction of quinolone drugs. It has been shown that *qnr* genes in *Vibrio* species contribute to adaptation to environmental stress. This involves response to cold shock and bile salts. The Qnr appear to have a role in the presence of stresses that may trigger changes in DNA supercoiling and DNA damage (Gil-Marqués, Jacoby and Hooper, 2021)

Qnr genes belong to a larger group known as pentapeptide repeat proteins (PRP). As the name suggests, PRPs are composed of repeating units of 5 amino acids with the current consensus being (A/C/S/V/T/L/I)/(D/N/S/K/E/I/R)/(L/F)/(S/T/R/E/Q/K/V/D)/(G/D/E/N/R/Q/K) (Zhang,

Ni and Kennedy, 2019). The PRP family consists of a variety of proteins that have a PRP fold. Very often the proteins are not functionally and evolutionary connected. They can be grouped into six main groups (Zhang and Kennedy, 2021):

- heterocyst glycolipid synthesis related
- manganese uptake related
- Topoisomerase acting PRP (TA-PRP)
- Ubiquitin E3 ligases
- Synaptic Vesicle Glycoprotein 2 receptors
- Plant and cyanobacteria proteins

This thesis will discuss the TA-PRP and the term PRP would be used to describe topoisomerase acting part members of the family.

TA-PRP structure can be described with a few main features. All of them are characterized by a right-handed quadrilateral beta helix. The helix gives them their square cross section. Each of the four faces are composed of five amino acids. The central amino acid is termed i, with the preceding two amino acids being i^{-2} and i^{-1} and the following two amino acids as $i^{+1}$and i^{+2}. The side chains of residues i and i^{-2} typically form the hydrophobic core of the structure while the side chains of the remaining three residues are part of the exterior (Hegde *et al.*, 2005; Vetting *et al.*, 2006). A 360° coil is made from four pentapeptide faces. Typically, the N- and C- termini of PRPs lie at the opposite ends of stacked coils. PRPs that exist as dimers in solution have C-terminal "dimerization domains" which consist of an alpha helix sandwiched between two beta strands. PRPs that target topoisomerases and for which high-resolution structures have been reported are all dimers. Some PRPs (like Qnr) possess loops protruding outside from the main core of the protein. The structure of QnrB1 as a representative of TA-PRP protein is depicted on **Figure 16 A**.

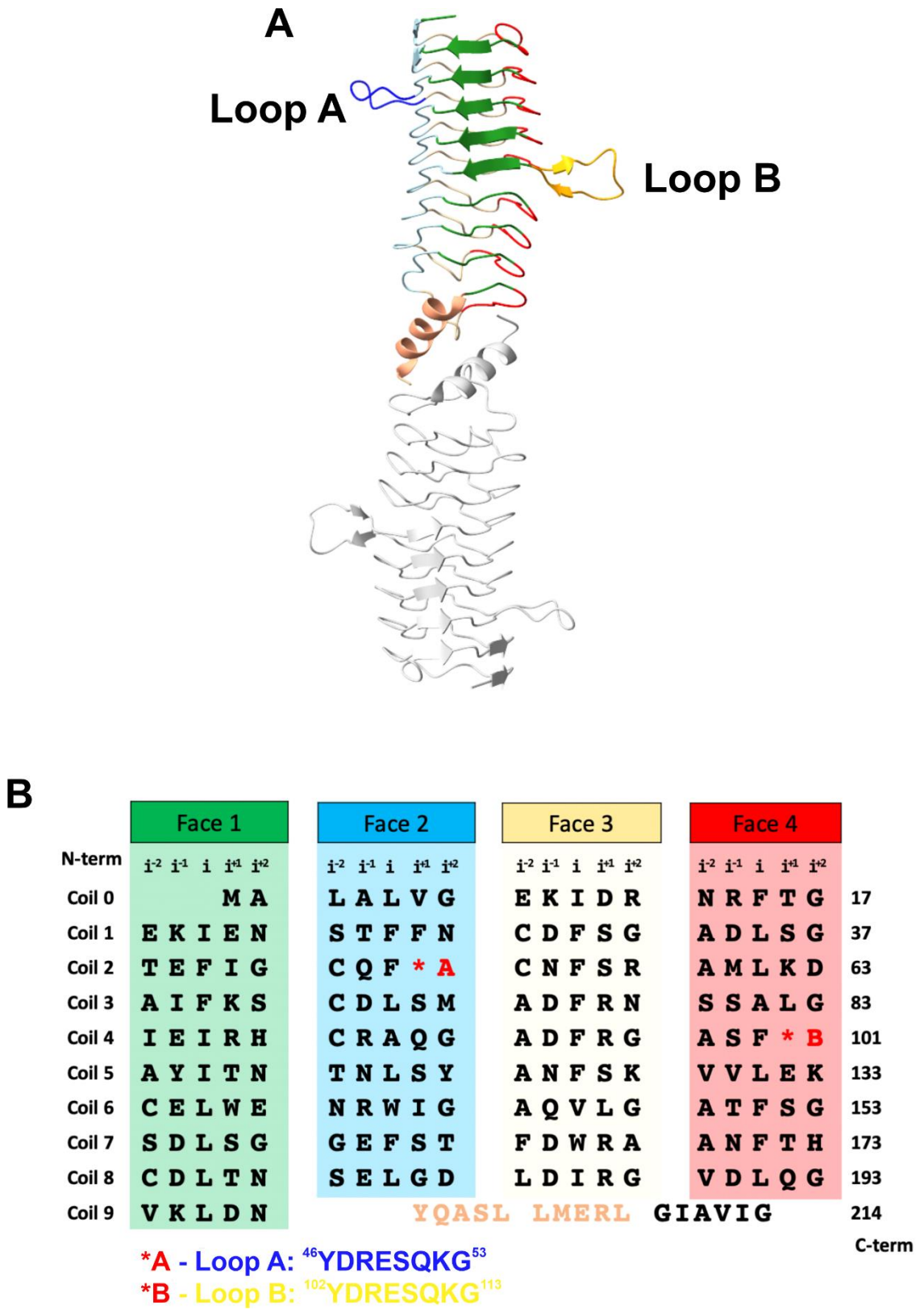

Figure 16. (A) The structure of QnrB1, a typical TA-PRP, is shown (PDB:2XTW). Loop A is coloured blue, loop B is coloured yellow. Alpha helix dimerization domain is coloured beige. The colours of PRP faces are same as in figure (B) QnrB1 PRP sequence diagram with the emphasis of faces formed by PRP motif.

The QnrA1 protein was shown to bind to DNA gyrase regardless of the presence of the quinolone. The protein was protecting the DNA gyrase supercoiling in *in vitro* setup. It was also established that PRP does not degrade the quinolone nor does it stimulate gyrase supercoiling by itself. QnrA1 did not protect topoisomerase IV against ciprofloxacin activity. (Tran and Jacoby, 2002). The protein was found to bind to GyrB and GyrA subunits as well as to the gyrase complex. QnrA1-DNA gyrase complexes were formed regardless the presence of DNA, ATP or CFX (Tran, Jacoby and Hooper, 2005a). Similar results were obtained for *E. coli* Topo IV (Tran, Jacoby and Hooper, 2005b)

The first structure for PRP was established for MfpA protein from *M. tuberculosis*. Before structural studies the protein encoded by the *mfpa* gene was show to confer only low level of resistance to ciprofloxacin and sparfloxacin in MIC assays (minimal inhibitory concentration) (4-8 fold) (Montero *et al.*, 2001) The PRP was shown to inhibit *E. coli* DNA gyrase in *in vitro* supercoiling assays and inhibit ATP-independent relaxation reactions (IC_{50} = 1.2 μM) (Hegde *et al.*, 2005).

QnrB1 is the only PMQR protein whose structure was experimentally determined. QnrB1 was identified originally in a *K. pneumoniae* ESBL strain from India. It has also been shown to be encoded in various multi-drug resistance plasmids. QnrB1 confers a moderate level of protection against quinolone drugs in an *in vivo* setup (8-16 fold) (Jacoby *et al.*, 2006). QnrB1 was reported to reverse ciprofloxacin inhibition of supercoiling activity of DNA gyrase in low concentrations (as low as 50 pM) and inhibit DNA gyrase supercoiling in higher concentrations (25 μM) (Jacoby *et al.*, 2006). The protein is 226-residues long and contains nine PRP coils composed of a mixture of type II and type IV β turns. Importantly, QnrB1 protein contains two loops: an 8-residue loop (Loop A: Y46-G53) in coil 2 connecting face 2 to face 3 and 12-residue loops (Loop B: S102–S113) projecting outward form from the corner between face 4 and face 1 joining coil 4 and coil 5) (**Figure 16 B**). As for all TA-PRPS, QnrB1 is a dimer with dimeric interface on the C-terminal end. The original crystal structure contains two dimers of a protein in the crystallographic asymmetric unit (Vetting, Hegde, Wang, *et al.*, 2011).

Recently, comprehensive studies of *Mycobacterium Smegmatis* MfpA was published. The protein was shown to inhibit negative supercoiling by *M. smegmatis* gyrase in the absence of fluoroquinolones. The protein decreased the level of quinolone induced DNA

cleavage and it was shown that the protective activity requires ATP hydrolysis. The structure of MsMfpA–MsGyrB47 complex has been determined (Feng *et al.*, 2021)

Another example of a genome encoded PRP conferring quinolone resistance is EfsQnr 3which was found in *Enterococcus faecalis.* The protein was shown to provide moderate resistance to quinolones. (Arsène and Leclercq, 2007). In *in vitro* assays EfsQnr was able to inhibit gyrase supercoiling activity. In the same time the relaxation activity of the enzyme was not impaired. EfsQnr protected the enzyme from ciprofloxacin inhibition. (Hegde *et al.*, 2011).

Other previously mentioned cleavage complex stabilising toxins, albicidin and Mccb17 also have the resistance factors among the TA-PRP group. The structures of TA-PRPs that has been extremally established has been depicted on **Figure 17**.

AlbG protein is located in the albicidin synthesis cluster. It has been shown to protect DNA gyrase from albicidin *in vitro*. Expression of the protein in *E. coli* cells conferred a 30-fold increase in resistance for albicidin in microbiological assays. AlbG was shown to inhibit DNA gyrase supercoiling activity in higher concentrations (IC_{50} = 6 μM) (Hashimi *et al.*, 2007). The structure of AlbG protein has been determined. Similarly, to QnrB1 and MfpA, AlbG folds into a right-handed quadrilateral β-helix with a dimer interface. AlbG possess one loop in its structure. Interestingly the loop deletion mutant of $AlbG_{\Delta 91–97}$ shown that the core structure of the protein was not disturbed regardless the deletion of the loop (Vetting, Hegde, Zhang, *et al.*, 2011).

McbG protein is located in a microcin B17 synthesis cluster. It was shown to provide resistance to microcin B17 for the producer strain. However, McbG resistance dependent mechanism is present together with an efflux pump-based mechanism (*mcbF* and *mcbE* genes). Interestingly, it was shown that McbG protein alone can provide immunity to microcin B17. This suggests that efflux pump mechanism and PRP based mechanism are complementary to each other (Garrido *et al.*, 1988). Unfortunately, so far no details of McbG mechanism are known nor the structure of the protein was experientially determined. There are also no reports of successful purification of the protein. The model established by AlphaPhold protein structure prediction based on neural network (Jumper *et al.*, 2021) shows that McbG does not possess well pronounced loop.

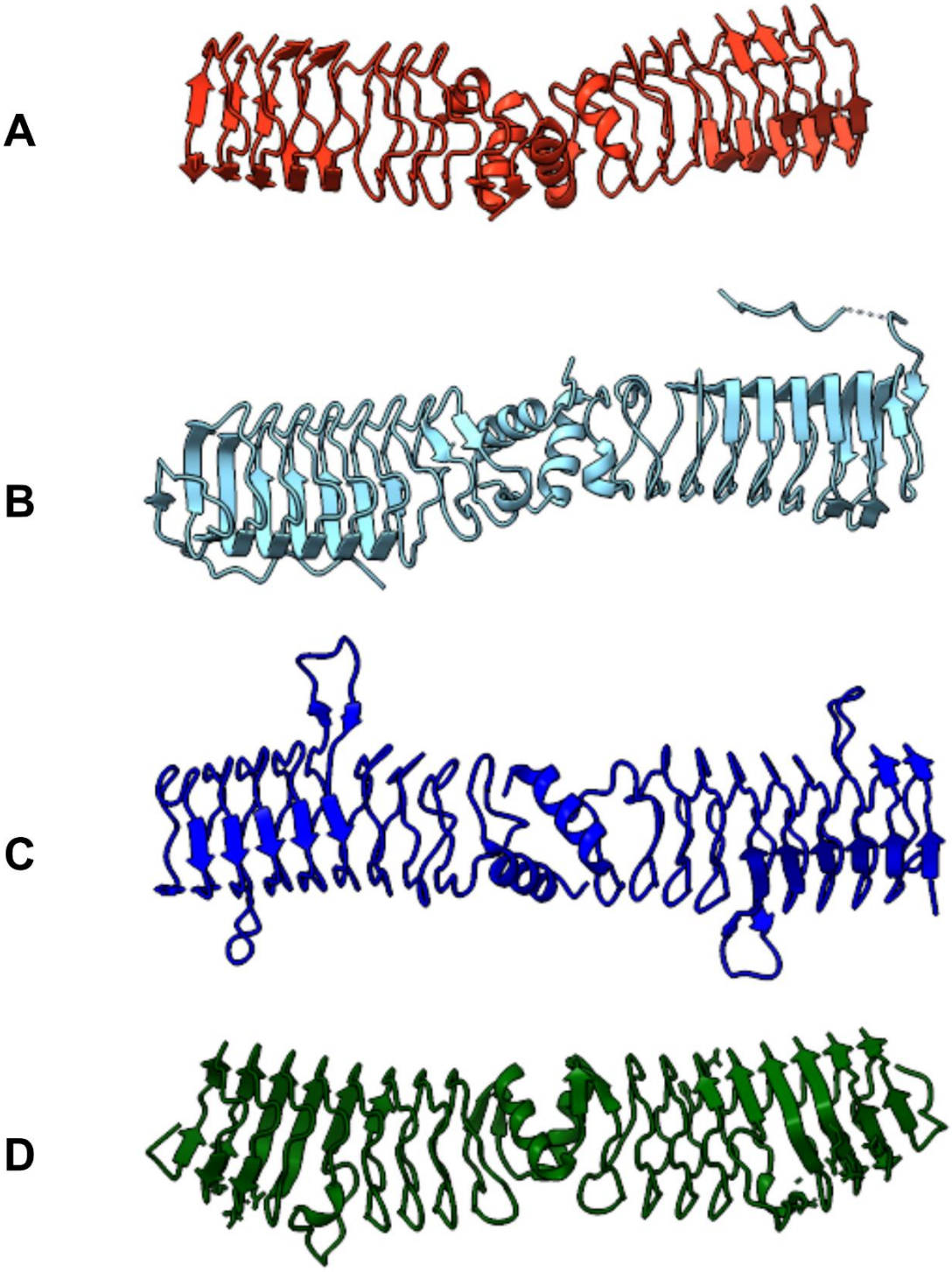

Figure 17. Structures of topoisomerase acting pentapeptide repeat proteins (A) MfpA from *Mycobacterium. Tuberculosis* (PDB:2bm4) (B) EfsQnr from *Enterococcus faecalis* (PDB:2W7Z) (C) QnrB1 from *Klebsiella Pneumoniae* (PDB:2XTW) *(*D) AlbG from *Xanthomonas albilineans* (PDB:2XT2).

There are three basic models of TA-PRP action. After the solving the structure of MfpA. Due to similar shape and charge distribution of PRP it was suggested that MfpA competes with dsDNA for binding to the region of the enzyme where DNA is bound and then

cleaved. In this model TA-PRPs mimic the G-segment and bind to the G-segment binding and cleavage site across the GyrA saddle. (Hegde *et al.*, 2005; Shah and Heddle, 2014). This model was supported by the fact that mutations of *gyrA* D87 of *M. Tuberculosis* gyrase prevented MfpA interaction with the enzyme. (Mérens *et al.*, 2009). This mutation was previously shown to increase DNA-gyrase binding stability (Barnard and Maxwell, 2001). The main unclear feature of the G-segment mimicry model is how the gyrase would be able to continue its supercoiling activity with no G-segment bound to the enzyme as the DNA competition would result in a drop or even abolition of supercoiling activity. Inhibition of supercoiling activity was observed in the case of *M. tuberculosis* MfpA and in the case of high concentrations of QnrB, EfsQnr and AlbG (Jacoby *et al.*, 2006; Hashimi *et al.*, 2007; Hegde *et al.*, 2011). However, these inhibitory concentrations for Qnr and EfsQnr and AlbG are significantly higher than those at EfsQnr which protection is observed. This suggested that the observed inhibition of TA-PRP is due to high non-physiological concentrations of the protein and does not explain the protective mechanism. This inhibition paradox makes the G-segment mimicry highly questionable.

A second mechanism was proposed for TA-PRPs to explain how protection against the action of FQ can be achieved without affecting supercoiling. It is suggested that rather than mimicking the initial bound state of DNA and competing for its binding site, the TA-PRPs recognize the quinolone-stabilized cleaved complex and interact with it. Interaction causes destabilization whereby the loss of quinolone from the binding site occurs. That allows the supercoiling reaction to proceed (Vetting, Hegde, Wang, *et al.*, 2011; Shah and Heddle, 2014).

In an alternative model for gyrase-targeting PRP, the protein also acts as a DNA mimic however it mimics the T-segment. In this model, TA-PRP is captured by the gyrase-DNA complex in which the G-segment is already bound. (Shah and Heddle, 2014). The authors of this model took into account the fact that some TA-PRPs possess loops. The loop (loop 2 of QnrB1 or AlbG loop) would be responsible for recognizing the conformation specific to the stabilised cleavage complex. This model also raises a question of the importance of the PRP loop for protection. The QnrB1 loop 2 has been established as necessary for protective activity (Jacoby *et al.*, 2013). This is problematic in context of the loopless PRP such as MfpA that would lack the part of the protein important for protection.

The T-segment mimicry model was recently buttressed by the structure and biochemical analysis of MfpA protein from *Mycobacterium Smegmatis.* The protein was found to be bound in the position where the T-segment would be located during passage after the N-gate of the enzyme. Additionally, the study shown that ATP hydrolysis is necessary for MfpA protective activity. The PRP itself was causing the stimulation of ATPase activity of DNA gyrase. The ATP seems to be needed for the enzyme to be "restarted" after releasing the cleavage complex stabilising drug. *M. Smegmatis* MfpA was not affecting relaxation reaction while being able to inhibit supercoiling. This is another observation that puts G-segment mimicry in question. If PRP would act as a G-segment mimic we should observe the inhibition of both relaxation and supercoiling.

While current data suggest a general role for T-segment mimicry, a universal model of TA-PRP activity is still lacking. Differences in observations obtained through the years suggests that maybe there is no one universal mechanism of action. Gathering more structural data about different cleavage stabilising toxins and TA-PRPs would add more input to the ongoing TA-PRP conundrum.

3. Aim of the study

The main aim of the study was to provide structural and biochemical information about the interactions between pentapeptide repeat proteins and *E. coli* DNA gyrase. The obtained data were used to try to explain the observed specificity of the inhibitory and protective action mediated by different PRPs. An updated model for pentapeptide repeat protein-mediated topoisomerase interaction with their targets was built based on the obtained results.

These goals were achieved via the following main objectives:

- Purification of QnrB1, AlbG and McbG proteins and their biochemical characterisation used to assess their ability to inhibit *E. coli* gyrase activity and/or rescue gyrase from fluoroquinolones and natural products (albicidin and microcin B17) in different conditions.
- Building and refinement of structural model of QnrB1-DNA-drug-gyrase complex using previously collected and processed cryo-EM data and introduction of structure-guided mutations

4. Materials and methods

The part of this chapter is based on the paper "Pentapeptide repeat protein QnrB1 requires ATP hydrolysis to rejuvenate poisoned gyrase complexes" (Mazurek *et al.*, 2021) containing methods used during QnrB1 experiments.

4.1. Materials

List of materials used in the study is presented in **Table 2**.

Table 2. List of materials used in the study.

Product	**Company**
20-12p-8 DNA	IDT
4–20% Mini-PROTEAN TGX Precast Protein Gels, 15-well, 15 µl	Bio-Rad
Acetic acid	Sigma
Acetonitrile for HPLC, gradient grade	VWR
Agarose	VWR
Alexa Fluor™ 488 5-TFP (Alexa Fluor™ 488 Carboxylic Acid, 2,3,5,6-Tetrafluorophenyl Ester), 5-isomer	Thermo
Ammonium sulphate	VWR
Ampicillin, Sodium Salt	Lab Empire
AMP-PNP	Merck
Boric acid	VWR
Bromophenol Blue	VWR
Calcium chloride	Sigma
Chloramphenicol	Lab Empire
Chloroform	Sigma
Ciprofloxacin	Sigma
Ciprofloxacin CIP 0.002-32 MIC Test Strips	Liofilchem
Deoxyribonuclease I from bovine pancreas	Sigma
Dithiothreitol	VWR
dNTP Mix (10 mM each)	Thermo Scientific
E. coli SPA-Tagged Collection; *gyrA*, *gyrB*	Dharmacon
EDTA	VWR
Ethanol 96%	VWR
Ethidium bromide solution	Sigma
FastDigest NcoI	Thermo Scientific
FastDigest *NcoI*	Thermo Scientific
FastDigest *NdeI*	Thermo Scientific
FastDigest XhoI	Thermo Scientific
FastDigest *XhoI*	Thermo Scientific
GeneJet Gel Extraction and DNA clean-up Micro kit	Thermo Scientific
Glycerol	VWR
Glycine	Lab Empire
Goat anti-Mouse IgG (H+L) Secondary Antibody, HRP-linked	Thermo Scientific
Hydrochloric acid	Sigma
Imidazole	VWR
Isoamyl alcohol	Sigma
Isopropyl β-D-1-thiogalactopyranoside	VWR
Kanamycin monosulfate	Lab Empire
L-Arginine, Hydrochloride	Sigma
LB Broth	Sigma
LB Broth with agar	Sigma

Methanol	VWR
Monoclonal ANTI-FLAG M2 antibody	Sigma
Monoclonal Anti-poly Histidine antibody	Sigma
Mueller Hinton Agar	Sigma
Mueller Hinton Broth	Sigma
Novobiocin	Sigma
Nuclease-Free Water (not DEPC-Treated)	Thermo Scientific
pBpa (H-p-Bz-Phe-OH)	Bachem
Phusion DNA Polymerase (2 U/µL); 5X Phusion HF Buffer (cat.	Thermo Scientific
Pierce ECL Western Blotting Substrate	Thermo Scientific
Pierce Protease Inhibitor Mini Tablets, EDTA-free	Thermo Scientific
PreScission Protease	Merck
PVDF Transfer Membrane	Thermo Scientific
Pyruvate Kinase/Lactic Dehydrogenase enzymes from rabbit muscle (PK/LDH)	Sigma
Sodium chloride	VWR
Sodium dodecyl sulfate (SDS), 20% Solution	Lab Empire
Sucrose	Sigma
T4 DNA Ligase (5 U/µL); 10X T4 DNA Ligase Buffer	Thermo Scientific
TEV Protease	Merck
Trifluoroacetic acid	VWR
Tris(Hydroxymethyl)aminomethane	VWR
Tween 20	VWR
Tycho NT.6 Capillaries	Nanotemper
β-Nicotinamide adenine dinucleotide, reduced disodium salt hydrate (NADH)	Merck

4.1.1. Laboratory equipment

List of laboratory equipment used in the study is presented in **Table 3**.

Table 3. List of laboratory equipment used during the study

Product	Company
AB104-S Analytical Balance	Mettler Toledo
ÅKTA Purifier 900 FPLC System	GE Healthcare
ChemiDoc XRS+ imaging system	Bio-Rad
Duomax 1030 Rocking Platform Shaker	Heidolph
Laboratory centrifuge 5424 R	Eppendorf
Laboratory incubator CLN 15	POL-EKO-APARATURA
LM-20 2UV (302nm/365nm) Benchtop UV Transilluminator	UVP
Mastercycler nexus X2	Eppendorf
MicroPulser Electroporator	Bio-Rad
Mini-PROTEAN Tetra Cell and PowerPac Universal Power Supply	Bio-Rad
Mini-Sub® Cell GT Cell	Bio-Rad
PB602-S Laboratory balance	Mettler Toledo
PIPETMAN Classic automatic pipets	Gilson
RF-6000 spectrofluorimeter	Shimadzu
Thermomixer comfort	Eppendorf
Trans-Blot Turbo Transfer System	Bio-Rad
WIZARD IR Infrared Vortex Mixer	VELP Scientifica
ZWYR-240 Premium orbital benchtop shaking incubator	Labwit

4.1.2. Bacterial strains

List of bacterial strains used in the study is presented in **Table 4.**

Table 4 List of Bacterial strains used in the study**.**

Strain/Company	Purpose
5α NEB	General cloning strain
Dharmacon SPA tag strains of DY330 *gyrA, gyrB* Dharmacon	*In vivo* crosslinking experiments
E. coli BL21(DE3) Gold	General expression strain
E. coli One Shot BL21 Star (DE3)	General expression strain
OverExpress C43(DE3) pLysS	McbG expression trials
E. coli Lemo21™ (DE3)	
Tuner (DE3) Competent Cells	
Vibrio natriegens Vmax competent cells	

4.1.3. List of buffers

List of buffers used for protein purification and subsequent experiments is presented in **Table 5**.

Table 5 List of buffers used for protein purification and subsequent experiments

Buffer	Composition
QnrB1 lysis buffer	50 mM Tris-Cl pH 8.0, 200 mM $(NH_4)_2SO_4$, 20 mM imidazole [pH 8.0], 10% glycerol
QnrB1 wash buffer	50 mM Tris-Cl pH 8.0, 200 mM $(NH_4)_2SO_4$, 50 mM imidazole [pH 8.0], 10% glycerol
QnrB1 elution buffer	50 mM Tris-Cl pH 8.0, 200 mM $(NH_4)_2SO_4$, 250 mM imidazole [pH 8.0], 10% glycerol,
TGED-Arg	50 mM Tris-HCl pH 7.5, 50 mM arginine hydrochloride [pH 7.5], 10% glycerol, 1 mM EDTA, 2 mM DTT
PRP SEC buffer	20 mM Tris pH 7.5, 50 mM NaCl, 50 mM arginine hydrochloride [pH 7.5], 5% glycerol, 2 mM DTT
AlbG lysis buffer	50 mM Tris-Cl pH 8.0, 20 mM imidazole, 300 mM NaCl, 5% glycerol
AlbG wash buffer	50 mM Tris-Cl pH 8.0, 300 mM NaCl, 50 mM imidazole [pH 8.0], 5 % glycerol
AlbG/McbG elution buffer	50 mM Tris-Cl pH 8.0, 300 mM NaCl, 250 mM imidazole [pH 8.0], 5% glycerol,
McbG His-Trap buffer	50 mM Tris-Cl pH 8.0, 0.1% Triton X-100, 300 mM NaCl, 10 mM imidazole [pH 8.0], 50 mM arginine hydrochloride [pH 7.5], 10% glycerol
McbG His-Trap wash	50 mM Tris-Cl 8,50 mM NaCl, 40 mM imidazole [pH 8.0] 50 mM arginine hydrochloride [pH 7.5], 5% glycerol
High-salt McbG wash buffer	50 mM Tris-Cl pH 8, 1 M NaCl, 20 mM imidazole, 50 mM arginine hydrochloride [pH 7.5], 5% glycerol
TGED	50 mM Tris-HCl pH 7.5, 10% glycerol, 1 mM EDTA, 2 mM DTT
Gyrase lysis buffer	20 mM Na-HEPES pH 8.0, 500 mM NaCl, 20mM imidazole [pH 8.0], 10% glycerol
STREP buffer	20 mM Na-HEPES pH 8.0, 60mM NaCl, 1 mM EDTA, 1 mM DTT, 10% glycerol

Gyr B47 lysis buffer	50 mM Tris-Cl pH 7.5, 150 mM NaCl, 20 mM imidazole, 10% glycerol
Gyrase assay buffer	35 mM Tris-Cl pH 7.5, 24 mM KCl, 4 mM $MgCl_2$, 2 mM DTT, 1.8 mM spermidine, 1 mM ATP, 6.5 % glycerol, 0.1 mg/ml albumin
STEB	20% sucrose, 50 mM Tris-Cl pH 8, 5 mM EDTA, 0.25 mg/ml bromophenol blue
EMSA buffer	30 mM Tris-Cl pH 7.5, 75 mM KCl, 6% glycerol, 2 mM $MgCl_2$, 1 mM DTT
Pull-down buffer	25 mM Tris-Cl pH 7.5, 5 mM $MgCl_2$, 50 mM KCl and 5% glycerol
Protein labelling buffer	25 mM Na-HEPES pH 7.0, 10% glycerol, 200 mM KCl and 1 mM TCEP
Fluorescence polarisation buffer	50 mM Tris-HCl, pH 7.5, 0.5 mM TCEP, 10 mM $MgCl_2$, 30 mM potassium glutamate, 5 % glycerol
TBM buffer	90 mM Tris-borate pH 7.5, 4 mM $MgCl_2$
cryo-EM buffer	25 mM Na-HEPES pH 8, 30 mM potassium acetate, 2.5 mM magnesium acetate, 0.5 mM TCEP

4.2. Methods

4.2.1. Bacterial cell transformation protocol

4.2.1.1. Transformation of chemo-competent *Escherichia coli*

An aliquot of 50 µl chemo-competent bacterial cells prepared according to the Inoue method (Green and Sambrook, 2020) was incubated with 50 ng of plasmid DNA for 20 minutes on ice. The cells were subsequently transferred to a heat block set for 42°C for 45 seconds and then cooled on ice for 1 minute. After addition of 1 ml of LB liquid medium the cells were further incubated for 90 minutes at 37 °C with shaking. The cells were plated on a LB plate with appropriate antibiotic and incubated overnight at 37°C.

4.2.1.2. Transformation of electrocompetent *Escherichia coli*

5 µl of electrocompetent cells prepared according to our standard laboratory protocol (Renzette, 2011) were mixed with 20 ng of plasmid DNA and transferred to an electroporation cuvette. Cells were electroporated using a 0.1 cm electroporation cuvette at a voltage of 1.8 kV for one pulse using BioRad Micropulser (typical pulse time being 5.5 ms). 1 ml LB liquid medium was immediately added after electroporation. The cells were then incubated for 90 minutes at 37 °C with shaking. The cells were plated on a LB plate with appropriate antibiotic and incubated overnight at 37°C.

4.2.2. Cloning procedures

The polymerase chain reaction (PCR) was used for sub-cloning of genes. The PCR reactions were carried out according to the Phusion DNA Polymerase (Thermo) manufacturer's guidelines. A typical 20 µl PCR reaction was run with 0.5 -1 µM of each primer, 1 ng of template DNA, 1 U of polymerase, 200 µM dNTPs (equimolar deoxynucleotide triphosphates, dGTP, dCTP, dATP and dTTP), 1 x PCR buffer and nuclease free water to the required volume. Reactions were incubated in a Mastercycler Nexus (Eppendorf) thermocycler. For all reactions, one PCR program was used, for which cycling conditions are listed in **Table 6**.

Table 6. Standard PCR program used in procedure gene cloning.

Reaction step	Temperature	Time [minuses]
Initial denaturation	98ºC	1:00
Denaturation	98ºC	0:30
Annealing	55ºC	0:30
Extension	72ºC	0:30/1000bp
Go to "Denaturation" step	30 x	
Final extension	72ºC	5:00

The products of PCR reactions were separated on 1% TAE agarose gels stained with Ethidium Bromide (EtBr). Samples were mixed with DNA loading buffer before loading on the gel. DNA fragments of appropriate size were excised from the gel and the DNA was isolated using a GeneJET Gel Extraction (Thermo) kit.

PCR products and vectors were digested for 2h at 37ºC. The compositions of both vector and insert digestion reactions are shown in **Table 7**.

Table 7 Standard digestion reactions composition.

Vector digestion		**DNA insert digestion**	
Component	**Volume**	**Component**	**Volume**
10X FD Green Buffer	4 µl	10X FD Buffer	2 µl
*Nco*I/*NdeI*-FD	2 µl	*NdeI* -FD	1 µl
*Xho*I-FD	2 µl	*Xho*I-FD	1 µl
vector	500 ng	DNA insert	100-200 ng
NF-H_2O	Up to 40 µl	NF-H_2O	Up to 20 µl
Total Volume:	**40 µl**	**Total Volume:**	**20 µl**

DNA ligations were conducted with 1 µl T4 DNA ligase (5 U) Units (Thermo) in a 10 µl reaction, as according to manufacturer's guidelines. After the reaction, *E. coli* 5α (NEB) chemical competent cells were transformed with ligation mixtures. Verification of insert cloning was performed by colony PCR of selected bacterial colonies. Positive colonies were inoculated in LB medium overnight and plasmids were isolated from obtained cultures using GeneJET Plasmid Miniprep Kit (Thermo) according to the protocol provided by the manufacturer. Sanger DNA sequencing of isolated constructs were performed by Eurofins. Lists of plasmids and primers used in the study are presented in supplementary tables **S1** and **S2**.

Site-directed mutagenesis was used to introduce mutations into the *qnrB1* gene. Mutations involved replacement of codon for single amino acids with the amber stop

codon – TAG, which is recognized by orthogonal suppressor tRNA to incorporate *p*Bpa (*para*-benzoyl-phenylalanine)

The overlap extension PCR method was used to introduce mutations by using mismatched primers (Higuchi, Krummel and Saiki, 1988). In this method, to introduce single-codon mutations, four different primers are used:

- forward and reverse primers complementary to the beginning and the end of the gene respectively,
- forward and reverse mutation-introducing primers complementary to the site where mutation is introduced except for the mismatch between template DNA and mutated codon.

The first round of PCR consisted of two concurrent reactions carried out on the same DNA template but with different primers:

1. *qnrB1* forward primer (For_qnrB1_NcoI_6xHis) and mutation-introducing reverse primer (e.g., Rev_Y123TAG)
2. Mutation-introducing forward primer (e.g., For_Y123TAG) and *qnrB1* reverse primer (Rev_qnrB1_XhoI_TAA).

After isolation of the products of these 2 reactions the second round of PCR was carried out. The products of the two previous reactions were mixed together in equal volumes (0.5 µl each) and two *qnrB1* gene primers (For_qnrB1_NcoI_6xHis and Rev_qnrB1_XhoI_TAA) were added to the reaction. The products of site-directed mutagenesis PCR were analysed on agarose gel and ligated into a pBAD vector as described above. Similarly, after plasmid isolation Sanger DNA sequencing of isolated constructs were performed by Eurofins.

4.2.3. MIC measurements

Minimal inhibitory concentrations of compounds were measured by broth microdilution in 96-well plates as described by the Clinical & Laboratory Standards Institute (Patel J.B., Cockerill R.F., Bradford A.P., Eliopoulos M.G., Hindler A.J., Jenkins G.S., Lewis S.J., Limbago B., Miller A.L., Nicolau P.D., Pwell M., Swenson M.J., Traczewski M.M., Turnidge J.D., 2015). *E. coli* BW25113 cultures transformed with appropriate plasmids were cultured in Mueller-Hinton Broth (MHB). 3-hour cultures were diluted to

correspond with the 0.5 McFarland standard. Series of 2-fold dilutions of drugs solutions prepared in MHB were dispensed on 96 well plate (50 µl per well). 50 µl 10-fold dilution of 0.5 McFarland bacterial cultures were then added to the drugs on the plate. Then the plate was incubated at 37°C overnight. The MIC was defined as the lowest concentration of drug where no significant bacterial growth was observed. Each experiment contained a sterility control as well as drug-free control. All measurements were performed as triplicates. The error is expressed by standard deviation of the mean.

4.2.4. QnrB1 protein purification

Plasmid pET28-QnrB1 containing the *qnrB1* open reading frame with a C-terminal hexa-histidine tag was transformed into BL21 (DE3) Gold cells. 3 L of TB liquid media supplemented with 30 µg/ml kanamycin were inoculated with 30 ml of starter overnight culture and incubated at 37°C with shaking to $OD_{600} = 0.8$. After induction with 500 µM IPTG the temperature was reduced to 24°C and the cultures were incubated overnight with shaking. Cells were harvested by centrifugation at 7000 g for 30 minutes at 4°C. Pellets were resuspended in QnrB1 lysis buffer (50 mM Tris-Cl pH 8.0, 200 mM $(NH_4)_2SO_4$, 10% glycerol, 20 mM imidazole) supplemented with protease inhibitors (Pierce). Resuspended cells were incubated for 30 minutes on ice with 1 mg/ml lysozyme with periodic mixing. Cells were lysed using a French press and lysate was cleared by centrifugation at 87 000 g for 30 minutes at 4°C. QnrB1 was purified by Ni-affinity chromatography (HisTrap HP 5 ml, Cytiva). The column was equilibrated with QnrB1 lysis buffer and after loading the lysate washed with 20 CVs of QnrB1 wash buffer. The fractions were eluted with an QnrB1 elution buffer (50 mM Tris-Cl pH 8.0, 200 mM $(NH_4)_2SO_4$, 10% glycerol, 250 mM imidazole). Fractions containing protein were pooled and dialysed overnight against buffer A-Arg (50 mM Tris-HCl pH 7.5, 50 mM arginine hydrochloride, 10% glycerol, 1 mM EDTA, 2 mM DTT) and loaded on a MonoQ HR 16/10 ion exchange column (Cytiva). Peak fractions eluted over a 0-1 M NaCl gradient were pooled, concentrated, and loaded onto a 10/300 Superdex S75 Increase column (Cytiva) previously equilibrated with PRP sec buffer. Peak fractions were concentrated, flash-frozen in liquid N_2 and stored at -80°C.

4.2.5. AlbG protein purification

Plasmid pET28-AlbG containing cloned *albG* gene with hexa-histidine N-terminal tag has been transformed into BL21 (DE3) Gold cells (Agilent). Plates were incubated overnight in 37°C. 3 L of LB media with kanamycin added to the final concentration of 30 μg/ml were inoculated with 30 ml of overnight culture prepared from a few colonies of transformed cells. The culture was incubated with shaking to OD_{600} = 0.6. Protein production was induced by adding 500 μM IPTG. The culture was incubated at 24°C overnight. Cells were collected by centrifugation at 7000 g for 30 minutes at 4°C. The obtained pellet was resuspended in AlbG lysis buffer, which was supplemented with protease inhibitors (Pierce). Obtained solution was incubated for 30 minutes on ice with mixing with 1 mg/ml lysozyme and 5 μg/ml deoxyribonuclease I. Avestin EmulsiFlex-C3 was used to lyse the cells. The lysate was cleared by centrifugation at 87 000 g for 45 minutes at 4°C. Supernatant was filtered and loaded on a 5 ml HP HisTrap column (Cytiva). The column was previously equilibrated with an AlbG lysis buffer. After loading, the column was washed with 100 ml of AlbG wash buffer. Protein was eluted using an AlbG elution buffer. Protein presence was checked using the Bradford method (Bradford, 1976). Fractions containing protein were pooled and dialysed overnight against the TGED buffer. The dialysate was loaded on HiTrap Q XL 5 ml ion exchange column (Cytiva). The column was washed with 10% stepwise gradient of TGED buffer with 1 M NaCl. AlbG protein eluted at 30% of TGED buffer with 1 M NaCl. Fractions were analysed on SDS-PAGE gel. Fractions containing AlbG protein were pooled and concentrated using 30 kDa cut off Amicon and loaded on a 10/300 Superdex S75 Increase SEC column (Cytiva) equilibrated with PRP sec buffer. After size exclusion chromatography peak fractions were collected, concentrated and frozen in liquid N_2. Protein was stored at -80°C.

4.2.6. McbG protein purification

4.2.6.1. Affinity chromatography followed by Ion-exchange

Cells were collected by centrifugation at 6500 g for 15 minutes at 4°C. Obtained pellet were resuspended in McbG His-Trap buffer, which was supplemented with protease inhibitors (Pierce). The Obtained solution was incubated for 30 minutes on ice with mixing with 1 mg/ml lysozyme and 5 μg/ml deoxyribonuclease I. Avestin EmulsiFlex-

C3 was used to lyse the cells. The lysate was cleared by centrifugation at 87 000 g for 45 minutes at 4°C. Supernatant was filtered and loaded on 5 ml HP HisTrap column (Cytiva). The column was previously equilibrated with the McbG His-Trap buffer. After loading, the column was washed with 100 ml of McbG His-Trap wash buffer and after with 100 ml of high-salt McbG wash buffer. Protein was eluted using McbG elution buffer. Protein presence was measured using the Bradford method. Collected fractions were inspected on SDS-PAGE gel. Fractions containing McbG protein were diluted and dialysed against theTGED buffer with 50 mM $(NH_4)_2SO_4$. Obtained dialysate was loaded on MonoQ HR 16/10 (Cytiva) ion exchange column pre-equilibrated with TGED buffer with 50 mM $(NH_4)_2SO_4$. The column was washed with a 10% stepwise gradient of TGED buffer with 1M NaCl. McbG protein was eluted at 30% of TGED buffer with 1M NaCl. Fractions were analysed on SDS-PAGE gel. Fractions containing McbG protein were pooled and concentrated using 30 kDa cut off Amicon and loaded on a 10/300 Superdex S75 Increase SEC column (Cytiva) equilibrated with PRP SEC buffer. After size exclusion chromatography peak fractions were collected, concentrated and frozen in liquid N_2. Protein was stored in -80°C.

4.2.6.2. Hydrophobic interaction (HIC) chromatography

The HP HisTrap column purification was performed as described in the Ion-exchange section (see above). Fractions containing protein were pooled and dialysed overnight against TGED buffer with 50 mM L-Arg-Cl and 500 mM $(NH_4)_2SO_4$. After dialysis concentration of $(NH4)_2SO_4$ was adjusted to 1.5 M and the dialysate was loaded on HiTrap Phenyl Sepharose (high-sub) column (Cytiva). The column was washed with 10 CV of TGED 50 mM Arg-Cl buffer with 1.5 M $(NH4)_2SO_4$. Gradient of decreasing salt 1.5-0 M was performed over 200 ml. Fractions were collected and inspected on SDS-PAGE gels. Fractions containing the protein of interest were pooled and loaded on a HiTrap Heparin HP 5 ml column (Cytiva) preequilibrated in TGED 50 mM L-Arg-Cl. A stepwise gradient with increasing salt concentration (0.1-1 M) was performed. Fractions were collected and inspected on SDS-PAGE gel. Fractions containing McbG protein were collected and dialysed overnight against TGED with 200 mM $(NH_4)_2SO_4$. After dialysis protein was stored at -80°C.

4.2.7. Purification of QnrB1 *para*-benzoyl-phenylalanine (*p*Bpa) mutants

BL21 Star (DE3) cells (Thermo) were transformed with plasmids pBAD-*qnrB1[x]pBpa,* carrying *qnrB1* amber gene with N-terminal hexa-histidine tag and pEVOL-*p*Bpa plasmid (Young *et al.*, 2010) (carrying tRNA synthetase/tRNA pair for incorporation of a photoactive non-canonical amino acid, p-benzoyl-l-phenylalanine). Plates were incubated in 37°C overnight. 100 ml of LB media supplemented with 30 μg/ml kanamycin and 100 μg/ml ampicillin was inoculated with 1:100 ratio of overnight culture set from colonies obtained in a procedure described above. The culture was incubated at 37°C with shaking till it reached OD_{600} = 0.3. At this moment *para*-benzoyl-phenylalanine (*p*Bpa) was added to final concentration of 1 mM. Incubation was continued till OD_{600} reached 0.6. Subsequently, cells were induced by adding arabinose to 10 mM final concentration. The culture was then continued for 6 h at 37 °C. The cells were collected by centrifugation at 8500g for 30 minutes at 4°C. Obtained pellets were resuspended in QnrB1 lysis buffer supplemented with protease inhibitors (Pierce). Obtained solution was incubated for 30 minutes on ice with mixing with 1 mg/ml lysozyme and 5 μg/ml deoxyribonuclease I. Avestin EmulsiFlex-C3 was used to lyse the cells. The lysate was cleared by centrifugation at 87 000 g for 45 minutes at 4°C. Supernatant was filtered and loaded on 5 ml HP HisTrap column (Cytiva). The column was previously equilibrated with QnrB1 lysis buffer. After loading, the column was washed with 100 ml of QnrB1 wash buffer. Protein was eluted using QnrB1 elution buffer. Protein presence was checked using Bradford method. Fractions containing protein were subsequently pooled and the buffer was exchanged using PD-10 Desalting Columns (Cytiva) preequilibrated with QnrB1 storage buffer. Samples were concentrated to desired concentration, snap-frozen in liquid N_2 and stored at -80°C.

4.2.8. Purification of gyrase-targeting toxins

Microcin B17 was obtained according to the procedure described before (Metelev *et al.*, 2013). Briefly, *Escherichia coli* BW25113 cells were transformed with pBAD-*mcbABCDEFG*. Obtained cells were cultured in 2 L of 2xYT media until OD_{600} = 0.7, induced with 10 mM arabinose and left overnight at 37°C with shaking. The cells were collected by centrifugation at 8500 g for 30 minutes at 4°C resuspended in 100 mM acetic acid/1 mM EDTA (*ethylenediaminetetraacetic acid)* solution and lysed by boiling for 10 min in a water bath. The obtained lysate was clarified by centrifugation at 12 000g for 40

minutes and loaded on to BondElute 10 g C18 cartridge (Agilent), equilibrated with 0.1% TFA. The cartridge was extensively washed first with 20 CV 0.1% TFA, then with 20 CV of 10% MeCN in 0.1% TFA. Elution was performed using 30% MeCN in 0.1% TFA. The eluate was vacuum dried, dissolved in 10% DMSO and further purified by HPLC using COSMOSIL 5C18-MS-II 120Å 5µm, 10.0x 150 mm column. The column was equilibrated in 0.1% TFA. The bound material was eluted with a linear gradient of acetonitrile in 0.1% TFA (from 0 to 50% acetonitrile in 30 min).
Albicidin was produced using a total synthesis approach was a gift from Prof. Roderich Süssmuth (Berlin Institute of Technology) (Kretz *et al.*, 2015).

4.2.9. Purification of gyrase subunits and domains

Plasmids pET28b GyrA/B Twin-tag bearing appropriate gyrase subunits genes with cleavable N-terminally deca-His-tag and C-terminally Twin-Strep-tag (Vanden Broeck *et al.*, 2019) were transformed into BL21 (DE3) Gold cells (Agilent). Plates were incubated according to the previously described procedure. 2 L of TB culture supplemented with 100 µg/ml kanamycin for each gyrase subunit was prepared from overnight culture from obtained cells. Cells were cultured at 37°C with shaking until OD_{600} reached 0.75, when they were induced with 500 µM IPTG and incubated for an extra 4 h at 37°C with shaking. Cells were harvested as described for other proteins. Pellets were resuspended in Gyrase lysis buffer which was supplemented with protease inhibitors (Pierce). Obtained solution was incubated for 30 minutes on ice with mixing with 1 mg/ml lysozyme and 5 µg/ml deoxyribonuclease I. EmulsiFlex-C3 was used to lyse the cells. The obtained lysate was filtered and loaded on 5 ml HisTrap column preequilibrated in Gyrase lysis buffer. Column was then washed with 20 CV of Gyrase lysis buffer. Bound proteins were eluted using Gyrase lysis buffer supplemented with 250 mM imidazole. Fractions containing protein were then loaded on a 5 ml StrepTtrap HP column pre-equilibrated with STREP buffer. The column was then washed with 20 CV of STREP buffer. Bound protein was eluted using STREP buffer containing 3 mM desthiobiotin. Both 10-His tag and Twin-Strep tag were subsequently cleaved using P3C and TEV proteases (mass ratio 1:1:50 P3C-TEV-GyrA) overnight at 4 °C. Proteins were then loaded on HiTrap Q HP (Cytvia) column pre-equilibrated with TGED buffer. The column was then washed with 10 CV of TGED buffer containing 100 mM NaCl. Proteins were eluted with a gradient (0.1-1 M) of NaCl in TGED over 5 CVs. Fractions containing protein were collected and dialysed

overnight against TGED buffer. Proteins were concentrated to desired concentration and frozen in -80°C.

4.2.9.1. Purification of Flag-tagged gyrase subunits

Full-length *E. coli* GyrA-FLAG and 3xFLAG-GyrB subunits were purified similarly to (Maxwell and Howells, 1999). Plasmids pET28b containing corresponding genes were transformed into BL21 (DE3) Gold (Agilent). For GyrA, 2 L of TB culture supplemented with 100 µg/ml ampicillin was incubated at 37°C with shaking until OD_{600} reached 0.75, induced with 500 µM (IPTG) and incubated for a further 4 hours at 37°C. Cells were harvested by centrifugation. Pellets were resuspended in TGED buffer and supplemented with protease inhibitor cocktail (Pierce). Cells were lysed using Avestin EmulsiFlexC3 and cell debris removed by centrifugation at 40 000g for 20 minutes at 4°C. Clarified lysate was loaded onto 10 ml Q XL column (GE Healthcare) in TGED buffer, washed with 10 CV of TGED, 10 CV of TGED supplemented with 0.1 M NaCl and eluted with gradient (0.1-1 M) of NaCl in TGED over 5 CVs. Collected fractions were dialysed into TGED overnight at 4°C and further purified by MonoQ HR 16/10 using the same method as described for Q XL. Peak fractions were pooled together, concentrated using Amicon concentrators (Millipore) and loaded onto a Superdex 200 Increase 10/300 (Cytiva) column equilibrated in TGED. Fractions containing GyrA were aliquoted, frozen in liquid nitrogen and stored at -80°C.

For GyrB, 2 L of TB culture was grown at 37°C with shaking to OD_{600} = 0.8, induced with 500 µM IPTG and incubated for a further 3 hours at 28°C. Cells were lysed and processed in TGED as described for GyrA and protein was purified using heparin affinity (Heparin FF 16/10 column) and anion exchange (MonoQ HR 16/10 column) chromatography (Cytiva), eluting with a 0-1 M gradient of NaCl. Peak fractions from MonoQ were pooled, dialysed into TGED, concentrated using Amicon and aliquoted and frozen at -80°C.

4.2.9.2. Purification of GyrB43

E. coli gyrase B 43 kDa domain (GyrB43) was purified following the described procedure (Hearnshaw *et al.*, 2015). The plasmid pAJ1 (Ali *et al.*, 1993) was transformed into BL21 (DE3) Gold (Agilent) cells. 1 L culture of TB medium was inoculated with overnight culture of transformed cells and was incubated at 37°C with shaking to OD_{600} = 0.8 when

it was induced with 500 μM IPTG. The temperature was reduced to 25°C and the culture was continued overnight. Cells were harvested as described for other proteins. Cell lysis was performed according to the same procedure as for other proteins. Pellets were resuspended in the TGED buffer. The lysate was loaded on a Q XL column pre-equilibrated in the TGED buffer. The column was then washed with 10 CV of TGED and 10 CV of TGED containing 100 mM NaCl. Elution was performed using the TGED buffer with 1M NaCl. Bound protein was eluted using gradient elution (0.1-1M) of NaCl in the TGED buffer over 5 CVs. Fractions containing protein of interest were combined, and ammonium sulphate was added to 1.5 M. Salt-adjusted fractions were loaded to 10 ml Phenyl Sepharose HS FF (Cytiva) column equilibrated in 1.5M $(NH_4)_2SO_4$ and protein was eluted by 20 CV gradient from 1.5 M to 0 $(NH_4)_2SO_4$. Collected fractions were pooled together, dialysed overnight against the TGED and loaded onto a MonoQ column16/10 (Cytiva) column as described for GyrA and GyrB proteins. Peak fractions from MonoQ were pooled, dialysed overnight into TGED, concentrated to 10 mg/ml, aliquoted, frozen in liquid N_2 and stored at -80°C.

4.2.9.3. Purification of Gyrase B47

Gyrase B 47 kDa domain (Toprim) was purified as described in (Vos *et al.*, 2014). 2 L culture of BL21 Gold cells (DE3) (Agilent) Gold pET28-GyrB47 was grown in TB medium at 37°C with shaking. Cells were induced with 500 μM IPTG at OD_{600} = 0.75. After induction, the cells were grown further for 4 hours at 37°C. Cells were harvested as described for other proteins. Cell lysis was performed according to the same procedure as for other proteins. Pellets were resuspended in Gyr B47 lysis buffer. After lysis, filtered lysate was loaded on 5 ml HisTrap FF column (Cytvia) pre-equilibrated with Gyr B47 lysis buffer. The column was washed with 20 CVs of lysis buffer. Bound protein was eluted with a lysis buffer containing 250 mM imidazole. Fractions containing protein were pooled and dialysed overnight against the TGED buffer. The protein was then loaded on a 5 Q HP column (Cytiva). Q column purification was performed as described for gyrase B43. Peak fractions were dialysed overnight into TGED and further purified on a 5 ml Q HP column (Cytiva). A step gradient of NaCl was used and protein eluted at 40% NaCl. Fractions containing GyrB47 were pooled concentrated and flash-frozen in liquid N_2 and stored at -80°C

4.2.9.4. Purification of Gyrase A59

Gyrase A 59 kDa fragment was purified as described in (R. J. Reece and Maxwell, 1991). Plasmid pAJR10.18 was transformed into BL21(DE3) Gold cells. 2 L of culture was grown in LB at 37°C to OD_{600} = 0.85, induced with 0.5 mM IPTG, and grown for further 4 hours at 37°C. Cells were lysed by sonication in TGED. Lysate was cleared by centrifugation at 87 000 g for 30 minutes at 4°C and GyrA59 was purified first on a 16/10 Heparin FF (Cytiva) column using a 0.1-1 M gradient of NaCl in TGED. After overnight dialysis to TGED, GyrA59 was further purified on MonoQ (16/10, Cytiva) using a gradient 0-0.7 M NaCl over 6 CV. Fractions containing GyrA59 were pooled, concentrated and loaded onto a Superdex 200 16/600 gel filtration column. Pure protein, concentrated to ~5 mg/ml was aliquoted, flash-frozen in liquid N_2 and stored at -80°C.

4.2.10. Gyrase activity assays

4.2.10.1. Gyrase supercoiling assay

In a gyrase supercoiling assay, 1 unit of *E. coli* DNA gyrase was incubated in 30 µl of reaction volume in Gyrase assay buffer with 500 ng of relaxed pBR322 plasmid (Inspiralis Ltd.) (1 unit is defined as the amount of DNA gyrase needed to fully supercoil 500 ng of relaxed pBR322 plasmid in 30 minutes at 37°C in a 30 µl reaction). Where necessary, proteins and toxins were replaced with an equal volume of appropriate buffer. 30 µl of Chloroform: isoamyl alcohol (24:1) and 30 µl of STEB were used to stop the reaction in appropriate timepoints. Obtained aqueous layers from assays were run on 1 % agarose gels in TAE at 80 V for 180 minutes. After competition the gels were stained with 10 µg/ml ethidium bromide solution (Sigma) for 15 minutes. Subsequently the gels were destained with TAE buffer for 15 minutes and visualised using a ChemiDoc MP System (Bio-Rad). Analysis and quantification were performed using Fiji software (Schindelin *et al.*, 2012) . Gyrase relaxation assays were carried out in a similar manner, but ATP and spermidine were omitted and ~5 U of gyrase were used.

Percentage of supercoiled DNA was plotted against QnrB1 concentration and the data was fitted to the equation: $\%SC = ae^{b[QnrB1]}$, where a and b are function parameters found after fitting the function using Origin (Pro), Version 2020 b. IC_{50} (concentration of QnrB1 required for 50% supercoiling inhibition) was calculated from the fitted function.

4.2.10.2. Gyrase cleavage assay

5 U of gyrase were used in a gyrase cleavage assay. The reaction was carried out at 37°C for 1 h in 30 µl of reaction volume in the gyrase assay buffer with 500 ng pBR322 plasmid. Reaction was terminated by adding sodium dodecyl sulphate (SDS) to a final concentration of 0.2% and proteinase K to a final concentration of 0.2 mg/ml followed by incubation for 30 minutes at 37°C. 30 µl of chloroform: isoamyl alcohol (24:1) and 30 µl of STEB buffer was added to separate proteins from DNA and the obtained aqueous phase was loaded on 1 % agarose TAE gel. The gel was run for 120 minutes at 90 V. The gels were visualised using a ChemiDoc XRS+ System (Bio-rad). Analysis and quantification were performed using Fiji software. The amount of cleaved DNA in each lane was quantified and the data were fitted to the equation $\%\,\text{DNA cleavage} = \%\,\max\text{cleavage}\ \frac{[\text{CFX}]}{\text{EC50}_{cfx} + [\text{CFX}]}$ where EC50_{cfx} is concentration of ciprofloxacin in which 50% of maximum cleavage activity is observed. The EC50_{cfx} values were calculated from the fitted function.

Cleavage of short DNA fragments was performed according to different procedure. The 20 nM DNA fragment (with the exception of the 76 bp fragment where 30 nM was used) was incubated with 5 U of DNA gyrase for 30 minutes. Reaction was terminated by adding sodium dodecyl sulphate (SDS) to final concentration of 0.2% and proteinase K followed by incubation for 30 minutes at 37°C. 30 µl of Chloroform: isoamyl alcohol (24:1) and 30 µl of was added to separate proteins from DNA and obtained aqueous phase was loaded on 4-20% TBE polyacrylamide gels (Thermo).

Time-courses of gyrase mediated DNA cleavage was performed as follows: 100 U of *E. coli* gyrase was incubated at 25 °C in 400 µl reactions with Gyrase assay buffer (for Ca^{2+} induced cleavage, $MgCl_2$ was replaced by $CaCl_2$) and 500 ng relaxed pBR322 DNA (Inspiralis Ltd). Appropriate buffer was supplemented with 1 mM ATP or 0.5 mM ADPNP. At selected time points, 20 µl aliquots were pipetted and stopped by addition of SDS and EDTA to final concentrations of 0.5% and 250 mM respectively. After finishing the time course, samples were treated with proteinase K (0.2 mg/ml) for 30 minutes at 37°C, extracted by chloroform: isoamyl alcohol (24:1) and mixed with STEB buffer. Obtained aqueous layers from time course time points were run on 1% agarose TAE gels at 90 V for 120 minutes. Once complete, the gels were stained with 10 µg/ml ethidium

bromide solution (Sigma) for 15 minutes and de-stained with TAE buffer for 15 minutes and visualised.

Cleavage complex stability assays were performed as follows: an initial 60 µl reaction was set up with 80 U of DNA gyrase in gyrase assay buffer 50 nM of pBR322 DNA and 20 uM CFX, or 1 µM albicidin for AlbG containing assays. The reaction was incubated for 10 minutes at 37°C. Then, 20 µl of the reaction was diluted 20-fold with a gyrase assay buffer supplemented with 5 µM QnrB1 or 5 µM AlbG. At selected times, 20 µl of each reaction was pipetted out to separate Eppendorf tubes and mixed with SDS (5 %) and EDTA (250 mM). After finishing the time course, collected samples were treated with proteinase K (0.2 mg/ml) for 30 minutes at 37°C, then a chloroform-isoamyl alcohol mixture (24:1) and STEB were added. Obtained aqueous layers from certain time points were run on 1% agarose TAE gel at 90 V for 120 minutes. Once complete, the gels were stained with 10 µg/ml ethidium bromide solution (Sigma) for 15 minutes and destained with TAE buffer for 15 minutes and visualised.

4.2.10.3. ATPase assays

Full length gyrase and GyrB 43 ATPase assays were carried out according to the protocol provided by Inspiralis Ltd based on Tamura & Gellert (40). Each reaction contained 50 mM Tris-Cl (pH 7.5), 1 mM EDTA, 5 mM magnesium chloride, 5 mM DTT, 10 % (w/v) glycerol, 0.8 mM PEP, 0.4 mM NADH and ~1U of PK/LDH mix (Sigma). For GyrB43 assays, the concentration of GyrB43 was 4 µM. For gyrase assays, 50 nM gyrase tetramer (A_2B_2) was used. Linear pBR322 DNA (Inspiralis) was used at 10.5 nM where indicated. Assays were performed in microtitre plates with a reaction volume of 100 µl. The absorbance at 340 nm was measured continuously in a plate reader (SpectraMAX190, Molecular Devices) and used to evaluate the oxidation of NADH (using an extinction coefficient of 6.22 mM^{-1} cm^{-1}), which relates stoichiometrically to the production of ADP. The results were fitted to a Michaelis – Menten plot according to equation $V = Vmax(\frac{[ATP]}{K_m+[ATP]})$ or Hill equation $V = Vmax\frac{[QnrB1]^n}{{K_m}^n+[QnrB1]^n}$ using Origin (Pro), Version 2020 b, (OriginLab Corporation). Novobiocin (50 µM) was used as a control for gyrase-independent ATPase activity.

4.2.11. DNA fragments production

DNA fragments (300-100 bp) were obtained by amplification from the pBR322 template, followed by purification (GeneJet Gel Extraction and DNA Cleanup Micro kit, Thermo). The synthesis of 76 base complementary oligonucleotides fragment was ordered from an outside company (Sigma). The 20-12p-8 DNA used for Cryo-EM sample preparation was ordered in IDT.

4.2.12. Pull-down experiments

5 μM purified FLAG-QnrB1/AlbG/HIS-McbG was mixed with 0.65 μM gyrase A_2B_2 complex or appropriate gyrase subunit/subdomain in 20 μl of pull-down buffer. For the experiments with ADPNP, the nucleotide (1 mM) was added 30 mins before QnrB1 to induce GyrB dimerisation and the reaction was pre-incubated for 30 minutes at room temperature together with a control reaction. An equal amount of equilibrated ANTI-FLAG M2 agarose (Sigma) or in the case of HIS-McbG, HisPur Ni-NTA Resin (Thermo) was added to each reaction. After addition of PRP, reactions were incubated for a further 60 min at room temperature with gentle shaking. Resin was washed three times with TGE (20 mM Tris-Cl pH 7.5, 10% glycerol, 100 mM NaCl) and eluted with 50 μg/ml (final concentration) of 3xFLAG peptide (Sigma) in TGE. Load and eluate material were analysed by SDS-PAGE.

4.2.13. Fluorescence anisotropy measurements

QnrB1 was N-terminally labelled with AlexaFluor 488-carboxylic acid-2,3,5,6-tetrafluorophenyl ester-5 isomer (5-TFP, Thermo), according to a procedure described for YacG protein (32). Briefly, purified QnrB1-His was exchanged to amino labelling buffer. A 15 times molar excess of AlexaFluor 488-5-TFP over QnrB1 was added to the QnrB1 solution. The reaction was incubated in 25°C for 1 h with shaking. Unreacted dye was quenched by adding 1 M L-lysine dissolved in 20 mM Tris-HCl pH 7.5 (final lysine concentration 130 mM) and incubating the reaction at 37˚C for 30 minutes. Free dye was separated from labelled protein using Superdex S75 increase 10/300 GL column (Cytiva), equilibrated with QnrB1 storage buffer.

Fluorescence measurements were carried out with a RF-6000 spectrofluorometer (Shimadzu) fitted with a polarizer. The assays were carried out at specific

excitation/emission wavelengths for Alexa-488 of 488/520 nm. For QnrB1 binding to gyrase, 50 nM labelled QnrB1 was mixed in an EMSA buffer with appropriate gyrase subunit(s) and incubated for 10 minutes at room temperature in darkness. When 1 mM ADPNP was used, the samples were incubated for additional 1 h at room temperature with addition of 2 mM $MgCl_2$. Curves were fitted using Origin (Pro)Version 2020b, (OriginLab Corporation) according to standard one site specific binding equation: $Binding = \frac{B_{max}*x}{Kd*x}$ where K_d is dissociation constant x is QnrB1 concentration and B_{max} is maximum binding.

QnrB1/DNA binding competition assays were performed as follows: 90 bp Cy5-labelled oligonucleotide encompassing the strong gyrase binding site from plasmid pBR322 was ordered from Sigma and annealed with an antisense unlabelled oligo by heating to 99°C and gradual cooling. The sequences of ordered nucleotides are presented in **Table 8**.

Table 8. Oligonucleotides used to prepare 90 bp Cy5 labelled oligonucleotide duplex encompassing strong gyrase binding site.

Name	**Sequence (5'-3')**
F_90 bp	Cy5=CGCTGGGCTACGTCTTGCTGGCGTTCGCGACGCGAGGCTGGATGGCCTTCCCCATTATG ATTCTTCTCGCTTCCGGCGGCATCGGGATGC
R_90bp	GCATCCCGATGCCGCCGGAAGCGAGAAGAATCATAATGGGGAAGGCCATCCAGCCTCGCGTCG CGAACGCCAGCAAGACGTAGCCCAGCG

To measure the ability of QnrB1 to compete with DNA, 20 nM 90 bp Cy5-DNA fragment complex was mixed in a fluorescence polarisation buffer with 1 μM gyrase (A_2B_2) and increasing concentrations of label-free QnrB1. The assays were carried out at specific excitation/emission wavelengths for Cy5 of 600/666 nm. The optimal concentration of the gyrase complex for binding experiments was established beforehand by mixing 20 nM 90 bp Cy5-DNA and increasing concentrations of gyrase in the above-mentioned buffer. To measure the ability of DNA to compete with QnrB1, 50 nM AlexaFluor488-labelled QnrB1 was mixed with 1 μM gyrase and increasing concentration of unlabelled linearised pBR322 (Inspiralis). The assays were carried out at specific excitation/emission wavelengths for Alexa-488 of 488/520 nm.

4.2.14. Electrophoretic mobility shift assays (EMSA)

147 bp pBR322 dsDNA fragment encompassing known strong gyrase binding site (Fisher *et al.*, 1981) was produced by PCR and purified with Thermo Scientific GeneJet Gel Extraction and DNA Cleanup Micro kit. 20 nM of the fragment was mixed with 0.2 μM of reconstituted gyrase in the EMSA buffer. QnrB1 or AlbG were added as indicated. In control reactions, QnrB1/AlbG were replaced by their storage buffers. Reactions were incubated for 30 min at 25°C and run on 6% polyacrylamide gels in TBM buffer (90 mM Tris-borate, pH 7.5, 4 mM $MgCl_2$) at 150 V at room temperature. After the run gels were stained with SYBR Gold (Thermo) for 20 mins and visualized under UV light.

Amount of DNA was quantified using Fiji software (Schindelin *et al.*, 2012). The data were fitted to the standard one site specific binding equation: $\text{Binding} = \frac{\text{Bmax}*[\text{QnrB1}]}{\text{IC}_{50_{QnrB1}}*[\text{QnrB1}]}$ using Origin (Pro), Version 2020 b software.

4.2.15. Protein stability measurement

Tycho Scanner (Nanotemper) was used to analyse protein stability. 2mg/ml McbG and QnrB1 proteins were loaded into Tycho NT.6 Capillaries (NanoTemper) and the measurement was performed on the default instrument program. QnrB1 protein was used as a reference of PRP protein unfolding. The Data was analysed using machine built in software.

4.2.16. Liquid chromatography and tandem mass spectrometry (LC-MS/MS)

The samples were prepared using paramagnetic bead technology based on the Single-Pot Solid-Phase-enhanced Sample Preparation (SP3) (extraction method based on hydrophilic interaction mechanism) for optimal and efficient extraction and desalting of analysed proteins. (Hughes *et al.*, 2014) Two types of Speed Beads were mixed in a ratio 1:1: GE45152105050250 and GE65152105050250 (Sigma-Aldrich). The proteins were reduced with dithiothreitol, alkylated with iodoacetamide and digested with Trypsin/Lys-C Mix (Promega).

Peptides were analysed using an UltiMate 3000 RSLCnano System coupled with Q Exactive mass spectrometer (Thermo Fisher Scientific) through DPV-550 Digital PicoView nanospray source (New Objective). Sample was loaded onto a trap column

(Acclaim PepMap 100 C18, 75 μm x 20 mm, 3 μm particle, 100 Å pore size, Thermo Fisher Scientific) in 2% acetonitrile with 0.05% TFA at a flow rate of 5 μl/min and further resolved on an analytical column (Acclaim PepMap RSLC C18, 75 μm x 500 mm, 2 μm particle, 100 Å pore size, Thermo Fisher Scientific) with a 2 h gradient of acetonitrile (from 2% to 40%) in 0.05% formic acid at a flow rate of 250 nl/min. The Q Exactive was operated in a data dependent mode using the Top12 method. Full-scan MS spectra were acquired with a resolution of 70,000 at m/z 200 with an automatic gain control (AGC target) of 10^6. The MS/MS spectra were acquired with a resolution of 17,500 at m/z 200 with an AGC target of 5×10^5. The maximum ion accumulation times for the full MS and the MS/MS scans were 120 ms and 60 ms respectively. Peptides were dynamically excluded from fragmentation within 30 seconds.

The RAW file was processed by the Proteome Discoverer platform (v.1.4, Thermo Fisher Scientific) and searched using locally installed MASCOT search engine (v.2.5.1, Matrix Science) against two different databases: the SwissProt database with Escherichia coli taxonomy restriction (release June 2020, 23149 sequences) and the SwissProt database with Proteobacteria taxonomy restriction (release June 2020, 198550 sequences).

The following parameters were applied: fixed modification - cysteine carbamidomethylation; variable modifications - methionine oxidation; the peptide mass tolerance - 10 ppm; fragment mass tolerance - 20 mmu. Only tryptic peptides with up to one missed cleavage site were considered. Target Decoy PSM Validator was applied with the maximum false discovery rate (FDR) of 0.01 for the SwissProt database searches and 0.05 for the TrEMBL database and reference proteome searches.

4.2.17. Cryo-electron microscopy

Sample preparation and data analysis was performed by Dr Dmitry Ghilarov.

4.2.17.1. Cryo-electron microscopy sample preparation

E. coli GyrA and GyrB subunits were mixed in equimolar proportions to reconstitute the full DNA gyrase enzyme. 20-12p-8 DNA (20 bp palindromic DNA molecule with a nick after the eighth base and 5′ phosphorylated following base) (Srikannathasan *et al.*, 2015) was added to the complex in a 1:1 ratio resulting in a final concentration of gyrase-DNA complex ~10 μM. The reconstituted complex was buffer exchanged by dialysis at 4°C overnight to cryo-EM buffer with the addition of 50 μM moxifloxacin (MFX). The subsequent day the complex was supplemented with 250 μM MFX and 1 mM ATP (for EcGyr-QnrB1 + ATP complex) or with just 250 μM CFX (for EcGyr-QnrB1 - ATP complex) and incubated for 30 minutes at 37°C. 8 mM CHAPSO was added, and sample was centrifuged (1 h at 21 000 g) to remove potential aggregates.

4.2.17.2. Cryo-electron microscopy data collection and analysis.

Aliquots of 4 μl of reconstituted complexes (~10 mg/ml) were applied to glow-discharged (Leica, 60 s/8 mA) Quantifoil holey carbon grids (R2/1, 300 copper mesh). After 30 s of incubation with 95% chamber humidity at 10°C, the grids were blotted for 6 s and plunge-frozen in liquid ethane using a Vitrobot mark IV (FEI).

Cryo-EM data were collected at the Polish national cryo-EM facility SOLARIS with a Titan Krios G3i microscope (Thermo Fisher Scientific) operated at 300 kV, and images were collected at a nominal magnification of ×105 000 resulting in a calibrated physical pixel size of 0.86 Å per pixel. The images were recorded in counting mode on a K3 electron direct detector (Gatan) equipped with GIF BIO Quantum energy filter operated with a slit width of 20 eV. A dose rate of 15 electrons per pixel per second was used, and exposure time was set to generate a total dose of ~40 electrons/Å^2 over 40 movie frames.

Processing of both datasets was done in cryoSPARC 3+ and RELION software (Punjani *et al.*, 2017; Zivanov *et al.*, 2018). Movies were dose-weighted and motion and CTF corrected in patch mode. Resulting micrographs were manually curated and micrographs without defects and CTF estimated <5 Å selected for further analysis. Particles were picked first with TOPAZ (Bepler *et al.*, 2019) followed by cryoSPARC template picker.

2x2 binned particles were subjected to several rounds of 2D classification. Cleaned particles went through unsupervised 3D classification first in cryoSPARC (*Ab initio*) and, following refinement and export, in Relion (unsupervised 3D classification with angular search, and masked focussed classification without angular search). Particles from homogenous classes were re-extracted in cryoSPARC as unbinned particles using updated coordinates. Non-uniform refinement of this particle set with local CTF correction resulted in maps reaching global resolution of 3.2 Å (ATP dataset) and 3.4 Å (nucleotide-free dataset). Local filtering and cryoSPARC auto-sharpening were used to aid model building.

4.2.17.3. Model building

The initial model of gyrase:QnrB1 complex was built in ChimeraX (Pettersen *et al.*, 2021). The closest available *E. coli* structures of DNA gyrase (PDB:6RKW - structure of the complete *E. coli* DNA Gyrase, 6RKV - *E. coli* DNA Gyrase - DNA binding and cleavage domain) (Vanden Broeck *et al.*, 2019) were used as a starting point for rigid body fitting. The structure of GyrB43 in the Qnr-binding conformation was modelled using template-homology modelling by SWISS-model server with MsGyrB47:MfpA (PDB: 6ZT5) (Feng *et al.*, 2021) as a template model (Waterhouse *et al.*, 2018). Fitted structures were stripped of all ions and water molecules. The protein fragments with no corresponding density in obtained cryo-EM maps were removed from obtained atomic models. The structure of 20-12p-8 DNA was copied from *Staphylococcus aureus* DNA gyrase structure (PDB:5CDP) (Chan *et al.*, 2015). Dimers of QnrB1 were rigid body fitted using previously published atomic model of the protein (PDB:2XTW) (Vetting, Hegde, Wang, *et al.*, 2011). Prepared starting model contained GyrA (amino acids 8-525) – incorporating winged helix domain, tower domain, and coil-coiled domain with the exception of CTD. For GyrB amino acids 2-790 remained in the model encompassing full GHKL and transducer domains with Toprim missing only last the 14 amino acids. The obtained rigid body fitted model of the DNA:gyrase:QnrB1 complex was subsequently refined using phenix.real.refine suite (Afonine *et al.*, 2018). All refinements rounds were done using real space fitting and global gradient-driven minimization with NCS restraints, Ramachandran restraints and secondary structure restraints obtained using ksdssp algorithm (Kabsch and Sander, 1983). Between cycles of refinement the model was inspected in COOT where missing amino acids and poorly resolved regions were

manually refined (Emsley *et al.*, 2010). Atomic model and constraint dictionary of moxifloxacin were generated with the Grade server (http://grade.globalphasing.org). Moxifloxacin was manually fit in COOT. For this, *Staphylococcus aureus* DNA gyrase structure with bound moxifloxacin (PDB:5CDQ) (Chan *et al.*, 2015) was aligned to the model using Matchmaker tool in ChimeraX (Meng *et al.*, 2006), the MFX molecules from *S. aureus* gyrase model were merged into *E. coli* complex and the MFX models were manually refined using COOT. Obtained final model was used to refine B-factors in phenix. real.refine. MolProbity was used to validate the obtained structures (Williams *et al.*, 2018).

5. Results

5.1. *In vivo* activities of PRPs

In order to compare protective activity of PRPs against their presumed cognate toxins (CFX, ALB and MccB17), the genes encoding respective proteins (without any additional protein purification tags) were cloned into arabinose-inducible pBAD plasmids. Those plasmids were transformed into *E. coli* BW25113 (*ΔaraBAD).* Empty pBAD vector was used as a control. The MIC values for transformed strains were determined using microdilution method (see **Table 9**). Induction of QnrB1 led to a16-fold increase of CFX MIC compared to control plasmid. Induction of McbG led to a 4-fold increase of MIC whereas no change in MIC was observed upon AlbG induction. The tests with ALB shown >357-fold increase upon AlbG induction (higher concentrations could not be tested due to limitation in albicidin solubility), but induction of QnrB1 did not show any change in ALB MIC value. Induction of McbG lead to only a 5-fold increase of ALB MIC. Finally, MICs for MccB17 were increased 26-fold for the McbG producing strain. AlbG and QnrB1 induction led to a 4-fold and 2-fold increase of MccB17 MIC, respectively. The QnrB1 loop B deletion mutant was previously demonstrated as the mutant with no protective activity in gyrase assays (Vetting, Hegde, Wang, *et al.*, 2011). Also it was shown that the deletion of three amino acids in the loop leads to disappearance of protective activity of QnrB1 in MIC assays (Jacoby *et al.*, 2013). AlbG loop deletion mutant (AlbG $\Delta_{91\text{-}97}$) prepared based on structural data showing that the AlbG protein is forming stable PRP dimer without the loop is the "loopless" homologue of QnrB1 loop B deletion mutant. AlbG $\Delta_{91\text{-}97}$ shown drastically reduced MIC value for albicidin showing only 2-fold protection.

The possibility of an AlbG loop being a determinant of the specificity of protection was also tested: for this, a chimeric variant was designed where its loop (AlbG amino acids 91-97) was replaced by the QnrB1 loop B sequence (QnrB1 amino acids 102-113) creating $AlbG_{QnrB1\ 106\text{-}108}$. The obtained chimeric QnrB1 mutant shown no protective effect for any of the tested drugs. Similarly, a chimeric QnrB1 bearing the AlbG loop $QnrB1_{AlbG\ 91\text{-}97}$ shown no protective activity (data not shown).

The obtained MICs results clearly indicate that PRPs protection is specific to their cognate toxins. It has already been shown that loop 2 deletion mutant of QnrB1 is incapable of protecting gyrase against inhibition by ciprofloxacin (Vetting, Hegde, Wang, *et al.*,

2011). The fact that AlbG loop deletion mutant shows significantly reduced protection against albicidin is in line with the MIC data available for loop deletion variant of QnrB1 where the mutant shown no protective activity (Jacoby *et al.*, 2013). These data further highlight the importance of loops for PRP activity.

Table 9. Obtained MIC values. Measured MICs of albicidin (ALB), ciprofloxacin (CFX) and microcin B17 (MccB17) for *E. coli* BW25113 strain transformed with empty vector (pBAD) or plasmids expressing PRPs: QnrB1, McbG, AlbG and AlbG $\Delta_{91\text{-}97}$.

	Toxin					
	ALB		MccB17		CFX	
Plasmid	Obtained MIC [μM]	Fold change	Obtained MIC [μM]	Fold change	Obtained MIC [μM]	Fold change
pBAD	0.028 ± 0.005	1	0.58 ± 0.09	1	0.016 ± 0.004	1
pBAD-QnrB1	0.023 ± 0.008	1	1.3 ± 0.1	2	0.25 ± 0.06	16
pBAD-McbG	0.13 ± 0.02	5	>15	>26	0.12 ± 0.03	8
pBAD-AlbG	>10	>357	2.6 ± 0.2	4	0.016 ± 0.004	1
pBAD-AlbG $\Delta_{91\text{-}97}$	0.062 ± 0.009	2	-	-	-	-

Unfortunately, structural data for McbG protein is not available, while different protein structure prediction tools produced conflicting results; therefore, it was not possible to pick loop-specific residues to be mutated with confidence in this case. Without certainty, introduced mutations might cause misfolding of the entire protein, thus this has not been tried.

5.2. PRPs biochemical characterisation

5.2.1. QnrB1

QnrB1 protein as the most studied TA-PRP can be treated as model protein for the Qnr protein family. The fact that its 3D structure is known and its host organism is *Klebsiella pneumoniae* from the *Enterobacteriacea*e family simplifies the experiments which can be performed using a closely related *E. coli* host.

5.2.1.1. Protein purification

QnrB1 protein was expressed as hexa-histidine-tagged protein and purified using immobilized metal affinity chromatography (IMAC) using HisTrap Fast Flow (Cytvia) column as first step (**Figure 18 A**). Eluted fractions seem to be well purified from

contaminating proteins. After overnight dialysis into low-salt buffer the obtained protein was loaded on MonoQ ion-exchange column and further purified (**Figure 18 B**). Finally, collected fractions form MonoQ column were concentrated, and the buffer was exchanged using a Superdex S75 Increase gel filtration column. This method is a modification of a previously published protocol of QnrB1 purification which did not include dialysis and ion-exchange steps (Hegde *et al.*, 2011). The modification resulted from the fact that when the previously published purification method was followed, the protein after IMAC step was precipitating during freezing; moreover, obtained final specimen after gel filtration was showing high level of nuclease contamination resulting in non-specific DNA degradation in subsequent gyrase assays. Addition of the ion-exchange step allowed production of a nuclease – free and stable protein that could be used in the assays with DNA.

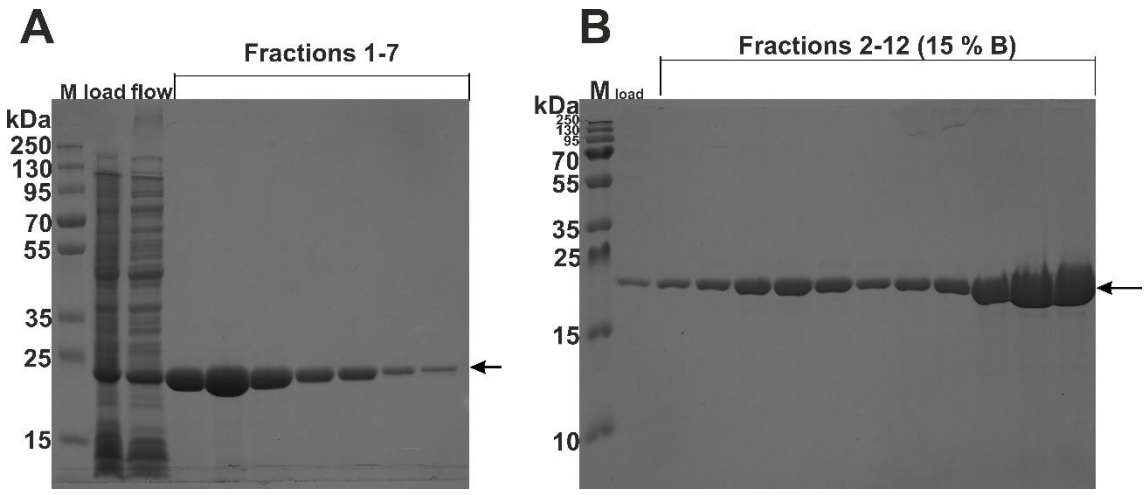

Figure 18 SDS-PAGE gels from each stage of purification of HIS-QnrB1. (**A**) Gel showing HISTrap purification step (load – fraction loaded on the column after cell lysis, flow – flowthrough from HisTrap Fast Flow column, Fractions 2-7 contains every second fraction (10 µl from 5 ml of eluted fractions form HisTrap Fast Flow column) (**B**) Gel showing fractions from MonoQ ion-exchange column purification step (load – material loaded on the column, fractions 2-12 (15% B) – fractions collected from elution with 15% of buffer B).

5.2.1.2. QnrB1 activity in gyrase supercoiling assays

To test the ability of QnrB1 to protect DNA gyrase from CFX inhibition, a gyrase supercoiling assay was performed with increasing concentrations of QnrB1 and 5 µM CFX. QnrB1 offered limited protection without being able to restore full supercoiling in the presence of 5 µM CFX (**Figure 19 A**). Estimated $EC_{50\ QnrB1}$ (concentration of QnrB1 required to observe half of maximum protective effect) for the protein equalled 0.2 µM.

It could be also seen that higher concentrations (> 10 μM) of QnrB1 lead to gyrase inhibition. This effect was further studied separately in the supercoiling assay without CFX present. Estimated $IC_{50\ QnrB1}$ (concentration of QnrB1 required to observe half of maximum inhibition of supercoiling) was ~ 11 μM which is > 50 times higher than $EC_{50\ QnrB1}$ value (**Figure 19 B**). The importance of loop B amino acids of QnrB1 for its protection activity was already shown in MIC assays performed in previous studies where QnrB1 $\Delta_{106\text{-}108}$ mutant (ΔTTR) lost the protective ability in MIC assays against ciprofloxacin (Jacoby *et al.*, 2013). When tested in the same set of supercoiling assays, the ΔTTR mutant shown no protection against CFX but was still able to inhibit gyrase supercoiling reaction when tested without the drug to the similar extent as WT QnrB1. (**Figure 19 CD)**. These results suggest that TTR sequence located in the loop 2 of QnrB1 is important for protection against CFX activity although likely not essential for the interaction with gyrase. The inhibitory effect observed by high concentrations of QnrB1 (>10 μM) suggest that the protein is competing with the DNA binding thus preventing supercoiling as was proposed earlier for MfpA. My results obtained for the protective activity of QnrB1 against ciprofloxacin in supercoiling reactions correlated well with the previous reports (Vetting, Hegde, Wang, *et al.*, 2011). The inhibition of supercoiling by increasing concentration of QnrB1 is similar to observations for homologous PRPs MtMfpA, MsMfpA and EfsQnr where increasing concentration of protein similarly inhibited the supercoiling reaction (Hegde *et al.*, 2005, 2011; Feng *et al.*, 2021).

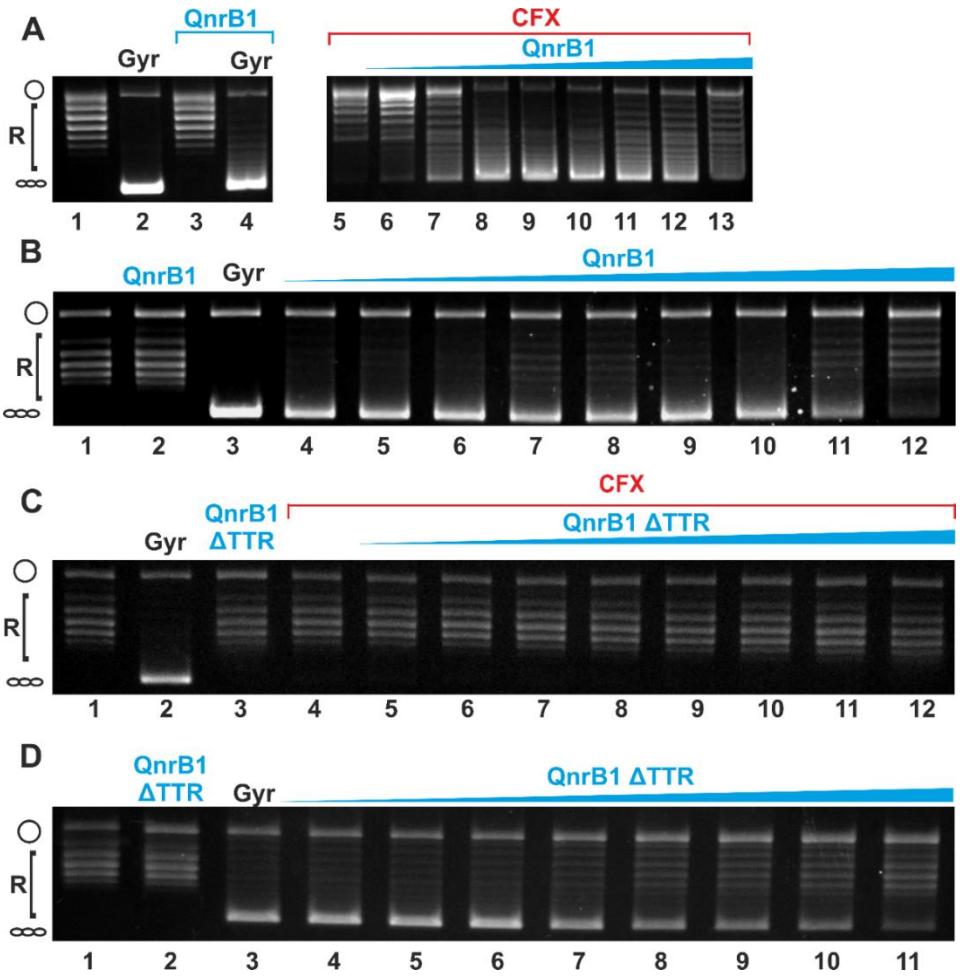

Figure 19. (**A**) Plasmid supercoiling assay showing: lane 1: relaxed pBR322, lane 2: supercoiling by 1 U of gyrase, lane 3: lack of detectable nuclease activity in the purified QnrB1 (50 μM QnrB1) and lane 4: partial inhibition of gyrase by 50 μM QnrB1; lanes 6–13: gyrase inhibition by CFX (5 μM) and rescue by increasing concentrations of QnrB1 (0.04, 0.2, 1, 5, 10, 20, 25, 50 μM). Positions of negatively supercoiled and relaxed DNA are indicated by the graphics at the left (same notation used in other Figures); (**B**) Plasmid supercoiling assay showing the inhibitory effect of high concentrations of QnrB1. Lane 1: relaxed pBR322, lane 2: no nuclease activity was observed upon addition of 50 μM QnrB1, Lane 3: gyrase and relaxed pBR322 lanes 4-12: effect of increasing concentration of QnrB1 on gyrase supercoiling activity (0.0016; 0.008; 0.04; 0.2; 1; 5; 10; 20; 40 μM); (**C**) Plasmid supercoiling assay showing lack of protection by QnrB1 ΔTTR. Lane 1: relaxed pBR322; lane 2: nuclease control (pBR322+50 μM QnrB1 ΔTTR); lane 3: gyrase, 1 U; lane 4: gyrase and 5 μM CFX; lanes 5-12: gyrase and 5 μM CFX and increasing concentration of QnrB1 ΔTTR (0.0016; 0.008; 0.04; 0.2; 1; 5; 10; 25; 50 μM); (**D**) Plasmid supercoiling assay showing inhibitory effect of high concentrations of QnrB1 ΔTTR. Lane 1: relaxed pBR322, lane 2: nuclease control (pBR322+50 μM QnrB1 ΔTTR); lane 3: gyrase and relaxed pBR322; lanes 4-11: effect of increasing concentration of QnrB1 on gyrase supercoiling activity (0.0016; 0.008; 0.04; 0.2; 1; 5; 10; 25; 50 μM). Figure adapted from (Mazurek *et al.*, 2021) .

In the reverse setup where 5 μM QnrB1 were tested against increasing concentrations of CFX, it can be seen that the protective effect is present in the range of almost all concentrations of the drug tested, but is declining when higher concentrations of drug are used (>20 μM, **Figure 20 AB**). To quantify the effects, CFX IC_{50} (half maximal inhibitory concentration) values were determined with and without QnrB1. For this, the amount of

supercoiled DNA was measured and plotted as the function of ciprofloxacin concentration. The data was fit to the curve: $y = ae^{bx}$ where x is a ciprofloxacin concentration and y equals the percentage of supercoiled DNA equal to percent of supercoiled DNA and a and b are function parameters. In the presence of QnrB1 the value reached 6.34 μM which is almost 8 times higher than the value observed in the absence of protein (0.81 μM).

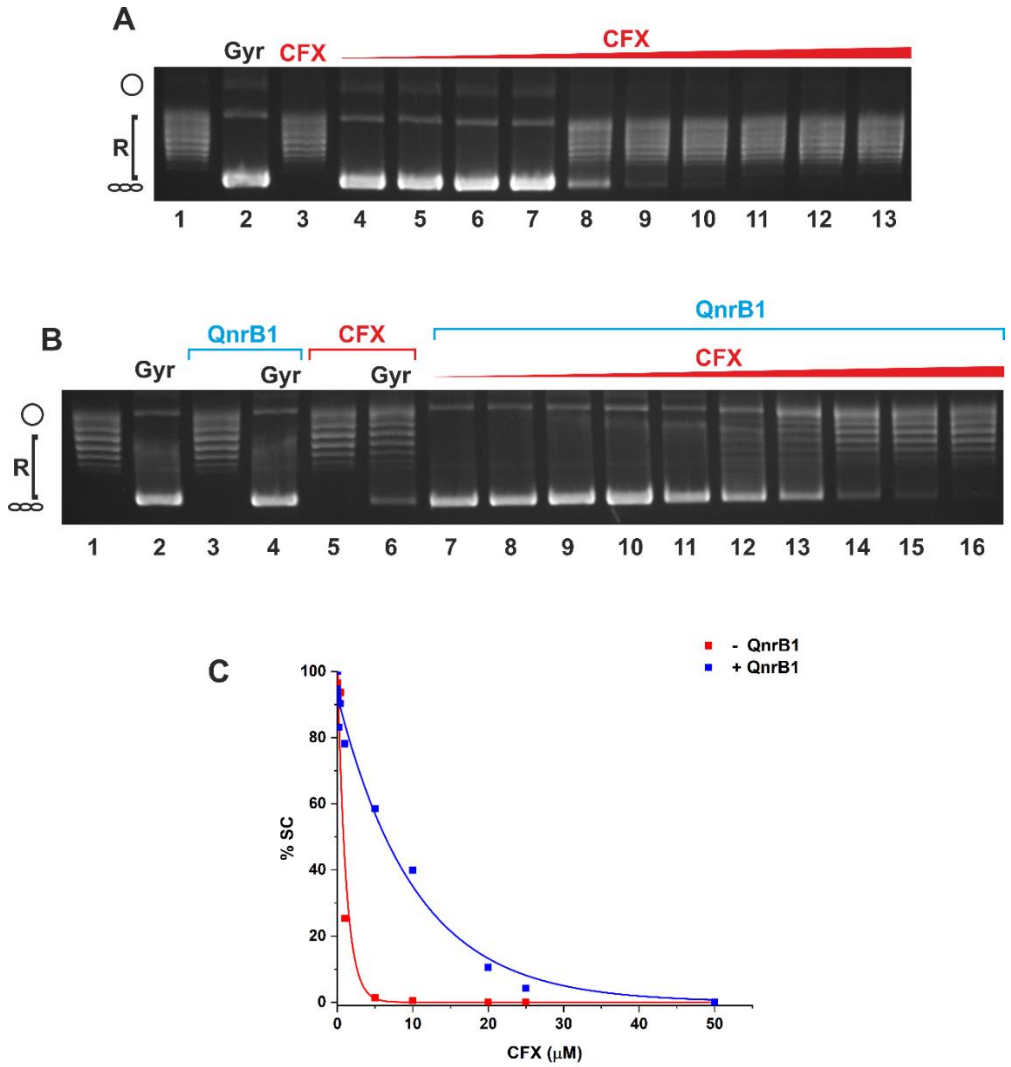

Figure 20 (**A**) Plasmid supercoiling assay showing inhibitory effect of ciprofloxacin: lane 1: relaxed pBR322, lane 2: supercoiling by 1 U of gyrase, lane 3: control for the lack of detectable nuclease activity in 5 μM ciprofloxacin w/o gyrase; lane 4 – 13 inhibition of gyrase supercoiling by increasing concentration of ciprofloxacin (0.0016; 0.08; 0.4; 0.2; 1; 5; 10; 20; 25; 50μM). Positions of negatively supercoiled and relaxed DNA are indicated by the graphics at the left (**B**) Plasmid supercoiling assay showing the protective effect of 5 μM QnrB1 against increasing concentration of ciprofloxacin. Lane 1: relaxed pBR322, lane 2: no nuclease activity was observed upon addition of 50 μM QnrB1, Lane 3: DNA supercoiling in the presence of 50 μM QnrB1; lane 5: no detectable nuclease activity of 5 μM ciprofloxacin w/o gyrase lane 6: inhibition of supercoiling by 5 μM ciprofloxacin; lanes 7-16: protective effect of 5 μM QnrB1 against increasing concentration of ciprofloxacin (0.0016; 0.08; 0.4; 0.2; 1; 5; 10; 20; 25; 50μM). (**C**) Percentage of supercoiled DNA in the presence (blue) and absence (red) of QnrB1 quantified and plotted. Fit curves are shown.

5.2.1.3. Activity in cleavage assays

QnrB1 protection of supercoiling reaction has been postulated due to the fact that QnrB1 reduces the amount of cleaved DNA in the presence of CFX. The cleavage assays can directly show the amount of linear DNA in the reaction allowing to track the change in more quantitative manner. The ability of QnrB1 to rescue DNA gyrase from CFX inhibition was also tested by carrying out DNA gyrase cleavage assays (**Figure 21**). The amount of cleaved DNA in each lane was quantified and the data were fit to the equation $\%\,\text{DNA cleavage} = \%\,\text{max cleavage}\ \frac{[\text{CFX}]}{\text{EC50}_{cfx} + [\text{CFX}]}$ where EC50_{cfx} is concentration of ciprofloxacin in which 50% of maximum cleavage activity is observed. The EC50_{cfx} values were calculated from the fit function. In the absence of QnrB1 the EC50_{cfx} is 0.86 ± 0.09 μM and $\%\,\text{max cleavage}$ was 60 ± 1 %. When QnrB1 was added to the reaction the EC50_{cfx} 1.08 ± 0.32 μM and $\%\,\text{max cleavage}$ is 32 ± 2. Maximum cleavage value dropped twice upon addition of QnrB1 while EC50_{cfx} values for both reactions are similar. Protective activity of QnrB1 in the cleavage assay was already reported but there was no quantification of the phenomenon (Vetting, Hegde, Wang, *et al.*, 2011).

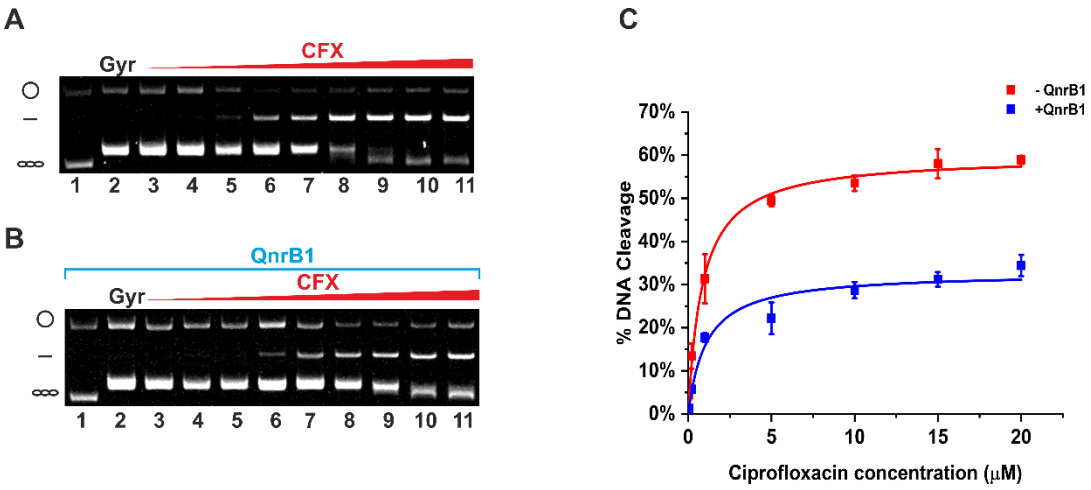

Figure 21. QnrB1 decreases the amount of cleaved DNA in the cleavage assay with ciprofloxacin. (**A**) DNA gyrase (5 U) cleavage reactions with increasing amounts of ciprofloxacin run in the presence of ethidium bromide (EtBr). (**B**) DNA gyrase (5 U) cleavage reactions with increasing amounts of ciprofloxacin in presence of 5 μM QnrB1, run on an EtBr gel. Lane 1, relaxed pBR322. Lane 2, relaxed pBR322 with DNA gyrase. Lanes 3–11, relaxed pBR322 gyrase and increasing concentrations of ciprofloxacin (0.0016, 0.008, 0.04, 0.2, 1, 5, 10, 15, 20 μM) (C) Cleaved DNA in the presence (blue) and absence (red) of QnrB1 quantified and plotted. Error bars represent standard deviation (SD) of 3 independent experiments. The fit lines are presented. Figure adapted from (Mazurek *et al.*, 2021) .

In reverse setup when increasing amounts of QnrB1 were tested with fixed CFX concentration the protective effect was also observed. A lower amount of cleaved DNA can be seen especially in the range of 0.04 μM – 25 μM (**Figure 22**).

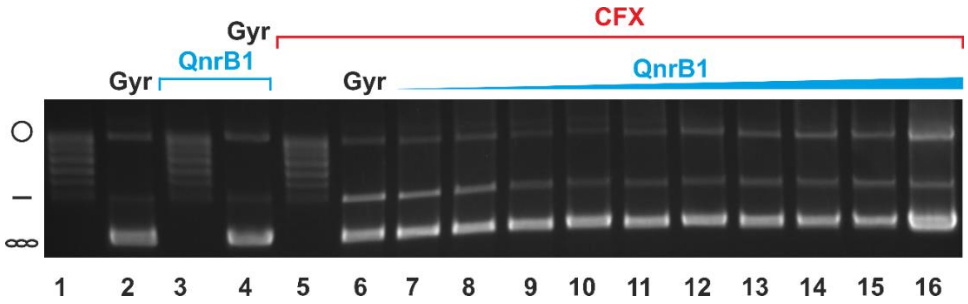

Figure 22. DNA cleavage assay with fixed amount of CFX (0.25 μM) and relaxed DNA as substrate. Lane 1: relaxed pBR322; Lane 2: 5 U of gyrase complex with relaxed pBR322; Lane 3: nuclease control of 50 μM QnrB1; Lane 4: 50 μM QnrB1 with 5 U of gyrase complex; Lane 5: 0.25 μM CFX without DNA gyrase; Lanes 6-16: 0.25 μM CFX with increasing concentration of QnrB1 (0,0.0016,0.008,0.04,0.2,1,5,10,20,25,50 μM)

When negatively supercoiled DNA was used in the assay the protective effect was also manifested (**Figure 23**) and seemed to be more pronounced in lower concentrations of ciprofloxacin. $IC50_{cfx}$ and % max cleavage values for these assays are 0.28 ± 0.09 μM and 51 ± 3 for the reaction without QnrB1 and 4.12 ± 0.89 μM and 46 ± 3 for the reaction with QnrB1. It can be seen that in the case of reaction where negatively supercoiled DNA is used as a substrate, $EC50_{cfx}$ value decreased almost 15 times but the value of % max cleavage is very similar. The difference between obtained results for different DNA substrates could be due to preferential gyrase CFX-induced cleavage of negatively supercoiled DNA.

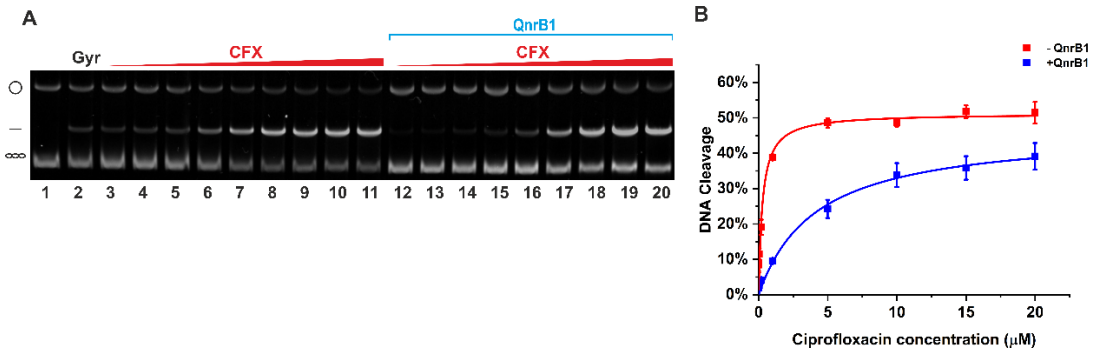

Figure 23. DNA cleavage assay with gyrase A_2B_2 complex and negatively supercoiled DNA as a substrate. Lane 1: negatively supercoiled pBR322; lane 2: negatively supercoiled pBR322 and 5 U (20 nM) A_2B_2; lanes 3 – 11: effect of increasing concentration of ciprofloxacin on DNA cleavage (0.0016; 0.008; 0.04; 0.2; 1; 5; 10; 15; 20 μM). Lanes 12 – 20: effect of increasing concentration of ciprofloxacin on DNA cleavage (same concentrations) in the presence of 5 μM QnrB1. (B) Graph showing dependence of DNA cleavage (percent) from ciprofloxacin concentration for A_2B_2 with (blue squares) and without (red squares) QnrB1. Error bars represent standard deviation (SD) of 3 independent experiments. Figure adapted from (Mazurek *et al.*, 2021) .

Fluoroquinolones can induce DNA cleavage in reactions with truncated gyrase complexes lacking GyrB ATPase domains or CTDs of GyrA (Kampranis and Maxwell, 1996). To test the ability of QnrB1 to protect these truncated constructs, cleavage assays using $GyrA59_2/B_2$ and $GyrA_2/B47_2$ complexes with negatively supercoiled DNA as a substrate were performed. A protective effect of QnrB1 was observed when the $GyrA59_2/B_2$ enzyme complex was used (**Figure 24 AB**). Addition of 5 μM QnrB1 reduced the amount of cleaved DNA however the effect was less pronounced than in the case of cleavage with the full gyrase complex. The parameters obtained from fit curve shown almost 4-fold drop in $EC50_{cfx}$ value with % max cleavage value on the same level ($EC50_{cfx}$ of 2.25 ± 0.44 μM and 64 ± 3 % max cleavage for the reaction in the absence of PRP and $EC50_{cfx}$ of 8.01 ± 1.54 μM and 69 ± 5 of % max cleavage with QnB1 present). When $GyrA_2/B47_2$ enzyme was used there was no measurable protective effect observed. (**Figure 24 C**). The observed protective effect in the case of $GyrA59_2/B_2$ implies that DNA wrapping is not necessary for QnrB1 activity, whilst the strict requirement of ATPase domains is shown by the outcome of the $GyrA_2/B47_2$ assay.

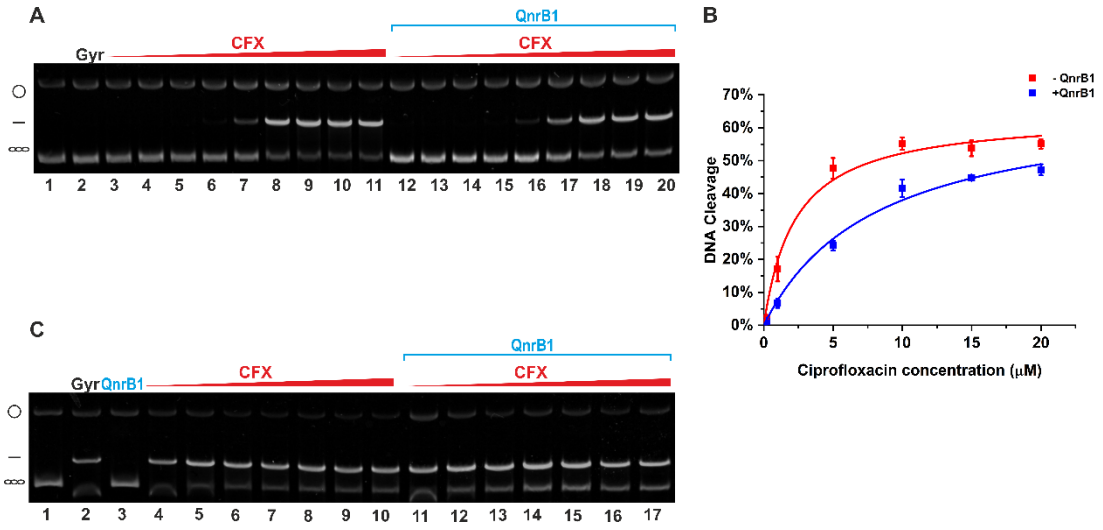

Figure 24. (**A**) DNA cleavage assay with gyrase $A59_2B_2$ complex. Lane 1: negatively supercoiled pBR322; lane 2: negatively supercoiled pBR322 and 20 nM gyrase A592B2 complex; lanes 3 – 11: effect of increasing concentration of ciprofloxacin on DNA cleavage (0.0016; 0.008; 0.04; 0.2; 1; 5; 10; 15; 20 μM) in presence of 5 μM QnrB1. (**B**) Plot of dependence of DNA cleavage (percent) from ciprofloxacin concentration for A592B2 with (blue squares) and without (red squares) QnrB1. Error bars represent standard deviation (SD) of 3 independent experiments. (**C**) DNA cleavage assay with gyrase A_2B47_2 complex. Lane 1: negatively supercoiled pBR322; lane 2: negatively supercoiled pBR322 and 20 nM gyrase A_2B47_2 complex; lane 3 5 μM QnrB1 incubated with DNA (nuclease absence control),4 – 10: effect of increasing concentration of ciprofloxacin on DNA cleavage (0.2; 1; 5; 10; 20; 25; 50 μM). Lanes 11 – 17: effect of increasing concentration of ciprofloxacin on DNA cleavage (0.2; 1; 5; 10; 20; 25; 50 μM) in presence of 5 μM QnrB1. Figure adapted from (Mazurek *et al.*, 2021) .

Gyrase BA core fusion which is devoid of GyrB43 and GyrA C-terminal domains (CTDs), but still able to cleave DNA in the presence of CFX (Schoeffler, May and Berger, 2010) was also tested to check if QnrB1 will be able to protect the enzyme from drug induced cleavage. PRP could not rescue the enzyme from drug activity even at concentrations as high as 50 μM. (**Figure 25**). The lack of protective effect in the context of BA core fusion enzyme can be explained by the absence of ATPase domains in the latter, as was shown by the$GyrA_2/B47_2$ assay (**Figure 24 C**).

There are two possible explanations for this requirement: either PRPs directly interact with ATPase domain to offer protection against CFX induced cleavage or, alternatively, ATP binding to the gyrase or ATP hydrolysis might be required.

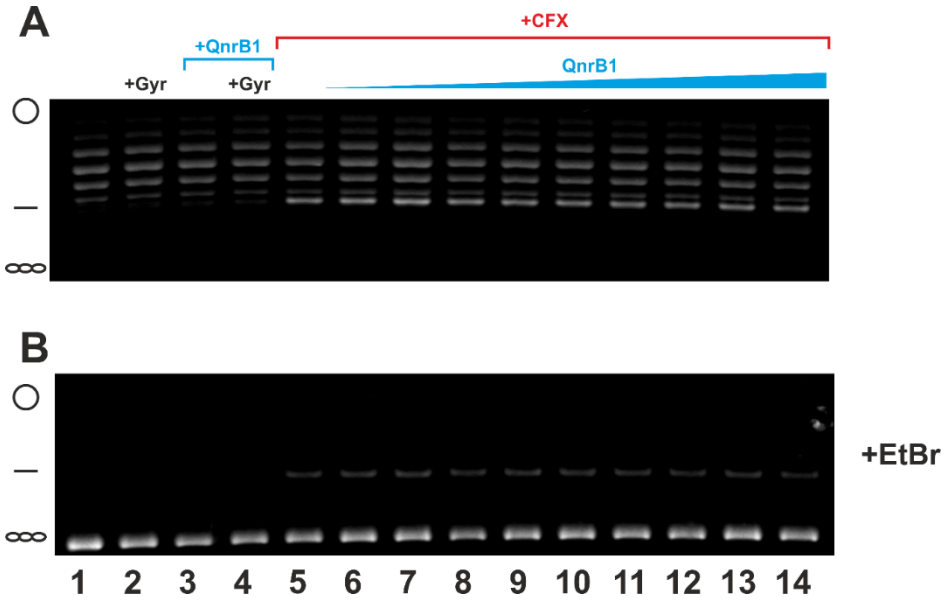

Figure 25. CFX-stimulated cleavage reactions with GyrBA core fusion enzyme and QnrB1**.** DNA cleavage assay with gyrase BA-core fusion enzyme. Lane 1: relaxed pBR322, lane 2: relaxed pBR322 with 20 nM enzyme, lane 3: 50 μM QnrB1 incubated with relaxed pBR322 (nuclease control), lane 4: 50 μM QnrB1 incubated with gyrase BA-core fusion enzyme. Lane 5: effect of 5 μM CFX incubation with relaxed pBR322 and 20 nM enzyme, Lanes 6 -14: effect of increasing concentration of QnrB1 (0.0016; 0.008; 0.04; 0.2; 1; 5; 10; 25; 50 μM) on DNA cleavage in the presence of 5 μM CFX. (**A**) reactions run on gel without ethidium bromide present in gel, (**B**) reactions run on gel with ethidium bromide present in gel.

To assess the potential role of the nucleotide in QnrB1 protection activity, time-course cleavage experiments were performed to monitor CFX-dependent cleavage complex formation in three different conditions: in the presence of ATP or its non-hydrolysable analogue ADPNP, or in the absence of nucleotide. In these assays nucleotides were added last to give QnrB1 an opportunity to bind to gyrase before nucleotide-induced N-gate dimerization. There was no visible effect on cleavage in presence of ADPNP or when the nucleotide was not present in the mixture (**Figure 26 AB**). It is known that G-segment

DNA binding and cleavage generally do not require ATP thus the observed necessity of nucleotide hydrolysis implies that the PRP mechanism is not based on simple G-segment mimicry and drug removal from the gyrase complex. As ADPNP presence was not able to restore QnrB1 activity, we concluded that nucleotide binding itself is not enough to manifest PRP activity. In the presence of ADPNP the enzyme is stabilised in the state where the N-gate is clamped shut since the enzyme cannot reset without ATP hydrolysis (Basu *et al.*, 2012). In this state, the enzyme cannot capture another T-segment to initiate the next round of strand passage. Thus, the ADPNP data suggests mode of action of QnrB1 is associated with the movement of ATPase domains associated with T-segment capture and passage, which presumably creates a conformation accessible to the PRP.

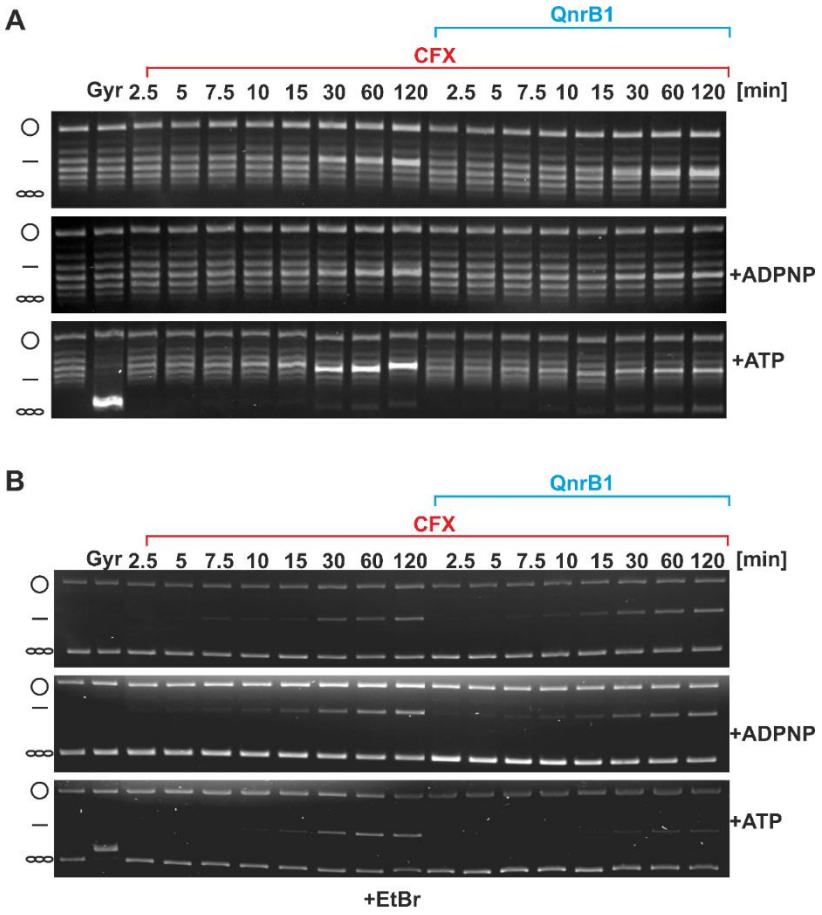

Figure 26. (**A**) Time courses of DNA cleavage. The reactions contained 5 μM ciprofloxacin and 5 μM QnrB1 (as indicated) and were run without nucleotide, with ADPNP or ATP. After completion, the reactions were run on a gel without EtBr. (**B**) Same reactions run in the presence of EtBr. The amount of cleaved DNA is reduced when 5 μM QnrB1 is present and if ATP was added to the reaction. Figure adapted from (Mazurek *et al.*, 2021) .

From the previous experiments a picture emerges of QnrB1 actively rejuvenating stabilised cleavage complexes rather than simply preventing drug binding. To more directly test whether QnrB1 can destabilize cleavage complex after its formation, I

utilised a cleavage complex stability assay. In this assay gyrase is preincubated with a high molar excess of ciprofloxacin in the presence of ATP. Then the reaction is diluted with the buffer containing PRP, and the aliquots of the reaction are taken at given timepoints. The aliquoted mixture is treated with SDS and EDTA to denaturate the enzyme bound to DNA (SDS) and prevent re-ligation of cleaved DNA ends by chelating the catalytic metal (EDTA). The samples representing different endpoints were then visualised on EtBr containing gel. It was clearly observed that in the presence of QnrB1 the amount of cleaved DNA rapidly drops, whereas in the control reaction the cleavage complex remained stable for at least 2 h. The effect was also clearly visible from the plot representing quantified amount of cleaved DNA (**Figure 27 A**). This result implies that QnrB1 is able to destabilise an existing cleavage complex since the PRP is added after preincubation period. The influence on the cleavage complex could also explain the inhibitory activity of high concentrations of QnrB1 on gyrase: the protein might destabilise the temporary cleavage complex that is natively present during normal gyrase catalytic cycle. Further tests of QnrB1 influence on cleavage complex formation was done by calcium cleavage assays. In this assays $MgCl_2$ is replaced with $CaCl_2$.which leads to the stabilisation of cleavage complex without adding drug (Osheroff and Zechiedrich, 1987). When 50 μM QnrB1 was added to the time-course cleavage reaction in the presence of $CaCl_2$, a reduction in amount of linear DNA was observed (**Figure 27 B**). To summarise, the necessity of ATP and the fact that preincubation with ADPNP leads to lack of QnrB1 protection suggests that ATP hydrolysis is required for the PRP to act, whilst the reduction of cleavage (drug and Ca^{2+} induced) suggests that the PRP acts by reducing the amount of formed cleavage complex.

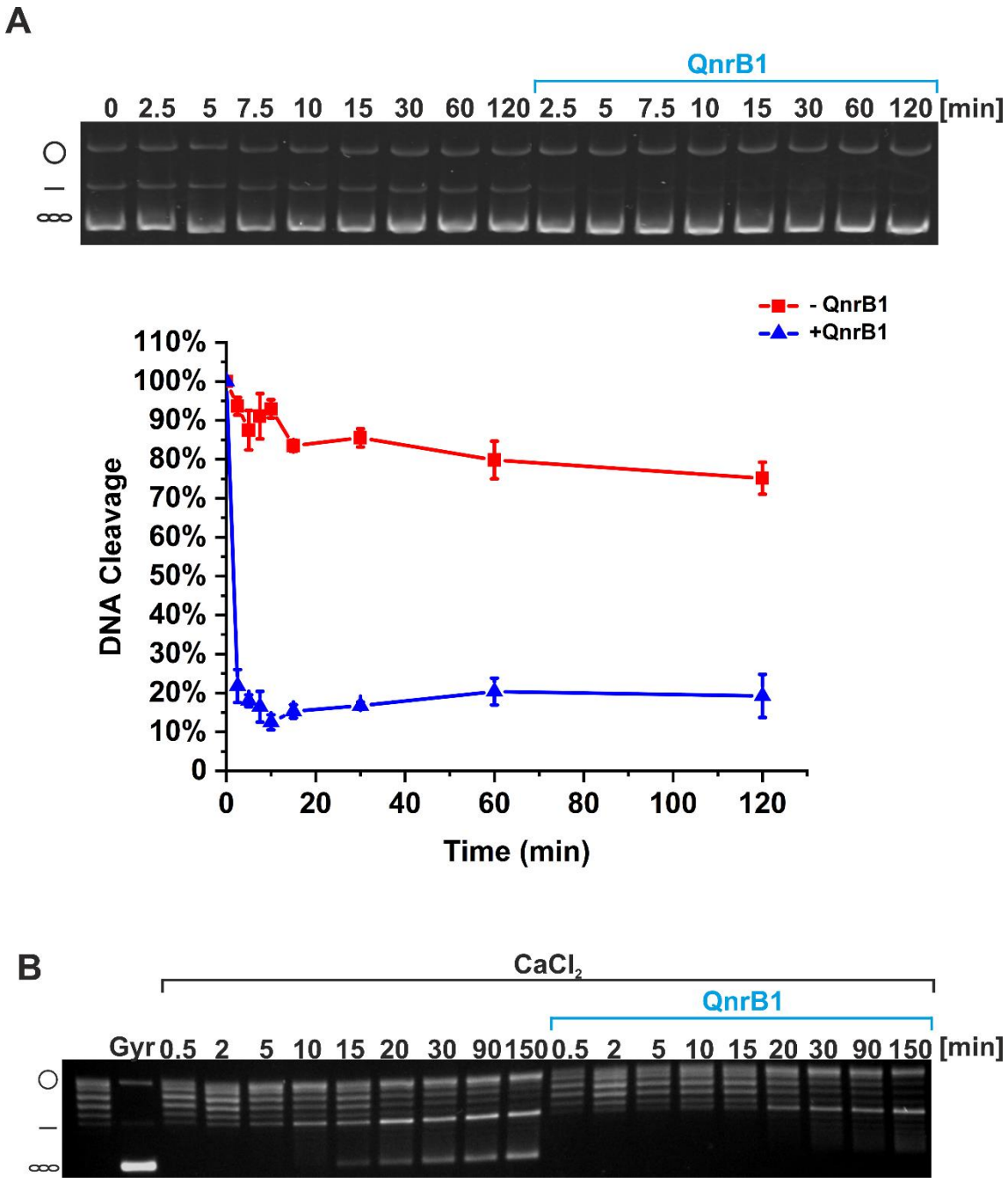

Figure 27. (**A**) (Top) Cleavage complex stability determined in the presence of 5μM QnrB1. Initial DNA cleavage reactions were incubated with 80 U of gyrase and 20 μM ciprofloxacin and were incubated for 10 min at 37 ˚C to reach equilibrium and then diluted 20-fold with reaction buffer with or without 5 μM QnrB1 and further incubated. The samples were run on an EtBr gel. (Bottom) Percentage of linear DNA was quantified and plotted. Level of DNA cleavage at time 0 was set to 100%. Error bars represent the SD of at least three independent experiments. (**B**) Time course of 4 $CaCl_2$ induced cleavage. The reactions contained 4 mM $CaCl_2$, and 50 μM QnrB1. Where there was no $CaCl_2$ it was replaced with 4 mM $MgCl_2$. Figure adapted from (Mazurek *et al.*, 2021) .

It has been shown that DNA gyrase can cleave short linear DNA fragments in the presence of quinolone antibiotics(Cove, Tingey and Maxwell, 1997). To check the influence of QnrB1 on cleavage induced by CFX on shorter DNA strands, and completely rule out the role of DNA wrapping in PRP mechanism, cleavage assays were performed using short

fragments of DNA (79 bp, 100 bp, 133 bp, 147 bp, 220 bp, 300 bp). QnrB1 was able to reduce the amount of cleavage regardless of the length of tested DNA fragments (**Figure 28**). Those results together with results obtained for $GyrA59_2/B_2$ cleavage assays (**Figure 24 AB**) show that QnrB1 does not need wrapped DNA to act.

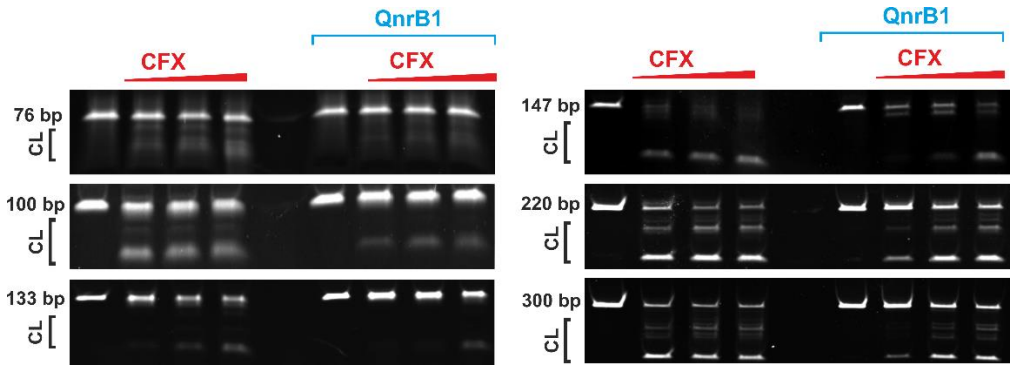

Figure 28. **Cleavage of short DNA fragments by DNA gyrase and protection by QnrB1**. Length of fragments (in base pairs) is indicated at the left. CL – cleaved DNA. 50 nM gyrase complex is present in each reaction. QnrB1 (5 μM) and CFX (0.1, 1, 10 μM) were added as indicated. Figure adapted from (Mazurek *et al.*, 2021) .

5.2.1.4. Activity in gyrase relaxation assays

The function of ATP in the mechanism of DNA gyrase is thought to be in driving top-to-bottom strand passage of the T-segment through the enzyme, the process that might open up the route for the QnrB1 to access the bound drug/catalytic centre. However, DNA gyrase in absence of ATP is able to relax negatively supercoiled DNA (Gellert *et al.*, 1977; Sugino *et al.*, 1977) in a reaction where strand passage is believed to proceed in the reverse direction (bottom to top) (Kampranis and Maxwell, 1996). Strikingly, this reaction was not inhibited by QnrB1 at any concentration. Actually, QnrB1 concentration-dependent *stimulation* of relaxation activity was observed (**Figure 29 A**). The effect was best observed in the presence of high QnrB1 concentrations (~20 μM) in a time-course relaxation assay (**Figure 29 B**). The relaxation stimulation effect was abolished when CFX was present in the reaction and the inhibition of relaxation can be observed upon higher QnrB1 concentrations under this condition (**Figure 29 C**). Despite the absence of ATP, QnrB1 is still able to act on gyrase. Therefore, ATP hydrolysis is not required for QnrB1 binding. At the same time, absence of inhibition in the relaxation experiment does rule out the hypothesis that QnrB1 interacts with ATPase domains dispensable for the relaxation reaction.

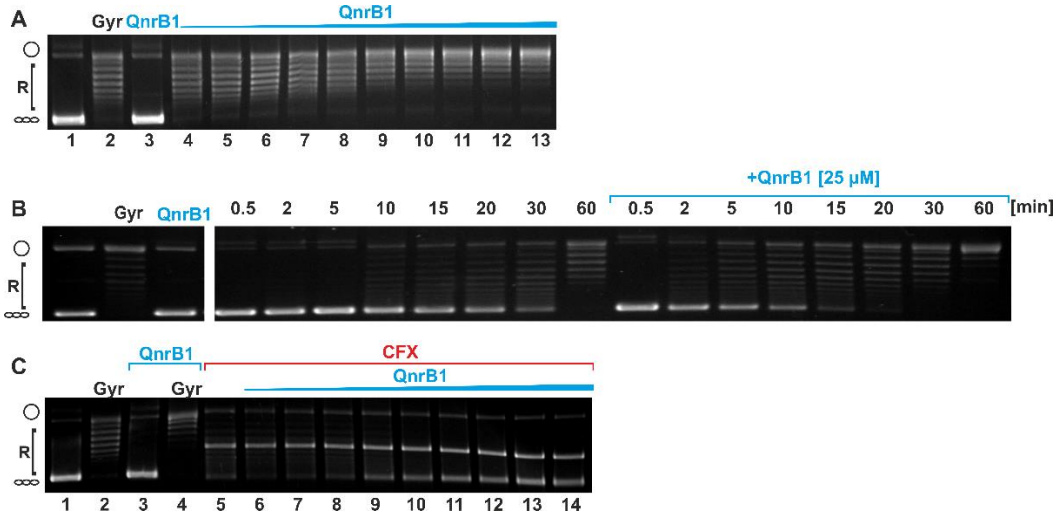

Figure 29. Effect of QnrB1 on ATP-independent relaxation**.** (**A**) Relaxation of negatively supercoiled DNA in presence of increasing QnrB1 concentrations. Lane 1: negatively supercoiled pBR322; lane 2: relaxation by gyrase; lane 3: lack of detectable nuclease activity in the purified QnrB1 (50 µM QnrB1); lanes 4-13: relaxation in presence of increasing concentrations of QnrB1 (0.0016, 0.008; 0.04; 0.2; 1; 5; 10; 20; 25; 50 µM). **(B)** Time course of DNA relaxation in presence of QnrB1. Gyr: DNA and gyrase after 60 minutes. QnrB1: nuclease control (50 µM QnrB1+DNA). Time points are indicated above the lanes. **(C)** Relaxation of negatively supercoiled DNA in the presence of ciprofloxacin and increasing QnrB1 concentrations. Samples were treated with SDS and proteinase K to release cleaved DNA. Lane 1: negatively supercoiled pBR322; lane 2: relaxation by 20 nM gyrase; lane 3: lack of detectable nuclease activity in the purified QnrB1 (50 µM QnrB1); lane 4: relaxation in the presence of 50 µM QnrB1; lanes 5-14: DNA relaxation in the presence of CFX (5 µM) and (6-14) the effect of increasing concentrations of QnrB1 (0.008; 0.04; 0.2; 1; 5; 10; 20; 25; 50 µM). Figure adapted from (Mazurek *et al.*, 2021) .

To further test the requirement for strand passage, relaxation activities of $A59_2/B_2$ and $A_2/B47_2$ gyrase complexes were tested. Gyrase complexes $A59_2/B_2$ (capable of performing ATP-dependent relaxation) and $A_2/B47_2$ (capable of performing ATP-independent relaxation). $A59_2/B_2$ complex does not is lack the CTD domain so the rapping of DNA is not possible during the reaction. $A_2/B47_2$ complex is not able to perform ATP hydrolysis due to the fact that ATPase domain is deleted. The reaction conditions and results of those relaxation assays are presented in **Table 10**.

Table 10. Conditions and result of relaxation assay with truncated gyrase enzymes with QnrB1 and ciprofloxacin**.**

Enzyme complex	$A59_2/B_2$		$A_2/B47_2$	
Relaxation ATP dependence	Dependent		Not dependent	
CFX presence	-	+	-	+
QnrB1 influence	Inhibition of relaxation reaction	Lack of protection	Stimulation of relaxation reaction	Lack of protection

In both cases the protection effect was not observed in the presence of ciprofloxacin (**Figure 30 AB**). The reaction of ATP – dependent relaxation by $A59/B_2$ was strongly

inhibited by PRP. However, the effects of Qnrb1 tested in those relaxation assays without the drug were different. ATP-dependent relaxation was again inhibited, ATP-independent relaxation was stimulated similarly like in the case of A_2B_2 gyrase complex ATP independent relaxation. (**Figure 30 CD**, **Figure 29 A**). The strand passage occurring during ATP - independent relaxation performed by A_2/B47$_2$ complex is not driven by ATP hydrolysis. In ATP – dependent relaxation by A59/B_2 the strand passage is believed to occur in top to bottom manner (N-gate to C-gate) akin to Topo IV or eukaryotic Topo II (Kampranis and Maxwell, 1996). manner yet QnrB1 is still not able to rescue the relaxation reaction. These results together suggest that QnrB1 is able to inhibit gyrase reactions and provide protection against FQs only when "standard" top to bottom strand passage, coupled with ATP hydrolysis is happening. Potentially the inhibition could result from the decreased DNA capture by the enzyme in presence of PRP due to the fact of competition between QnrB1 and T-segment for binding to the GyrB subunit.

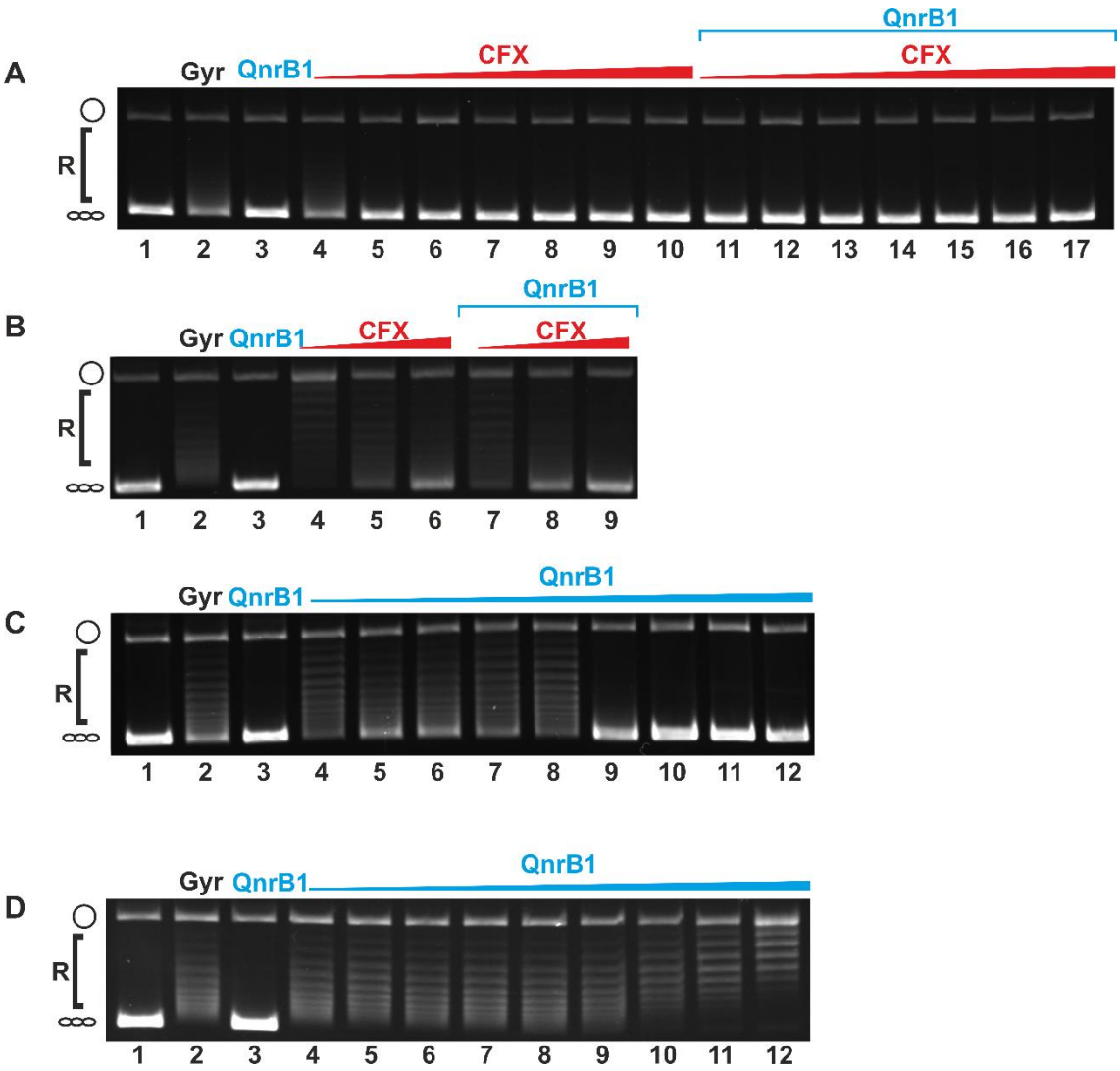

Figure 30. Effects of QnrB1 on relaxation by truncated gyrase enzymes: ATP-dependent (by $A59_2/B_2$) and ATP-independent (by $A_2/B47_2$). (**A)** $A59_2/B_2$ ATP-dependent relaxation assay in presence of increasing concentration of ciprofloxacin and 5 μM QnrB1. Lane 1: negatively supercoiled pBR322; lane 2: relaxation by $A59_2/B_2$; lane 3: relaxation in the presence of 50 μM QnrB1; lanes 4-10: DNA relaxation in the presence of increasing concentrations of CFX (0.2; 1; 5; 10; 20; 25; 50 μM); lanes 11-17: DNA relaxation in the presence of increasing concentrations of CFX (as before) and 5 μM QnrB1. (**B**) $A_2/B47_2$ ATP-independent relaxation assay in the presence of increasing concentrations of ciprofloxacin and 5 μM QnrB1. Lane 1: negatively supercoiled pBR32; lane 2: relaxation by $A_2/B47_2$; lane 3: relaxation in the presence of 50 μM QnrB1; lanes 4-6: DNA relaxation in the presence of increasing concentrations of CFX (20; 35; 50 μM); lanes 7-9: DNA relaxation in the presence of increasing concentrations of CFX (as before) and 5 μM QnrB1 (**C**) $A59_2/B_2$ ATP-dependent relaxation assay in the presence of increasing concentrations of QnrB1. Lane 1: negatively supercoiled pBR322; lane 2: relaxation by $A59_2/B_2$; lane 3: relaxation in the presence of 40 μM QnrB1; lanes 4-12: DNA relaxation in the presence of increasing concentrations of QnrB1 (0.0016; 0.008; 0.04; 0.2; 1; 5; 10; 20; 40 μM). All of above-described reactions contain standard supercoiling buffer with ATP. (**D**) $A_2/B47_2$ ATP-independent relaxation assay in the presence of increasing concentrations of QnrB1. Lane 1: negatively supercoiled pBR322; lane 2: relaxation by $A_2/B47_2$; lane 3: relaxation in the presence of 40 μM QnrB1; lanes 4-12: DNA relaxation in the presence of increasing concentrations of QnrB1 (0.0016; 0.008; 0.04; 0.2; 1; 5; 10; 20; 40 μM). Figure adapted from (Mazurek *et al.*, 2021) .

5.2.1.5. QnrB1 influence on DNA binding

EMSA experiments, reporting the formation of the wrapped DNA-bound gyrase complex, were performed to test QnrB1 influence on DNA binding by gyrase. Increasing concentrations of QnrB1 were found to outcompete 147 bp fragment containing the strong gyrase binding site from plasmid pBR322 (**Figure 31 A**). The amounts of bound and free DNA were quantified using a densitometry approach. Obtained values of fraction of free DNA were then plotted as a function of QnrB1 concentration. The QnrB1 IC_{50} value of DNA competition was calculated from standard one site specific binding equation: $\text{Binding} = \frac{\text{Fmax}*[\text{QnrB1}]}{\text{IC}_{50\,QnrB1}*[\text{QnrB1}]}$ where Fmax is the maximum fraction of free DNA and IC_{50} is the QnrB1 concentration that is needed for 50 % inhibition of DNA binding. After fitting the curve, the IC_{50} parameter equalled 10.93 ± 0.58 μM. (**Figure 31 B**). This value is ~5 times lower than estimated value of EC_{50} of QnrB1 protective activity in gyrase supercoiling reaction (**Figure 19 A**) This result is in line with the values required for the inhibition of supercoiling in the presence of high concentration of QnrB1 (>10 μM) (**Figure 19 B**). It seems that QnrB1 at high concentrations is competing with DNA to bind to DNA gyrase. At the same time, in the presence of 5 μM CFX that is known to stabilise DNA binding, competition effect of QnrB1 was not observed even in concentration as high as 40 μM (**Figure 31 C**).

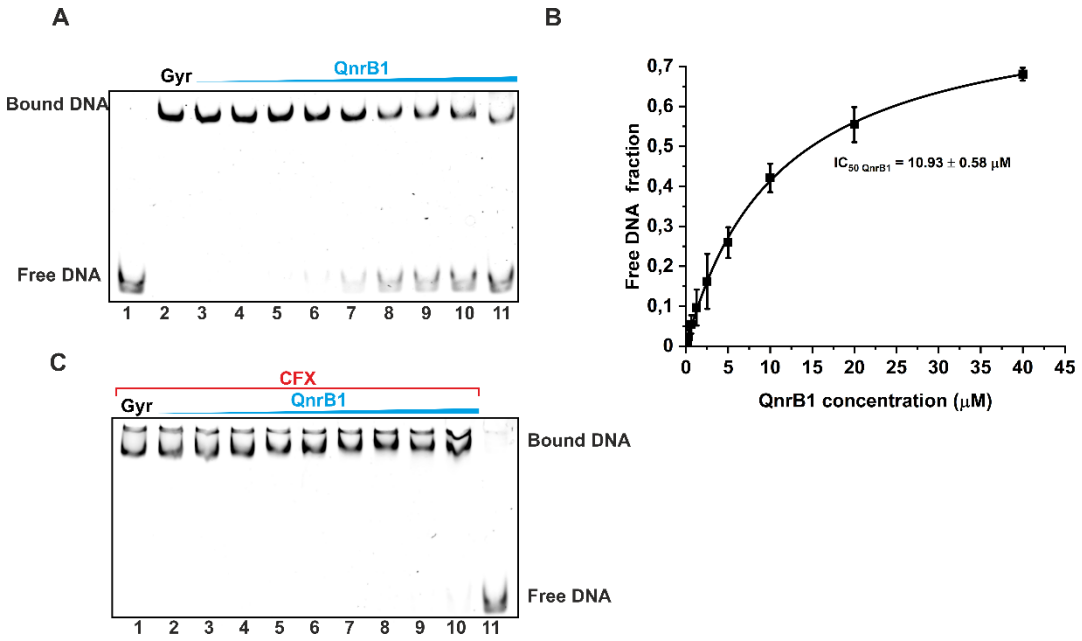

Figure 31. Effects of QnrB1 on DNA binding by gyrase**.** (**A**) EMSA showing the effect of increasing concentration of QnrB1 on DNA binding. Shown is SYBR Gold-stained 6% TBM gel. Lane 1: free 147 bp DNA; lane 2: gyrase (200 nM) added to DNA; lanes 3-11: effect of increasing concentrations (0.2; 0.3; 0.6; 1.3; 2.5; 5; 10; 20; 40 μM) of QnrB1 on DNA binding by gyrase. (**B**) Graph showing dependence of free DNA fraction on concentration of QnrB1. IC_{50} value for QnrB1 is calculated from the fit curve. Error bars are expressed as the standard deviation of three independent experiments. (**C**) Effect of increasing concentration of QnrB1 on DNA binding in the presence of 5 μM CFX. Lane 1: gyrase, DNA and 5 μM CFX; lane 2-10: effect of increasing concentration (0.2; 0.3; 0.6; 1.3; 2.5; 5; 10; 20; 40 μM) of QnrB1 on DNA binding by DNA gyrase; lane 11: free DNA. Figure adapted from (Mazurek *et al.*, 2021) .

Fluorescence anisotropy has been previously used to measure competition between 37 bp DNA fragment and protein YacG for binding to the DNA gyrase (Vos *et al.*, 2014). A similar methodology was used to measure competition between QnrB1 and DNA. Cy-5 labelled 90 bp pBR322 containing the gyrase binding site was used in the experiment. 20 nM of DNA and 1 μM gyrase complex was mixed with increasing concentrations of label-free QnrB1. The significant drop in fluorescence anisotropy was observed starting from 5 μM QnrB1 (**Figure 32 A**). Unfortunately, due to aggregation of QnrB1, higher concentrations than 40 μM could not be used in the assay which prevented us from reaching the lower plateau of the anisotropy curve. No fit was performed since competition parameters could not be calculated with certainty.

The reverse setup was also prepared: for this, 50 nM Alexa-488 N-terminal labelled QnrB1 was preincubated with 1 μM gyrase complex. Increasing amounts of label-free 90 bp fragment of pBR322 containing the strong gyrase binding site was titrated into the reaction. The change in fluorescence anisotropy was also observed in this case pointing at specific competition of QnrB1 and DNA. The drop in fluorescence was observed

starting from 3.8 μM concentration of base pairs (**Figure 32 B**). To summarise, both DNA binding assay strongly support the competition between QnrB1 and DNA.

.

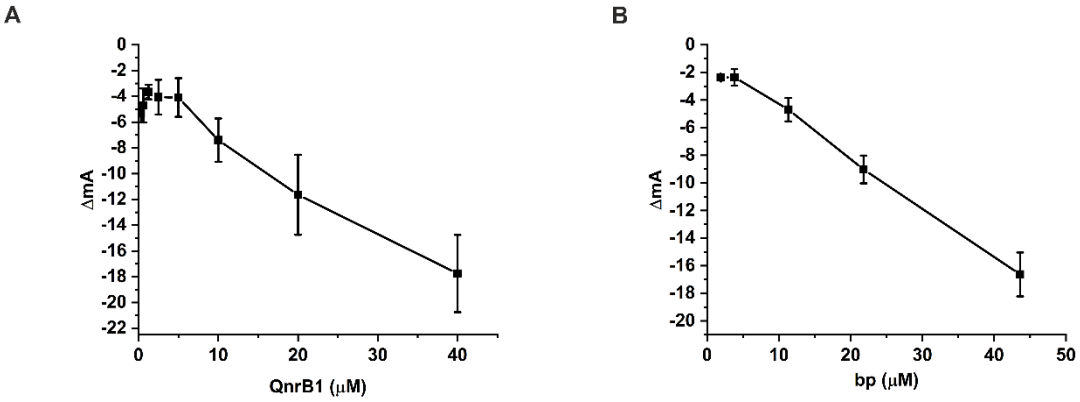

Figure 32. (**A**) Fluorescence anisotropy measurement of QnrB1 displacement by increasing concentration of linear DNA (linear 90 bp pBR322). 50 nM Alexa-488-QnrB1 and 1 μM DNA gyrase complex was used in reaction. Concentrations of linear DNA calculated as concentration of base pairs (bp) were as follows: (2; 4; 11; 22; 44 μM). (**B**) Fluorescence anisotropy measurement of DNA displacement by increasing concentration of QnrB1. 20 nM 90 bp DNA-Cy5 and 1 μM DNA gyrase complex was used in reaction. Concentrations of QnrB1 were as follows: (0.3125; 0.625; 1.25; 2.5; 5; 10; 20; 40 μM). Figure adapted from (Mazurek *et al.*, 2021) .

5.2.1.6. Influence on gyrase ATPase activity

Previous experiments clearly shown importance of ATP hydrolysis by the enzyme for QnrB1 activity. If interacting with ATPase domains, the PRP could be able to influence the hydrolysis itself. ATPase activity assays were performed to check the influence of QnrB1 on intrinsic and DNA-stimulated ATPase activity of DNA gyrase. In the absence of DNA, 5 μM QnrB1 stimulated the ATP hydrolysis rate about threefold. The DNA-stimulated rate was not affected. (**Figure 33 A**). When the isolated GyrB43 (ATPase subunit) subunit was tested, the observed ATPase reaction rate upon addition of QnrB1 was ∼17 times higher than the observed rate with no QnrB1 (**Figure 33 B**). QnrB1 ΔTTR previously tested in supercoiling assays (**Figure 19 D**) stimulated the B43 gyrase subdomain to the same extent as full-length QnrB1 **Figure 33 C**).

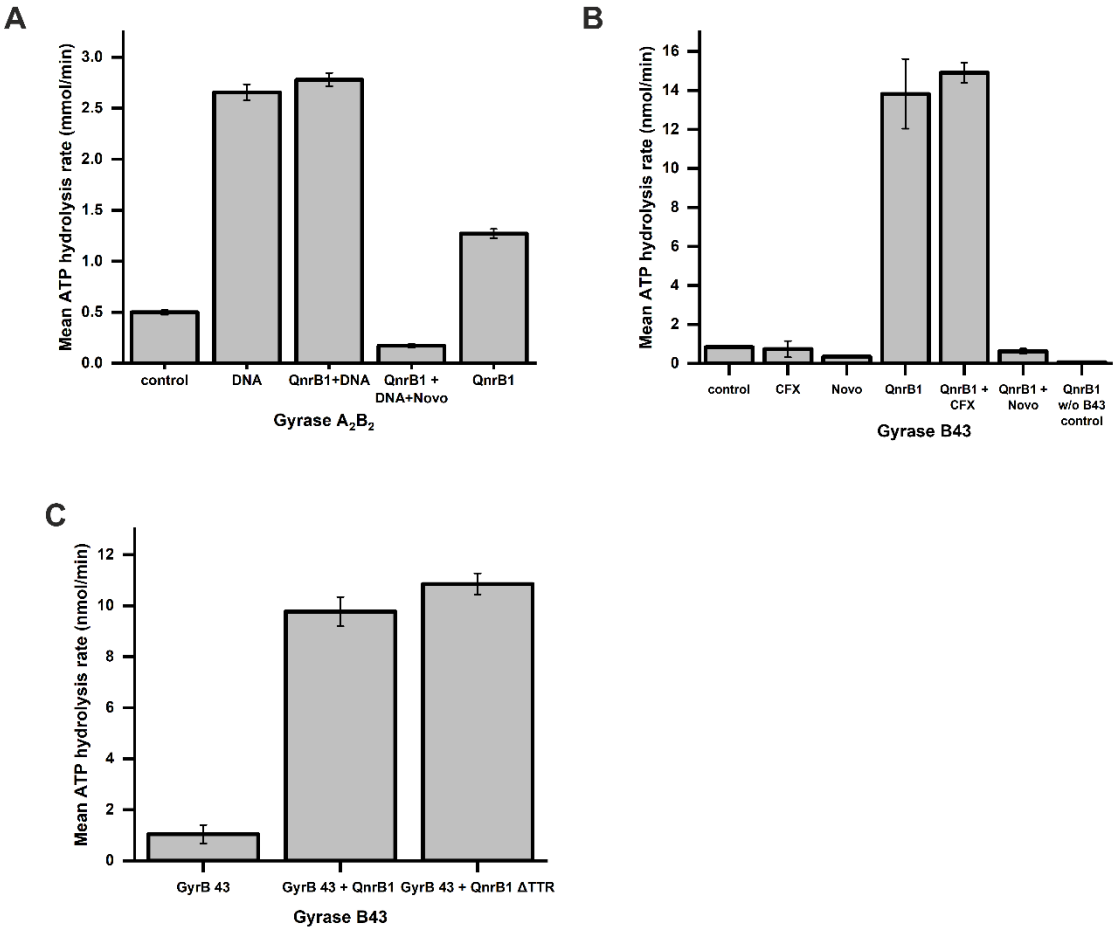

Figure 33. (**A**) ATPase rate data for 50 nM gyrase (A_2B_2) complex mixed with: 10 nM DNA; 10 nM DNA and 5 μM QnrB1;10 nM DNA ,5 μM QnrB1 and 50 μM novobiocin; 5 μM QnrB1. (**B**) ATPase rate data for 4 μM GyrB43 mixed with QnrB1, drugs and DNA as indicated. DNA was used at 10 nM, novobiocin (Novo) at 50 μM, CFX at 5 μM and QnrB1 at 5 μM. (**C**) ATPase rate data for 4 μM GyrB43 mixed with 5 μM QnrB1 and 5 μM QnrB1 ΔTTR. Error bars are expressed as the standard deviation of three independent experiments. (**C**) ATPase rate data for 4 μM GyrB43 mixed with 5 μM QnrB1 and 5 μM QnrB1 ΔTTR. Error bars are expressed as the standard deviation of three independent experiments. Figure adapted from (Mazurek *et al.*, 2021) .

To check PRP influence on ATPase hydrolysis kinetics I carried out a series of assays with increasing substrate (ATP) concentration and 5 μM QnrB1. The ATPase rate was then plotted as a function of ATP concentration. GyrB43 stimulation followed Michaelis– Menten kinetics described with equation $V = Vmax\frac{[ATP]}{K_m+[ATP]}$ with calculated values: (Vmax(–QnrB1) = 0.986 ± 0.075 nmol/min) vs (Vmax(+QnrB1) = 17.1 ± 1.1 nmol/min). K_m values for ATP for GyrB43 ATPase stimulated reactions are in the same order of magnitude as values for non-stimulated reactions ($K_{m\,-\,QnrB1}$ = 0.46 ± 0.15 mM, $K_{m\,+\,QnrB1}$ = 0.96 ± 0.17 mM) (**Figure 34 A**). Vmax value increased 17-times whilst K_m value was not altered significantly.

When increasing concentration of QnrB1 were added to ATPase assay with 4 μM B43 gyrase domain and constant amount of ATP (1 mM), the stimulation effect of ATP rate shown QnrB1 – concentration dependency. When plotted, the reaction hyperbolic shape. After performing a fit to Hill equation $V = Vmax\frac{[QnrB1]^n}{{K_m}^n+[QnrB1]^n}$ where n is Hill coefficient, the obtained parameters (Km = 3.61 ± 0.57 μM, Vmax = 15.19 ± 0.62 nmol/min and n = 1.07 ± 0.18) suggests that the QnrB1 binding to the GyrB43 domain is non cooperative (**Figure 34 B**) (Weiss, 1997).

QnrB1 Δ106-108 mutant was stimulating the ATPase activity of B43 to the same extent, suggesting that the residues that are important for protective activity of protein are not necessary for interaction with the B43 gyrase domain. Observed ATPase stimulation effect once again suggests the importance of ATP hydrolysis in PRP activity. the Similar results were obtained for the 'loopless' homolog of QnrB1 from *Mycobacterium smegmatis* (MsMfpA), where the addition of PRP led to the 10-fold stimulation of ATP hydrolysis (Feng *et al.*, 2021).

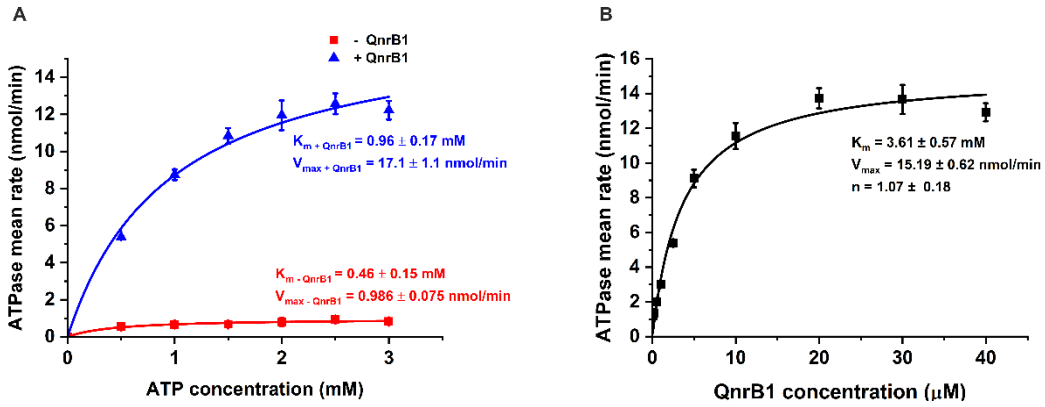

Figure 34. (**A**) ATPase rate data and Michaelis-Menten fits for series of experiments conducted with different concentrations of ATP with (blue) or without (red) 5 μM QnrB1 for GyrB43. (**B**) ATPase rates and Michaelis-Menten fit for series of assays conducted with 4 μM GyrB43 conducted with different concentrations of QnrB1 at constant concentration of ATP (1 mM). For all plots, error bars are expressed as the standard deviation of three independent experiments for the rate (nmol/min). Figure adapted from (Mazurek *et al.*, 2021) .

5.2.1.7. Direct studies of QnrB1-Gyrase interaction

Previously presented experiments provided indirect evidence for the physical interaction of PRP and gyrase, therefore I designed a set of binding experiments to directly show the level of interaction between the proteins. First, pull-down experiments were carried out to examine QnrB1 binding to gyrase subunits. N – terminally FLAG tagged QnrB1 protein was mixed with purified GyrA, GyrB or gyrase complex, incubated with a resin

conjugated with anti-FLAG-specific antibody, and the unbound proteins were washed by a low-salt buffer and analysed by SDS-PAGE. QnrB1 bearing an N-terminal FLAG (DYKDDDDK) (Hopp *et al.*, 1988) epitope tag was able to interact with GyrB subunit alone and as a part of the gyrase complex. When FLAG-QnrB1 was incubated with the GyrA subunit, the GyrA was not observed in pull-down eluates. but as expected GyrA subunit was found in pull-down eluates in the context of full gyrase complex due to elution, when GyrB subunit was also present (GyrB is strongly bounded to GyrA when mixed as a complex). This pattern can be explained if we propose that the main interaction occurs between QnrB1 and GyrB subunit, and this interaction does not prevent the formation of the gyrase complex.

As addition of ADPNP leads to irreversible GyrB N-gate dimerization, thus I tested whether formation of a dimer precludes interaction with QnrB1. Indeed, preincubation of reactions with ADPNP led to complete disappearance of gyrase subunits in eluates as observed on a gel shown in **Figure 35**. This effect correlates with the observation of lack of QnrB1 cleavage protection activity in gyrase assays when a non-hydrolysable analogue of nucleotide is present in the reaction (**Figure 26**). The lack of interaction upon addition of ADPNP was also observed in the case of GyrB subunit alone. Observed lack of pull-down on those samples implies that the QnrB1 binding site is likely located on the interface of GyrB subunit forming the inner cavity interacting with T-segment DNA.

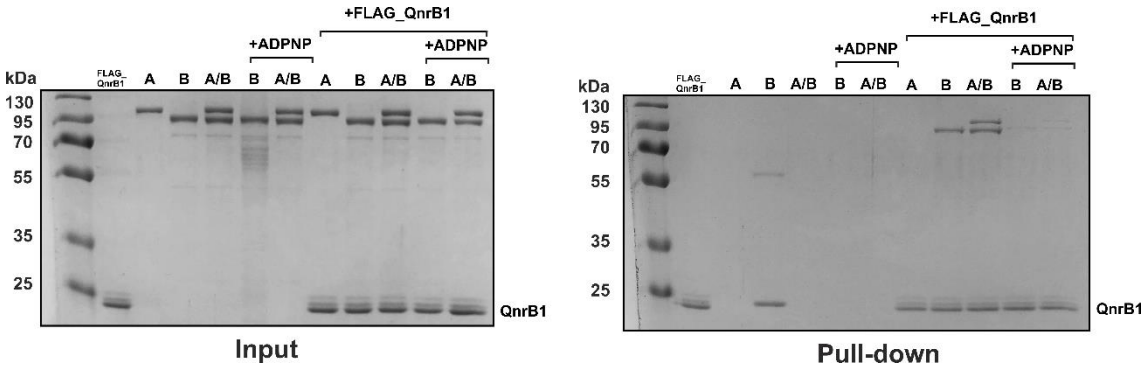

Figure 35. Pull-down assay with N-terminally FLAG-tagged QnrB1 and purified GyrA, GyrB and A_2B_2 complex. *Left* – input, *right* – pull-down (eluates from M2 (α-FLAG) agarose). A Coomassie stained SDS-PAGE gel is shown. Line containing gyrase B control on pull-down gel is contaminated with light and heavy chains of anti-FLAG antibody. Figure adapted from (Mazurek *et al.*, 2021) .

Further, I investigated the influence of $\Delta_{106\text{-}108}$ deletion in QnrB1 for the interaction. The interaction between N-terminally-FLAG tagged QnrB1$\Delta_{106\text{-}108}$ or QnrB1Δ_{106} mutants and GyrB was weakened, but not completely abolished (**Figure 36**).

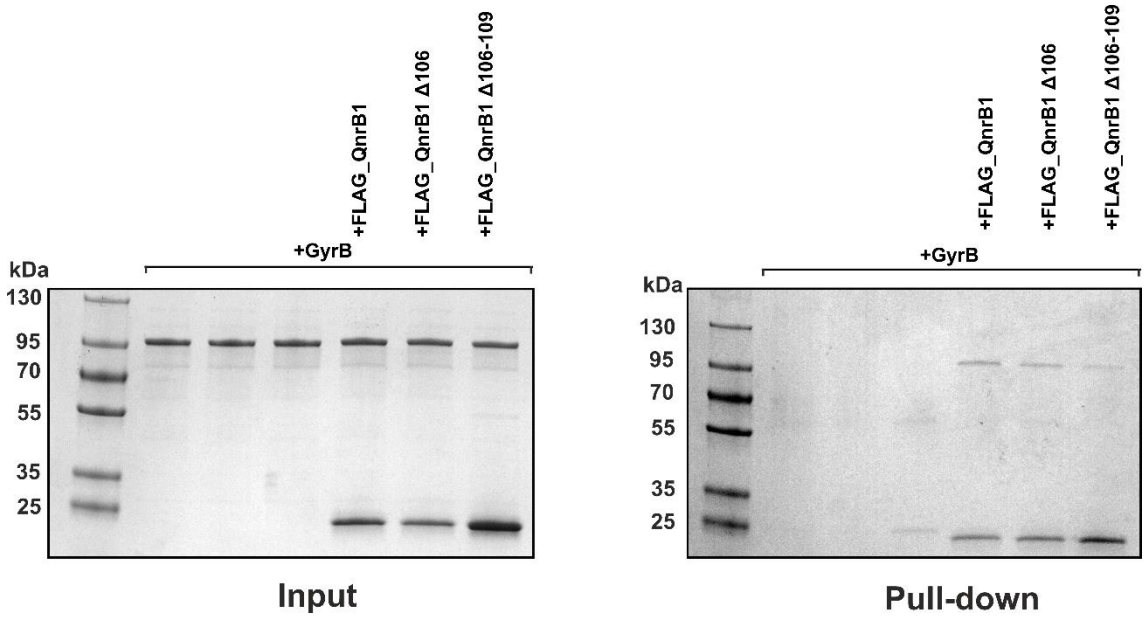

Figure 36. Pull-down assay with N-terminally FLAG-tagged QnrB1 Δ_{106} and QnrB1 $\Delta_{106\text{-}108}$ with purified GyrB. *Left* – input, *right* – pull-down (eluates from M2 (α-FLAG) agarose). A Coomassie stained SDS-PAGE gel is shown. Figure adapted from (Mazurek *et al.*, 2021) .

To rule out possible interference of N-terminal FLAG tag with binding to the GyrA, the reverse pull-down experiment was carried out where C-terminally 6x-His-tagged QnrB1 was mixed with 3xFLAG-GyrB, 3xFLAG-GyrB/GyrA complex or GyrB/GyrA-FLAG complex. Pull-down was observed only when a FLAG-tagged GyrB subunit was present. In this setup preincubation of reaction with ADPNP also abolished the binding (**Figure 37**).

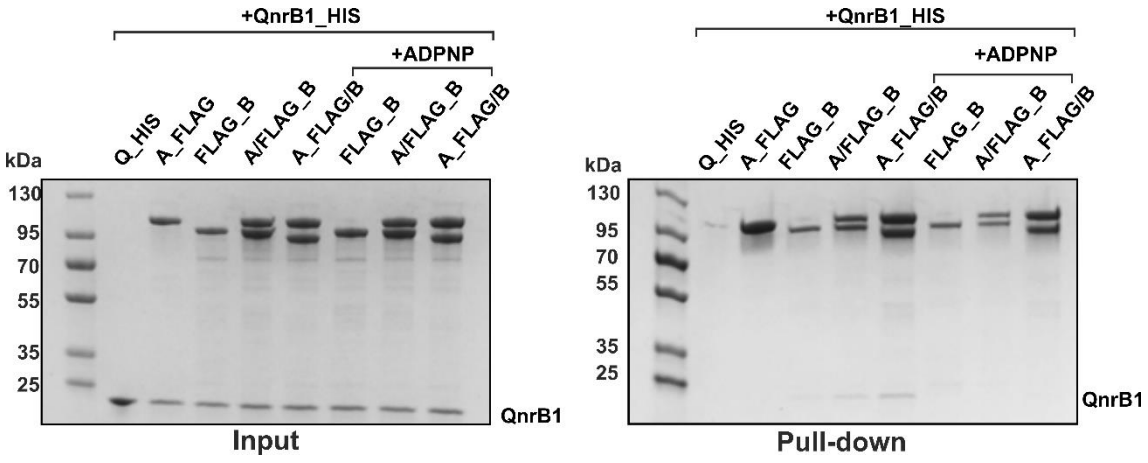

Figure 37. Pull-down assay with 3xFLAG-GyrB, GyrA-FLAG, 3xFLAG-GyrB/GyrA complex or GyrB/GyrA-FLAG complex with C-terminally his-tagged QnrB1. *Left* – input, *right* – pull-down (eluates from M2 (α-FLAG) agarose). A Coomassie stained SDS-PAGE gel is shown.

Smaller parts of gyrase B subunit were also tested for their ability to co-precipitate with N-terminally FLAG tagged QnrB1. Out of all the subdomains tested only the full-length GyrB subunit was able to interact with the QnrB1 protein (**Figure 38**).

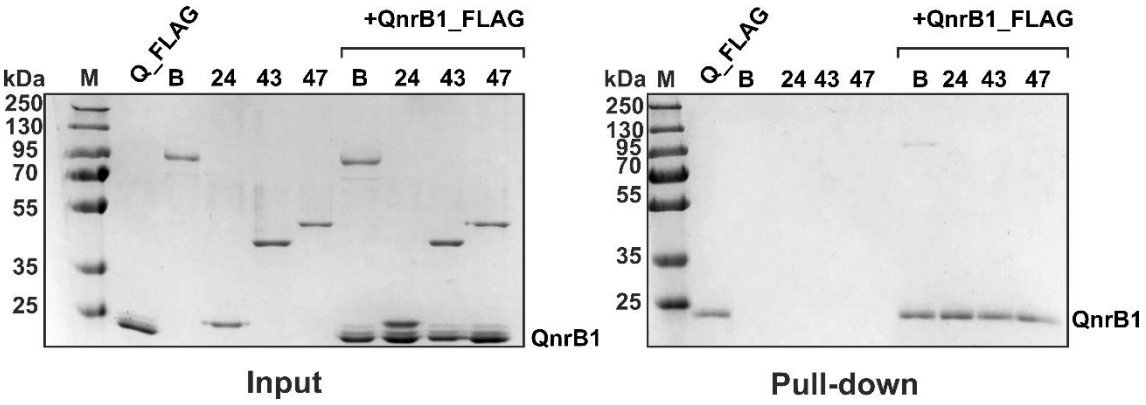

Figure 38. Pull-down assay with N-terminally FLAG-tagged QnrB1 and gyrase sub domains. Gyr B, B24, B43, B47 (Toprimm). *Left* – input, *right* – pull-down (eluates from M2 (α-FLAG) agarose). A Coomassie stained SDS-PAGE gel is shown.

Pull-down methods could not be used to quantify the binding affinity. To determine the binding constant of QnrB1 I carried out fluorescence anisotropy measurements with N-terminally labelled [Alexa488]-QnrB1. After plotting change in fluorescence as function of gyrase subunit/complex concentration the data was fit using the standard one site specific binding equation: $Binding = \frac{B_{max}*x}{Kd*x}$ where x is the concentration of the gyrase subunit/ complex. Estimated Kd for QnrB1/gyrase A_2B_2 complex was 0.08 ± 0.01 μM; $K_{d\ GyrB43}$ equalled 1.77 ± 0.22 μM K_{GyrB} for the full-length GyrB -2.53 ± 0.74 μM. The binding for GyrB did not reach full saturation even at >10 μM [GyrB] (higher concentration could not be tested due to the increasing viscosity). Isolated GyrA subunit was the weakest binder with K_d of 3.9 ± 1.2 μM. Preincubation with ADPNP decreased the binding of QnrB1 to GyrB subunits: QnrB1 bound to GyrB with K_d of 3.8 ± 1.2 μM and to GyrB43 with K_d = 12.2± 2.7. K_d for gyrase complex preincubated with ADPNP increased >20-fold to 1.78 ± 0.31 μM (**Figure 39**). We conclude that QnrB1 likely preferably binds to GyrB in the context of a full gyrase complex. The data obtained in fluorescence anisotropy experiments supports the observations from pull down experiments (**Figure 38**). The fact that preincubation with non-hydrolysable analogue of nucleotide abolishes the interaction with enzyme in pull-down assays and is causing the rise of binding constants in fluorescence anisotropy measurements suggests that QnrB1 might be binding inside the GyrB dimer cavity.

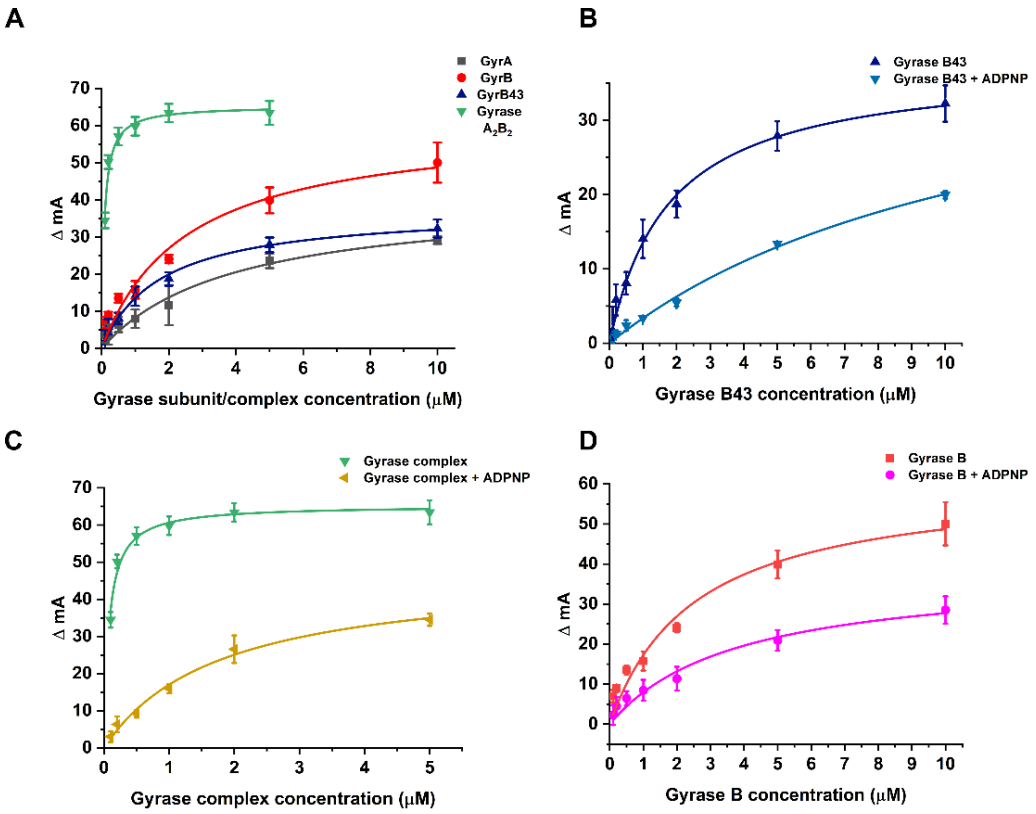

Figure 39. Interaction of gyrase subunits with Alexa-488-labelled QnrB1 measured by fluorescence anisotropy. (**A**) Fluorescence anisotropy assay showing binding of individual gyrase subunits and A_2B_2 complex to QnrB1. Solid curves represent one-site binding fits. Gray square – GyrA; red circle – GyrB; blue triangle – GyrB43; green triangle – gyrase A_2B_2 complex. (**B**) GyrB, $K_d = 2.53 \pm 0.74$; K_d (+ADPNP) $= 3.8 \pm 1.2$; (**C**) GyrB43, ($K_d = 1.77 \pm 0.22$, K_d (+ADPNP) was 12.2 ± 2.7); (**D**) Gyrase A_2B_2 complex, solid curves represent one-site binding fits ($K_d = 0.08 \pm 0.01$ μM, K_d (+ADPNP) $= 1.78 \pm 0.31$ μM). ΔmA indicates the change in anisotropy (in milli - units). Error bars are expressed as the standard deviation of three independent experiments. Figure adapted from (Mazurek *et al.*, 2021) .

5.2.1.8. Crosslinking experiments

To find out which residues of QnrB1 are possibly involved in the interaction with DNA gyrase I used site-specific crosslinking. For this, I incorporated an orthogonal photo-crosslinkable amino acid p-benzoyl-phenylalanine (*p*Bpa) in the desired locations within the PRP. Genetically encoded photo-crosslinking amino acids enable probing of protein–protein interaction interfaces in a position-dependent manner (Mishra *et al.*, 2020). Artificially evolved to recognise the pBpa aminoacyl-tRNA synthetase/tRNA pair from *Methanococcus jannaschii* encoded on plasmid pEVOL-pBpa. The plasmid was co-transformed into an *E. coli* expression strain together with a pBAD plasmid bearing a *qnrB1* gene modified to contain an amber stop codon (TAG) in the desired position (Chin *et al.*, 2002). The benzophenone moiety of the orthogonal pBpa is a widely used photo-crosslinker that can be activated with light of approximately wavelength 350–365 nm. The formed diradical is short-lived and typically inserts into C–H bonds of side chains

and the peptide backbone at the distance range of 3.1 Å, although larger labelling radii are possible due to rotations and flexibility at the *p*Bpa side chain and the surrounding environment (Dormán *et al.*, 2016). To select potential positions for pBpa incorporation the ConSurf web server was used. The server analyses the evolutionary conservation of the amino acids of the macromolecule to reveal regions that are important for structure and function. The level of evolutionary conservation of an individual amino acid of the protein reflects its importance for the structural integrity and function of the protein (Ashkenazy *et al.*, 2016). This approach could be used as a screening method for selecting positions to analyse in crosslinking experiments. After the analysis of QnrB1 protein structure (PDB:2XTW) the server produced a numerically estimated and colour coded visualisation of evolutionary conservation of amino acid positions of QnrB1 (**Figure 40**).

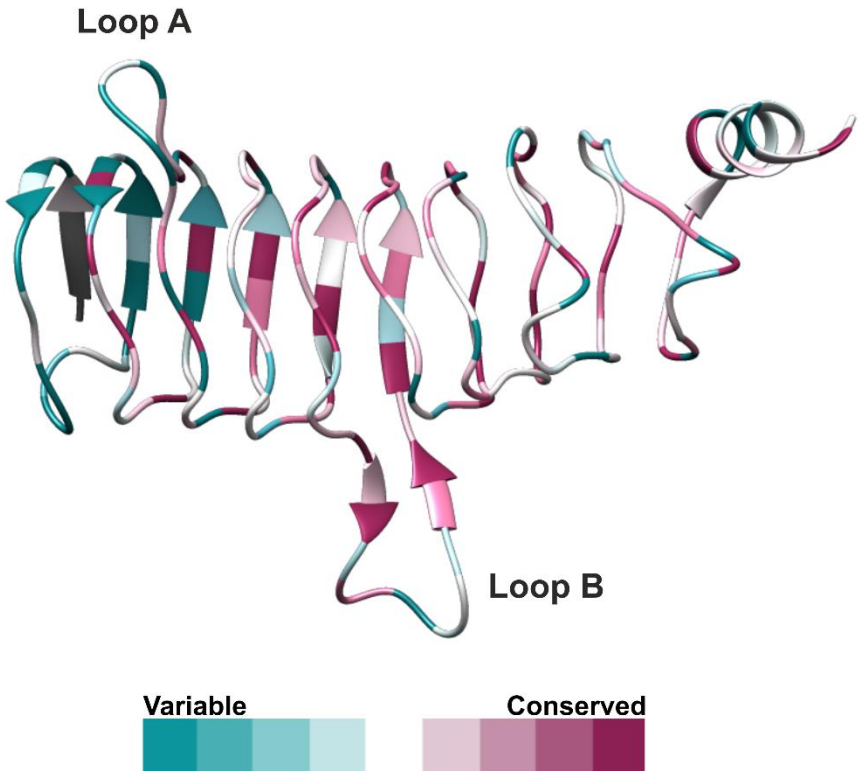

Figure 40. Cartoon representation of QnrB1 (PDB: 2XTW) with colour-coded ConSurf conservation scores.

We analysed ConSurf data and took non-conserved residues out of consideration due to the fact that there is low possibility of their importance in interaction (Capra and Singh, 2007). Highly conserved buried residues with an obvious PRP structural role were also excluded. This approach yielded 29 surface-exposed residues that were screened by substitution of UV-crosslinkable amino acid (**Table 11**) (**Figure 41**).

Table 11. List of QnrB1 residues replaced with *p*Bpa; **bold** are residues, which produced UV crosslinks.

QnrB1 position	PRP position (Jacoby *et al.*, 2013)
N27	i^{+2}
R48	loop A
Q51	loop A
I65	i^{-1}
M73	i^{+2}
R77	i^{+1}
G83	i^{+2}
E85	i^{-1}
R90	i^{-1}
D95	i^{-1}
I105	loop B
T106	loop B
T107	loop B
R108	loop B
T109	loop B
F111	loop B
S113	loop B
T117	i^{+1}
N120	i^{-1}
Y123	i^{+1}
N125	i^{-1}
E132	i^{+1}
E138	i^{+2}
R140	i^{-1}
D155	i^{-1}
S157	i^{+1}
R167	i^{+1}
D175	i^{-1}
R187	i^{+1}

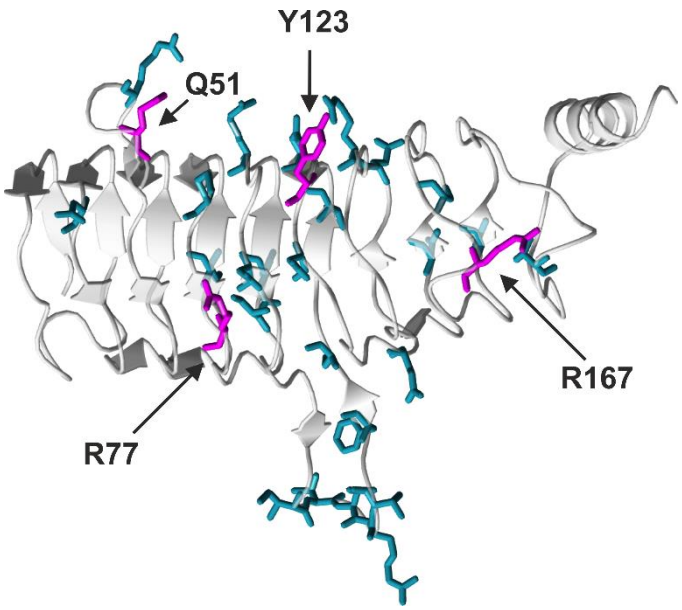

Figure 41. A cartoon representation of QnrB1 monomer (grey, PDB: 2XTW). Residues chosen for crosslinking experiments are displayed as dark cyan cylinders. Residues that produce crosslinks when replaced with *p*Bpa are marked with arrows and displayed as magenta cylinders. Figure adapted from (Mazurek *et al.*, 2021) .

E. coli DY330 strain derivatives, in which chromosomal *gyrA* or *gyrB* genes are fused with SPA purification tags (GyrA-SPA and GyrB-SPA) (Zeghouf *et al.*, 2004; Sutormin *et al.*, 2019) were used as hosts for expression of QnrB1 *p*Bpa variants. SPA tag contains a 3xFLAG sequence that was later used to detect the protein by Western blot procedure (Rigaut *et al.*, 1999). *In vivo* crosslinking shown that out of 29 selected residues four (Q51, R77, Y123, R167) produced crosslinks, all of them with the GyrB (**Figure 42** and **Supplementary Figures S1-3**). All four crosslinked residues were found on face 2 of QnrB1 (**Figure 41**).

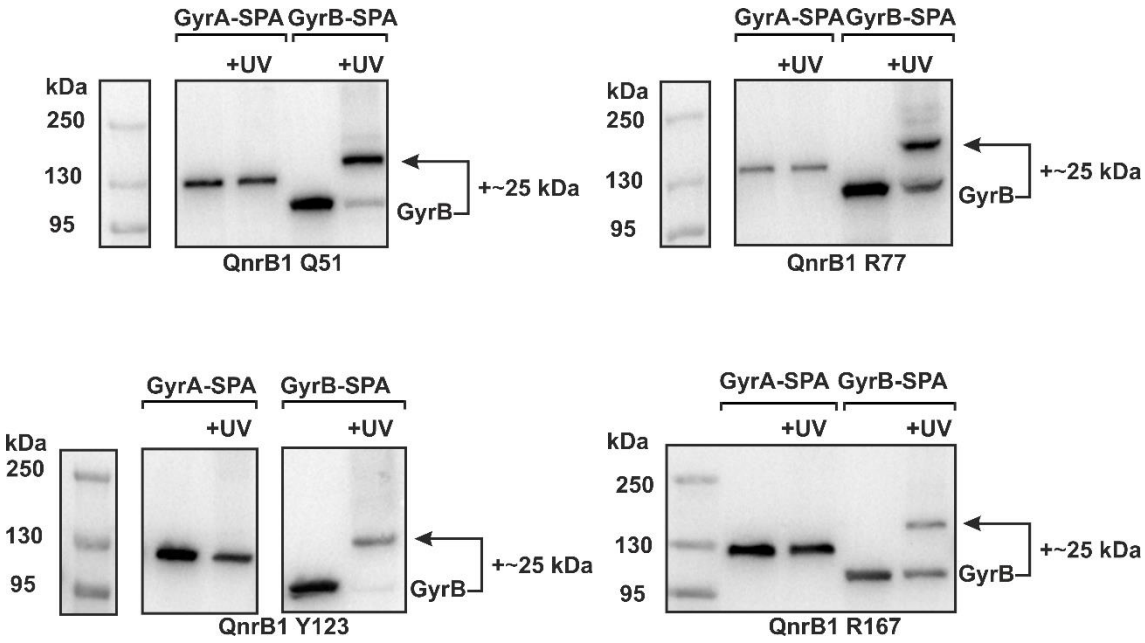

Figure 42. *In vivo* crosslinking anti-FLAG western blots of QnrB1 Q51, R77, Y123 and R167 *p*Bpa variants to chromosomally encoded GyrA-SPA and GyrB-SPA in *E. coli*. Visible band-shifts correspond to an increase in molecular weight of ~25 kDa, roughly equivalent to QnrB1. Western blot membranes are shown after chemiluminescence imaging. Figure adapted from (Mazurek *et al.*, 2021) .

To confirm results obtained using *in vivo* crosslinking approach, experiments were repeated *in vitro* with purified Q51*p*Bpa, R77*p*Bpa, Y123*p*Bpa and R167*p*Bpa QnrB1 variants and FLAG-tagged *E. coli* gyrase subunits described in pull-down experiments. In this setup Q51*p*Bpa and Y123*p*Bpa were found to crosslink strongly to GyrB whereas R77*p*Bpa and R167*p*Bpa gave weaker crosslinks also to the same subunit. Q51*p*Bpa and Y123*p*Bpa *in vitro* crosslinks were visible on SDS-PAGE Coomassie-stained gels while R77*p*Bpa and R167*p*Bpa crosslinks were seen only after visualising them using Western blot (**Figure 43**). The mass shift observed on a gel corresponded to a single QnrB1 molecule but additional shifted species were observed as weaker bands, corresponding to the attachment of two QnrB1 molecules. The crosslink band corresponding for attachment of two Qnrb1 molecules was very strong for GyrB-Y123*p*Bpa but in the case of the crosslinking with GyrA/B complex it completely disappeared

.

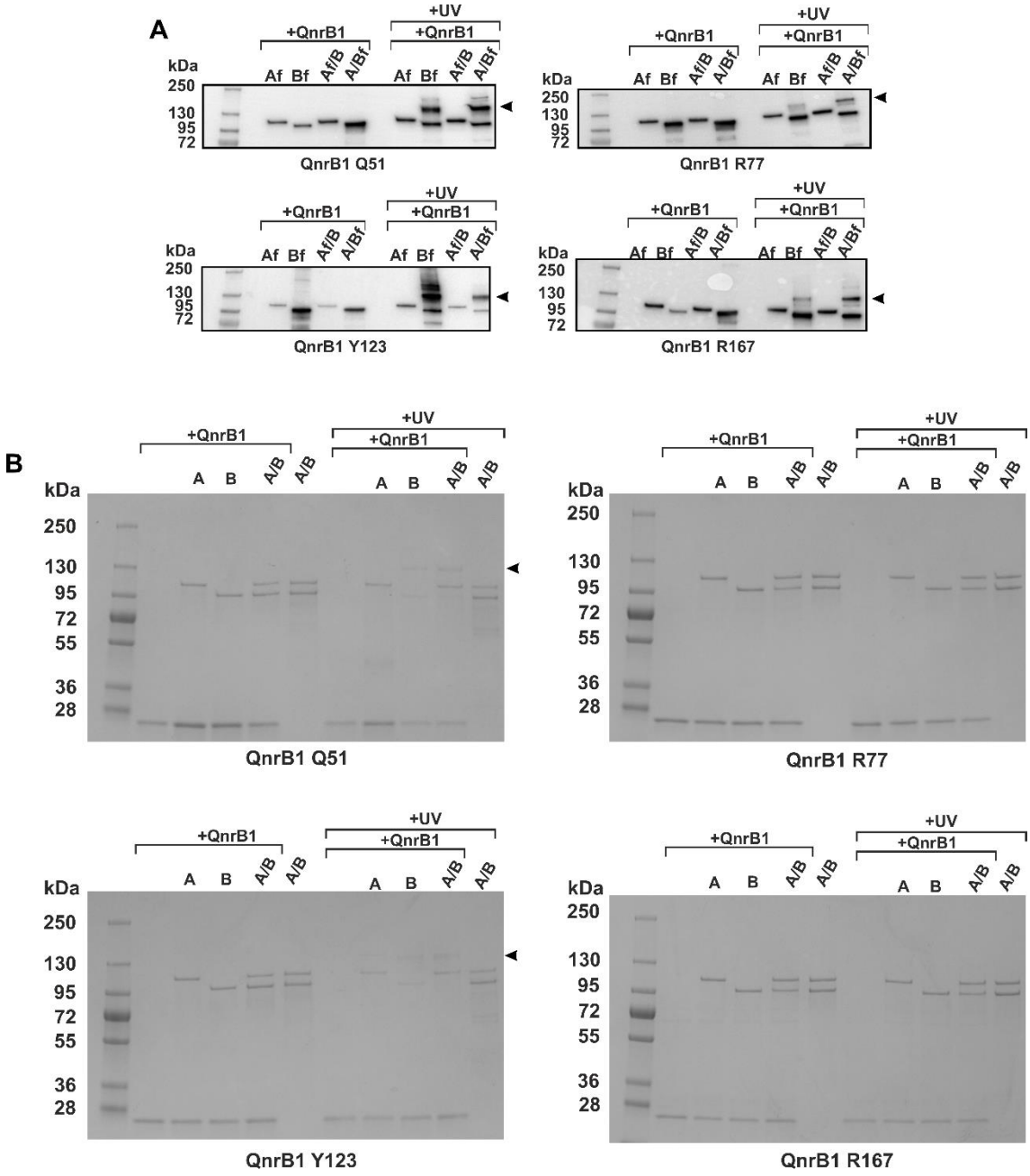

Figure 43. (A) *In vitro* crosslinking anti-FLAG western blots of QnrB1 Q51, R77, Y123 and R167 *p*Bpa variants with different FLAG-tagged gyrase subunits and mixtures of both tagged and untagged subunits (GyrA/3xFLAG-GyrB or GyrA-FLAG/GyrB) (Af- C-terminally FLAG GyrA; Bf- N-terminally 3xFLAG GyrB). Crosslinks are indicated by an arrow. (B) *In vitro* crosslinking SDS-PAGE Coomassie-stained gels of QnrB1 Q51, R77, Y123 and R167 *p*Bpa crosslinks. Tag-less gyrase proteins were used in those reactions. Crosslinks are indicated by an arrow.

Q51*p*Bpa and Y123*p*Bpa were the two mutants that produced strong visible bands on SDS-PAGE Coomassie-stained gels after the crosslinking reaction. We decided to perform further experiments for these two mutants and purified GyrB subdomains to establish the minimal unit of gyrase complex required for the interaction with QnrB1. Both QnrB1-*p*Bpa variants were approximately stoichiometrically crosslinked to GyrB

and to the GyrB43 domains but shown almost no crosslinking in the case of GyrB24 domain or TOPRIM (GyrB47) (very weak band was detected for TOPRIM-Y123*p*Bpa) (**Figure 44**).

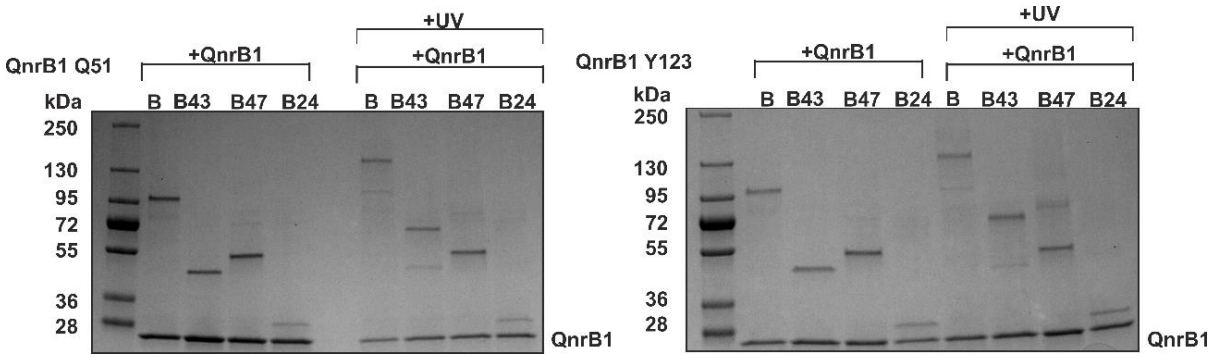

Figure 44. SDS-PAGE gels showing UV – induced crosslinking of QnrB1 Q51 *p*Bpa and QnrB1 Y123 *p*Bpa with different gyrase B subdomains. 5 µM of QnrB1 and 0.4 µM of indicated gyrase subunit was used in the reaction. (left) crosslink with QnrB1 Q51 *p*Bpa; (right) crosslink with QnrB1 Y123 *p*Bpa. Figure adapted from (Mazurek *et al.*, 2021) .

Competition experiments with wild type QnrB1 (QnrB1 WT) and QnrB1 Y123*p*Bpa were subsequently performed to prove the specificity of observed crosslinks. Increasing amounts of WT QnrB1 were added to the crosslinking reactions with GyrB and QnrB1 Y123*p*Bpa or GyrB43 and QnrB1 Y123*p*Bpa. In both reactions increasing amounts of unmodified protein prevented the crosslinking reaction. (**Figure 45**).

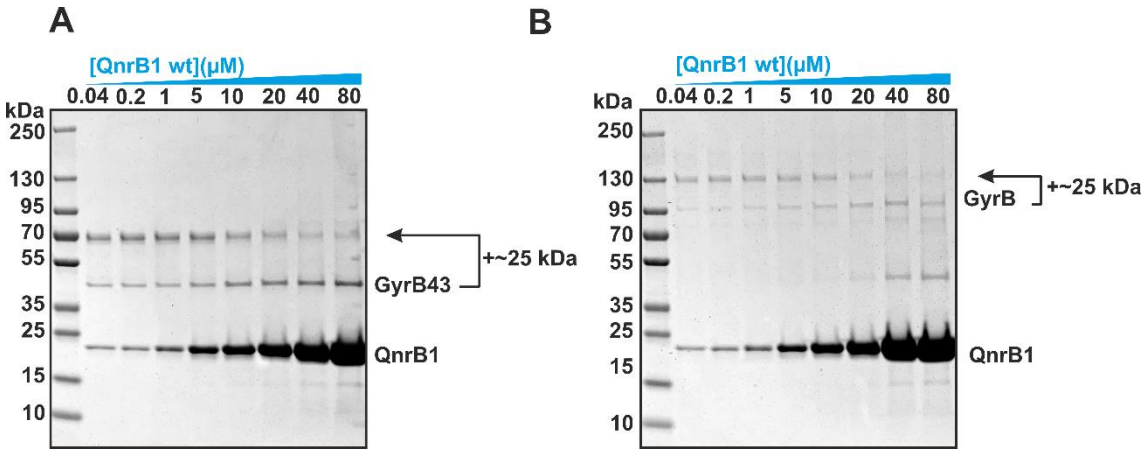

Figure 45. Competition crosslinking experiment with QnrB1wt (wild type) and QnrB1 Y123*p*Bpa**.** (**A**) GyrB43 subunit. Each reaction consisted of 0.4 µM GyrB43, 5 µM QnrB1 Y123*p*Bpa and increasing concentration of unlabelled WT QnrB1 **(B)** GyrB subunit. Each reaction consisted of 0.4 µM GyrB, 5 µM QnrB1 Y123*p*Bpa and increasing concentrations of unlabelled WT QnrB1. Band-shifts corresponding to QnrB1 crosslinking are indicated. Coomassie-stained SDS-PAGE gels are shown. Figure adapted from (Mazurek *et al.*, 2021).

The results described above show that *p*Bpa residues substituting Q51, R77, Y123 and R167 QnrB1 are within a close distance to the GyrB subunit; therefore, these residues might comprise an interaction interface. *In vivo* results shown no crosslinking to GyrA

suggesting very specific interaction to the GyrB subunit. *In vitro* crosslinking results for Q51 and Y123 variants in the case of separate GyrB subdomains shown strongest crosslinking to GyrB43. The observed crosslinking to the GyrB43 subdomain correlates with the ATPase stimulation effect (cf. section **5.2.1.6**), pull-down and fluorescence anisotropy data. Thus, QnrB1 seems to be interacting with the ATPase domain of gyrase B subunit and stimulates ATP hydrolysis.

The previously tested requirement of QnrB for nucleotide hydrolysis was also tested in a crosslinking experiment. GyrB and GyrB43 were incubated with 1 mM ADPNP before a crosslinking reaction with QnrB1 Y123*p*Bpa. Samples were collected at given time points to monitor the crosslinking reaction. Pre-incubation with ADPNP largely prevented crosslinking with full-length GyrB (**Figure 46 A**). No inhibition was observed for GyrB43 (**Figure 46 B**). To check the importance of the $\Delta_{106\text{-}108}$ QnrB1 loop deletion, the ability of the QnrB1 ΔTTR mutant (Y123pBpa $\Delta_{106\text{-}108}$) to crosslink to GyrB was also tested. No difference was observed between crosslinking of the mutant and wild-type QnrB1 (**Figure 46 C**). Since gyrase subunits were preincubated with ADPNP before adding QnrB1 to the reaction, the N-gate formed by GyrB ATPase subunits is likely in the dimerised state. Therefore, a possible explanation for a significant abolishment of crosslinking observed in these conditions is that QnrB1 molecule is unable to get inside the cavity of the GyrB dimer (cf. section **5.2.1.7**). Crosslinking results for Y123pBpa $\Delta_{106\text{-}108}$ show that the ΔTTR loop mutant is still able to interact with DNA gyrase.

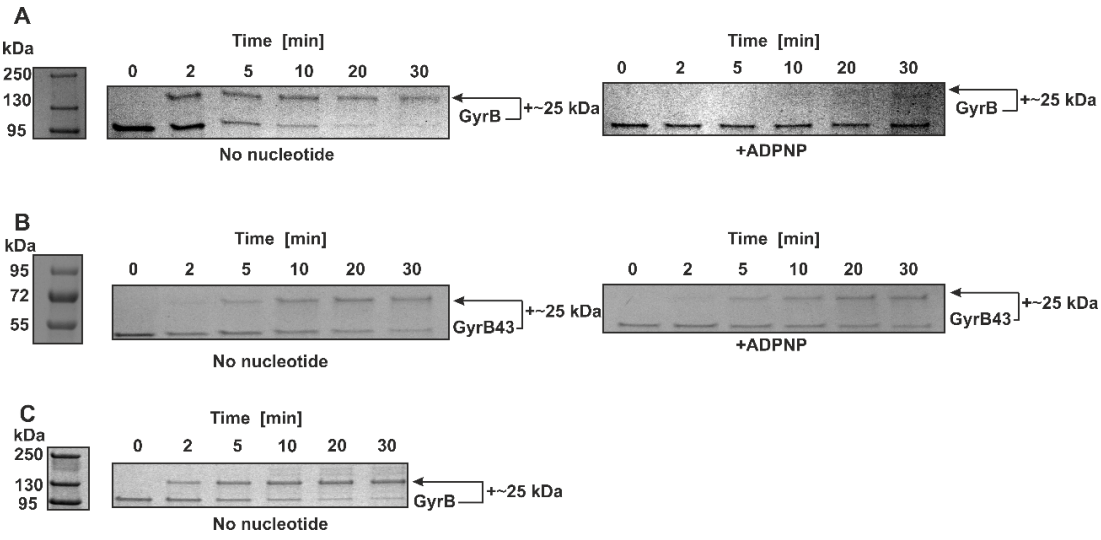

Figure 46. Time course of in vitro crosslinking of GyrB and GyrB43 to QnrB1Y123pBpa. (**A**) Crosslink to gyrase B subunit with (right) and without (left) ADPNP. (**B**) Crosslink to gyrase B43 with (right) and without (left) ADPNP. (**C**) Crosslinking of QnrB1 Y123pBpa ΔTTR mutant. Coomassie-stained SDS-PAGE gels are shown. Band-shifts corresponding to QnrB1 crosslinking are indicated. Figure adapted from (Mazurek *et al.*, 2021) .

A time course experiment to monitor crosslinking QnrB1 Y123 *p*Bpa to the full A_2B_2 gyrase complex was also performed in the presence of linear PBR322 plasmid DNA to check influence of DNA binding on the interaction between the PRP and the gyrase complex. Similarly, to previous results in the presence of ADPNP resulted in reduced amount of crosslink. (**Figure 47**).

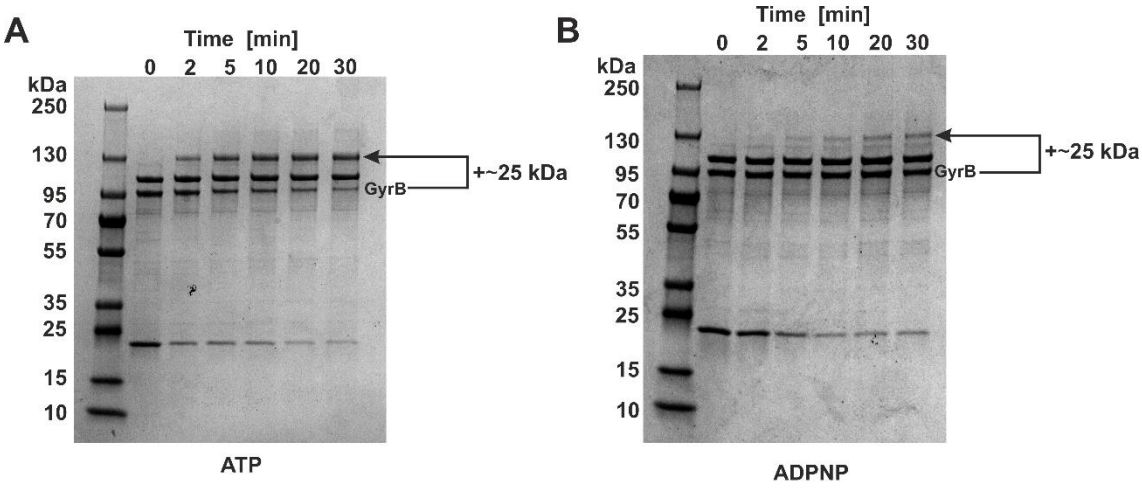

Figure 47. Time course of in vitro crosslinking of gyrase complex and linear PBR322 plasmid DNA with QnrB1 Y123pBpa. (**A**) Crosslink of QnrB1 Y123pBpa with ATP present. (**B**) Crosslink of QnrB1 Y123pBpa with ADPNP present. Coomassie-stained SDS-PAGE gels are shown. Band-shifts corresponding to QnrB1 crosslinking are indicated.

The crosslinking experiments were performed to check which exact positions in QnrB1 are responsible for interaction with DNA gyrase. Only four residues (Q51, R77, Y123, R167) Presented significant crosslinking in the assays. All four were specifically crosslinking to the GyrB subunit inside the bacterial cell. Further experiments with purified QnrB1*pbpa* proteins and gyrase subunits shown that the crosslinking site is located within the GyrB43 domain. This result is in-line with the results obtained for ATPase stimulation where isolated GyrB43 domain was activated by addition of PRP protein. The QnrB1 Y123*p*Bpa and Q51*p*Bpa were the strongest crosslinking mutants being able to produce crosslinks visible without the usage of immunological methods of detection. In the case of QnrB1 Y123*p*Bpa a weak band for GyrB47 crosslink was also observed. The crosslinking results clearly position the QnrB1 binding site in the GyrB subunit.

The possibility of performing crosslinking reactions with gyrase subunits gave the opportunity to test the influence of ADPNP on the QnrB1 binding on-site. Preincubation

with ADPNP lead to a significant decrease in the amount of crosslink in the case of GyrB subunit tested alone or in the case of the full gyrase complex. No additional crosslinks were observed when GyrA was present in crosslinking reactions when QnrB1 Y123*p*Bpa was tested. In the case of GyrB43, preincubation with ADPNP did not result in a decrease of crosslinked product. The PRP could be interacting with dimerised GyrB43 from the "bottom" exposed site due to the truncation of the enzyme (Brino *et al.,* 2000).This is another piece of evidence to suggest that the QnrB1 must be entering the gyrase complex through the N-gate and its main interaction site is inside the GyrB dimer.

5.2.2. AlbG

The peptide toxin albicidin, due to its high activity against fluoroquinolone resistant bacteria, shows significant promise as a potential founding structure for developing novel topoisomerase-targeting antibiotics (Hashimi, 2019; Michalczyk *et al.*, 2023). The AlbG protein present in the albicidin biosynthetic gene cluster confers 30 fold increase in resistance to albicidin among *E. coli* cells (Hashimi *et al.*, 2007). Due to its structural and sequence similarity to Qnr proteins, AlbG could potentially have a similar mode of action. My *in vivo* results already shown that AlbG, when expressed in *E. coli*, provides highly specific protection against albicidin. The fact that AlbG originates from *Xanthomonas albilineans*, a representative of a different bacterial genus Xanthomonadaceae could potentially indicate a slightly different mode of interaction with DNA gyrase (Hashimi *et al.*, 2008). The amino acid sequence of *Xanthomonas albilineans* gyrase shown 62% identity to *E. coli* GyrA and 60% identity to *E. coli* GyrB. Nevertheless, information about the interaction of AlbG and *E. coli gyrase* would help to determine if the two PRPs have the same mode of action. Therefore, I carried out a series of biochemical experiments to gather further information about the interaction of this PRP and the *E. coli* gyrase.

5.2.2.1. Protein purification

AlbG protein was expressed as a N-terminally hexa-histidine-tagged protein. The purification procedure was similar to the one used for QnrB1 protein; AlbG was purified using immobilized metal affinity chromatography (IMAC) using HISTrap column as the first step (**Figure 48 A**). After overnight dialysis into the ion exchange buffer, the obtained protein was loaded onto a MonoQ ion-exchange column and further purified

(**Figure 48 B**). Finally collected fractions form the MonoQ column were concentrated and the buffer was exchanged using the Superdex S75 Increase gel filtration column.

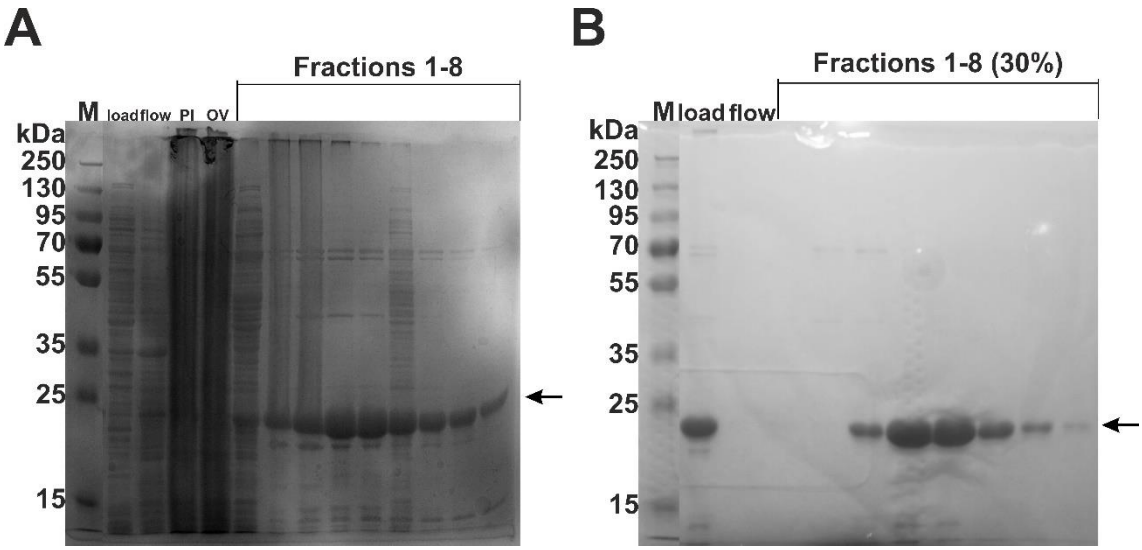

Figure 48. SDS-PAGE gels from each stage of purification of HIS-AlbG. (**A**) Gel showing HISTrap purification step (load – fraction loaded on the column after cell lysis, flow – flowthrough from HISTrap column, Fractions 1-8 – fractions eluted form HISTrap column (10 µl from 5 ml of eluted fractions form HISTrap column) (**B**) Gel showing fractions from MonoQ ion-exchange column purification step (load – material loaded on the column, fractions 1- 8(30% B) – fractions collected after elution with 30% of buffer B).

5.2.2.2. Activity in gyrase supercoiling assays

Purified AlbG protein was tested for protection activity in a gyrase supercoiling assay similarly to QnrB1. Increasing concentration of AlbG was tested against 3.3 µM ALB. The protein provided a protective effect (supercoiling was restored) over a wide range of concentrations (**Figure 49 A**) with estimated EC_{50} AlbG = 1.2 µM. In contrast to QnrB1, AlbG did not inhibit *E. coli* gyrase at any concentration tested (up to 25 µM) (**Figure 49 B**) (see also section **5.2.1.2**).

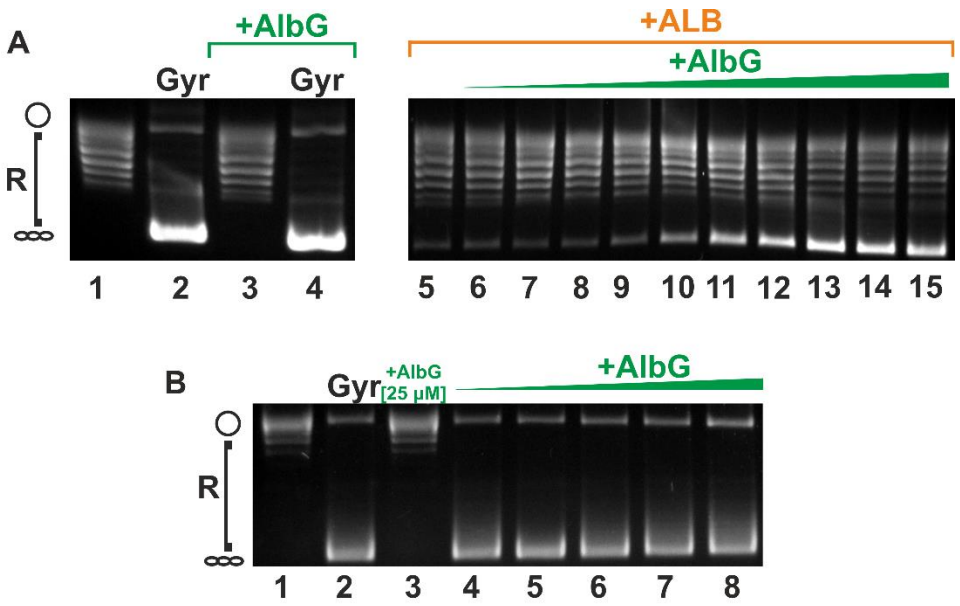

Figure 49. (**A**) Plasmid supercoiling assay showing (*left*): lane 1: relaxed pBR322; lane 2: supercoiling by 1 U of gyrase; lane 3: lack of detectable nuclease activity in the purified AlbG (50 µM) and lane 4: lack of effect of 50 µM AlbG on gyrase supercoiling; (*right*) gyrase inhibition by ALB (3.3 µM) and partial rescue by increasing concentrations of AlbG (0.0016; 0.008; 0.04; 0.2; 1; 5; 10; 20; 25; 50 µM). (**B**) Plasmid supercoiling assay showing the inhibitory effect of high concentrations of AlbG. Lane 1: relaxed pBR322, lane 2: gyrase and relaxed pBR322 no nuclease activity was observed upon addition of 25 µM AlbG, Lane 3: no nuclease activity was observed upon addition of 25 µM AlbG, lanes 4-8: effect of increasing concentration of QnrB1 on gyrase supercoiling activity (0.2; 1; 5; 10; 25).

MIC tests performed with various PRPs (**Table 9**) shown high specificity of proteins toward their cognate toxins in a cellular context. Supercoiling assays were performed to further investigate the specificity of QnrB1 and AlbG *in vitro* with the purified enzyme. Neither QnrB1, nor AlbG shown any protective activity when tested *in vitro* against albicidin and ciprofloxacin respectively (**Figure 50**). This result supports the data obtained for MIC tests, proving there is no cross-protective effect provided by QnrB1 and AlbG.

s

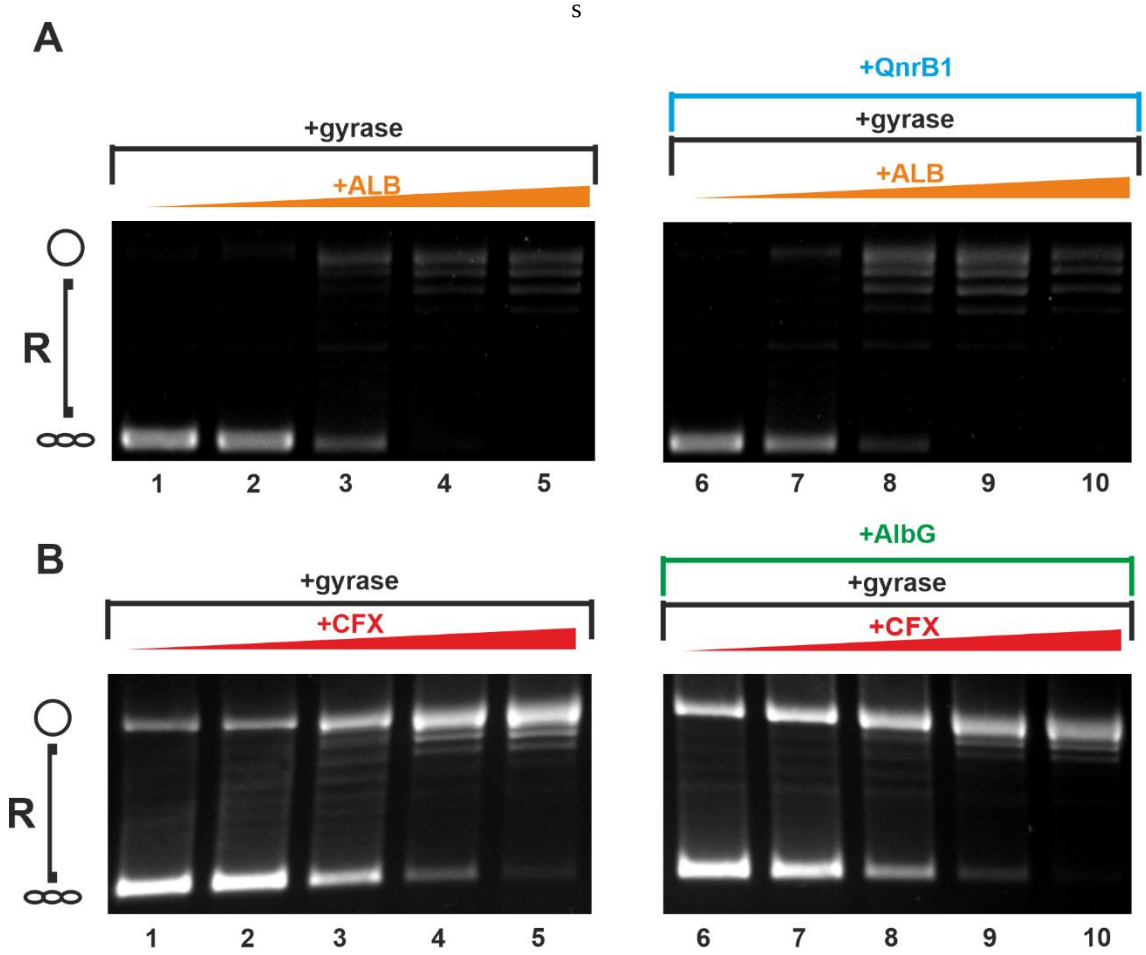

Figure 50. (A) Left gel shows gyrase supercoiling inhibition by increasing concentrations of albicidin lanes 1-5 (0.016; 0.16; 1.6; 16; 160 [µM]). Right gel, effect of the addition of 5 µM QnrB1 to the same reactions (lanes 6 – 10) (B). Left, lanes 1-5: gyrase supercoiling inhibition by increasing concentrations of ciprofloxacin (0.016; 0.08; 0.4; 2; 10 µM); right, lanes 6 – 10: effect of adding 5 µM AlbG to the reactions.

AlbG protein was previously shown to confer immunity to albicidin when expressed in *E. coli* strain but the toxin and the protein were never tested together in an *in vitro* gyrase assay (Hashimi *et al.*, 2007; Vetting, Hegde, Zhang, *et al.*, 2011). Results obtained in supercoiling assays show AlbG protects *E. coli* gyrase from an inhibition by albicidin and the effect is toxin-specific.

5.2.2.3. Activity in gyrase cleavage assays

Similarly, to the pipeline developed for QnrB1, we have tested the influence of AlbG on DNA cleavage induced by albicidin. Increasing amounts of albicidin were added to the cleavage reaction with relaxed DNA and 5 µM AlbG. In contrast to what was observed with QnrB1 and CFX, the cleavage reduction, although very noticeable, was not consistent across the concentration range i.e., the protective effect faded away with higher concentrations of albicidin (**Figure 51**). This behaviour can be explained by the higher

affinity of albicidin towards *E. coli* DNA gyrase (K_d = 50 nM) (Michalczyk *et al.*, 2023) and resulting higher stability of formed complexes.

Similarly as in the case of QnrB1 the amount of cleaved DNA in each lane has been quantified and the data were fit to the equation $\%\,\text{DNA cleavage} = \%\,\text{max cleavage}\ \frac{[\text{ALB}]}{\text{EC50}_{ALB} + [\text{ALB}]}$ where $\text{EC}_{50_{ALB}}$ is concentration of albicidin in which 50% of maximum cleavage activity is observed. The EC50_{ALB} values were calculated from the fit function. In the absence of AlbG the $\text{EC}_{50_{ALB}}$ is 0.15 ± 0.06 μM and $\%\,\text{max cleavage}$ was 43 ± 2 %. When AlbG was present in the reaction the calculated values were 15.25 ± 6.36 μM for $\text{EC}_{50_{ALB}}$ $\%\,\text{max cleavage}$ equalled $78 \pm 18\,\%$. It needs to be noted that the values have significantly higher errors for the fit for the reaction in the presence of PRP since the curve does not reach a plateau (Sebaugh, 2011). In the case of AlbG, in contrast to QnrB,1 the EC_{50} value of the toxin is significantly increased (~100x) whereas % max cleavage stays at a similar level (cf. section **5.2.1.3**). The observed difference could be a result of the fact that the albicidin stabilised cleavage complex has a longer half-life. Formed cleavage complexes with albicidin seem to show higher stability.

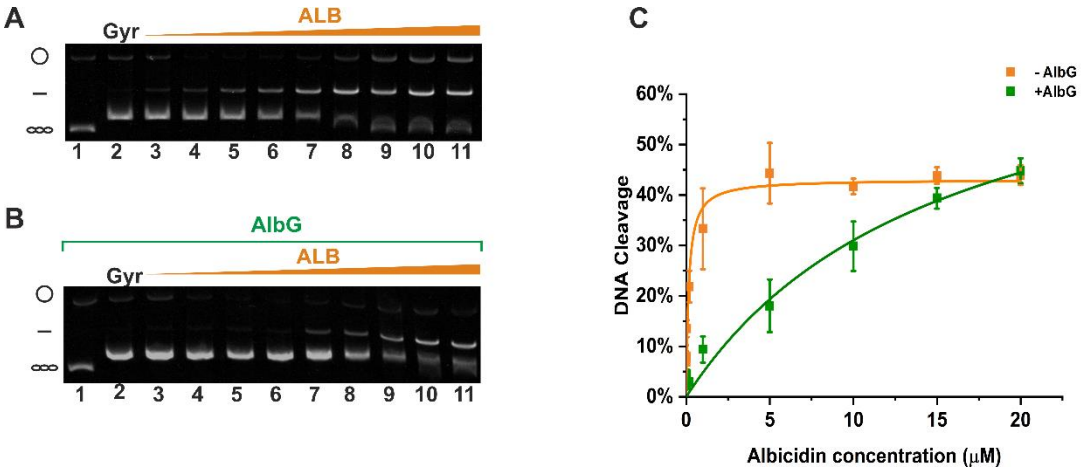

Figure 51. (**A**) DNA gyrase (5 U) cleavage reactions with the increasing amount of albicidin run on EtBr gel. (**B**) DNA gyrase (5 U) cleavage reactions with the increasing amount of albicidin in the presence of 5 μM AlbG run on EtBr gel. Lane 1, relaxed pBR322. Lane 2, relaxed pBR322 with DNA gyrase. Lanes 3 - 11 contain relaxed pBR322 gyrase and increasing concentrations of albicidin (0.0016; 0.008; 0.04; 0.2; 1; 5; 10; 15; 20μM) (**C**) Cleaved DNA in the absence (*orange*) and presence (*green*) of AlbG quantified and plotted. Error bars represent standard deviation (SD) of 3 independent experiments.

When the cleavage reaction was tested in the reverse setup, increasing concentration of AlbG with a fixed amount of poison, the protective effect was less pronounced. Lower

cleavage activity was observed starting from 10 µM of AlbG in the reaction. The effect is less pronounced compared to QnrB1 results in the same setup (**Figure 52**).

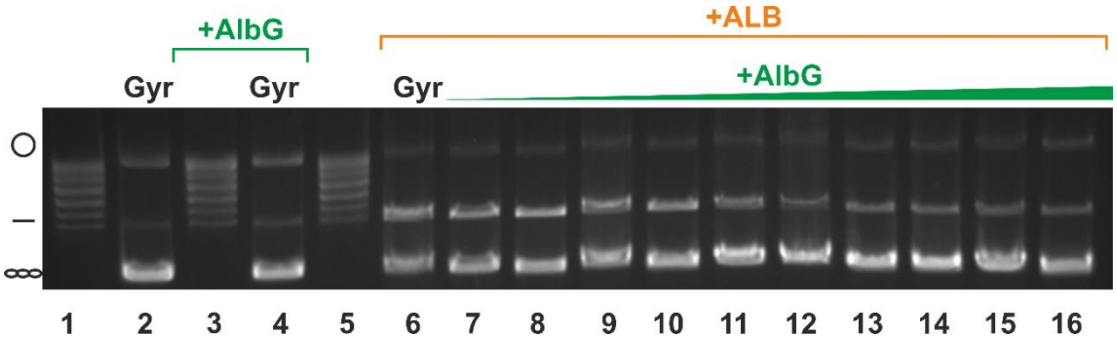

Figure 52. DNA cleavage assay with fixed amount of ALB (0.16 µM). Lane 1: relaxed pBR322; Lane 2: 5 U of gyrase complex with: relaxed pBR322; Lane 3: nuclease control of 50 µM AlbG; Lane 4: 50 µM AlbG with 5 U of gyrase complex; Lane 5: 0.16 µM ALB without DNA gyrase; Lanes 6-16: 0.16 µM ALB with increasing concentration of AlbG (0,0.0016,0.008,0.04,0.2,1,5,10,20,25,50)

When negatively supercoiled DNA was used in a cleavage setup with albicidin, the results were different compared to observations with QnrB1 and ciprofloxacin. When the gyrase A_2B_2 complex was incubated with albicidin and increasing amounts of AlbG and supercoiled pBR322, there was no concentration-dependent cleavage protection effect observed (**Figure 53**).

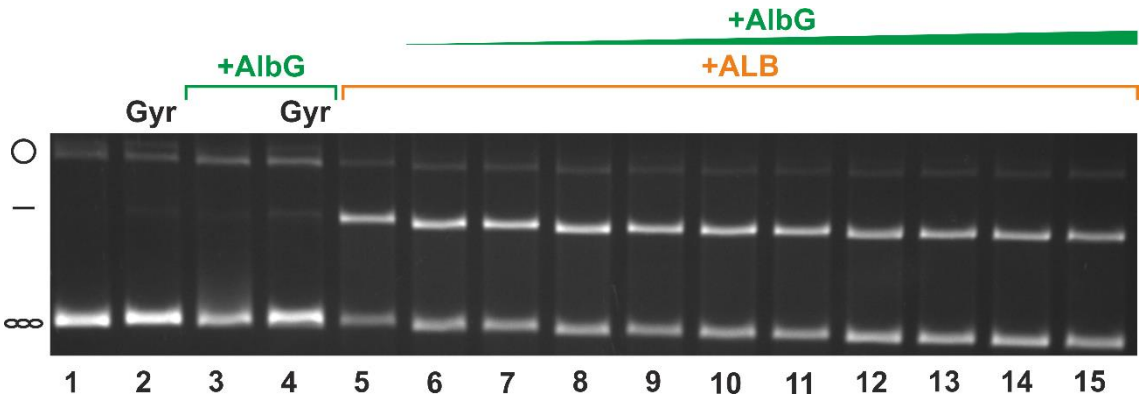

Figure 53. DNA cleavage assay with gyrase A_2B_2 complex with fixed amount of ALB (30 µM) and negatively supercoiled DNA. Lane 1: supercoiled pBR322; Lane 2: 5 U of gyrase complex with relaxed pBR322; Lane 3: nuclease control of 50 µM AlbG; Lane 4: 50 µM AlbG with 5 U of gyrase complex; Lanes 5-15: 30 µM ALB with increasing concentration of AlbG (0,0.0016,0.008,0.04,0.2,1,5,10,20,25,50)

Similarly, when Gyr $A59_2/B_2$ complex was used in the cleavage assay there was no protective effect observed regardless of AlbG concentration used (**Figure 54**). It has to be noted that due to high concentration of albicidin required to observe cleavage in these conditions (30 µM) the protective effect on cleavage could be hard to identify which corresponds to the data from **Figure 51 C**. The albicidin was observed to be unstable and poorly soluble which hampered interpretation of the assay results.

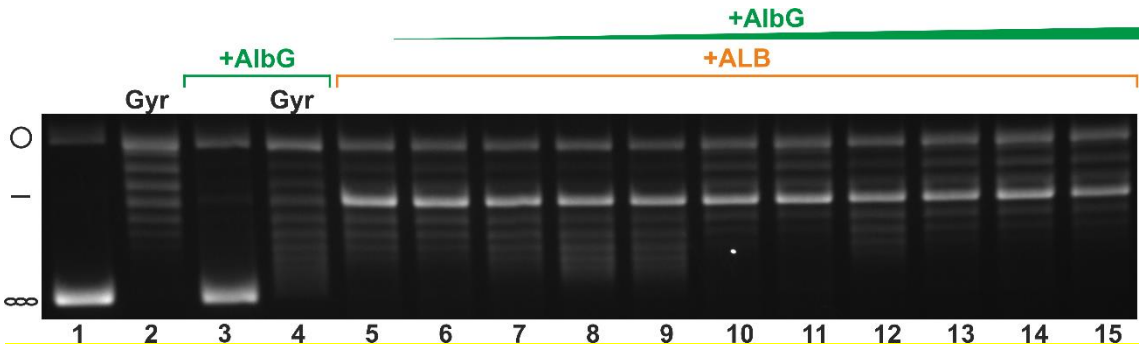

Figure 54. DNA cleavage assay with $GyrA59_2/B_2$ complex and fixed amount of ALB (30 μM). Lane 1: supercoiled pBR322; Lane 2: 5 U of gyrase complex with: relaxed pBR322; Lane 3: nuclease control of 50 μM AlbG; Lane 4: 50 μM AlbG with 5 U of gyrase complex; Lanes 5-15: 30 μM ALB with increasing concentration of AlbG (0,0.0016,0.008,0.04,0.2,1,5,10,20,25,50).

To see if the presence of nucleotide hydrolysis would also have influence on AlbG protective activity against albicidin the cleavage assay without nucleotide and its non-hydrolysable analogue ADPNP was compared with the assay performed in the presence of ATP. Weak protection was observed in the presence of ATP for reactions with higher concentrations of AlbG (**Figure 55**). In the case of albicidin the analysis of influence of nucleotide hydrolysis is more complicated since the activity of the toxin depends on nucleotide presence. Albicidin shows weak activity without nucleotide also in the presence of ADPNP the toxin shows reduced activity. Only in the presence of ATP the full cleavage has been reported. (Hashimi *et al.*, 2007).

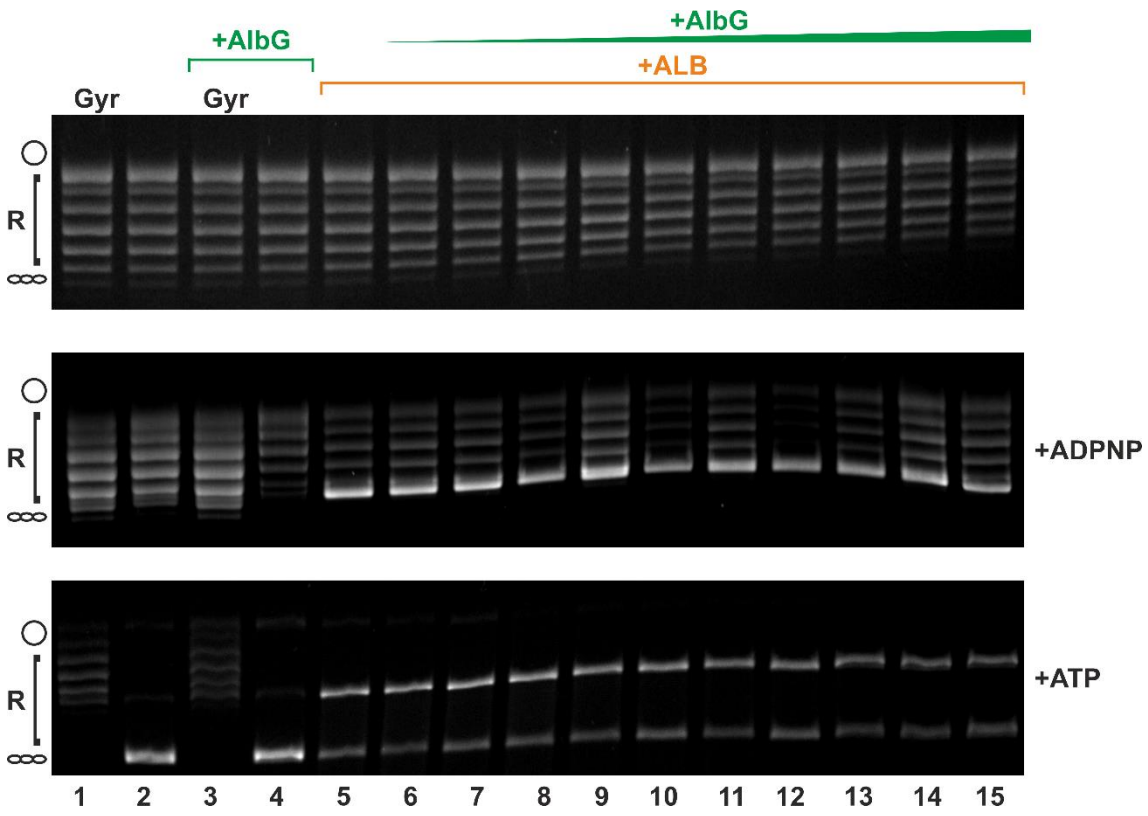

Figure 55. DNA cleavage assay with gyrase complex and fixed amount of ALB (30 μM). Lane 1: supercoiled pBR322; Lane 2: 5 U of gyrase complex with: relaxed pBR322; Lane 3: nuclease control of 50 μM AlbG; Lane 4: 50 μM AlbG with 5 U of gyrase complex; Lanes 5-15: 30 μM ALB with increasing concentration of AlbG (0,0.0016,0.008,0.04,0.2,1,5,10,20,25,50).

We next tested whether AlbG can destabilise the gyrase cleavage complex formed by ALB. Once AlbG was added to the reaction, a drop in the amount of cleaved DNA could be observed (**Figure 56**). However, the reduction was not as high as in the case of QnrB1. Interestingly, after 10 minutes of incubation, the level of cleavage returned to the starting point. This behaviour is very different to the one observed for QnrB1 protein when cleavage level was low for the entire time of the reaction once the protein was added and CFX was diluted (cf. **Figure 27**). Similarly, as in the case with the cleavage reactions, this effect could be due to the fact that used concentration of albicidin (1 μM) is still high relative to the IC_{50} and the protective effect of PRP could be counteracted by the toxin that is still rebinding to the gyrase cleavage complex. Established IC_{50} values for albicidin are in the 50 nM range and the toxin was observed to be far more effective cleavage inducer than ciprofloxacin (Hashimi *et al.*, 2008; Michalczyk *et al.*, 2023). The fact of using high concentration of Albicidin and possibly a too low concentration of AlbG probably prevented observation of a durable effect of cleavage complex destabilisation.

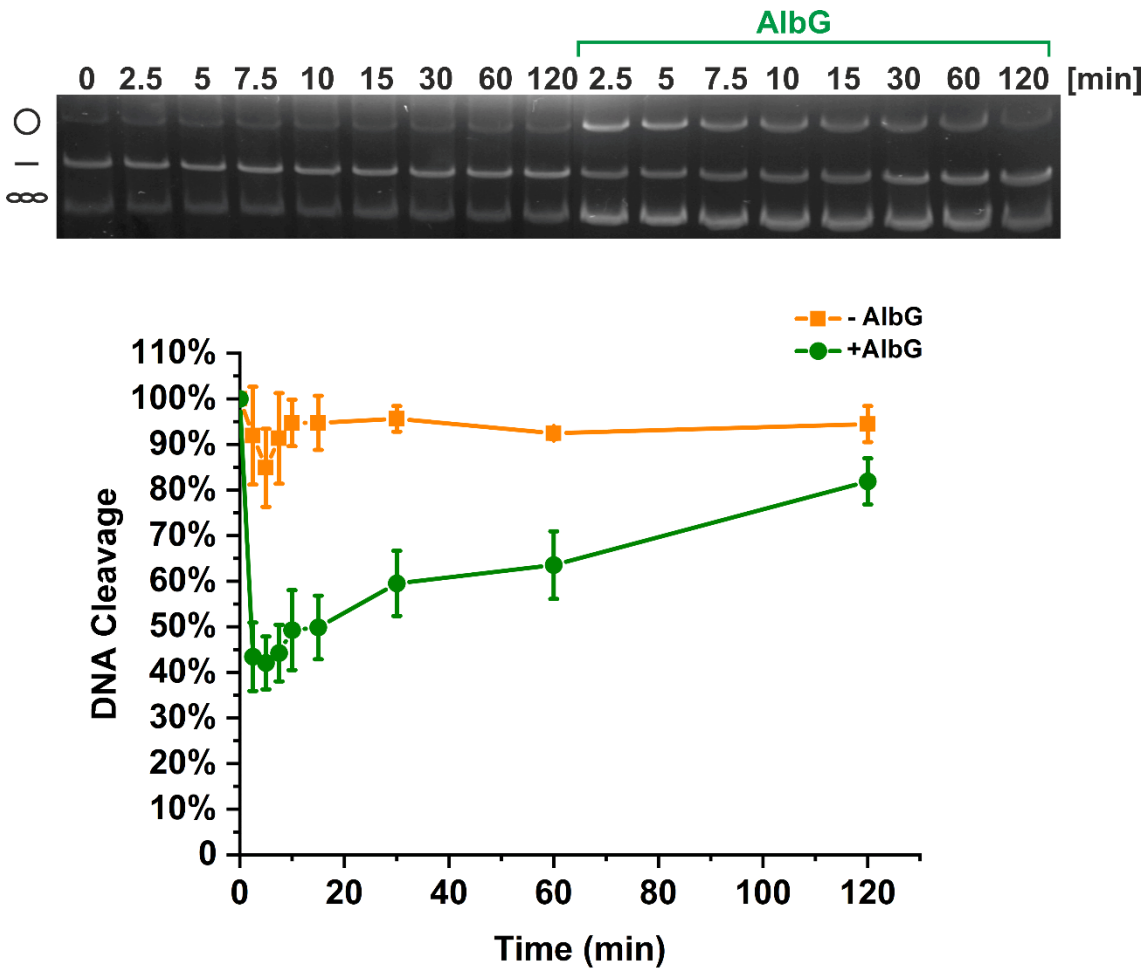

Figure 56. Cleavage complex stability determined in the presence of 5 µM AlbG. Initial DNA cleavage reactions with 80 U of gyrase and 1 µM albicidin were incubated for 10 minutes at 37°C to come to equilibrium and then diluted 20-fold with reaction buffer with or without 5 µM AlbG. (*Top*) The samples ran on the EtBr gel. (*Bottom*) Linear DNA was quantified and plotted. Level of DNA cleavage at time 0 was set to 100%. Error bars represent the SD of at least three independent experiments.

5.2.2.4. Activity in gyrase relaxation assays

AlbG protein was also tested for the capacity to restore an ATP-independent relaxation of negatively supercoiled DNA by the gyrase complex A_2B_2 inhibited by albicidin 10 µM AlbG was tested against increasing concentrations of albicidin, and relaxation reaction was monitored. The cleavage induced by ALB in these conditions is not rescued by PRP (**Figure 57 A**). When tested in reverse conditions (increasing concentration of AlbG) the PRP also shown no protective effect for ALB inhibited relaxation. Similarly, to QnrB1, slight inhibition of relaxation in the presence of toxin was observed (**Figure 57 B**). In contrast to QnrB1, AlbG did not influence the ATP-independent relaxation on its own (**Figure 57 C**) (cf. section **5.2.1.4**).

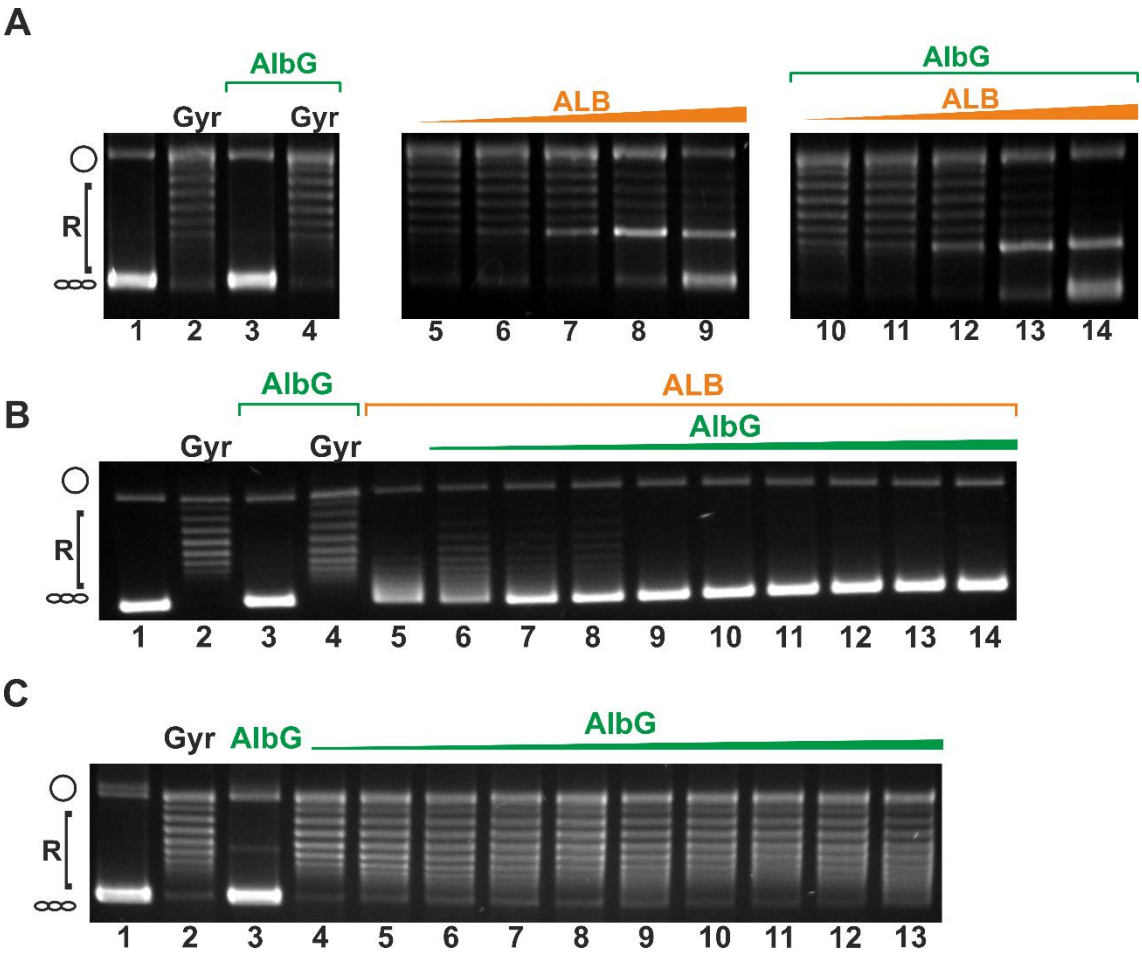

Figure 57. (**A**) ATP-independent relaxation inhibited by ALB is not rescued by AlbG. Different concentrations of ALB (indicated) were tested against 10 µM AlbG. lane 1: negatively supercoiled pBR322, lane 2: relaxation by gyrase, lane 3: lack of detectable nuclease activity in the purified AlbG (10 µM AlbG) lane 4: lack of relaxation promotion by 10 µM AlbG; (*right*) lanes 5-9: DNA cleavage by gyrase with increasing concentration of ALB, lanes 10-14 and lack rescue by increasing concentrations of AlbG (0,016; 0,16; 1,6; 16; 160; [µM]). (**B**) Relaxation assay of negatively supercoiled DNA in the presence of albicidin and increasing AlbG concentration. No protection is observed. Instead, inhibition can be spotted with high concentration of AlbG. lane 1: negatively supercoiled pBR322, lane 2: relaxation by gyrase, lane 3: lack of detectable nuclease activity in the purified AlbG (50 µM AlbG) lane 4: relaxation in the presence of 50 µM AlbG; lanes 5-14: DNA relaxation in the presence of ALB (5 µM) and lack rescue by increasing concentrations of AlbG (0,008; 0,04; 0,2; 1; 5; 10; 20; 25; 50 [µM]). (**C**) Relaxation assay of negatively supercoiled DNA in the presence of increasing AlbG concentration. lane 1: negatively supercoiled pBR322, lane 2: relaxation by gyrase, lane 3: relaxation in the presence of 50 µM AlbG; lanes 4-13: DNA relaxation in the presence of increasing concentrations of AlbG (0,0016, 0,008; 0,04; 0,2; 1; 5; 10; 20; 25; 50 [µM]).

5.2.2.5. AlbG influence on DNA binding

To assess AlbG ability to displace DNA from the DNA gyrase complex, an EMSA assay was performed. AlbG was not able to outcompete the bound 147 bp linear fragment containing SGS of pBR 322 DNA regardless of concentration tested (**Figure 58**). This observation shows that AlbG behaves differently to QnrB1 which efficiently outcompeted the DNA from the gyrase complex (compare with **Figure 31**).

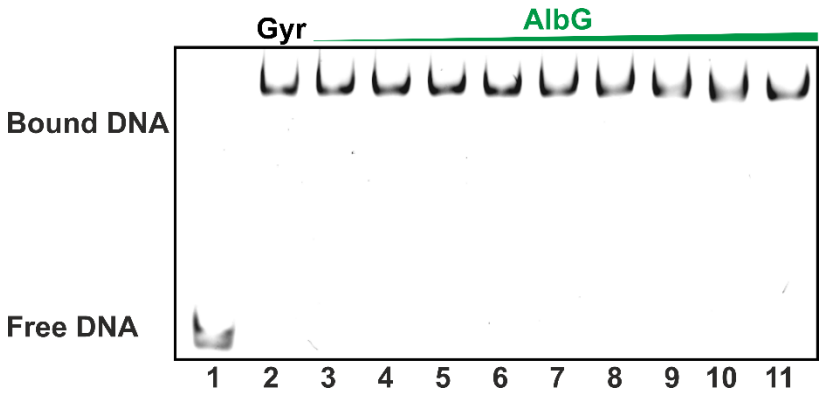

Figure 58. Effect of increasing concentration of AlbG on DNA binding. Lane 1: free DNA, Lane 2: gyrase complex added to DNA, Lane 3-11: increasing concentration of QnrB1 effect on DNA binding by DNA gyrase [0,1; 0,2; 0,5; 1; 2; 4; 12; 35; 70 µM]. AlbG does not out compete DNA from DNA gyrase complex.

5.2.2.6. Activity in gyrase ATPase assay

Following results obtained for QnrB1, we have tested if AlbG affects the ATPase activity of gyrase. Interestingly, in contrast to QnrB1, AlbG shown no stimulation of the B43 subunit (**Figure 59**) (cf. **Figure 33 C**). Together with results from DNA competition assay and different behaviour in relaxation and gyrase cleavage and supercoiling assays, the observations for AlbG suggest different mode of interaction with *E. coli* DNA gyrase; potentially AlbG shows less affinity to gyrase without bound albicidin which explains lack of inhibition.

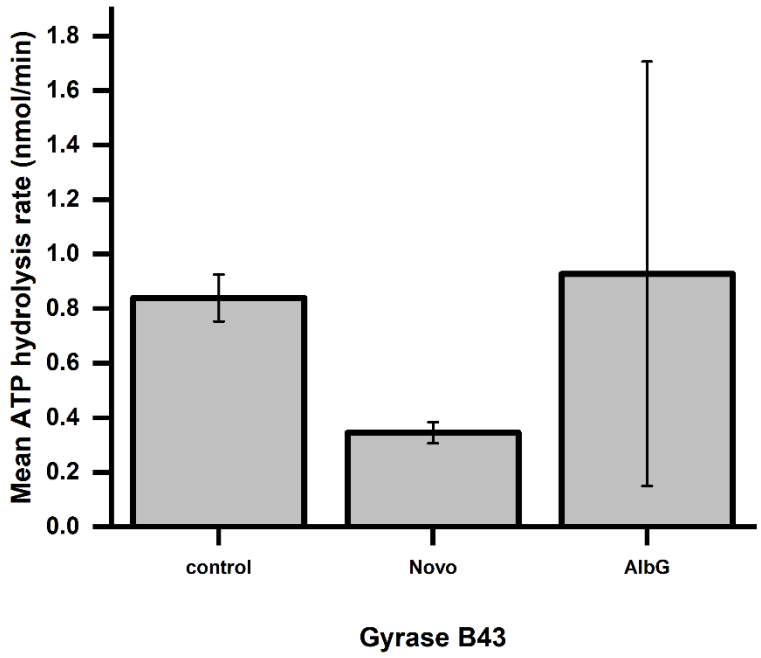

Figure 59. ATPase rate data for 4 µM GyrB43 in the presence of 50 µM novobiocin (Novo) or 5 µM AlbG. Error bars are expressed as the standard deviation of three independent experiments.

5.2.2.1. Direct studies of AlbG-Gyrase interaction

To further confirm our assumptions, we carried out a pull down assay using N-terminally-FLAG tagged AlbG and gyrase subunits. In stark contrast to QnrB1, N-FLAG-AlbG was not interacting with any gyrase subunits or with gyrase A_2B_2 complex (**Figure 60**). (The bands visible in pull-down gel are also present in the control without AlbG and arise due to non-specific interaction with M2 resin). Compared to QnrB1 pull-down results there is no enrichment in gyrase subunits in any eluates (cf. section **6.2.1.7**).

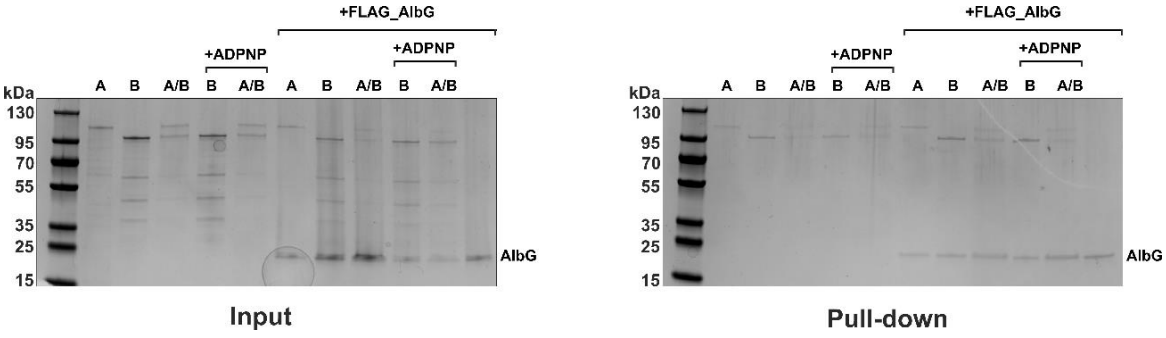

Figure 60. Pull-down assay with N-terminally FLAG-tagged AlbG and purified GyrA, GyrB and A_2B_2 complex. *Left* – input, *right* – pull-down (eluates from M2 (α-FLAG) agarose). A Coomassie stained SDS-PAGE gel is shown.

Negative pull-down result suggests lower binding affinity of AlbG to *E. coli* gyrase complex than the one observed for QnrB1 protein.

5.2.2.2. Crosslinking experiments

Prompted with positive results for QnrB1 pBpa crosslinking we carried out a similar experiment with AlbG. Structural alignment of QnrB1 and AlbG was performed with "Matchmaker" program incorporated in ChimeraX software using the Needleman–Wunsch algorithm and BLOSUM-62 matrix (Pettersen *et al.*, 2021). Out of four crosslinking QnrB1 residues, residue QnrB1 Y123 overlapped with an equally positioned residue in AlbG D109. (**Figure 61 A**). AlbG and QnrB1 share only moderate sequence homology (22%) so a structural match could suggest a similar location of those residues. Indeed, when AlbG D109 was substituted with benzoyl-phenylalanine (*p*Bpa) and *in vivo* crosslinking experiment was performed, an intensive band corresponding to the crosslink to *E. coli* GyrB was observed on the gel (**Figure 61 B**)

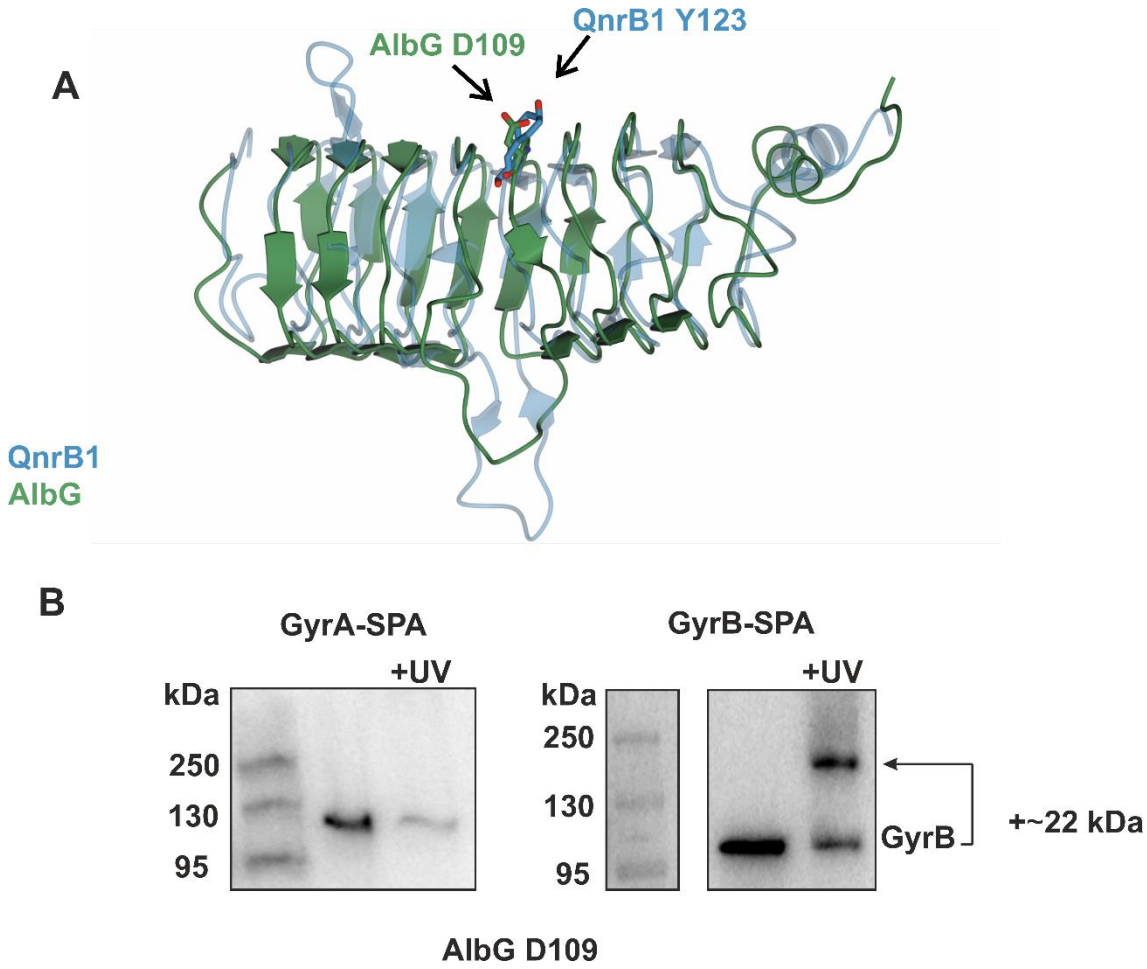

Figure 61. Structural alignment of QnrB1 and AlbG. (**A**) Cartoon representations of QnrB1 (PDB:2XTW; blue) and AlbG (PDB:2XT2; green) superimposed by secondary structure matching in ChimeraX software. Highlighted are QnrB1 Y123 and structurally homologous AlbG D109. (**B**). Western blot showing in vivo crosslinking of AlbG D109pBpa to *E. coli* GyrA-SPA and GyrB-SPA.

In crosslinking experiments with purified GyrB similar results as for QnrB1 were observed. The crosslink band was visible in the absence of nucleotide, but when 1 mM ADPNP was added to the reaction, crosslinking was significantly reduced (**Figure 62 A**). Equally, AlbG was found to crosslink to GyrB43 (**Figure 62 B**).

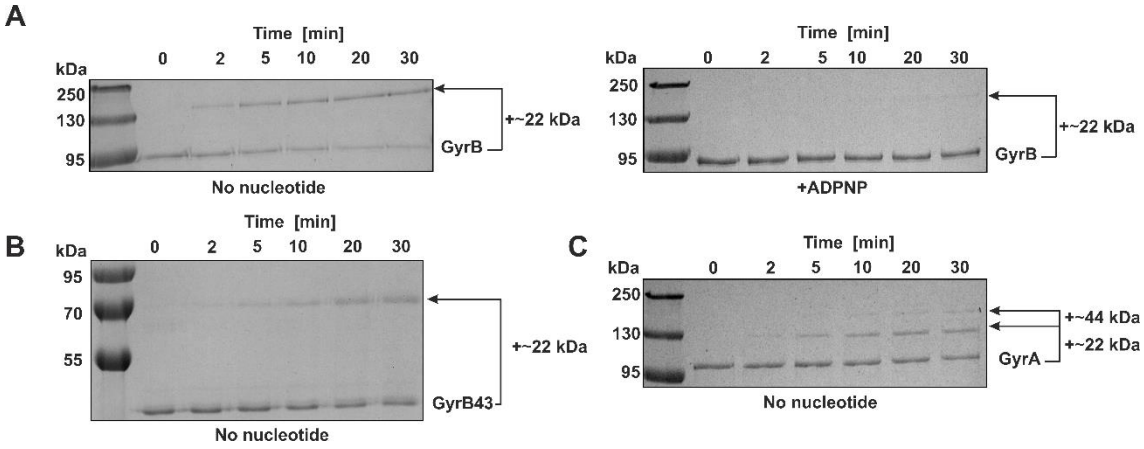

Figure 62. *In vitro time* course crosslinking SDS-PAGE Coomassie-stained gels of AlbG D109 *p*Bpa crosslinks with *E. coli* gyrase subunits. Tag-less gyrase subunits were used in those reactions. Crosslinks are indicated by an arrow. Reaction contained 400 nM of gyrase subunit and 5 μM AlbG protein (**A**) *left* time course crosslinking to gyrase B with no nucleotide present, *right* time course crosslinking to gyrase B in the presence of 1 mM ADPNP. (**B**) time course crosslinking to gyrase B43 subdomain. Crosslink with AlbG is indicated with an arrow. (**C**) Time course crosslinking to gyrase A. Crosslink with AlbG is indicated with an arrow.

Surprisingly, in the case of AlbG crosslinking to the GyrA subunit was also observed: an additional band is appearing in the range of molecular masses corresponding to one or two AlbG monomers (22-44 kDa) (**Figure 62 C**). Such behaviour could be observed due to the fact that GyrA subunit is natively interacting with GyrB subunit, GyrA on its own can present an interface that is normally not exposed and thus would not be normally found interacting with AlbG. To cross out this possibility of nonspecific interaction between GyrA and AlbG D109 pBpa, the *in vitro* experiment was performed using gyrase holocomplex. A similar amount of crosslinking to GyrA was still observed. Further investigation shown that addition of ADPNP is causing the disappearance of GyrB crosslinking band while the GyrA crosslinked band is still present (**Figure 63 AB**). The fact that the band corresponding to GyrA crosslink is not disappearing after the incubation with ADPNP suggests that there is an additional interface for AlbG interaction compared with QnrB1.

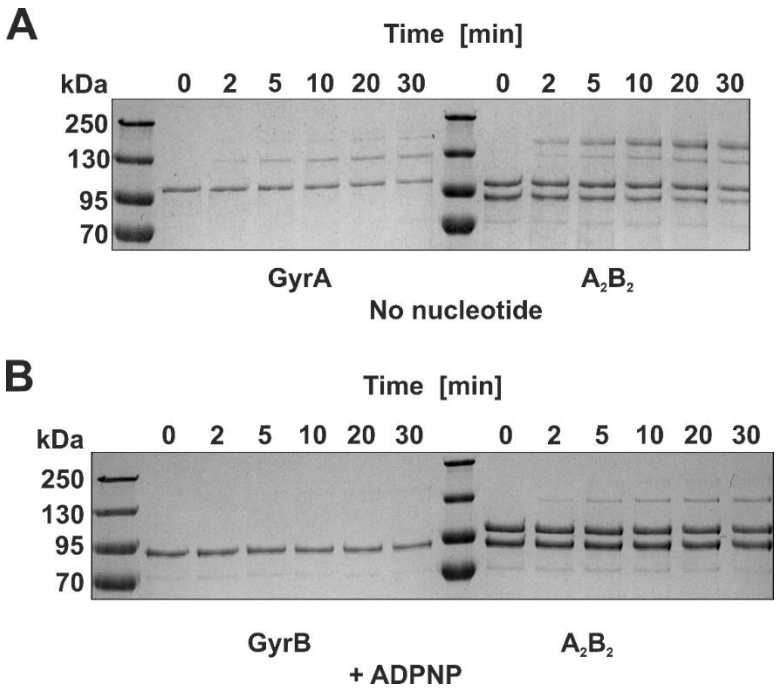

Figure 63. *In vitro time* course crosslinking SDS-PAGE Coomassie-stained gels of AlbG D109 *p*Bpa crosslinks with gyrase complex. GyrA and GyrB crosslinking reactions are shown as a reference of molecular weight of crosslinked bands of independent gyrase subunits.

This result is different to the behaviour of QnrB1 Y123 *p*Bpa. In the case of QnrB1 crosslink to GyrA was never observed *in vitro* nor *in vivo crosslinking* assays. However, the AlbG D109 *p*Bpa GyrA crosslink was not detected in *vivo* similarly like QnrB1 Y123 *p*Bpa (cf section Crosslinking experiments **5.2.1.8**).

AlbG seems to bind to *E. coli* DNA gyrase in a slightly different way. The interaction was not detected in pull-down experiments which potentially means that the PRP interaction is weaker compared to QnrB1. The AlbG was not causing ATPase stimulation and the relaxation stimulation was not observed as well. Crosslinking results indicates that there is an additional interaction interface located on GyrA subunit.

5.2.3. McbG

McbG protein from *E. coli* microcin B17 cluster is responsible for host immunity against produced toxin. In *in vivo* studies of the protein shown high activity and specificity towards MccB17 (Garrido *et al.*, 1988). To date there is no experimental structural data available on McbG apart from the predicted model generated by AlphaFold (AF-P05530-F1). The predicted structure is showing only a small loop present in the structure (5 amino acids). There are no reports available on McbG biochemical activity, thus I have

attempted to produce and characterise this PRP to possibly determine its structure and compare structure-activity relationship with other PRPs.

5.2.3.1. Expression trials

Expression and purification of McbG protein has not been described before in any publication. We have made an attempt to purify McbG in order to perform biochemical and structural studies. N-terminally hexa-His-tagged protein was expressed in *E. coli* BL21 (DE3) Gold using pET-28 vector. A slightly modified purification method based on the QnrB1 purification was used (see Methods section) to obtain pure protein (**Figure 64**). McbG was expressed as N-terminally hexa-histidine-tagged protein and purified using immobilized metal affinity chromatography (IMAC) using HisTrap HP (Cytvia) column as first step. Eluted fractions were highly contaminated in comparison to the fractions obtained during QnrB1 purification. Protein was also found to be unstable and prone to precipitation shortly after elution from HisTrap column. After overnight dialysis into a low-salt ion exchange buffer the obtained protein was loaded on the MonoQ ion-exchange column and further purified. Finally, collected fractions from the MonoQ column were concentrated, and the buffer was exchanged using a Superdex S75 Increase gel filtration column. The final yield of purification was low (0.5 mg of protein from 1 L of medium) and obtained protein was precipitating a short time after the final step of purification once stored in the PRP sec buffer. Addition of 200 mM $(NH_4)_2SO_4$ led to solubilisation of the protein but it was not active in later gyrase assays. Modification of the protocol to use hydrophobic interaction (HIC) chromatography instead of an ion-exchange column was tried and did not result in any increase in protein stability or amount of collected material (data not shown).

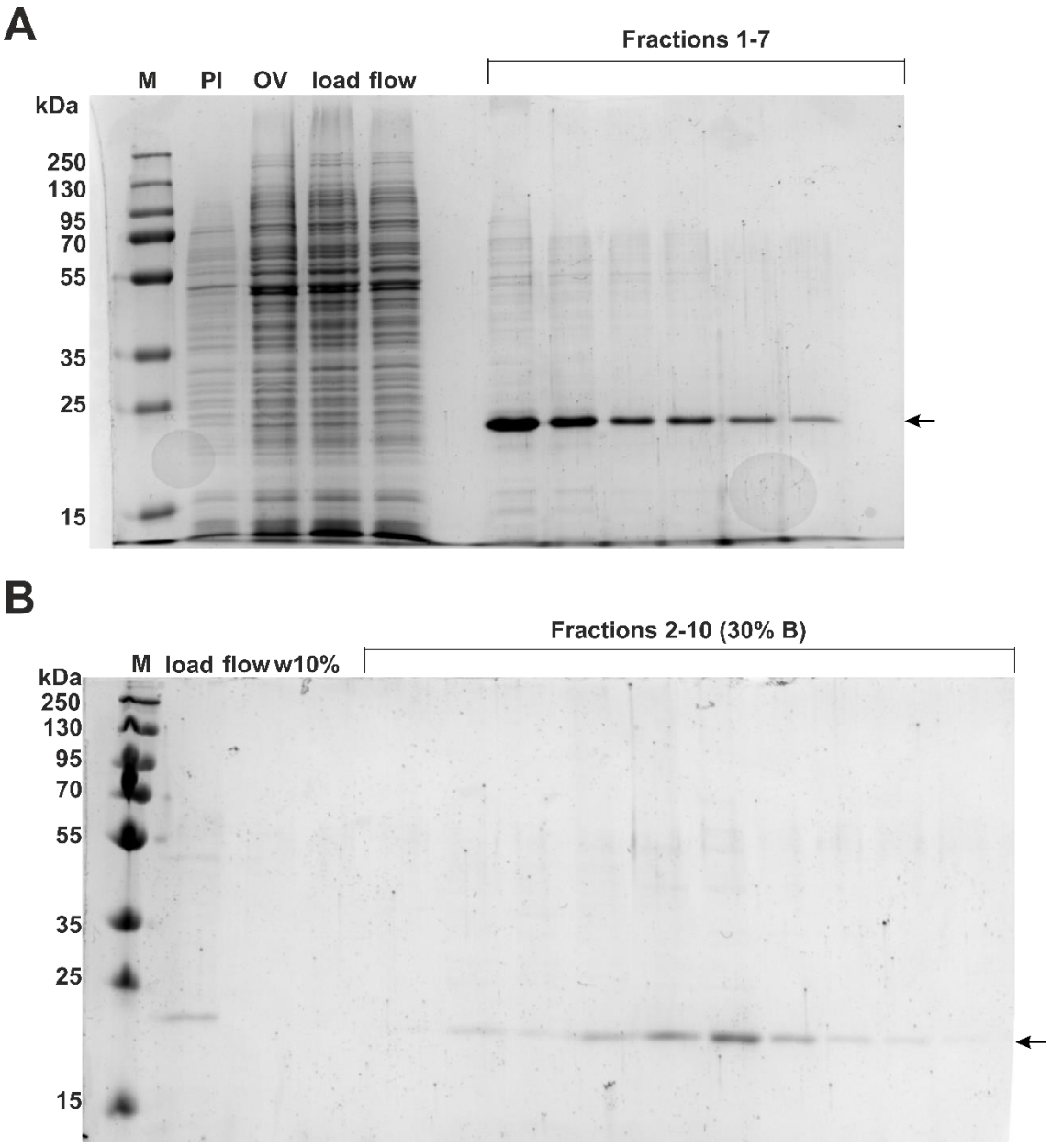

Figure 64. SDS-PAGE gels from each stage of purification of HIS-McbG. (**A**) Gel showing HisTrap™ Fast Flow purification step (PI- pre-induced cells, OV- cells from overnight induced culture, load – fraction loaded on the column after cell lysis, flow – flowthrough from HisTrap Fast Flow column, Fractions 1-7 (10 µl from 5 ml of eluted fractions form HisTrap Fast Flow column). (**B**) Gel showing fractions from MonoQ ion-exchange column purification step (load – material loaded on the column, flow – flowthrough, w10% - fraction washed from the column with 10% of buffer B, fractions 2-10 (30% B) – fractions collected from elution with 30% of buffer B.

To overcome the problem of low yield of purification, different expression systems were tested in order to obtain stable protein and enhance the yield of protein production. The expression host, expression plasmid and result of the expression trial are shown in **Table 12**. None of the tested conditions resulted in significant increase of protein stability and amount after purification.

Table 12. Expression systems used during expression of McbG protein optimisation attempts

Expression host	**McbG Expression plasmid/ McbG construct**	**System description**	**Result (protein yield, stability)**
E. coli BL21(DE3) Gold	pET-28a N-term HIS McbG	Basic bacterial expression setup	0.5 mg / 1 L of medium, unstable protein
E. coli BL21(DE3) Gold	pBAD HIS B N-term HIS McbG	Arabinose regulated protein expression; lower promoter leakage compared T7 promoters	0.5 mg / 1 L of medium, unstable protein
E. coli One Shot™ BL21 Star (DE3)	pET 28a/ pBAD HIS B N-term HIS McbG	Mutation in the RNaseE gene (rne131) that reduces levels of endogenous RNases and mRNA degradation, increased the stability of mRNA transcripts and increasing protein yield	0.2 mg / 1 L of medium, unstable protein
OverExpress™ C43(DE3) pLysS	Pet 28a/ pBAD HIS B N-term HIS McbG	This strain has at least one mutation, which prevents cell death associated with expression of many recombinant toxic proteins. Cells containing pLysS produce a small amount of T7 lysozyme – inhibitor of T7 polymerase thus stabilising recombinants encoding toxic proteins	0.5 mg / 1 L of medium, unstable protein
E. coli One Shot BL21 Star (DE3) pGro7	Pet 28a N-term HIS McbG	pGro7 is an arabinose induced plasmid that contains Gro ES- Gro EL proteins - molecular chaperone complexes that help to fold proteins inside the cell	0.5 mg / 1 L of medium, unstable protein
E. coli One Shot BL21 Star pColA *gyrA + gyrB*	pBAD HISB N-term HIS McbG	Potentially McbG protein could be interacting with host gyrase causing toxicity. In this case, induction of pColA plasmid before pBAD will lead to overexpression of gyrase proteins which should work as a sink for excess McbG	0.4 mg / 1 L of medium, unstable protein, high contamination with DNA
E. coli One Shot BL21 Star pColA gyrA_	pBAD HISB N-term HIS McbG	As above. BA_fusion protein is less toxic itself when expressed but can potentially still work as a binding partner for McbG	0.5 mg / 1 L of medium, unstable protein

gyrB_fusion protein			
E. coli Lemo21 (DE3)	Pet 28a N-term HIS McbG	Lemo 21 (DE3) *E. coli* strain allows tuneable expression of lysozyme which works is an inhibitor of T7 RNA polymerase. The level of lysozyme expression is modulated by adding L-rhamnose to the expression culture which allows tuneable expression of the protein encoded on the plasmid with T7 promoter/	No expression detected regardless L-rhamnose concentration used
Tuner™ (DE3) Competent Cells	Pet 28a N-term HIS McbG	*E. coli* Tuner are lacZY deletion mutants of BL21 and enable adjustable levels of protein expression throughout all cells in the culture. The lac permease (lacY) mutation allows uniform entry of IPTG into all cells in the population which allows homogeneous level of induction of protein expression	0.5 mg / 1 L of medium, unstable protein
E. coli BL21(DE3) Gold	pET 28a N-term Strep-tag II - McbG	The Strep-tag II is a short peptide detecting the protein. (8 amino acids, WSHPQFEK), which binds with high selectivity to Strep-Tactin, an engineered streptavidin. StrepTrap HP column is used to purify the fusion protein.	No expression observed
E. coli BL21(DE3) Gold	pET 28a N-term HIS-FLAG McbG	The FLAG-tag is a short peptide (8 amino acids DYKDDDDK), which is an antigen that is recognised by anti-flag affinity resin which could be later used for pull-down assays.	No expression observed
Vibrio natriegens Vmax competent cells	Pet 28a N-term HIS McbG	*Vibrio natriegens* is a Gram-negative, non-pathogenic marine bacterium (Hoff *et al.*, 2020). It is considered the fastest growing free-living bacterium, with a doubling time between 7 and 10 min under optimal conditions. The organism was tailored for expression of proteins form plasmid containing T7 promoter by	0.1 mg / 1 L of medium, unstable protein

		considered the integrating the T7 RNA polymerase cassette into *V. natriegens* genome (Weinstock *et al.*, 2016).	
E. coli BL21(DE3) Gold	Pet 28a N-term HIS McbG	Hydrophobic interaction chromatography used as a second step of purification	No significant difference between yield and stability of obtained protein
E. coli BL21(DE3) Gold	Pet 28a N-term MBP-HIS McbG	It is known that fusions of maltose binding protein with protein (MBP) of interest can increase protein solubility. This method is commonly used for expressing and purifying poorly soluble proteins (Fox and Waugh, 2003).	Rapid protein precipitation after MBP tag cleavage. MBP-McbG inactive in gyrase assays.

5.2.3.2. McbG Crystallography trails

His-tagged Protein obtained from purifications form *E. coli* BL21(DE3) Gold, *E. coli* One Shot BL21 Star (DE3 and OverExpress C43(DE3) pLysS was used for crystallographic screens using crystallographic screens listed in table. A Mosquito HTS robot was used to set 0.2 µl or 0.4 µl drops. Crystallographic screens used are presented in **Table 13**.

Table 13. Crystallographic screens used in McbG crystallisation tests.

Screen Name	Company
ClearStrategy I+II (sodium acetate pH 4.5/5.5)	Molecular Dimensions
ClearStrategy I+II (Tris pH 7.5/8.5)	
JCSG+	
LMB Screen	
MacroSol/Stura Footprint	
MemGold	

MIDAS	
Morpheus	
PACT premier	
ProPlex	
SG1 - ShotGun	
Structure 1/2	
NR-LBD + NR-LBD Extension	
MPD	Qiagen
Natrix1/Natrix2	Hampton
PEG/Salt	Jena BS

Unfortunately, none of the setups yielded protein crystals which could be used for X-ray crystallography. The only observed crystals were salt crystals which formed in conditions containing phosphate ions in the screen.

5.2.3.3. Activity in gyrase supercoiling assays.

Similarly, to QnrB1 an AlbG, His-McbG was tested in gyrase enzymatic assays. McbG was not showing any influence on gyrase supercoiling reaction. The protein was tested in various concentrations and time points but no observable influence on reaction was detected (**Figure 65 AB**).

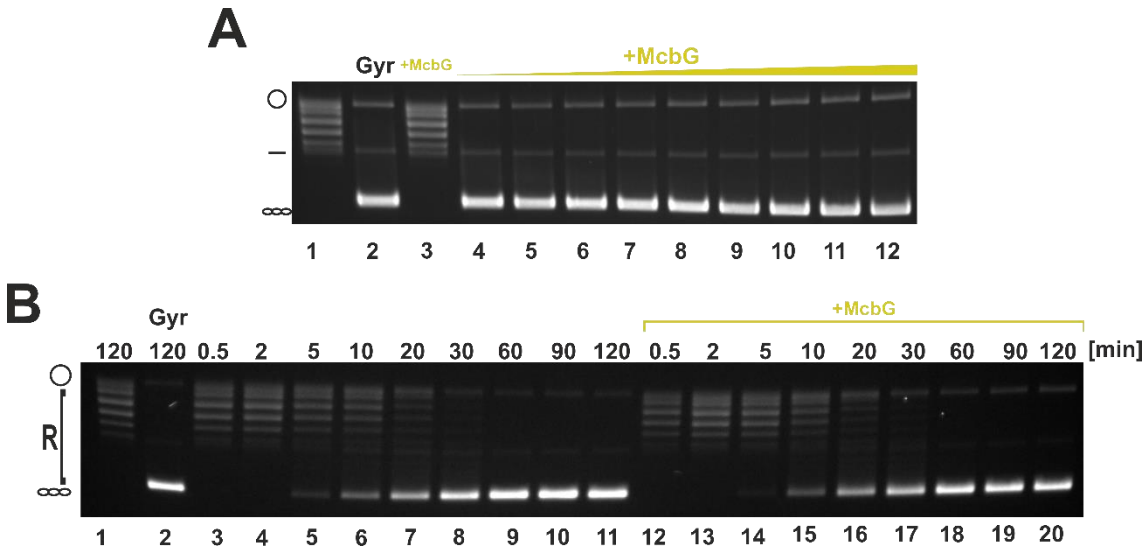

Figure 65. (**A**) Plasmid supercoiling assay with increasing concentration of McbG. Lane 1: relaxed pBR322, lane 2: gyrase and relaxed pBR322, Lane 3: no nuclease activity was observed upon addition of 50 μM McbG lanes 4-12: effect of increasing concentration of QnrB1 on gyrase supercoiling activity (0.008; 0.04; 0.2; 1; 5; 10; 20; 25; 50 μM). (**B**) Time course gyrase supercoiling assay in the presence of 50 μM McbG. Lane 1: Relaxed pBR322, lane 2: gyrase and relaxed pBR322 after 120 min of incubation, Lanes 3-11: time points of supercoiling reaction w/o McbG presence, lanes 12-20: time points of supercoiling reaction in the presence of 50 μM McbG.

5.2.3.4. Activity in gyrase cleavage assays

Since McbG was efficient in protecting cells against MccB17 in a microbiological assay, its protective activity was also tested in an *in vitro* assay. Increasing concentration of McbG was added to gyrase cleavage reaction induced by the presence of 20 μM MccB17. In time course cleavage assay addition of McbG lead to slight decrease in amount of cleaved DNA. Similarly, to supercoiling assay, cleavage was also tested in concentration dependent manner. Addition of McbG protein to the time-course supercoiling reaction resulted in visible restoration of DNA supercoiling. (**Figure 66 ABC**).

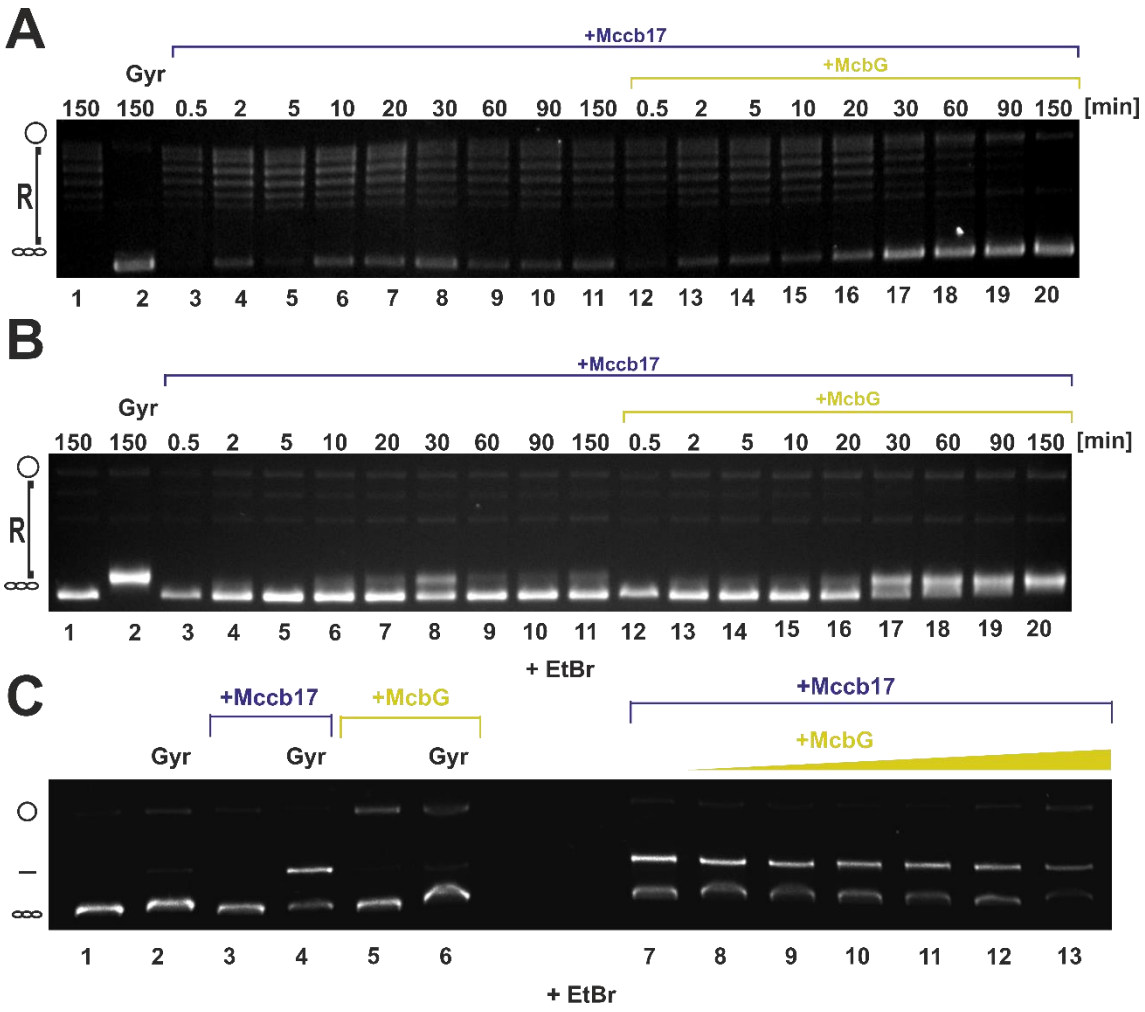

Figure 66. (**A**) Time course cleavage assay in the presence of 20 µM Mccb17 and 5 µM McbG. Lane 1: Relaxed pBR322, lane 2: gyrase and relaxed pBR322 after 150 min of incubation, Lanes 3-11: time points of supercoiling reaction w/o McbG presence, lanes 12-20: time points of supercoiling reaction in the presence of 1 µM McbG. (**B**) Gel described above run in the presence of EtBr (**C**) Gyrase cleavage activity assay in the presence of 20 µM Mccb17 and increasing concentration of McbG. Lane 1: relaxed pBR322, Lane 2: lane 2: gyrase and relaxed pBR32, Lane 3: no nuclease activity is present for 20 µM Mccb17; Lane 4: 20 µM Mcbb17 incubated with gyrase, Lane 5: no nuclease activity is observed for 40 µM McbG, Lane 6: 40 µM McbG incubated with gyrase, Lanes 7-13: effect of increasing concentration of McbG on gyrase cleavage activity in the presence of 20 µM Mccb17 (no McbG, 0,2 ;1 ;5;10;20;40). The gel has been developed in the presence of EtBr.

5.2.3.5. Activity in gyrase ATPase assay

The obtained data for QnrB1 suggested that one of potential PRP activities is stimulation of ATPase reaction. The McbG was tested in the same setup where GyrB43 was treated with 5 µM McbG (**Figure 67**).

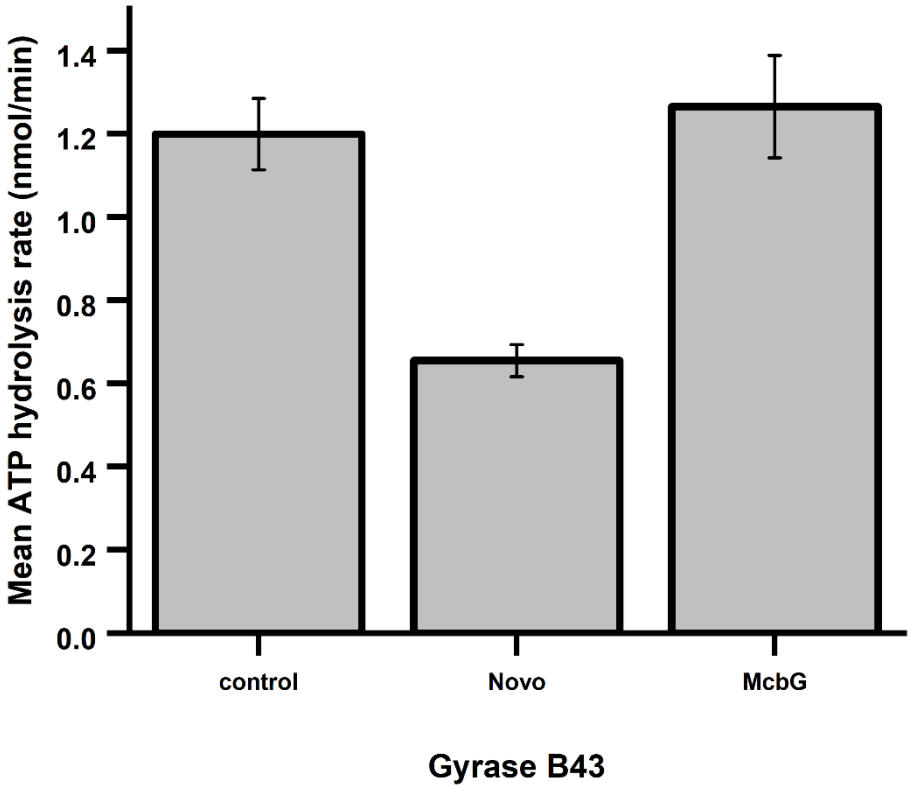

Figure 67. ATPase rate data for 4 μM GyrB43 mixed with 50 μM novobiocin (Novo) and 5 μM McbG. Error bars are expressed as the standard deviation of three independent experiments.

No stimulation effect was observed in this experiment. McbG seems not to be interacting with ATPase domain. It is also possible that the protein has low stability and is unable to interact with the enzyme during the assay.

5.2.3.6. McbG protein stability test

It can be hypothesised that the produced McbG protein is misfolded which could be the reason for lack of observable activity. It would explain low stability, high tendency for precipitation and lack of observed crystals during trails. Tycho Scanner (Nanotemper) was used to study if protein tertiary structure is intact. The method is based on measuring the changes in the intrinsic fluorescence, detected at both 350 nm and 330 nm, from tryptophan and tyrosine residues in the protein. The thermal ramp is applied and the ratio of 350 nm and 330 nm fluorescence is plotted. The peak of the first derivative of the plot indicates inflection temperature (Ti). Another PRP protein, QnrB1 was used as a reference. Purified HIS-McbG produced a sigmoidal melting curve with an inflection point Ti = 66.9ºC which is close to Ti value for QnrB1 Ti = 60.2 ºC (**Figure 68**). The

curve has a reverse profile compared to the QnrB1 curve. This can be explained by the fact that McbG protein do not possess tryptophan residues. Difference of 350 nm / 330 nm ratio (Δ Ratio) for McbG is 0.22 which is close to QnrB1's Δ Ratio (0.25). The similarity of Ti and Δ Ratio suggests correct folding of McbG.

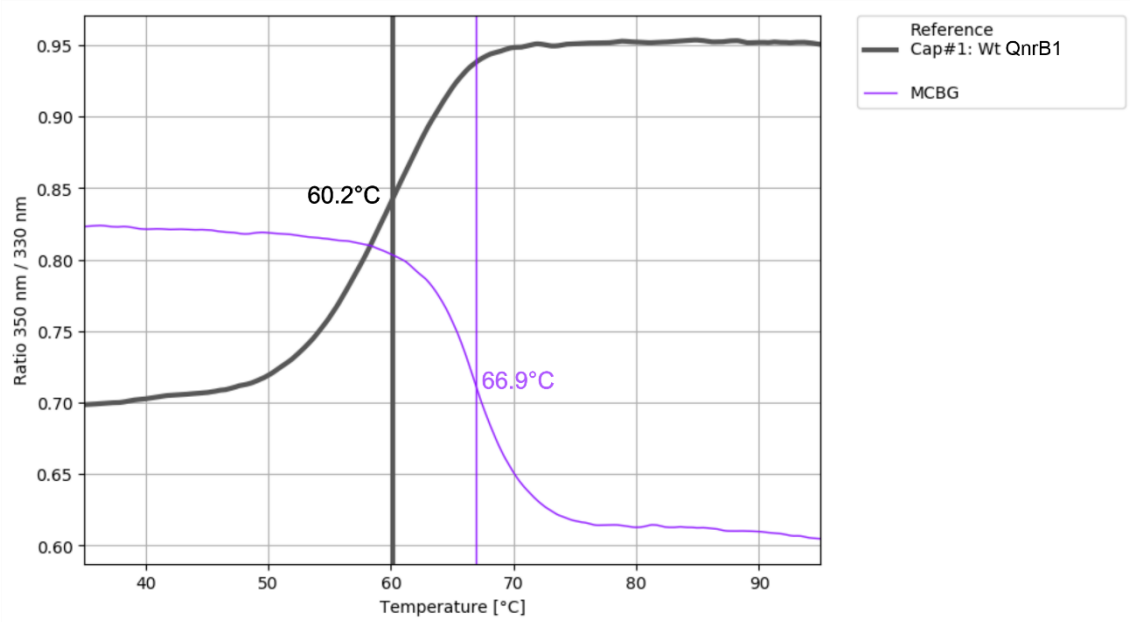

Figure 68. Graph showing a ratio of 350 nm and 330 fluorescence for 1 µM McbG protein (violet line) and 1 µM QnrB1 protein (dark line). Inflection points are indicated accordingly.

5.2.3.7. Direct McbG-Gyrase interaction studies

Because the results from the gyrase assays were inconclusive, I sought more evidence for direct interaction of McbG and *E. coli* gyrase. Similarly, as in the case of QnrB1 and AlbG, a pull-down assay was used to directly study the interaction of proteins. Due to the unavailability of FLAG-tagged McbG, His-McbG together with HisPur Ni-NTA resin was used. Bands corresponding to DNA gyrase were observed only when the gyrase complex was added into the mixture (**Figure 69**). Surprisingly pull-down was also observed in the case of reaction in the presence of 1 mM ADPNP. Observed pull-down suggests that the McbG protein is able to interact with the gyrase complex. The lack of pull-down in the case where GyrA and GyrB subunits were tested alone could suggest that the McbG is interacting with the interface created between GyrA and GyrB by gyrase hetero-tetramer. Unfortunately, the result cannot be directly compared with the results for QnrB1 and AlbG pull-downs since different resins have been used in the experiment.

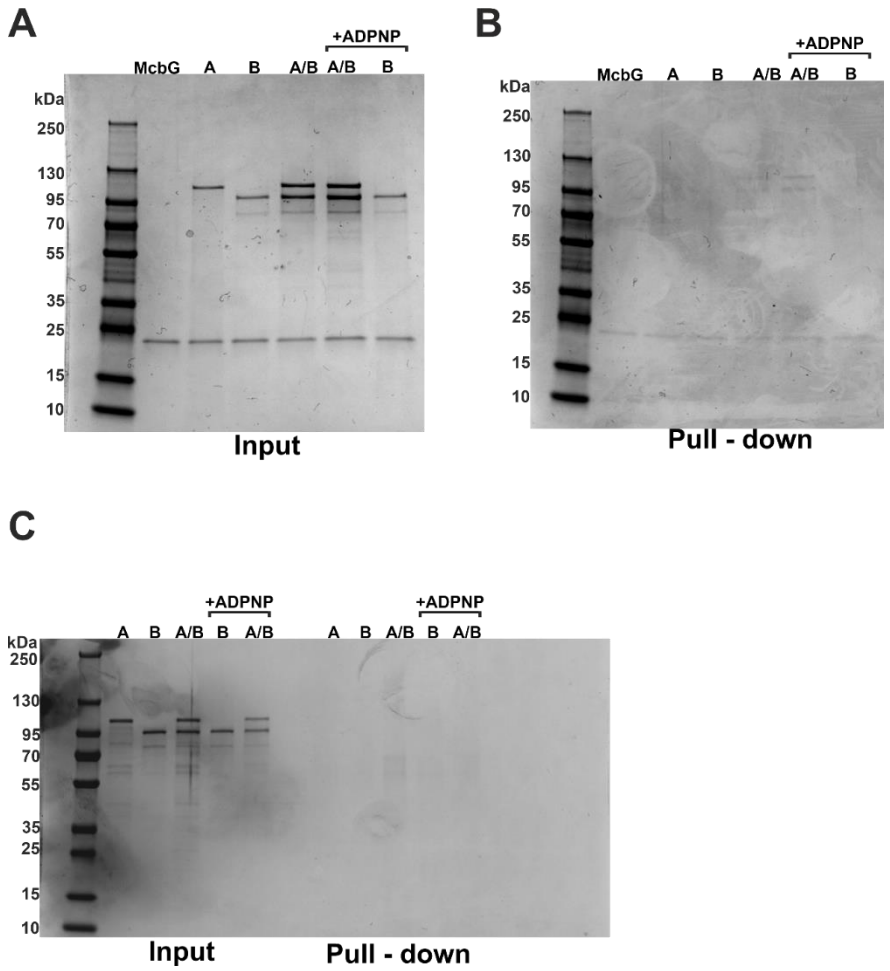

Figure 69 Pull-down assay with N-terminally HIS-tagged McbG and purified GyrA, GyrB and A_2B_2 complex. A – input – samples with 5 μM HIS-McbG, B – pull-down (eluates from HisPur™ Ni-NTA Resin) of samples with HIS McbG. C – control mock pull-down experiment with no McbG present. A Coomassie stained SDS-PAGE gel is shown.

5.2.3.8. Mass-spectrometry identification of GyrA and GyrB proteins in purified sample of McbG protein

Since gyrase proteins were observed to interact with HIS-McbG protein *in vitro*, it was possible that a small amount of expression host gyrase subunits would copurify with overexpressed McbG protein. After purification of HIS-McbG in *E. coli* expression system liquid chromatography coupled with tandem mass spectrometry (LC-MS/MS) was used to detect possible copurification of small amounts of *E. coli* gyrase subunits with His-McbG. Such an approach was shown to be successful despite the fact that one of the interacting partners could be produced and copurified at a lower level of magnitude (Vobruba *et al.*, 2020) The specimen after all purification steps was analysed to check for presence of purification contaminants. Indeed, GyrA and GyrB proteins appeared in the

top four positions in mass spectrometry results (**Table 14**). The result was consistent regardless of the purification method used (see *Methods* section). As expected, McbG protein gave the highest score for match confidence. Both GyrA and GyrB proteins shown significant coverage and score. The fact of identification of cAMP-activated global transcriptional regulator with good confidence could be explained since CRP is a common contaminant during IMAC chromatography (Bolanos-Garcia and Davies, 2006). Fourth protein on the list, RNA-binding protein Hfq, is identified significantly less reliably than previous identified proteins. This fact suggests that the copurification of McbG and gyrase subunits is not accidental.

Table 14. LC-MS/MS identification of proteins GyrA and GyrB in a sample obtained after purification of HIS-tagged McbG protein in *E. coli* BL21(DE3) Gold sorted by descending score value (top four positions are presented from MASCOT search engine) **Score -** The sum of the ion scores of all peptides that were identified. **Coverage -** The percentage of the protein sequence covered by identified peptides. **# Proteins -** The number of identified proteins in a protein group, **# Unique Peptides - The** number of peptide sequences that are unique to a protein group. **# Peptides -** The total number of distinct peptide sequences identified in the protein group **# PSM's -** The number of peptide spectrum matches.

Accession	Description	Score	Coverage %	# Proteins	# Unique Peptides	# Peptides	# PSMs
P05530	Protein McbG OS=Escherichia coli GN=mcbG PE=4 SV=1 - [MCBG_ECOLX]	5742 5.92	96.79	1	25	25	1403
P0ACK0	cAMP-activated global transcriptional regulator CRP OS=Escherichia coli O157:H7 GN=crp PE=3 SV=1 - [CRP_ECO57]	7785 .49	61.43	1	14	14	204
P0AES7	DNA gyrase subunit B OS=Escherichia coli O157:H7 GN=gyrB PE=3 SV=2 - [GYRB_ECO57]	2351 .35	53.86	1	32	32	60
P0AES4	DNA gyrase subunit A OS=Escherichia coli (strain K12) GN=gyrA PE=1 SV=1 - [GYRA_ECOLI]	1433 .35	36.00	1	26	26	38
A7ZV41	RNA-binding protein Hfq OS=Escherichia coli O139:H28 (strain E24377A / ETEC) GN=hfq PE=3 SV=1 - [HFQ_ECO24]	892. 27	50.98	2	5	5	23
P0AA45	Ribosomal small subunit pseudouridine synthase A OS=Escherichia coli O157:H7 GN=rsuA PE=3 SV=1 - [RSUA_ECO57]	207. 54	33.33	1	5	5	7

Altogether it can be seen that McbG is interacting with *E. coli* DNA gyrase. The effects observed in gyrase assays are less pronounced compared to QnrB1 and AlbG. The protein has low stability once purified. This is not observed for other tested PRPs.

5.3. Structure of QnrB1-gyrase-DNA-MFX complex

Previous results have shown that QnrB1 is interacting with the purified gyrase complex. After incubation of gyrase holo-complex and QnrB1, GyrA and GyrB subunits were present in the eluate after pull down. To understand the mechanism of interaction between PRP and gyrase, cryo-EM was used to obtain the structure of QnrB1-gyrase (GyrBA)-DNA-MFX complex. Previously described double-nicked 20-12p-8 DNA was used together with MFX to trap the enzyme in the cleavage state. The 20-12p-8 DNA duplex consists of 12-mer and an 8-mer and has an artificial nick in the DNA at each cleavage site, such as the 5' nucleotide of the 12-mer ends with a 5' phosphate. Such a system was previously successfully used to obtain structure of cleavage complex of *S. aureus* DNA gyrase (Chan *et al.*, 2015). The DNA gyrase purification for cryo-EM was based on another reported cryo-EM structure of gyrase(Vanden Broeck *et al.*, 2019).

The complexes were obtained in two different conditions: without the nucleotide, and with an addition of ATP to observe the effect of ATP hydrolysis on QnrB1 interaction.

Single-particle analysis of collected data revealed two different complexes with rod-like QnrB1 bound to DNA gyrase. After performing 3D classification, two DNA-bound structures were determined, at resolutions of 3.2 and 3.4-Å respectively for nucleotide-free and ATP conditions. In both QnrB1-DNA-GyrBA (with and without ATP) complexes, the whole gyrase tetramer was observed with the exception of GyrA CTDs (GyrA 8-525, GyrB 27-790). Statistics for obtained models are presented in **Table 15**. The overall structure and cryo-EM maps are presented in **Figure 70**.

Table 15. Refinement statistics of EcGyr QnrB1 models

Model	**EcGyr-QnrB1-no_ATP**	**EcGyr-QnrB1-with_ATP**
Model resolution (Å)	3.2	3.4
Model composition		
Non-hydrogen atoms	27623	27600
Protein residues	3400	3396
Nucleotides	60	60
Ligands	6 (2 MFX; 4 MG)	6 (2 MFX; 4 MG)
Mean B factors (Å^2)		
Protein	164.11	50.31
Nucleotide	77.86	34.84
Ligands	103.22	43.57
R.m.s. deviations		
Bond lengths (Å)	0.007	0.008
Bond angles (°)	0.988	1.279
Validation		
MolProbity score	1.72	1.58
Clashscore	2.64	2.44
Ramachandran plot		
Favoured (%)	92.43	91.83
Allowed (%)	7.57	8.17
Disallowed (%)	0.00	0.00

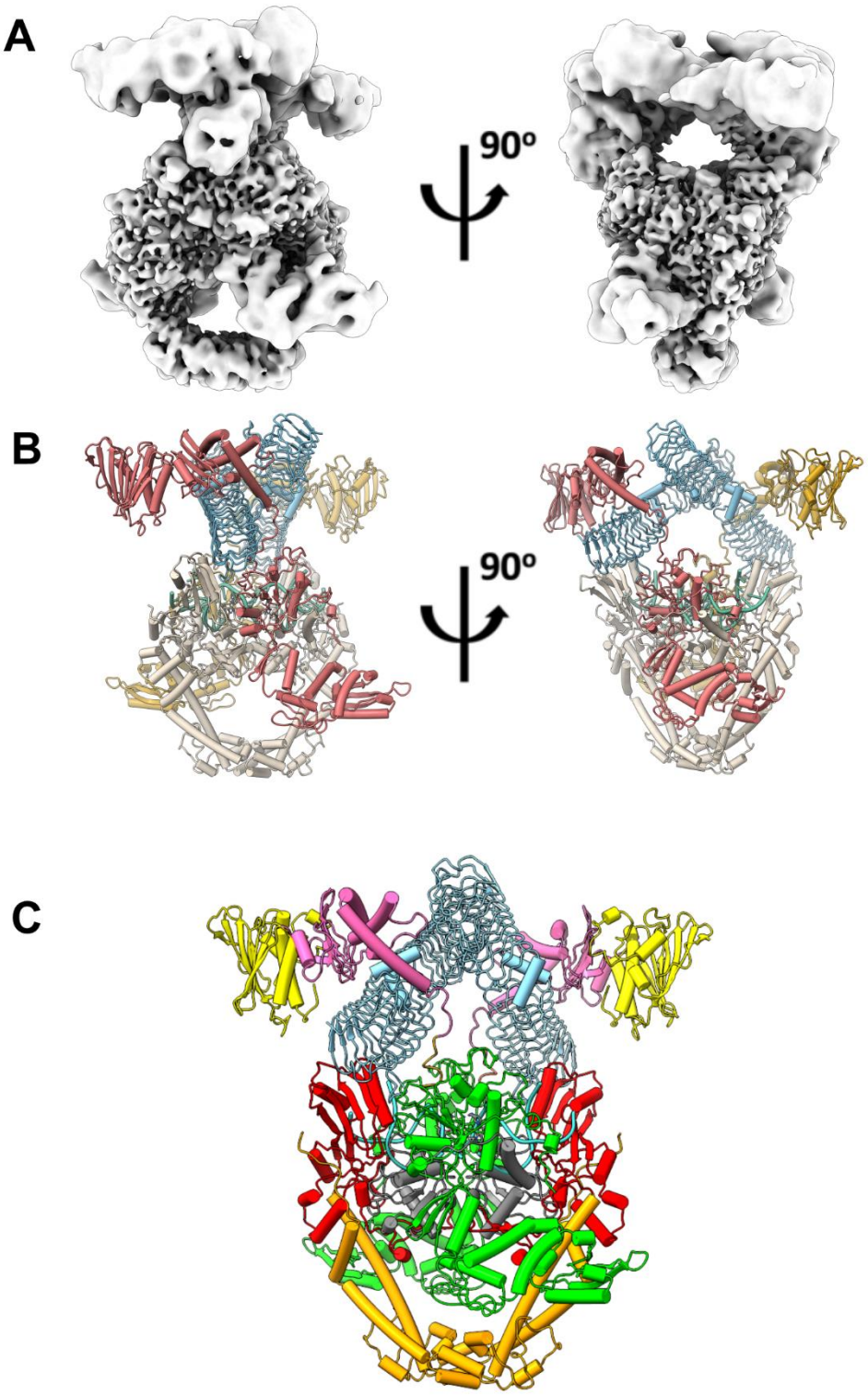

Figure 70. (**A**) Cryo-EM maps of gyrase: DNA: QnrB1 complex (EcGyr-QnrB1-no_ATP) represented as grey mesh. (**B**) Overall molecular models obtained after model building and refinement procedure (EcGyr-QnrB1-no_ATP). Alpha helices are represented as cylinders and beta strands as arrows. QnrB1 - blue, GyrA - white, GyrB1-coral, GyrB2- golden, DNA- turquoise (**C**) Positions of individual domains in obtained gyrase: QnrB1: DNA complex: ATPase domain (B24) – yellow; transducer – pink; TOPRIM – lime, WHD – grey, TOWER – red, Coiled coil – orange, DNA – turquoise.

Compared to previously published cryo-EM structure of *E. coli* DNA gyrase (Vanden Broeck *et al.*, 2019) the quality of data for both QnrB1-gyrase-DNA-MFX complexes allowed us to model previously absent loops in GyrA and GyrB (GyrA 422-427, 443-446 and GyrB 474-483). Due to the fact that only 20 bp-long DNA was used, the GyrA CTDs did not wrap the DNA and were too flexible to be observed as clear density that would allow model building.

Both obtained conformations have 2-fold symmetry and consist of the "core" cleavage-reunion domain, two dimers of QnrB1 located in the gap between GyrA TOWER and GyrB TOPRIM, and ATPase domains of GyrB "covering" QnrB1 on top (**Figure 71**).

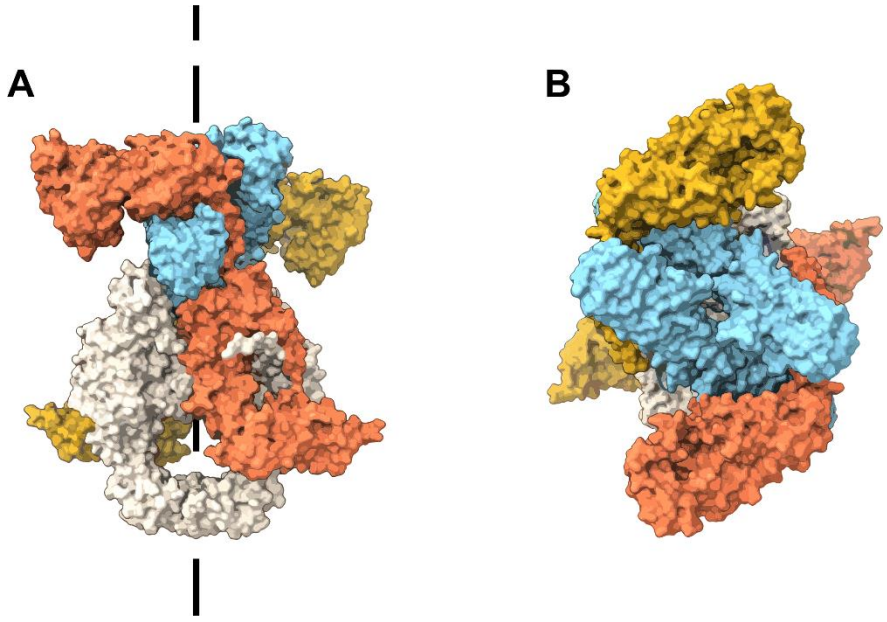

Figure 71. Overall view of DNA gyrase: DNA: QnrB1 complex (EcGyr-QnrB1-no_ATP) presented as molecular surface (solvent-excluded surfaces). C2 symmetry axis of the complex is depicted as a dashed line. (**A**) Side view, (**B**) Top view. QnrB1 - blue, GyrA - white, GyrB1-coral, GyrB2- golden

The structure of GyrBA "core" is similar but not identical to the reported *E. coli* gyrase structures (6RKU and 6RKV); the distance between two adjacent GyrA protomers is closer to 6RKU (closed state, RMSD 1.6 Å) than to that of the pre-opening state of gyrase (6RKV, RMSD of 2.3 Å).

The mode of binding of double-nicked DNA, and the cleavage site show high similarity to the previous crystal structures of *S. aureus* (Chan *et al.*, 2015) and mycobacterial (Blower *et al.*, 2016) gyrase cleavage-reunion core with fluoroquinolones. Calculated RMSD of superposition with *S. aureus* cleavage-reunion core structure (PDB: 5cdq) was 1.2 Å. Two molecules of MFX are bound between the DNA bases from both sides of cleaved DNA fragments inhibiting DNA re-ligation. (**Figure 72**)

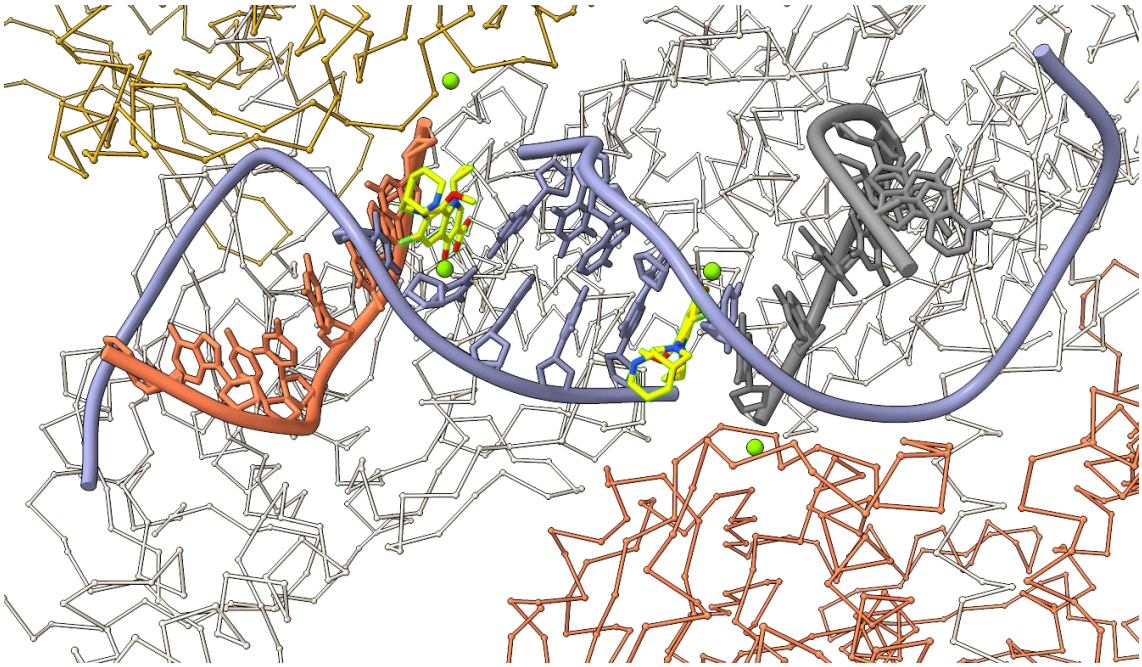

Figure 72. Binding site of two moxifloxacin molecules within the cleavage-reunion core of *Ec*Gyr (EcGyr-QnrB1-no_ATP). For clarity the protein chains are represented as C-alpha backbone (sticks). DNA sugar phosphate-backbone is represented as ribbon and nucleotides presented as sticks. Magnesium ions are presented as green spheres GyrA - white, GyrB1-coral GyrB2- golden. MFX molecules are presented as yellow sticks.

The MFX molecules show good fit to the model (CC :0.80) and contain the density for the associated Mg $^{2+}$ ion which connects the drug molecule to the Asp87 and Ser83 (water-metal-ion bridge). The "B" site metal (Bax *et al.*, 2019) which is coordinated by the side chains of GyrB D498 and D500 is also unambiguous (CC 0.80). (**Figure 73**).

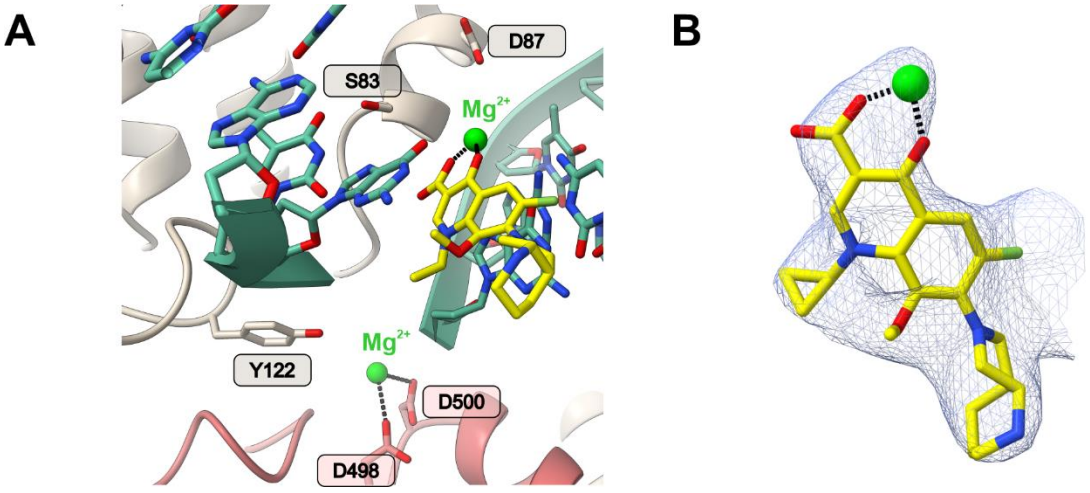

Figure 73. Close-up view of the MFX binding site captured in the which? complex. (**A**) Single MFX molecule (shown as yellow sticks) binding is presented together with the magnesium ion interacting with drug molecule (water-metal-ion bridge). The "B" site Mg^{2+} ion coordinated by the side chains of GyrB D498 and D500 is also presented. The base pairs of neighbouring nucleotides are presented as sticks. The protein residues S83, D87 and Y122 for GyrA and D498 and D500 for GyrB are presented as sticks. (**B**) Coulomb potential density for the MFX molecule.

In course of work for this PhD thesis it was established that ATP was strictly required for QnrB1 to be able to rescue gyrase-fluoroquinolone complexes from inhibition.

After analysis and model building for QnrB1- GyrBA-DNA dataset collected in the presence of ATP (EcGyr-QnrB1-with_ATP) it became obvious that the addition of ATP led to the striking structural rearrangement of the GyrB43 domain. The ATPase domains move > 90 Å and rotate 90° to interact each with an opposite QnrB1 monomer as compared to the nucleotide-free state (see **Figure 74**). In the nucleotide-free structure GyrB43 is covering the QnrB1 from the top interacting with the same QnrB1 monomer that binds to the TOWER domain, in the ATP structure GyrB43 approaches a different protomer in QnrB1 dimer, supporting it from the bottom. Further detailed 3D classification analysis shown that while both conformations of ATPase domains were observed in nucleotide-free and ATP datasets, the particles were distributed between them in the opposite ways. This fact is pointing at the role of ATP as a potential conformational switch for GyrB43.

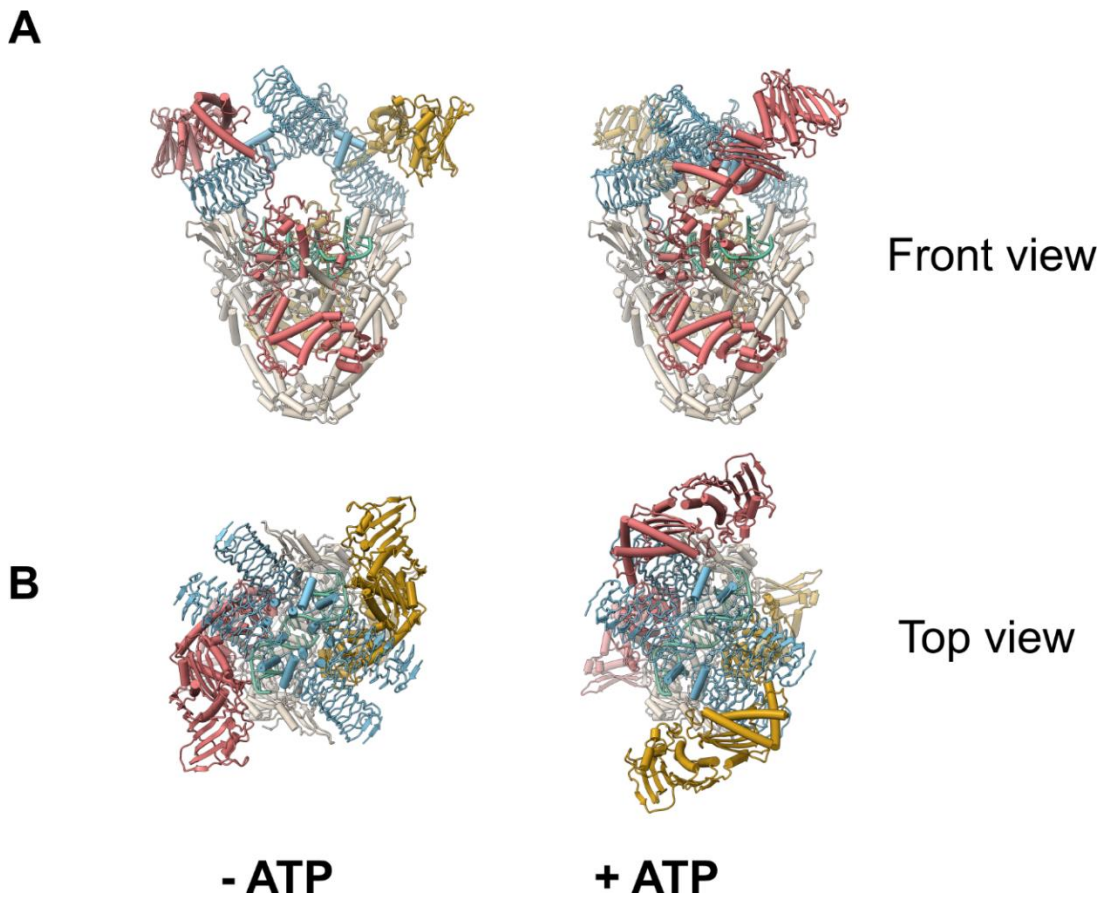

Figure 74. Comparison of structures: EcGyr-QnrB1-no_ATP – *left*, EcGyr-QnrB1-with_ATP – *right*. The structures are superimposed according to the gyrase core position. (**A**) Front view, (**B**) top view. Alpha helices are represented as cylinders and beta strands as arrows. QnrB1 - sky blue, GyrA - white, GyrB1- coral, GyrB2- goldenrod.

In the majority of topoisomerase II structures solved so far, nucleotide analogue ADPNP was used resulting in the stabilisation of state where ATPase domains formed an interlocked dimer in the middle of the space above the G-segment; it was hypothesized that T-segment capture occurs inside the cavity formed by ATPase domains. This led authors of a recent study of MfpA:MtGyrB47 complex (PDB: 6ZT5) to propose a similar model for the MfpA capture in the context of the holoenzyme (Feng *et al.*, 2021). Cryo-EM structures of gyrase: DNA: QnrB1 complex show unambiguous density for the linker region (389-402) between ATPase and transducer domain that position each ATPase/transducer domain next to the TOPRIM from the same, rather than the opposite GyrB subunit. Compared to the published *E. coli* gyrase structure, where this region is clearly visualised (PDB: 6RKW) this linker has significantly different orientation. It is highly probable that the linker conformation is altered by the conformation change of the enzyme due to QnrB1 interaction (**Figure 75**).

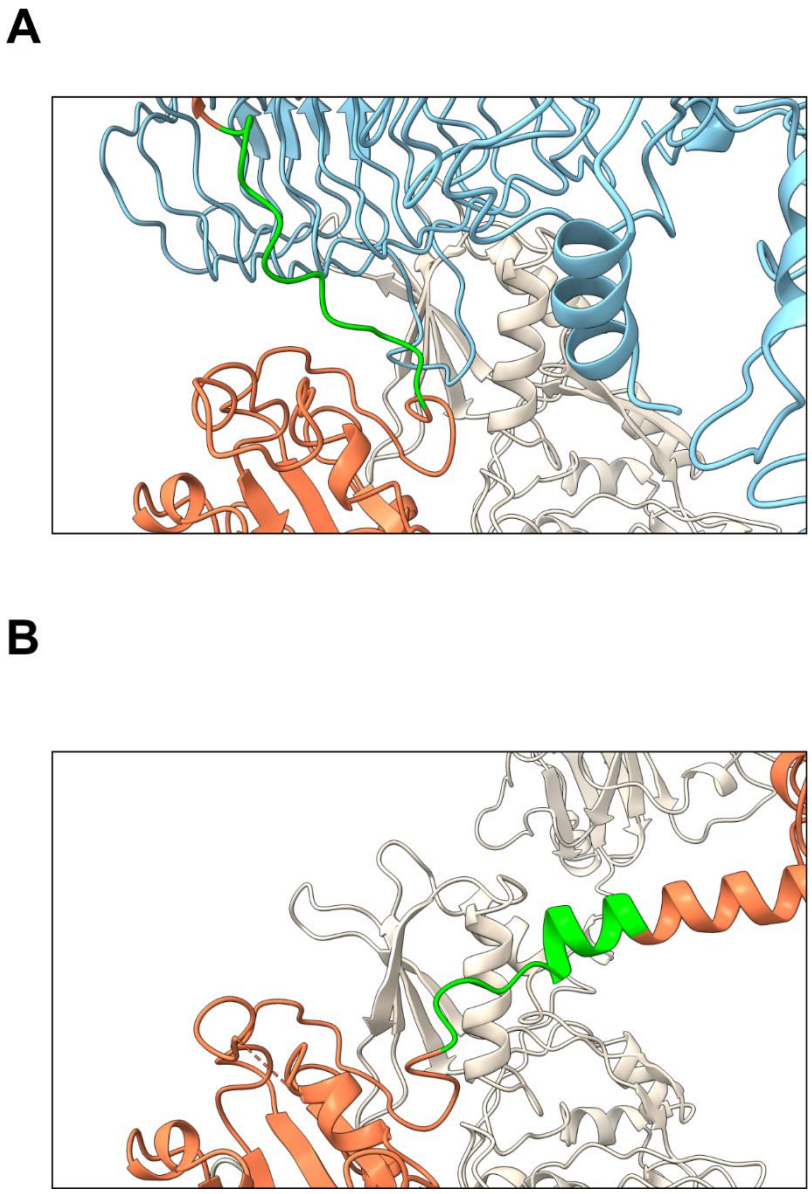

Figure 75. Comparison of structure of GyrB linker 389-402 and orientation of GyrB ATPase domains in *E. coli* gyrase: DNA: QnrB1 complex and published *E. coli* gyrase-DNA holo-complex structure (6RKW). The linker is coloured green, Qnr - blue, GyrA - white, GyrB-coral. (**A**) Structure of the linker in QnrB1: DNA: gyrase complex. (EcGyr-QnrB1-no_ATP) (**B**) Structure of linker from *E. coli* gyrase holo-complex (PDB: 6RKW), the linker is coloured green

Interestingly, the position of ATPase domains is more similar to the one observed in extremely 'open' structure of DNA *Mycobacterium tuberculosis* gyrase (6GAV) (Petrella *et al.*, 2019) or of *Streptococcus pneumoniae* Topo IV (PDB:4I3H) (Laponogov *et al.*, 2013).

Crystal structure of a topoisomerase-acting PRP from *Mycobacterium smegmatis* (MfpA) was determined as bound to mycobacterial GyrB47 domain (PDB: 6ZT5) (Feng *et al.*, 2021). QnrB1 shares some level of similarity (25% sequential identity and presence of pentapeptide repeats) with mycobacterial protein, although MfpA does not have loops in

the structure. The model of the mycobacterial complex can be used nevertheless to compare the binding of QnrB1 with *E. coli* GyrB43 in obtained gyrase: DNA: QnrB1 complexes. MfpA and *M. smegmatis* GyrB47 interact in the similar manner when compared to QnrB1 and *E. coli*. The calculated RMSD value for superposition of GyrB47 domain *M. smegmatis* structure and GyrB43 (GyrB 27-790) of *E. coli* is 0.73 Å. The structures, although not identical (note different angle of the PRP approaching the ATPase domain), display overall conformational similarity (**Figure 76**).

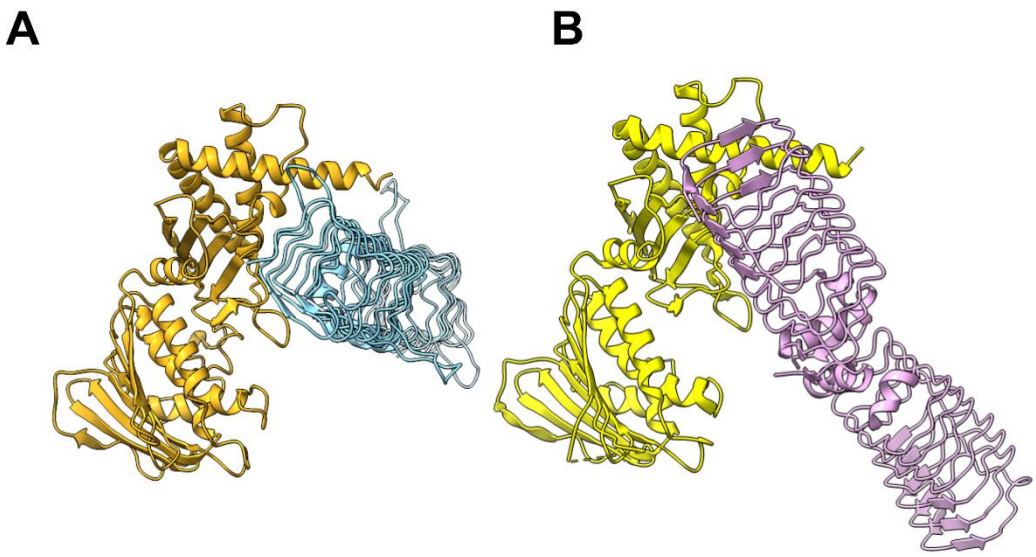

Figure 76. Structural comparison of *E. coli* GyrB ATPase/QnrB1 and *M. smegmatis* GyrB ATPase/MfpA. (**A**) Cryo-EM structure of *E. coli* ATPase domain and QnrB1 (this work). (**B**) X-ray diffraction structure of *M. smegmatis* ATPase domain and MfpA. PDB: 6ZT5 - The structures are oriented according B43 domain superposition. Qnr - blue, GyrB43- golden, MfpA - pink, GyrB47- yellow.

Within the EcGyrBA-DNA-QnrB1 complex, the major interaction surface is QnrB1 face 2 (Vetting, Hegde, Wang, *et al.*, 2011) that interacts with the ATPase domain . After analysis of the structure with the bioinformatic tool to detect salt bridges (ASBAAC: Automated Salt-Bridge and Aromatic-Aromatic Calculator) (Roy and Datta, 2018), four salt bridges were identified : (Qnr R48: GyrB E317, Qnr R90:GyrB E317, Qnr Y123:GyrB R386, and Qnr R140:GyrB D313). (**Figure 77 A**). Residues R48 and Y123 were previously shown to crosslink to GyrB43 (cf. section **5.2.1.8**). Residues Q51, R77 and R167 of QnrB1 that were also found crosslinking in the biochemical experiments were not found in the close vicinity to any potential interaction site. This suggests that potentially QnrB1 ‘probes’ multiple other positions relative to the GyrB43 that were not necessarily captured or occupied enough to show up in the cryo-EM experiments. The

crosslinking reaction is happening *in situ* during protein interaction, while cryo-EM structure represents a snapshot of the protein's conformation at a specific moment in time, and the conformations observed may not necessarily represent all possible conformations of the protein in solution.

The binding between QnrB1 and GyrB43 is structurally similar to the one observed between MfpA and MsGyrB47 (**Figure 77 B**) suggesting that the interaction between the PRP and ATPase domain is the important and conserved part of the mechanism, and is consistent with the biochemical data showing good agreement between the behaviour of QnrB1 and MfpA systems.

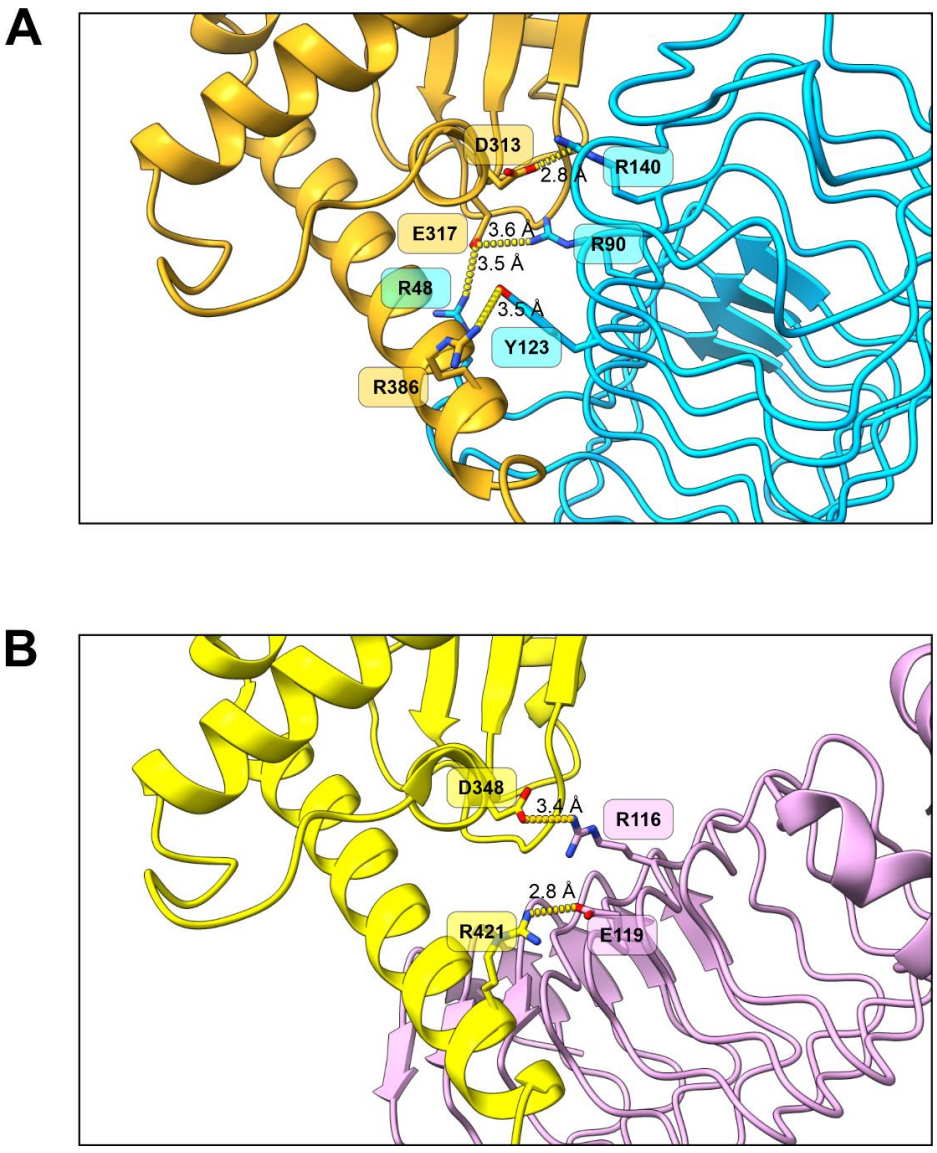

Figure 77. Comparison of interaction of PRPs with GyrB ATPase domains. (**A**) *E. coli* gyrase and QnrB1 (this work), (**B**) *M. smegmatis* GyrB47 / MfpA crystal structure (PDB: 6ZT5). Qnr - sky blue, GyrB43-gold, MfpA - pink, GyrB47 - yellow. Distances between potential interaction between atoms are presented as dark dashed lines. The measured distance is shown in Å. Heteroatoms of interacting residues are coloured (nitrogen - blue -, oxygen -red)

The important difference between MfpA, and QnrB1 is the presence of the loop B in Qnr protein which interacts with the GyrA subunit to position the protein in alignment with the TOWER domain. In each dimer of QnrB1, one monomer is bound between the GyrA TOWER domain and GyrB43. The loop B of QnrB1 fits in the hydrophobic pocket formed between the GyrB TOPRIM and GyrA TOWER domains. This interaction influences the conformation of the loop, such that it is different to the conformation observed in the crystal structure of the apo QnrB1(PDB: 2XTW) model (RMSD: 2.23 Å) (**Figure 78**).

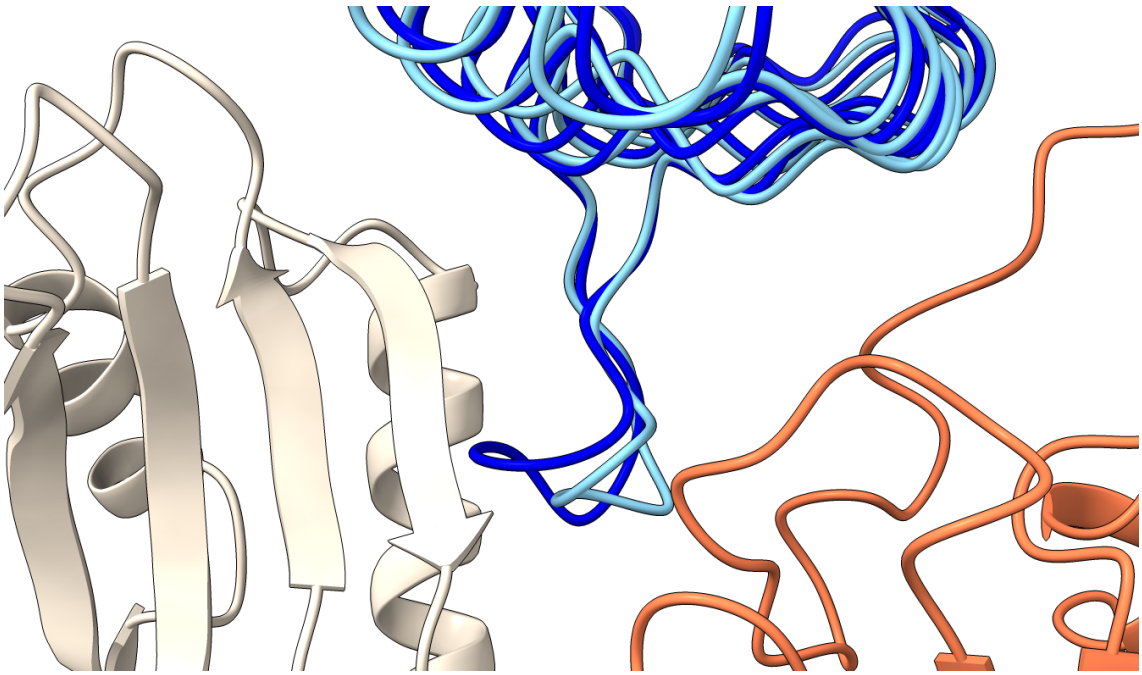

Figure 78 Superposition of a single chain of QnrB1 from the crystal structure (PDB:2XTW) with QnrB1 monomer bound in gyrase: DNA: QnrB1 complex. Qnr (PDB:2xtw) - dark blue, QnrB1 in gyrase: DNA: QnrB1 complex – light blue: GyrA - white, GyrB-coral,

The main residue of QnrB1 involved in loop positioning is F111, that occupies a hydrophobic pocket formed by the side chains of GyrA V281, A278, I289 and L292 (**Figure 79**). This interaction could influence the enzyme activity since the interaction between the two subunits of DNA gyrase is mediated by the TOWER domain, and changes in the conformation of the TOWER domain can affect the enzyme's activity.

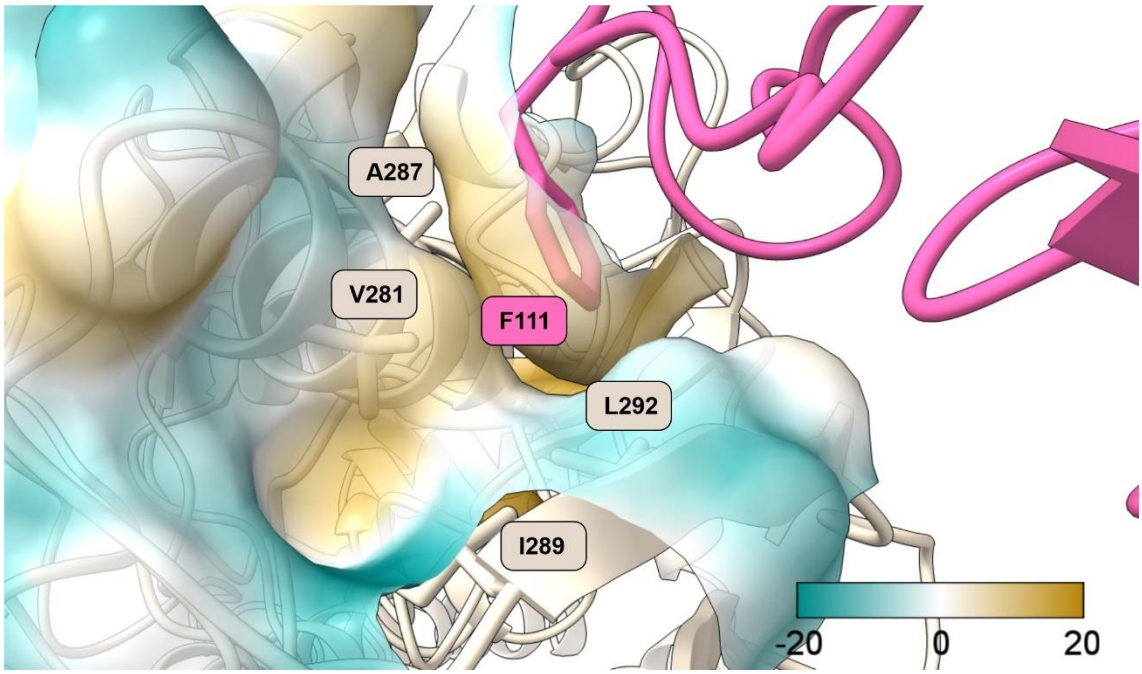

Figure 79. Interaction of QnrB1 loop B with the GyrA TOWER domain: hydrophobic pocket. Molecular surface (solvent-excluded surfaces) of GyrA TOWER domain and QnrB1 F111 residue is coloured according to hydrophobicity (-20- highly hydrophilic, 20- highly hydrophobic). Qnr - pink, GyrA - white. GyrA V281, A278, I289 and L292 and Qnrb1 F111 residues are presented as sticks.

The importance of this interaction is supported by the previous extensive data showing essentiality of loop for protection; moreover, it previously has been shown that a single alanine mutation in this position (QnrB1 F111) completely abolishes the protective activity of PRP (Jacoby *et al.*, 2013). The loop B structure is stabilised by the hydrogen bonding between N103 and T106. Residue T106 seems to interact with the main chain carbonyl of the residue L292 of GyrA. (**Figure 80**).

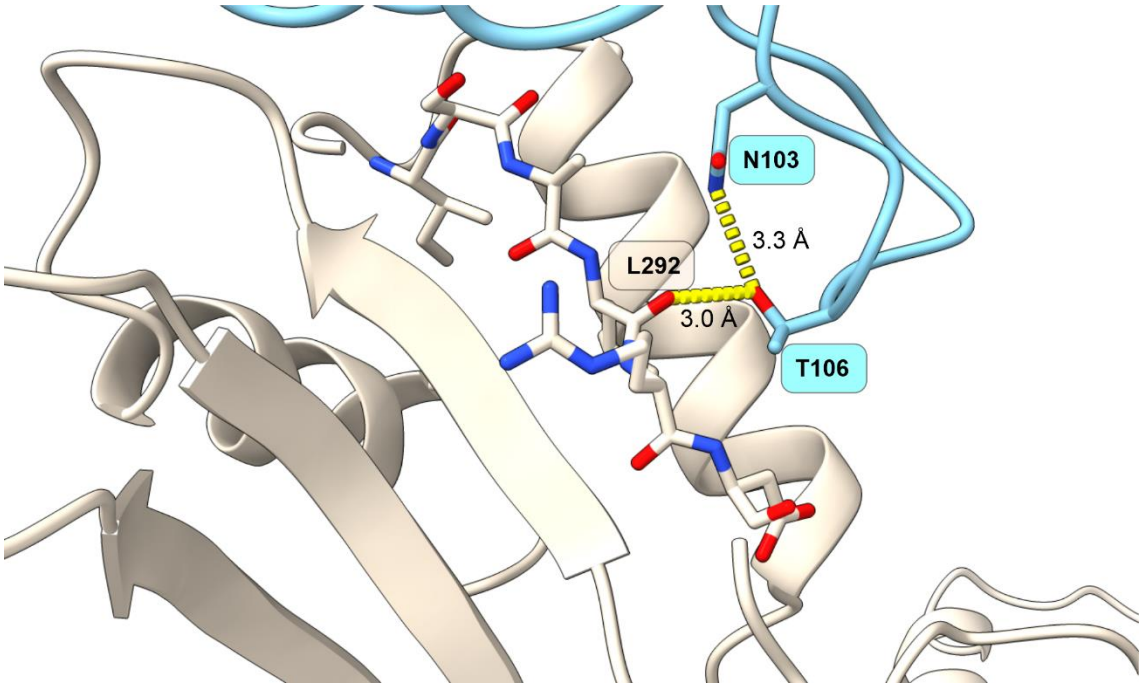

Figure 80. The hydrogen bonding between N103 and T106 in the QnrB1 loop B and potential salt bridges between QnrB1 T106 and GyrA L292. Distances between the interacting residues are presented as dark dashed lines. The measured distance is shown in Å. Residues 289-294 of GyrA TOWER and N103 and T106 of QnrB1 are presented as sticks and heteroatoms are coloured (nitrogen -blue, oxygen- red)

As was shown in the section representing biochemical experiments on QnrB1 and other studies, deletion of residues 106-108 within the loop B (ΔTTR) completely abolishes the protective activity of QnrB1 (Jacoby *et al.*, 2013) and at the same time does not affect its ability to inhibit gyrase or stimulate ATPase activity of GyrB43 (Mazurek *et al.*, 2021). Residues 286-298 of the TOWER domain of GyrA have been shown to be involved with interaction with QnrB1 in other studies where a crosslinking approach was used (Chen *et al.*, 2021). Together those two observations strongly imply that the loop B of QnrB1 is interacting with GyrA and this interaction, whilst not the strongest one, is key for ATP-stimulated rescue activity of the protein.

5.3.1. Structure-driven mutagenesis of QnrB1

Prompted by the fact that the residues R48, R140 and R190 of QnrB1 were found to form salt bridges with the GyrB, alanine mutants of QnrB1 were prepared by site-directed mutagenesis and their ability to confer CFX resistance was tested by MIC measurement. *E. coli* BW25113 strain was transformed with pBAD plasmids encoding appropriate mutated genes. 4 mutants of QnrB1 were tested: Y123A, R48A Y123A, R48A Y123A R146A and R48A R90A Y123A R146A. The single mutant Y123A already shown six-fold reduction of resistance compared to wtQnrB1. Every other mutation has shown an

additive effect on MIC (**Figure 81**). These results support the hypothesis that the face 2 of QnrB1 is interacting with GyrB43 and this interaction is essential for gyrase protection.

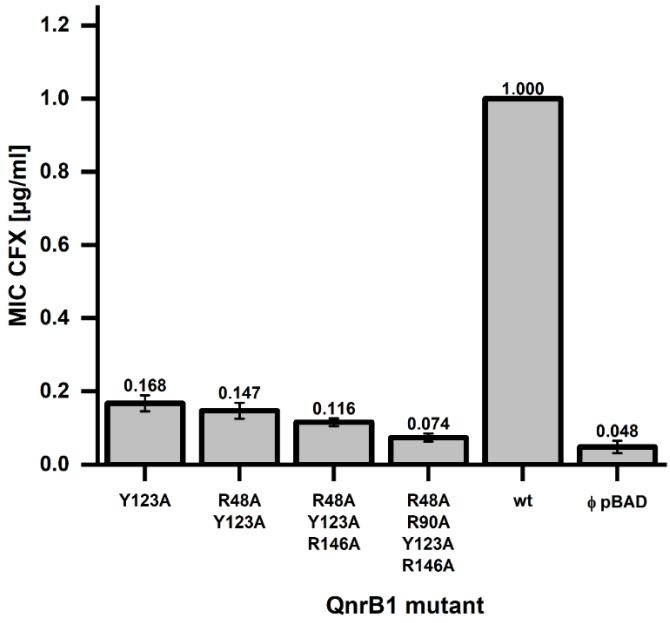

Figure 81. CFX MIC strip tests results for alanine mutants of QnrB1. WT – wild type QnrB1, Φ pBAD – empty vector. Error bars represent SD of three repetitions.

Data collected in Cryo-EM experiments and biochemical studies of QnrB1 suggests that there are two interaction interfaces that plays role in QnrB1 activity. Face 2 of QnrB1 seems to position the protein in the correct orientation in the context of DNA gyrase. Loop B interaction with the GyrA TOWER domain is also essential for protective activity. Only when those two interactions are present the QnrB1 protein is able to offer protection.

6. Discussion

The main aim of the study was to provide biochemical and structural data about the interaction between pentapeptide repeat proteins (PRPs) and *E. coli* DNA gyrase. QnrB1 from *Klebsiella pneumoniae*, AlbG from *Xanthomonas albilineans* and McbG from *Escherichia coli* were analysed in a series of experiments. Each of the analysed proteins was analysed together with its cognate toxin (QnrB1-fluoroquinolones, AlbG- albicidin, McbG – microcin B17). This approach where different PRPs are being studied in parallel allows to get a broad picture of PRP behaviour. Due to limitations in obtaining sufficient amounts of McbG protein and low activity of albicidin in biochemical assays, QnrB1 was studied most thoroughly. Nevertheless, the data obtained for AlbG and McbG are adding

important information about other PRP activity. During the study the cryo - EM methodology was used to elucidate the mechanism of PRP activity. Also, the information of interacting amino acids obtained from structural model were used to introduce structurally driven mutations in QnrB1. The cryo-EM data for complex of QnrB1-DNA-gyrase and ciprofloxacin [obtained by Dr Dmitry Ghilarov] that was used to build the molecular model of QnrB1 and DNA gyrase interaction is the first-ever structure that shows a PRP in the context of the full-length DNA gyrase. The previous structure capturing PRP interacting with a part of gyrase was complex between a homodimer of *Mycobacterium smegmatis* MfpA and a single copy of the *Mycobacterium smegmatis* DNA gyrase B47 subdomain (Feng *et al.*, 2021).

The first mechanism of PRPs was based on observations gathered for single PRP. The first proposed mechanism of PRP action (G-segment mimicry) was based on data for (MfpA) from *Mycobacterium tuberculosis* (Hegde *et al.*, 2005). The model suggested that MfpA (and consequently all) other topoisomerase-acting PRPs) was outcompeting DNA in the generation of the initial gyrase-DNA complex, sequestering the gyrase subunits and thus diminishing the formation of the gyrase-covalent DNA: fluoroquinolone complex. Data presented in this thesis suggest that the G-segment mimicry model of PRP mechanism is not correct. As the observations gathered during the thesis could not be explained using this theory.

Through the years, other models were proposed. Direct destabilisation of enzyme-drug-DNA complex by PRP (Vetting, Hegde, Wang, *et al.*, 2011) and T-segment mimicry (Shah and Heddle, 2014) were hypothesised based on gathered biochemical data and bioinformatical analysis of available PRP and DNA gyrase structures. T-segment mimicry model (Shah and Heddle, 2014) was strongly supported by the structural obtained for *Mycobacterium smegmatis* PRP MfpA interacting with *M. smegmatis* GyrB47 (Feng *et al.*, 2021) Data gathered in this thesis suggests that the actual PRP gyrase protection mechanism supports T-segment mimicry model wherein upon being captured as T-segment mimic the PRP is able to recognise the cleavage complex and destabilise it. It has to be noted that the data are also suggesting that possibly not all PRPs share exactly the same mechanism of action. In the discussion section the observations for all PRPs will be compared and the implications of results would be discussed in the context of gyrase mechanism.

6.1. Comparison of behaviour of tested PRPs in gyrase activity assays

Obtained results for biochemical assay shows difference between tested PRPs. Unfortunately, due to problems in McbG production and its instability some of the experiments were not performed for it. The results that could be compared have been presented in **Table 16.**

Table 16. Comparison of results obtained for PRP proteins in biochemical assays

	QnrB1	**AlbG**	**McbG**
Supercoiling rescue in the presence of cognate toxin	YES	YES	YES
Supercoiling inhibition by high concentration of protein	YES	NO	NO
Cleavage reduction in the presence of cognate toxin	YES	YES	YES
Relaxation stimulation	YES	NO	Experiment not performed
ATP independent relaxation protection	YES	NO	Experiment not performed
ATPase stimulation	YES	NO	NO
Competition in DNA binding	YES	NO	Experiment not performed
Gyrase subunit pull-down	YES (GyrB and gyrase complex)	NO	YES (gyrase complex)
*p*Bpa mutant crosslinking	To GyrB43 and GyrB	To GyrA and GyrB	Experiment not performed

The variety of obtained biochemical results indicates that the topoisomerase acting PRPs could share some degree of similarity in the case of mechanism of action but they interaction with DNA gyrase could differ in important details.

This thesis provided biochemical data about interaction of AlbG with *E. coli* gyrase. The AlbG protein did not show any influence on gyrase relaxation in any conditions tested. Potentially, AlbG interaction with *E. coli* DNA gyrase is not allowing the dislodging of the albicidin during the relaxation reaction. A large difference in ATPase stimulation between proteins directly shows that the interaction with DNA gyrase is different. This result is later buttressed by the fact that AlbG was not observed in pull-down eluates. Albicidin resistance protein also was not able to outcompete the DNA in competition assays.

It has to be noted that AlbG is the protein encoded in albicidin biosynthetic cluster (Hashimi *et al.,* 2007), The albicidin producer host gyrase has been shown to have distinct features. *X. albilineans* GyrA shows only 62% of identity compared to its *E. coli* counterpart. In the case of GyrB subunit the identity equals 61% The *X. albilineans* protein has two insertions, of 29 and 43 amino acids, in the C-terminal-region, which is involved in DNA wrapping and complex stability. *X. albilineans* was shown not to be able to perform ATP – independent relaxation even at high concentrations of enzyme. Only when *E.* coli GyrA was used together with *X. albilineans* GyrB the relaxation activity was observed (Hashimi *et al.*, 2008). Potentially AlbG as an immunity protein present in the producing host is tailored to its interaction with its host GyrA subunit. This would explain the difference in influence on relaxation assays performed using *E. coli* enzyme. This fact could also explain the fact that albicidin resistance protein was not able to outcompete the DNA in competition assays. To tackle those differences, it would be necessary to perform corresponding experiments using X. *albilineans* gyrase complex. Potentially in higher concentrations AlbG would be causing inhibition of X. *albilineans* gyrase like it is observed for QnrB1 and E. coli protein.

In the case of McbG, the fact that it is a protein originating from *E. coli* also could buttress the fact that co evolution of PRP inside a toxin cluster along with host gyrase could play a role in its specificity. McbG though shown most broad protection against tested toxins. Potentially some TA-PRPs could show higher level of "universal" binding to the enzyme allowing its interaction with different toxin stabilised cleavage complexes.

6.2. Specificity of PRP interactions with gyrase cleavage complexes stabilised by different toxins.

The originally proposed G-segment mimicry model for *M. tuberculosis* MfpA postulated the reduction of DNA binding to gyrase which would lead to inhibition of formation of toxic stabilised cleavage complexes. In this case the PRP-driven reduction of DNA binding should result in a similar level of protection against all toxins whose mode of action requires gyrase-DNA interaction complexes irrespectively of their precise binding site. QnrB1 was shown to not offer protection against proteinaceous gyrase poison CcdB (Kwak, Jacoby and Hooper, 2015) which site of interaction is located in the central cavity of GyrA dimer close the C-gate, nor against the natural product simocyclinone D8, which binds to the GyrA subunit in the 'saddle' region of the DNA displacing DNA (Jacoby, Corcoran and Hooper, 2015). What is more, QnrB1 was shown to have synergistic effect when tested together with simocyclinone D8 which will be rationalised later in this section. In the thesis all tested PRPs shown high level of specificity towards different gyrase poisons.

The structure of QnrB1: gyrase complex presented in the thesis shows that the PRP loop B is interacting with the GyrA Tower domain. This fact allows to speculate about the importance of the PRP loop in the specificity of the protection. The MIC data in the thesis clearly shows that the loop deletion mutant of AlbG is inactive. QnrB1 loop deletion mutant was shown to be inactive in previous studies (Vetting, Hegde, Wang, *et al.*, 2011; Jacoby *et al.*, 2013). The chimeric proteins AlbG $_{\text{QnrB1 106-108}}$ and QnrB1$_{\text{AlbG 91-97}}$ tested in the thesis to check the possibility that the loops are responsible for protective specificity were not showing any activity. This observation clearly shows that PRP specificity is not determined only by the loop. PRPs like MfpA from *Mycobacterium* and *Efs*Qnr from *Enterococcus faecalis* do not possess loops. This fact also shows that presence of loops is not necessarily required to interact with gyrase.

Another possibility is that the specificity of the PRP is determined by both the structure of the toxin-stabilised cleavage complex of the enzyme and the specific features of the PRP. In other words, we can hypothesise "toxin: gyrase: PRP" specificity rather than "toxin PRP" specificity. Recently established structure of albicidin-bound *E. coli* DNA gyrase shows changes in the position of GyrA subunits compared to MFX stabilised complexes. Albicidin also binds asymmetrically, which clearly distinguishes it from the

MFX (Michalczyk *et al.*, 2023). The differences in stabilised cleavage complex could prevent QnrB1 to bind and ultimately to perform its protective action.

In the case of McbG the structure of the protein has not been established experimentally. Different prediction tools position the potential loop in a similar place (amino acids 82-86) but the protrusion is not significantly exposed making it difficult to assign PRP loop features. The MccB17 stabilised cleavage complex could also be significantly different to the one observed in the case of MFX and albicidin. It would also lead to prevention of proper recognition of the complex by other PRPs.

To answer the questions about the PRP specificity it would be required to determine the structures of toxin-stabilised cleavage complexes of gyrase from PRP-encoding host organisms. The comparison of details would elucidate the main factors of observed specificity. The recent progress in using cryo-EM to illuminate the details of drug bound gyrase complexes makes the structural approach feasible.

6.3.Inhibitory effects of PRPs

The inhibitory conundrum of PRPs has been tackled in my work, being the dual nature of PRP proteins reported in other studies. PRPs were shown to inhibit DNA gyrase supercoiling and at the same time being able to protect it from the quinolone inhibition. For example, for the MfpA protein the inhibition of *E. coli* gyrase was observed in the concentration as low as 1 μM (Hegde *et al.*, 2005). Same report shown that 3 μM of *M. tuberculosis* MfpA inhibited *E. coli* DNA gyrase (Mérens *et al.*, 2009). At the same time, previously published data for Qnr protein seems not to support this observation. 320 nM QnrA1 was shown to reverse inhibition in the presence of 1.5 μM ciprofloxacin. QnrA1 did not cause inhibition even in the highest concentration tested (2 μM) (Tran, Jacoby and Hooper, 2005a). QnrB4 did not inhibit *E. coli* DNA gyrase supercoiling unless concentrations were at least as high as 30 μM while showing protective activity at 0.5 μM. First report of QnrB1 activity in gyrase assay claimed that 0.5 nM QnrB1 was sufficient to rescue supercoiling inhibition by 6 μM ciprofloxacin. The inhibition of gyrase by the Qnr protein was observed at 25 μM (Jacoby *et al.*, 2006). Similarly, the chromosomally encoded PRP from *Enterococcus faecalis* was protecting *E. coli* gyrase against ciprofloxacin at concentration of 0.2 μM, while the inhibitory effect of the protein was observed starting from 1 μM (Hegde *et al.*, 2011). Previous study of AlbG protein shown that it is able to partially inhibit *E. coli* DNA gyrase (IC_{50} (Hashimi *et al.*, 2007).

In the thesis the inhibition of *E. coli* DNA gyrase by AlbG was not observed. Out of all of the above-mentioned studies it seems that PRP proteins indeed inhibit *E. coli* DNA gyrase at higher concentrations that might not be directly related to the toxin-specific protection. In the presented thesis, estimated $EC_{50\ QnrB1}$ equalled 0.2 μM while $IC_{50\ QnrB1\ was}$ that equals 11 μM. $IC_{50\ QnrB1}$ is > 50 times higher than $EC_{50\ QnrB1}$ value. The inhibitory effect seems to be related to the likely non-physiological amount of Qnr protein in the assay (>10 000-fold higher than the enzyme needed for efficient supercoiling). The loop deletion QnrB1 $\Delta_{106\text{-}108}$ mutant was shown to be able to similarly inhibit gyrase supercoiling activity at concentrations higher > 10 μM albeit completely devoid of the protective activity. Probably it leads to the inhibition of the DNA binding that leads to decreased supercoiling activity of gyrase. This hypothesis is supported by the fact that the $IC_{50\ QnrB1\ value}$ of DNA binding inhibition in EMSA assay is correlating with $IC_{50\ QnrB1}$ in supercoiling assays (~ 10 μM). The supercoiling inhibition could be caused by the fact that QnrB1 binding seems to be incompatible with T-segment transportation through GyrB. In higher concentrations the QnrB1 would obstruct the usual route of the transported DNA segment. When no T-segment is present like in the case of $A59_2/B_2$ relaxation reactions the QnrB1 does not compete with the transported segment and interacts inside the cavity of the GyrB dimer normally occupied by the T-segment. This leads to inhibition of the reaction.

Stronger inhibitory effects of *Efs*Qnr and *M. tuberculosis* MfpA seem to be rare amongst TA-PRPs. *M. tuberculosis* MfpA was also shown to inhibit its host (*M. tuberculosis*) gyrase at 3 μM (Mérens *et al.*, 2009). Same report was not able to show any MfpA protective activity with *M. tuberculosis* gyrase in supercoiling assay (Mérens *et al.*, 2009). This shows that some TA-PRPs can show contradicting behaviour in *in vitro* assays. Recently another member of MfpA family, from *M. smegmatis*, was reported to inhibit *M. smegmatis* gyrase at concentrations higher than 10 μM while protective effect for the same enzyme was observed starting from 0.1 μM (Feng *et al.*, 2021). The data for MfpA proteins are contradicting each other. This fact cannot be simply explained by the difference in the proteins structure and sequence since both MfpA variants are similar and what is more the residues that was shown to be important for gyrase interaction in the case of *M. smegmatis* variant are located in the same positions in the case of *M. tuberculosis* protein. To address these discrepancies *M. tuberculosis* MfpA should be tested again in the context of *E. coli* and *M. tuberculosis* gyrase enzyme in a unified

experimental setup. *Efs*Qnr protein could be tested with *Enterococcus faecalis* gyrase due to the fact that PRP interaction might be tailored to host gyrase enzyme. Observed *E. coli* gyrase inhibition would then be an effect of nonspecific interaction with *Efs*Qnr and not happen in *E. faecalis*.

The EMSA results for QnrB1 where an increasing amount of protein was able to displace bounded 147 bp fragment show that the PRP is competing with DNA for the binding to the enzyme. However, the effect was observed only in very high concentrations of protein that are ~10-fold higher than required for protection (IC_{50}=~11 μM). The protein inhibitors competing with DNA for gyrase DNA binding site have much lower apparent IC_{50} ; for example an endogenous *E. coli* gyrase repressor YacG has an IC_{50} low as 35 nM (Vos *et al.*, 2014). The GyrI protein from *E. coli* which is another example of proteinaceous that competes with DNA shown K_d value of 0,5 μM for GyrA (Chatterji and Nagaraja, 2002). The example of YacG shows that proteins that have been tailored for gyrase inhibition can show ~1000 times higher affinity to the enzyme compared to the PRPs. Even the K_d value for GyrI is lower than observed IC_{50} values for PRP DNA competition This is another buttress for that the inhibition of DNA gyrase by PRP is happening in high excess of the protein over the enzyme.

6.4.QnrB1 dislodges cleavage complexes and requires ATP hydrolysis

QnrB1 has been shown to reduce the amount of the cleavage complex formed by addition of ciprofloxacin (Vetting, Hegde, Wang, *et al.*, 2011). The data presented in the thesis supports this observation. Addition of QnrB1 reduced the amount of cleaved DNA by ~50% for all concentrations of ciprofloxacin tested when relaxed DNA was used as a substrate.

The QnrB1 molecule seems to "recognise" the stalled complexes and destabilise them to induce releasing of the drug. Calcium cleavage assays carried out in the presence of QnrB1 show that the PRP is efficiently destabilising the cleavage complexes regardless of ciprofloxacin presence. It could mean that the conformation of the cleavage complex in the presence of calcium ions (closest to the native conformation) is allowing the QnrB1 to interact with the enzyme to rescue it from the stalled cleavage conformation. Potentially QnrB1 has some preference towards stabilised cleavage conformation of *E. coli* enzyme. The cleavage complex needs to be stabilised for some time to allow the QnrB1 interact. The presence of cleavage conformation in native gyrase cycle is too short

to allow QnrB1 to interact efficiently. The analysis of QnrB1 binding to stabilised gyrase cleavage complex could be performed to investigate this phenomenon.

It would be useful to carry out calcium cleavage experiments with other PRPs and gyrase enzymes from relevant organisms and compare the results. This will allow us to confirm whether the QnrB1 is indeed destabilising the cleavage complex with Ca2+ or these results are the consequence of decreased DNA binding to the gyrase. Further experiments with very short DNA fragments binding of which presumably should not be affected by QnrB1 according to our structural data could clarify this question.

The lower protection observed in the case of albicidin-induced cleavage and AlbG protection could be the result of higher potency of albicidin toward *E. coli* DNA gyrase than ciprofloxacin. The differences could also result from the mentioned fact that AlbG could be tailored to interact with *Xanthomonas* gyrase. The experiments performed with albicidin producing host could answer the question and give more info about the cleavage complex recognition.

Cleavage complex stability assays shown that QnrB1 and AlbG are able to disrupt the existing cleavage complex and allow the re-ligation of DNA. In this case PRP do not have to compete with the G-segment before its binding to prevent the formation of a cleavage complex with the drug like it was proposed in G-segment theory (Hegde *et al.*, 2005). Instead, the protein is destabilising the complex leading to removal of the drug from the stalled enzyme. This observation corresponds to the theory of cleavage complex destabilisation proposed by Vetting and co-workers. (Vetting, Hegde, Wang, *et al.*, 2011). The PRP seems to be tuned to interact with the conformation triggered by the stalling of the cleavage complex. This would also be in line with the specificity of PRP discussed in the previous section since binding of different toxins trigger slightly different conformations of the enzyme.

The cleavage assays revealed that the protection effect observed with QnrB1 and AlbG is dependent on ATP hydrolysis. Similar result was recently shown for MfpA protein form *M. smegmatis* (Feng *et al.*, 2021). The energy of ATP hydrolysis seems to be used to induce the drug removal in the presence of PRP protein. The fact that a similar result was obtained for three different PRPs indicates the importance of ATP hydrolysis as the general PRP mechanism.

6.5.The necessity of the strand passage for PRP activity

Since the dependency of inhibition of cleavage complex formation is strictly dependent on ATP hydrolysis two possible mechanisms could be postulated. Either the energy of ATP hydrolysis is needed to perform conformational changes to dislodge bound drug, or ATP- driven T-segment DNA passage provides the access to a temporally exposed drug binding pocket within gyrase. The strand passage requirement was suggested for two proteinaceous gyrase inhibitors that stabilise the cleavage complex: microcin B17 and CcdB. The strand passage occurring during DNA supercoiling or ATP - independent relaxation of negatively supercoiled DNA allows those toxins to bind to the enzyme (Pierrat and Maxwell, 2005; Smith and Maxwell, 2006). The observed protection from the CFX-induced cleavage by gyrase in the case of short linear DNA fragments (especially 76 and 100 bp) suggested that there is no necessity of DNA wrapping for QnrB1 for protective activity. Without the wrapping the T-segment could not be formed and transported through the DNA gate. In addition, ciprofloxacin-induced cleavage reaction by $GyrA59_2/B_2$ that lacks GyrA CTDs was successfully inhibited by addition of QnrB1. This truncated gyrase complex is unable to wrap the DNA, yet the protection is observed. $GyrA59_2/B_2$ ATP-dependent relaxation was not rescued by QnrB1 even though ATP hydrolysis is present and the strand passage is happening in “top-to-bottom” way (Kampranis and Maxwell, 1996). The lack of protection in the case $A_2/B47_2$ gyrase complex in cleavage and relaxation assays shows again that ATP hydrolysis is required for PRP activity. From those observations it can be concluded that ATP - driven strand passage is not essential for QnrB1 activity. The lack of inhibition of the $A_2/B47_2$ ATP-independent relaxation suggests that QnrB1 is only able to inhibit gyrase reactions which require normal top to bottom strand passage, coupled with ATP hydrolysis.

Together with the fact that QnrB1 and AlbG was able to dislodge preformed cleavage complexes it seems that PRP mechanism is based on cleavage complex recognition that does not require strand passage. Also, the lack of protection of relaxation reactions again shows that G-segment mimicry theory of PRP interaction is not correct. We should observe both relaxation and supercoiling reactions to be protected if the G-segment mimicry model would be valid: PRP should reduce general binding of DNA resulting in lower amount of stalled cleavage complexes.

Recent studies of MfpA protein from *M. Smegmatis* shown that mycobacterial PRP is not affecting ATP-dependent relaxation neither ATP-independent relaxation (Feng *et al.*, 2021). Unfortunately, in the study it was not established if the strand passage is strictly required for the observed protection. Similar relaxation experiments with different PRP should be performed to establish if the lack of necessity of strand passage for protection in universal feature. Also, the lack of AlbG activity in relaxation reaction is begs the question if PRP activity on relaxation reactions is not enzyme dependent. The tests with *X. albilineans* could answer the question if AlbG is able to offer protection for its "native" host gyrase in the case of relaxation reaction. *X. albilineans* gyrase has been shown to be unable to relax negatively supercoiled DNA (Hashimi *et al.*, 2008). It is possible that AlbG is not tailored for relaxation protection due to the fact that its host is not capable of performing the reaction.

6.6.The interaction of PRP with DNA gyrase

The high resemblance of the conformations of *E. coli* GyrB43 bound to QnrB1 and *M. smegmatis* GyrB47 bound to MfpA (Feng *et al.*, 2021) and the fact that both PRPs are showing stimulation of ATPase activity and ATP dependency of protection strongly suggests that these PRPs have a common way to interact with gyrase ATPase domain. In the case of MfpA protein it has been shown that salt bridges observed between the PRP and GyrB47 play an essential role in the interaction. For QnrB1 complex salt bridges in structurally homologous positions were also identified. Salt bridge between GyrB43_R386 and QnrB1_Y123 seems to be a counterpart for GyrB47_R421 and MfpA_E119. The other salt bridges observed for QnrB1_R90 and QnrB1_R140 are clearly correlating to the salt bridge between MfpA_R116 and GyrB47_R348. In the case of QnrB1 one extra salt bridge was identified: QnrB1_R48 – GyrB43_E317). R48 residue is located in the Qnr loop A that is not present in MfpA protein. Potentially in the case of QnrB1 the loop A is essential for the correct interaction with ATPase domain. The MIC result from the thesis for QnrB1 alanine mutants shown that Y123 seems to have the most critical impact on the QnrB1 protection activity. Other mutations have shown additive activity reduction effect. Those interactions are most likely responsible for ATPase stimulation effect. Interestingly, QnrB1 residues Q51, R77 and R167 which gave positive results in crosslinking did not seem to be directly interacting with any gyrase subunit. Those conformations when the residues would interact were probably not captured by

Cryo-EM experiments that represent the most abundant binding states of interacting molecules. When the reaction is not in equilibrium and it changes over time-resolved methods are more successful in representing the whole picture of the interaction. We also cannot exclude the possibility that BpA replacements altered conformation of the residues allowing interaction with the closest enzyme surface (GyrB43). Experiments performed for MsGyrB47 (R421A), and MsGyrB47 (D348A, R421A) shown that the stimulation of ATPase was decreased about twofold for the D348A mutant, and almost abolished for both MsGyrB47 (R421A) and MsGyrB47 (D348A, R421A) mutants (Feng *et al.*, 2021) It would be beneficial to perform similar ATPase stimulation activity studies for QnrB1 mutant for residues that have shown an impact on MIC results.

The necessity of ATP hydrolysis for QnrB1 activity and the fact that QnrB1 is unable to offer protection for complexes without an ATPase domain pointed to the importance of gyrase B subunit in QnrB1 interaction. The observed stimulation of ATPase activity of GyrB43 and gyrase complex and direct interaction studies show that GyrB43 is the one of the main interaction sites with gyrase enzyme. In all three types of binding experiments performed (FA, pull-downs, crosslinking) pre-incubation of GyrB, or A_2B_2 complex with ADPNP prevented or reduced QnrB1 binding. Additional studies of QnrB1 binding in the future could help to analyse the precise role of QnrB1 in ATPase stimulation and protective activity. It could be done by introducing the mutation in Walker motifs (responsible for binding phosphate in ATPase binding proteins) (Walker *et al.*, 1982) in GyrB43 subunit. It will allow QnrB1 to still interact with DNA gyrase and allow to study the role of ATP hydrolysis for protective activity.

Addition of ADPNP leads to narrowing and closure of the N-gate of DNA gyrase (Gubaev and Klostermeier, 2011). It would mean that in native conditions the QnrB1 is approaching the enzyme from “the top” of GyrB subunit. taking a route of the T-segment DNA rather binding in the pocket occupied by the G-segment. The closure of the N-gate is preventing the entrance of the protein “inside” the complex (**Figure 82**).

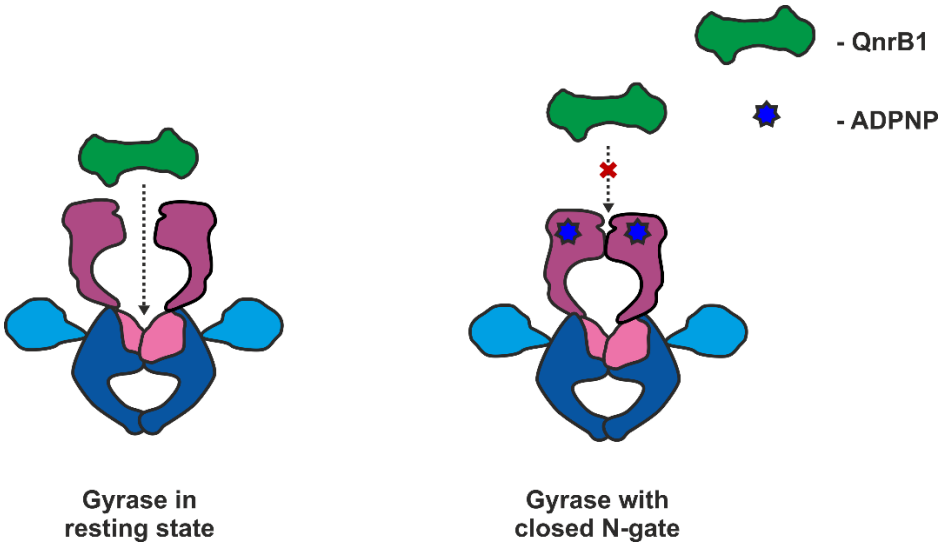

Figure 82. Schematical representation of influence of ADPNP binding for interaction of QnrB1 with gyrase enzyme. Green – QnrB1, dark purple – ATPase domain, light purple – TOPRIM, dark blue – WHD, tower, coiled coli domain of GyrA, light blue – GyrA CTD.

This is strongly in opposition to G-segment mimicry where PRP would be bound in place of G-segment that is not transported through the N-gate (Hegde *et al.*, 2005). The suggested T-segment mimicry model for the PRPs where the protein is captured and follows T-segment route during translocation assumes PRP would enter the enzyme through N-gate and then recognize some structural features of stabilised cleavage complex (Shah and Heddle, 2014). This would be true for the QnrB1 binding observed in the cryo-EM structure where loop 2 is interacting with GyrA TOWER domain. However, the PRP in this structure is not mimicking the native interaction of DNA with GyrB subunit. The structure of QnrB1: gyrase reveals interaction of GyrB linker 389-402 between the transducer and Toprim domains with QnrB1 face 4. The interaction with GyrB linker with QnrB1 together with induced ATPase hydrolysis could be responsible for the observed large conformational switch of ATPase domains upon addition of the nucleotide. The interaction of the transducer domain with QnrB1 is probably captured in crosslinking experiment with the GyrB43 domain, showing that QnrB1 is interacting with the domain even in the presence of ADPNP. The observed crosslinked band is likely due to interaction with QnrB1 with exposed domains from the "bottom" of the subunit. Similar interaction was suggested from the analysis of the structure of *M. smegmatis* MfpA and GyrB47 (Feng *et al.*, 2021).

The importance of loop B interaction and observed large ATPase domain conformational switch allows us to hypothesise about the mechanistic aspects of QnrB1-induced cleavage complex destabilisation. The QnrB1 could act as a lever that could induce complex

destabilisation due to its interaction with GyrA tower domain through loop B. The observed conformational change of ATPase domains powered by ATP hydrolysis could provide the force for the leveraged movement leading to destabilisation of stalled cleavage complex. This hypothesis should be analysed by performing additional structural studies. Time-resolved cryo-EM could provide information about the whole interaction of QnrB1 with gyrase complex throughout an entire cycle of interaction (Frank, 2017). The importance of conformational changes could be elucidated by FRET experiments allowing to probe the distances between gyrase subunits (Gubaev and Klostermeier, 2014).

The lack of protective activity of the QnrB1 Δ106-108 mutant could now be explained in the structural context. The T106 residue is interacting with GyrA L292 in the TOWER domain. The alanine mutation of each residue from 106-108 was shown to result in loss of protective activity of QnrB1 (Jacoby *et al.*, 2013). Therefore, the precise interaction of loop B with GyrA TOWER domain is important despite it is not the one providing the bulk of thermodynamic contribution for PRP binding. It has to be noted that when the QnrB1 *p*Bpa 106-108 mutant was probed by photo crosslinking, no crosslinking to gyrase A was observed. Possibly due to the fact that neighbouring residue mutated to *pBpa* is not interacting with L292 residue in the favourable orientation. In vivo crosslinking using *p*Bpa mutants has been shown to be strongly influenced by the vicinity of methionine residues. M104 of QnrB1 is potentially reducing the crosslinking reaction to L292. It has been shown that methionine residues are able to "internally quench" the crosslinking reaction of *p*Bpa (Lancia *et al.*, 2014). The crosslinking of QnrB1 T106_BpA was reported in other studies, however the data presented remains questionable (Chen *et al.*, 2021). Crosslinking analysis with different photo-crosslinkable amino acids like p-azido-l-phenylalanine (AzF) would be helpful to remove the discrepancies for observed crosslinks and structural data.

The gathered results are showing that loop B interaction is responsible for the protective effect and the interaction with GyrB43 is an independent process. It explains the observed ATPase stimulation activity in the case of QnrB1 Δ106-108 and inhibitory effect observed in high concentration of ΔTTR mutant. It could be argued that the ΔTTR mutant is interacting with GyrB43 obstructing DNA passage but is not able to induce cleavage complex destabilisation due to lack of proper conformation of loop B. The quantitative binding experiments (i.e., fluorescence anisotropy) and ATPase assay of QnrB1

individual loop deletion mutants could give an answer to the question of loops necessity for interacting with gyrase subunits. QnrB1 loop A deletion mutant would potentially present reduced binding to GyrB and lower stimulation of ATPase subunit. Loop B mutant should have reduced binding to GyrA subunit and the reduction of ATPase stimulation activity should lower be than in the case of loop B mutant.

Observed necessity of QnrB1 loop B for its activity begs a question how MfpA is able to offer protective activity against fluoroquinolones. Without structural data for the whole gyrase complex it is hard to exactly predict the interaction of the PRP with the Mycobacterial gyrase subunit A. Potentially the conformation of the enzyme allows the PRP to dislodge the fluoroquinolone just by interactions with face 2 of the PRP. The AlbG tested in the thesis has a smaller loop located on the same face as QnrB1 loop B yet the albicidin resistance protein was not offering the protection for ciprofloxacin induced cleavage. It suggests that the AlbG loop is tailored for interaction with the specific conformation induced by albicidin. The structure of albicidin bound *E. coli* gyrase revealed an intermediate catalytic state that can be placed between the partially open (pre-cleavage gepotidacin structure PDB:6RKV) and the fully open state (Topo IIα structure PDB:5ZEN. Unlike the FQs which bind to the enzyme symmetrically, the N-terminal end of albicidin occupies only one-half of the DNA cleavage site (Michalczyk *et al.*, 2023).

Other tested PRPs in this thesis did not stimulate ATPase activity. AlbG was not present in pull down eluates and in the case of McbG the interaction of protein was observed with both gyrase subunits regardless of ADPNP preincubation of mixture. The AlbG mutant D109*p*Bpa which seems to be structurally homologous to QnrB1 Y123*p*Bpa was crosslinking to both gyrase subunits *in vitro*. Those differences show that the interaction with different PRPs with the same gyrase enzymes may differ in details. In the case of AlbG, observed differences could be due to the mentioned fact that the PRP could be tailored for interaction with *Xanthomonas* gyrase. Based on the Cryo-EM model of QnrB1 and *E. coli* gyrase we can hypothesise about AlbG interaction with *Xanthomonas albilineans* gyrase. The smaller size of the AlbG loop potentially would require AlbG being closer to GyrA Tower domain to interact. This would make interaction with GyrB43 domain weaker since the PRP would be more distant from the ATPase domain. This could be a potential explanation of lack of observed ATPase stimulation by AlbG protein in the case of *E. coil* protein.

McbG could be interacting with the interface between gyrase subunits causing the pull down of both gyrase subunits to happen regardless of ADPNP preincubation. It would be worth to study the effect on ATPase stimulation in the case of a full gyrase complex in the presence of MccB17. The result could indicate the importance of the conformation of the enzyme for PRP interaction. To tackle the question of toxin binding importance for PRP interaction, it would be useful to obtain cryo-EM data for AlbG and McbG bound for gyrase with their cognate toxins. Significant differences of toxin binding induced conformations could result in different binding of PRPs. This would also help to explain observed differences in biochemical results.

6.7.PRP mechanism of action

Gathered data for tested PRPs suggests that the mechanism of action of PRPs shares some element of the T-segment mimicry model. The original G-segment DNA mimicry model is not supported by data presented in the thesis and reported by others (Mérens *et al.*, 2009; Vetting, Hegde, Wang, *et al.*, 2011). Two different steps of QnrB1 action can be seen after the analysis of presented data. The general binding of the PRP to the enzyme and drug-specific protection. The hypothesised T-segment mimicry where PRP acts as T-segment mimic (Shah and Heddle, 2014) seems to be valid for capture of the PRP . Also interaction with loop 2 and gyrase suggested in T-segment mimicry model (Shah and Heddle, 2014) is important for the protective activity of the QnrB1. The Qnrb1 interaction differs from the T-segment interaction with GyrB. The fact that QnrB1 is able to offer protection while T-segment cannot be formed shows that the PRP is able to recognise the stabilised cleavage complex. From those results a model proposed by Shah and Heddle seems to be most corresponding for gathered data (Shah and Heddle, 2014) (**Figure 83**).

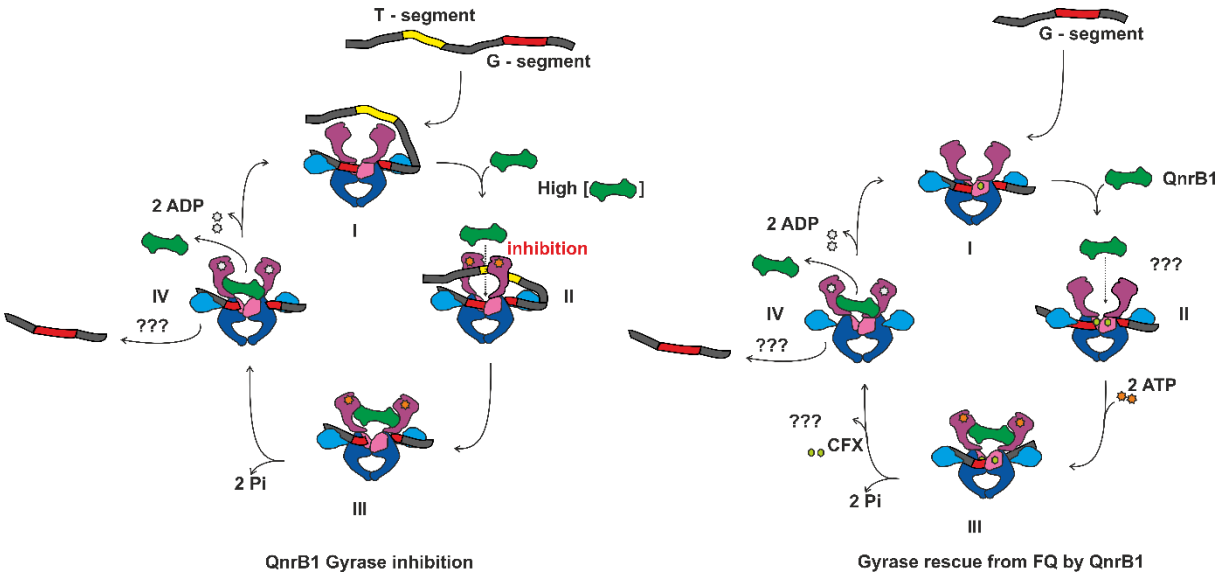

Figure 83. Potential mechanism of action of PRPs based on QnrB1. *QnrB1 gyrase inhibition*: I. DNA gyrase with bound G segment. II. At high concentrations, QnrB1 competes with the T-segment and binds to the ATP-operated clamp, preventing T-segment binding. III, IV. After ATP hydrolysis, QnrB1 is released, which might be accompanied by the release of DNA. *Gyrase rescue from FQ by QnrB1*: I. DNA gyrase cleavage complex formation. II. QnrB1 initial binding to the ATP-operated clamp (ATPase and transducer domains) in GyrB. III, IV. After ATP binding and hydrolysis, specific (loop-mediated) QnrB1 interaction results in fluoroquinolone removal and subsequent release of the PRP. This might be accompanied by the DNA release. Adapted from (Mazurek *et al.*, 2021).

QnrB1 follows the T-segment route in top to bottom strand passage. In higher concentrations it would lead to competition with T-segment and resulting supercoiling and ATP-dependent relaxation inhibition (**Figure 83**, "Gyrase inhibition"). It would also lead to the promotion of ATP- independent relaxation occurring in reverse direction due to the fact that the inhibition of top to bottom strand passage would shift the thermodynamic equilibrium of ATP-independent relaxation reaction towards higher relaxation. As QnrB1 binding is seemingly incompatible with productive DNA wrap, binding of QnrB1 would also lead to destabilisation of wrapped DNA complex which can be seen in EMSA/FA experiments.

In the case of the interaction with cleavage complex the QnrB1 would not have to compete with the T-segment and QnrB1 could interact with the enzyme presenting drug-specific protection. It is hard to answer the question of the fate of toxin molecules that are stabilising the cleavage complex. Assumption that QnrB1 activity leads to replacement of the toxin with the protein than leads to drug removal implies the necessity that QnrB1-stabilised conformation has the lower energy than the one stabilised by the toxin, The enzyme needs to be "restarted" after QnrB1 action otherwise enzyme would be constantly inhibited by the bounded PRP. Hence the observed requirement of ATP hydrolysis is

logical. It is an energy input needed to “re start” the protected enzyme. QnrB1 uses ATP hydrolysis to rejuvenate poisoned gyrase complexes. (**Figure 83**, “Gyrase rescue from FQ”).

It has to be asked if all the PRPs are sharing a similar mechanism. From the data presented for *M. smegmatis* MfpA it can be seen that QnrB1 and MfpA share very similar behaviour (Feng *et al.*, 2021). In the case of AlbG tested in this thesis similarities can be spotted but the details of the mechanism could be dependent on the native PRP target i.e., *X. albilineans* gyrase. The similar structural analysis like in the case of QnrB1 would need to be performed to find potential explanations for differences between QnrB1 and AlbG interaction with *E. coli* gyrase. Lack of information about MccB17 binding and McbG structure makes it difficult to hypothesise about McbG/gyrase interaction. The structure of McbG: gyrase: Mccb17 complex would give info about the nature of the McbG interaction. Due to the fact that cryo-EM needs less material it would be potentially easier to obtain the information of structure of McbG bound to DNA gyrase by this method than to determine structure of the isolated McbG by the X-ray crystallography (Peplow, 2020)

The presented model of PRP action does not fully answer the question about the importance of loops in determining the PRP specificity. The loop itself does not seem to be the only determinant, and potentially the loop presence is the reflection of structural differences of gyrase enzymes and is required for some PRPs to act. This would imply that the specificity is not only based on the gyrase targeting toxin itself, but enzyme structure needs to be factored in.

Similar mechanism to the described above has been proposed for TetM, a ribosome protection protein from *Enterococcus faecalis* conferring the resistance for ribosome targeting antibiotic, tetracycline. Tetracycline binds to the 30S ribosome subunit and act by blocking the A-site of the ribosome, resulting in the stalled irreversible complex. TetM has been shown to bind to tetracycline stalled ribosomes; upon TetM binding, the proline residue located in TetM loop III is driving the bound tetracycline away by interacting with tetracycline ribosome binding site nucleotide C1054 of the ribosome 16s rRNA. TetM binding to the ribosome leads to interaction of the C-terminal helix (CTH) from Tet M with 23S rRNA nucleotide A1913 and induces 16S rRNA decoding nucleotides A1492 and A1493 to flip out of helix 44 of the 16S rRNA. The loop III stabilisation is critical for the activity of TetM (Arenz *et al.*, 2015). The TetM protein is a GTPase that induces

the release of the drug in a GTP-hydrolysis dependent manner (Burdett, 1996). Energy coming from hydrolysis of triphosphates is used in both mechanisms as a trigger to rescue stalled enzyme. However, in the case of TetM the resistance factor is able to energise itself by its intrinsic GTPase activity. The QnrB1 activity is relying on the fact that DNA gyrase is an ATPase. The TetM GTPase activity has been also shown to be stimulated by the addition of ribosomes (Burdett, 1996). The mode of action of QnrB1 could be perceived as the gyrase analogue of the TetM mechanism.

7. Final conclusions

Since the first structure of PRP was established, it was debated what is the mechanism of action of those proteins. The first postulated G-segment mimicry mechanism seemed inconsistent and was never proved experimentally. Other possible mechanisms were proposed together with appearance of the new data. T-segment mimicry and direct recognition of the cleavage complex structural features emerged as valid alternatives for G-segment mimicry hypothesis. However, the models were never tested in biochemical assays. Also, no structural data were available for PRP interaction with the full gyrase complex.

The main aim of this thesis was to formulate a new, more appropriate model of PRP action based on biochemical and structural analysis. The model that is emerging from data obtained from the thesis incorporates elements of the T-segment DNA mimicry and suggests that some elements of PRPs interaction with DNA gyrase could apply to all of the proteins.

- PRP do not act as G-segment mimic
- Observed inhibitory effect is due to competition with the T-segment DNA binding and is only happening in non-physiological concentrations of the protein
- PRPs are binding in inner cavity of ATPase domain following the path of T-segment but the interaction with the subunit differs from the one observed for the T-segment DNA
- The interaction with ATPase domain leads to stimulation of ATP hydrolysis
- Pentapeptide repeat proteins requires ATP hydrolysis to rejuvenate poisoned gyrase complexes

- The observed specificity of PRP is more likely to be a resultant of the specific interaction of PRP with the specific gyrase complex stabilised by specific toxin (gyrase: toxin: PRP specificity).

To answer the question about the detailed mechanism of PRPs testing is required together with their host enzymes. Structure of AlbG bound to *X. albilineans* gyrase would shed light on observed differences between QnrB1 and AlbG. In the case of McbG it seems that for successful study, the problem of stability of the protein must be resolved first. It would also be valuable to obtain the structure of a microcin B17 gyrase complex with bound McbG. Finally, time-resolved cryo-EM methodology could provide the answer about the PRP mechanism in detail. The fate of the dislodged toxin and the mechanism of the enzyme "reset" would complement the PRP mechanism theory.

8. Bibliography

Adachi, T. *et al.* (1987) 'DNA sequence of the E. coli gyr B gene: application of a new sequencing strategy', *Nucleic Acids Research*, 15(2), pp. 771–784. doi: 10.1093/nar/15.2.771.

Afonine, P. V. *et al.* (2018) 'New tools for the analysis and validation of cryo-EM maps and atomic models', *Acta Crystallographica Section D: Structural Biology*, 74(9), pp. 814–840. doi: 10.1107/S2059798318009324.

Ahuja, S. D. *et al.* (2012) 'Multidrug Resistant Pulmonary Tuberculosis Treatment Regimens and Patient Outcomes: An Individual Patient Data Meta-analysis of 9,153 Patients', *PLoS Medicine*, 9(8). doi: 10.1371/journal.pmed.1001300.

Ali, J. A. *et al.* (1993) 'The 43-Kilodalton N-Terminal Fragment of the DNA Gyrase B Protein Hydrolyzes ATP and Binds Coumarin Drugs', *Biochemistry*, 32(10), pp. 2717–2724. doi: 10.1021/bi00061a033.

Allali, N. *et al.* (2002) 'The highly conserved TldD and TldE proteins of Escherichia coli are involved in microcin B17 processing and in CcdA degradation', *Journal of Bacteriology*, 184(12), pp. 3224–3231. doi: 10.1128/JB.184.12.3224-3231.2002.

Aravind, L., Leipe, D. D. and Koonin, E. V. (1998) 'Toprim - A conserved catalytic domain in type IA and II topoisomerases, DnaG-type primases, OLD family nucleases and RecR proteins', *Nucleic Acids Research*, 26(18), pp. 4205–4213. doi: 10.1093/nar/26.18.4205.

Arenz, S. *et al.* (2015) 'Cryo-EM structure of the tetracycline resistance protein TetM in complex with a translating ribosome at 3.9-Å resolution', *Proceedings of the National Academy of Sciences of the United States of America*, 112(17), pp. 5401–5406. doi: 10.1073/pnas.1501775112.

Arsène, S. and Leclercq, R. (2007) 'Role of a qnr-like, gene in the intrinsic resistance of Enterococcus faecalis to fluoroquinolones', *Antimicrobial Agents and Chemotherapy*, 51(9), pp. 3254–3258. doi: 10.1128/AAC.00274-07.

Asensio, C. *et al.* (1976) 'A new family of low molecular weight antibiotics from enterobacteria', *Biochemical and Biophysical Research Communications*, 69(1), pp. 7–14. doi: 10.1016/S0006-291X(76)80264-1.

Ashkenazy, H. *et al.* (2016) 'ConSurf 2016: an improved methodology to estimate and visualize evolutionary conservation in macromolecules', *Nucleic Acids Research*, 44(W1), pp. W344–W350. doi: 10.1093/nar/gkw408.

Avalos, E. *et al.* (2015) 'Frequency and geographic distribution of gyrA and gyrB mutations associated with fluoroquinolone resistance in clinical Mycobacterium tuberculosis isolates: A systematic review', *PLoS ONE*, 10(3), pp. 1–24. doi: 10.1371/journal.pone.0120470.

Bakshi, S. *et al.* (2012) 'Superresolution imaging of ribosomes and RNA polymerase in live Escherichia coli cells', *Molecular Microbiology*, 85(1), pp. 21–38. doi: 10.1111/j.1365-2958.2012.08081.x.

Baquero, F. and Moreno, F. (1984) 'The microcins', *FEMS Microbiology Letters*, 23(2–3), pp. 117–124. doi: 10.1111/j.1574-6968.1984.tb01046.x.

Barnard, F. M. and Maxwell, A. (2001) 'Interaction between DNA gyrase and quinolones: Effects of alanine mutations at GyrA subunit residues Ser83 and Asp87', *Antimicrobial Agents and Chemotherapy*, 45(7), pp. 1994–2000. doi: 10.1128/AAC.45.7.1994-2000.2001.

Basu, A. *et al.* (2012) 'ATP binding controls distinct structural transitions of Escherichia coli DNA gyrase in complex with DNA', *Nature Structural & Molecular Biology*, 19(5), pp. 538–546. doi: 10.1038/nsmb.2278.

Bates, A. D. *et al.* (2005) *DNA Topology*. Oxford University Press (Oxford bioscience). Available at: https://books.google.pl/books?id=WGBAGyzvQOUC.

Bates, A. D., Berger, J. M. and Maxwell, A. (2011) 'The ancestral role of ATP hydrolysis in type II

topoisomerases: Prevention of DNA double-strand breaks', *Nucleic Acids Research*, 39(15), pp. 6327–6339. doi: 10.1093/nar/gkr258.

Bates, A. D., O'Dea, M. H. and Gellert, M. (1996) 'Energy coupling in Escherichia coli DNA gyrase: The relationship between nucleotide binding, strand passage, and DNA supercoiling', *Biochemistry*, 35(5), pp. 1408–1416. doi: 10.1021/bi952433y.

Bax, B. D. *et al.* (2019) 'DNA Topoisomerase Inhibitors: Trapping a DNA-Cleaving Machine in Motion', *Journal of Molecular Biology*, 431(18), pp. 3427–3449. doi: 10.1016/j.jmb.2019.07.008.

Bellon, S. *et al.* (2004) 'Crystal Structures of Escherichia coli Topoisomerase IV ParE Subunit (24 and 43 Kilodaltons): A Single Residue Dictates Differences in Novobiocin Potency against Topoisomerase IV and DNA Gyrase', *Antimicrobial Agents and Chemotherapy*, 48(5), pp. 1856–1864. doi: 10.1128/AAC.48.5.1856-1864.2004.

Bepler, T. *et al.* (2019) 'Positive-unlabeled convolutional neural networks for particle picking in cryo-electron micrographs', *Nature Methods*, 16(11), pp. 1153–1160. doi: 10.1038/s41592-019-0575-8.

Berger, J. M. *et al.* (1996) 'Structure and mechanism of DNA topoisomerase II', *Nature*, pp. 225–232. doi: 10.1038/379225a0.

Berger, J. M. *et al.* (1998) 'Structural similarities between topoisomerases that cleave one or both DNA strands', *Proceedings of the National Academy of Sciences of the United States of America*, 95(14), pp. 7876–7881. doi: 10.1073/pnas.95.14.7876.

Bergerat, A. *et al.* (1997) 'An atypical topoisomerase II from archaea with implications for meiotic recombination', *Nature*, 386(6623), pp. 414–417. doi: 10.1038/386414a0.

Bergerat, A., Gadelle, D. and Forterre, P. (1994) 'Purification of a DNA topoisomerase II from the hyperthermophilic archaeon Sulfolobus shibatae. A thermostable enzyme with both bacterial and eucaryal features', *Journal of Biological Chemistry*, 269(44), pp. 27663–27669. doi: 10.1016/s0021-9258(18)47037-8.

Bhatnagar, K. and Wong, A. (2019) 'The mutational landscape of quinolone resistance in Escherichia coli', *PLoS ONE*, 14(11), pp. 1–18. doi: 10.1371/journal.pone.0224650.

Biedenbach, D. J. *et al.* (2016) 'In vitro activity of gepotidacin, a novel triazaacenaphthylene bacterial topoisomerase inhibitor, against a broad spectrum of bacterial pathogens', *Antimicrobial Agents and Chemotherapy*, 60(3), pp. 1918–1923. doi: 10.1128/AAC.02820-15.

Birch, R. G. and Patil, S. S. (1985) 'Preliminary characterization of an antibiotic produced by Xanthomonas albilineans which inhibits DNA synthesis in Escherichia coli', *Journal of General Microbiology*, 131(5), pp. 1069–1075. doi: 10.1099/00221287-131-5-1069.

Birch, R. G. and Patil, S. S. (1987) 'Correlation between albicidin production and chlorosis induction by Xanthomonas albilineans, the sugarcane leaf scald pathogen', *Physiological and Molecular Plant Pathology*, 30(2), pp. 199–206. doi: 10.1016/0885-5765(87)90033-6.

Birch, R. G., Pemberton, J. M. and Basnayake, W. V. S. (1990) 'Stable albicidin resistance in Escherichia coli involves an altered outer-membrane nucleoside uptake system', *Journal of General Microbiology*, 136(1), pp. 51–58. doi: 10.1099/00221287-136-1-51.

Bjergbaek, L. *et al.* (2000) 'Communication between the ATPase and cleavage/religation domains of human topoisomerase IIα', *Journal of Biological Chemistry*, 275(17), pp. 13041–13048. doi: 10.1074/jbc.275.17.13041.

Blair, J. M. A. *et al.* (2015) 'Molecular mechanisms of antibiotic resistance', *Nature Reviews Microbiology*, 13(1), pp. 42–51. doi: 10.1038/nrmicro3380.

Blower, T. R. *et al.* (2016) 'Crystal structure and stability of gyrase-fluoroquinolone cleaved complexes from Mycobacterium tuberculosis', *Proceedings of the National Academy of Sciences of the United States of America*, 113(7), pp. 1706–1713. doi: 10.1073/pnas.1525047113.

Bolanos-Garcia, V. M. and Davies, O. R. (2006) 'Structural analysis and classification of native proteins from E. coli commonly co-purified by immobilised metal affinity chromatography', *Biochimica et Biophysica Acta - General Subjects*, 1760(9), pp. 1304–1313. doi: 10.1016/j.bbagen.2006.03.027.

Bostock, J. M. *et al.* (2006) 'A DHA14 drug efflux gene from Xanthomonas albilineans confers high-level albicidin antibiotic resistance in Escherichia coli', *Journal of Applied Microbiology*, 101(1), pp. 151–160. doi: 10.1111/j.1365-2672.2006.02899.x.

Bradford, M. M. (1976) 'A rapid and sensitive method for the quantitation of microgram quantities of protein utilizing the principle of protein-dye binding', *Analytical Biochemistry*, 72(1–2), pp. 248–254. doi: 10.1016/0003-2697(76)90527-3.

Brino, L. *et al.* (2000) 'Dimerization of Escherichia coli DNA-gyrase B provides a structural mechanism for activating the ATPase catalytic center', *Journal of Biological Chemistry*, 275(13), pp. 9468–9475. doi: 10.1074/jbc.275.13.9468.

Vanden Broeck, A. *et al.* (2019) 'Cryo-EM structure of the complete E. coli DNA gyrase nucleoprotein complex', *Nature Communications*, 10(1), p. 4935. doi: 10.1038/s41467-019-12914-y.

Brown, P. O., Peebles, C. L. and Cozzarelli, N. R. (1979) 'A topoisomerase from Escherichia coli related to DNA gyrase', *Proceedings of the National Academy of Sciences of the United States of America*, 76(12), pp. 6110–6114. doi: 10.1073/pnas.76.12.6110.

Burdett, V. (1996) 'Tet(M)-promoted release of tetracycline from ribosomes is GTP dependent', *Journal of Bacteriology*, 178(11), pp. 3246–3251. doi: 10.1128/jb.178.11.3246-3251.1996.

Cabral, J. H. M. *et al.* (1997) 'Crystal structure of the breakage-reunion domain of DNA gyrase', *Nature*, 388(6645), pp. 903–906. doi: 10.1038/42294.

Capra, J. A. and Singh, M. (2007) 'Predicting functionally important residues from sequence conservation', *Bioinformatics*, 23(15), pp. 1875–1882. doi: 10.1093/bioinformatics/btm270.

Carret, G., Flandrois, J. P. and Lobry, J. R. (1991) 'Biphasic kinetics of bacterial killing by quinolones', *Journal of Antimicrobial Chemotherapy*, 27(3), pp. 319–327. doi: 10.1093/jac/27.3.319.

Carter, H. E. *et al.* (2023) 'Role of the Water–Metal Ion Bridge in Quinolone Interactions with Escherichia coli Gyrase', *International Journal of Molecular Sciences*, 24(3). doi: 10.3390/ijms24032879.

Del Castillo, F. J., Del Castillo, I. and Moreno, F. (2001) 'Construction and characterization of mutations at codon 751 of the Escherichia coli gyrB gene that confer resistance to the antimicrobial peptide microcin B17 and alter the activity of DNA gyrase', *Journal of Bacteriology*, 183(6), pp. 2137–2140. doi: 10.1128/JB.183.6.2137-2140.2001.

Cavaco, L. M. *et al.* (2009) 'qnrD, a novel gene conferring transferable quinolone resistance in Salmonella enterica serovar Kentucky and Bovismorbificans strains of human origin', *Antimicrobial Agents and Chemotherapy*, 53(2), pp. 603–608. doi: 10.1128/AAC.00997-08.

Chalapareddy, S. *et al.* (2016) 'Radicicol-Mediated Inhibition of Topoisomerase VIB-VIA Activity of the Human Malaria Parasite Plasmodium falciparum', *mSphere*. Edited by R. Dzikowski, 1(1), pp. 1–17. doi: 10.1128/mSphere.00025-15.

Champoux, J. J. (2001) 'DNA Topoisomerases: Structure, Function, and Mechanism', *Annual Review of Biochemistry*, 70(1), pp. 369–413. doi: 10.1146/annurev.biochem.70.1.369.

Champoux, J. J. and Dulbecco, R. (1972) 'An activity from mammalian cells that untwists superhelical DNA--a possible swivel for DNA replication (polyoma-ethidium bromide-mouse-embryo cells-dye binding assay).', *Proceedings of the National Academy of Sciences of the United States of America*, 69(1), pp. 143–146. doi: 10.1073/pnas.69.1.143.

Chan, P. F. *et al.* (2015) 'Structural basis of DNA gyrase inhibition by antibacterial QPT-1, anticancer drug etoposide and moxifloxacin', *Nature Communications*, 6, pp. 1–13. doi: 10.1038/ncomms10048.

Chatterji, M. *et al.* (2000) 'The additional 165 amino acids in the B protein of Escherichia coli DNA gyrase

have an important role in DNA binding', *Journal of Biological Chemistry*, 275(30), pp. 22888–22894. doi: 10.1074/jbc.M001047200.

Chatterji, M. and Nagaraja, V. (2002) 'GyrI: A counter-defensive strategy against proteinaceous inhibitors of DNA gyrase', *EMBO Reports*, 3(3), pp. 261–267. doi: 10.1093/embo-reports/kvf038.

Chen, C. *et al.* (2021) ' E. coli GyrA Tower Domain Interacts with QnrB1 Loop B and Plays an Important Role in QnrB1 Protection from Quinolone Inhibition ', *Antimicrobial Agents and Chemotherapy*, (April). doi: 10.1128/aac.00402-21.

Chin, J. W. *et al.* (2002) 'Addition of a photocrosslinking amino acid to the genetic code of Escherichia coli', *Proceedings of the National Academy of Sciences*, 99(17), pp. 11020–11024. doi: 10.1073/pnas.172226299.

Classen, S., Olland, S. and Berger, J. M. (2003) 'Structure of the topoisomerase II ATPase region and its mechanism of inhibition by the chemotherapeutic agent ICRF-187', *Proceedings of the National Academy of Sciences*, 100(19), pp. 10629–10634. doi: 10.1073/pnas.1832879100.

Cociancich, S. *et al.* (2015) 'The gyrase inhibitor albicidin consists of p-aminobenzoic acids and cyanoalanine', *Nature Chemical Biology*, 11(3), pp. 195–197. doi: 10.1038/nchembio.1734.

Confreres, A. and Maxwell, A. (1992) 'gyrB mutations which confer coumarin resistance also affect DNA supercoiling and ATP hydrolysis by Escherichia coli DNA gyrase', *Molecular Microbiology*, 6(12), pp. 1617–1624. doi: 10.1111/j.1365-2958.1992.tb00886.x.

Corbett, K. D. *et al.* (2005) 'The structural basis for substrate specificity in DNA topoisomerase IV', *Journal of Molecular Biology*, 351(3), pp. 545–561. doi: 10.1016/j.jmb.2005.06.029.

Corbett, K. D., Benedetti, P. and Berger, J. M. (2007) 'Holoenzyme assembly and ATP-mediated conformational dynamics of topoisomerase VI.', *Nature structural & molecular biology*, 14(7), pp. 611–9. doi: 10.1038/nsmb1264.

Corbett, K. D. and Berger, J. M. (2003) 'Structure of the topoisomerase VI-B subunit: Implications for type II topoisomerase mechanism and evolution', *EMBO Journal*, 22(1), pp. 151–163. doi: 10.1093/emboj/cdg008.

Correia, S. *et al.* (2017) 'Mechanisms of quinolone action and resistance: where do we stand?', *Journal of Medical Microbiology*, 66(5), pp. 551–559. doi: 10.1099/jmm.0.000475.

Cove, M. E., Tingey, A. P. and Maxwell, A. (1997) 'DNA gyrase can cleave short DNA fragments in the presence of quinolone drugs', *Nucleic Acids Research*, 25(14), pp. 2716–2722. doi: 10.1093/nar/25.14.2716.

Crumplin, G. C. and Smith, J. T. (1976) 'Nalidixic acid and bacterial chromosome replication', *Nature*, 260(5552), pp. 643–645. doi: 10.1038/260643a0.

Dar, M. A. *et al.* (2007) 'Molecular cloning of apicoplast-targeted Plasmodium falciparum DNA gyrase genes: Unique intrinsic ATPase activity and ATP-independent dimerization of PfGyrB subunit', *Eukaryotic Cell*, 6(3), pp. 398–412. doi: 10.1128/EC.00357-06.

Davagnino, J. *et al.* (1986) 'The DNA replication inhibitor microcin B17 is a forty-three-amino-acid protein containing sixty percent glycine', *Proteins: Structure, Function, and Bioinformatics*, 1(3), pp. 230–238. doi: 10.1002/prot.340010305.

Deibler, R. W., Rahmati, S. and Zechiedrich, E. L. (2001) 'Topoisomerase IV, alone, unknots DNA in E. coli', *Genes & Development*, 15(6), pp. 748–761. doi: 10.1101/gad.872301.

DiGate, R. J. and Marians, K. J. (1988) 'Identification of a potent decatenating enzyme from Escherichia coli', *Journal of Biological Chemistry*, 263(26), pp. 13366–13373. doi: 10.1016/s0021-9258(18)37713-5.

Dorman, C. J. and Dorman, M. J. (2016) 'DNA supercoiling is a fundamental regulatory principle in the control of bacterial gene expression', *Biophysical Reviews*, 8, pp. 89–100. doi: 10.1007/s12551-016-0238-2.

Dormán, G. *et al.* (2016) 'The Life of Pi Star: Exploring the Exciting and Forbidden Worlds of the Benzophenone Photophore', *Chemical Reviews*, 116(24), pp. 15284–15398. doi: 10.1021/acs.chemrev.6b00342.

Drlica, K. (1992) 'Control of bacterial DNA supercoiling', *Molecular Microbiology*, 6(4), pp. 425–433. doi: 10.1111/j.1365-2958.1992.tb01486.x.

Drlica, K. and Zhao, X. (2007) 'Mutant selection window hypothesis updated', *Clinical Infectious Diseases*, 44(5), pp. 681–688. doi: 10.1086/511642.

Dutta, R. and Inouye, M. (2000) 'GHKL, an emergent ATPase/kinase superfamily', *Trends in Biochemical Sciences*, 25(1), pp. 24–28. doi: 10.1016/S0968-0004(99)01503-0.

Edwards, M. J. *et al.* (2009) 'A Crystal Structure of the Bifunctional Antibiotic Simocyclinone D8, Bound to DNA Gyrase', *Science*, 326(5958), pp. 1415–1418. doi: 10.1126/science.1179123.

Emmerson, A. M. and Jones, A. M. (2003) 'The quinolones: Decades of development and use', *Journal of Antimicrobial Chemotherapy*, 51(SUPPL. 1), pp. 13–20. doi: 10.1093/jac/dkg208.

Emsley, P. *et al.* (2010) 'Features and development of Coot', *Acta Crystallographica Section D: Biological Crystallography*, 66(4), pp. 486–501. doi: 10.1107/S0907444910007493.

Evans-Roberts, K. M. *et al.* (2016) 'DNA gyrase is the target for the quinolone drug ciprofloxacin in arabidopsis thaliana', *Journal of Biological Chemistry*, 291(7), pp. 3136–3144. doi: 10.1074/jbc.M115.689554.

Feng, L. *et al.* (2021) 'The pentapeptide-repeat protein, MfpA, interacts with mycobacterial DNA gyrase as a DNA T-segment mimic', *Proceedings of the National Academy of Sciences*, 118(11), p. e2016705118. doi: 10.1073/pnas.2016705118.

Fisher, L. M. *et al.* (1981) 'Site-specific interaction of DNA gyrase with DNA.', *Proceedings of the National Academy of Sciences of the United States of America*, 78(7), pp. 4165–4169. doi: 10.1073/pnas.78.7.4165.

Fisher, L. M. *et al.* (1992) 'DNA supercoiling and relaxation by ATP-dependent DNA topoisomerases', *Philosophical Transactions of the Royal Society of London. Series B: Biological Sciences*, 336(1276), pp. 83–91. doi: 10.1098/rstb.1992.0047.

Forterre, P. (2006) 'DNA topoisomerase V: a new fold of mysterious origin', *Trends in Biotechnology*, 24(6), pp. 245–247. doi: 10.1016/j.tibtech.2006.04.006.

Forterre, P. *et al.* (2007) 'Origin and evolution of DNA topoisomerases', *Biochimie*, 89(4), pp. 427–446. doi: 10.1016/j.biochi.2006.12.009.

Fox, J. D. and Waugh, D. S. (2003) 'Maltose-binding protein as a solubility enhancer.', *Methods in molecular biology (Clifton, N.J.)*, 205, pp. 99–117. doi: 10.1385/1-59259-301-1:99.

Frank, J. (2017) 'Time-resolved cryo-electron microscopy: Recent progress', *Journal of Structural Biology*, 200(3), pp. 303–306. doi: 10.1016/j.jsb.2017.06.005.

Friedman, S. M., Lu, T. and Drlica, K. (2001) 'Mutation in the DNA gyrase A gene of Escherichia coli that expands the quinolone resistance-determining region', *Antimicrobial Agents and Chemotherapy*, 45(8), pp. 2378–2380. doi: 10.1128/AAC.45.8.2378-2380.2001.

Frohlich, R. F. *et al.* (2007) 'Tryptophane-205 of human topoisomerase I is essential for camptothecin inhibition of negative but not positive supercoil removal', *Nucleic Acids Research*, 35(18), pp. 6170–6180. doi: 10.1093/nar/gkm669.

Fujimoto-Nakamura, M. *et al.* (2005) 'Accumulation of mutations in both gyrB and parE genes is associated with high-level resistance to novobiocin in Staphylococcus aureus', *Antimicrobial Agents and Chemotherapy*, 49(9), pp. 3810–3815. doi: 10.1128/AAC.49.9.3810-3815.2005.

Gadelle, D. *et al.* (2003) 'Phylogenomics of type II DNA topoisomerases', *BioEssays*, 25(3), pp. 232–242.

doi: 10.1002/bies.10245.

Gadelle, D. *et al.* (2014) 'DNA topoisomerase VIII: A novel subfamily of type IIB topoisomerases encoded by free or integrated plasmids in Archaea and Bacteria', *Nucleic Acids Research*, 42(13), pp. 8578–8591. doi: 10.1093/nar/gku568.

Gajiwala, K. S. and Burley, S. K. (2000) 'Winged helix proteins', *Current Opinion in Structural Biology*, 10(1), pp. 110–116. doi: 10.1016/S0959-440X(99)00057-3.

Garrido, M. C. *et al.* (1988) 'The export of the DNA replication inhibitor Microcin B17 provides immunity for the host cell.', *The EMBO journal*, 7(6), pp. 1853–1862. doi: 10.1002/j.1460-2075.1988.tb03018.x.

Gellert, M. *et al.* (1976) 'DNA gyrase: an enzyme that introduces superhelical turns into DNA.', *Proceedings of the National Academy of Sciences of the United States of America*, 73(11), pp. 3872–3876. doi: 10.1073/pnas.73.11.3872.

Gellert, M. *et al.* (1977) 'Nalidixic acid resistance: A second genetic character involved in DNA gyrase activity', *Proceedings of the National Academy of Sciences of the United States of America*, 74(11), pp. 4772–4776. doi: 10.1073/pnas.74.11.4772.

Gellert, M., Fisher, L. M. and O'Dea, M. H. (1979) 'DNA gyrase: Purification and catalytic properties of a fragment of gyrase B protein', *Proceedings of the National Academy of Sciences of the United States of America*, 76(12), pp. 6289–6293. doi: 10.1073/pnas.76.12.6289.

Genilloud, O., Moreno, F. and Kolter, R. (1989) 'DNA sequence, products, and transcriptional pattern of the genes involved in production of the DNA replication inhibitor microcin B17', *Journal of Bacteriology*, 171(2), pp. 1126–1135. doi: 10.1128/jb.171.2.1126-1135.1989.

Gensberg, K., Jin, Y. F. and Piddock, L. J. V. (1995) 'A novel gyrB mutation in a fluoroquinolone-resistant clinical isolate of Salmonella typhimurium', *FEMS Microbiology Letters*, 132(1–2), pp. 57–60. doi: 10.1016/0378-1097(95)00287-F.

Ghilarov, D. *et al.* (2011) 'A major portion of DNA gyrase inhibitor microcin B17 undergoes an N,O-peptidyl shift during synthesis', *Journal of Biological Chemistry*, 286(30), pp. 26308–26318. doi: 10.1074/jbc.M111.241315.

Ghilarov, D. *et al.* (2019) 'Architecture of Microcin B17 Synthetase: An Octameric Protein Complex Converting a Ribosomally Synthesized Peptide into a DNA Gyrase Poison', *Molecular Cell*, 0(0), pp. 1–14. doi: 10.1016/j.molcel.2018.11.032.

Ghilarov, D. *et al.* (2021) 'Molecular mechanism of SbmA, a promiscuous transporter exploited by antimicrobial peptides', *Science Advances*, 7(37). doi: 10.1126/sciadv.abj5363.

Gibson, E. G. *et al.* (2019) 'Mechanistic and Structural Basis for the Actions of the Antibacterial Gepotidacin against Staphylococcus aureus Gyrase', *ACS Infectious Diseases*, 5(4), pp. 570–581. doi: 10.1021/acsinfecdis.8b00315.

Gil-Marqués, M. L., Jacoby, G. A. and Hooper, D. C. (2021) 'Analyzing Possible Native Functions of the Quinolone Resistance Gene qnr in Vibrio vulnificus', *Antimicrobial Agents and Chemotherapy*, 65(6). doi: 10.1128/AAC.00232-21.

Gmünder, H., Kuratli, K. and Keck, W. (1997) 'In the presence of subunit A inhibitors DNA gyrase cleaves DNA fragments as short as 20 bp at specific sites', *Nucleic Acids Research*, 25(3), pp. 604–610. doi: 10.1093/nar/25.3.604.

Goa, K. L., Bryson, H. M. and Markham, A. (1997) 'Sparfloxacin. A review of its antibacterial activity, pharmacokinetic properties, clinical efficacy and tolerability in lower respiratory tract infections', *Drugs*, 53(4), pp. 700–725. doi: 10.2165/00003495-199753040-00010.

Green, M. R. and Sambrook, J. (2020) 'The Inoue Method for Preparation and Transformation of Competent Escherichia coli: "Ultracompetent" Cells', *Cold Spring Harbor Protocols*, 2020(6), pp. 225–231. doi: 10.1101/pdb.prot101196.

Gubaev, A. and Klostermeier, D. (2011) 'DNA-induced narrowing of the gyrase N-gate coordinates T-segment capture and strand passage.', *Proceedings of the National Academy of Sciences of the United States of America*, 108(34), pp. 14085–90. doi: 10.1073/pnas.1102100108.

Gubaev, A. and Klostermeier, D. (2014) 'The mechanism of negative DNA supercoiling: A cascade of DNA-induced conformational changes prepares gyrase for strand passage', *DNA Repair*, 16(1), pp. 23–34. doi: 10.1016/j.dnarep.2014.01.011.

Guyer, B. M. and Whitford, G. M. (1975) 'Oxolinic acid in urinary tract infection a multi-centre trial', *Current Medical Research and Opinion*, 2(10), pp. 636–640. doi: 10.1185/03007997409111876.

Harmon, F. G., DiGate, R. J. and Kowalczykowski, S. C. (1999) 'RecQ Helicase and Topoisomerase III Comprise a Novel DNA Strand Passage Function', *Molecular Cell*, 3(5), pp. 611–620. doi: 10.1016/s1097-2765(00)80354-8.

Hashimi, S. M. *et al.* (2007) 'The phytotoxin albicidin is a novel inhibitor of DNA gyrase', *Antimicrobial Agents and Chemotherapy*, 51(1), pp. 181–187. doi: 10.1128/AAC.00918-06.

Hashimi, S. M. *et al.* (2008) 'DNA gyrase from the albicidin producer Xanthomonas albilineans has multiple-antibiotic-resistance and unusual enzymatic properties.', *Antimicrobial agents and chemotherapy*, 52(4), pp. 1382–1390. doi: 10.1128/AAC.01551-07.

Hashimi, S. M. (2019) 'Albicidin, a potent DNA gyrase inhibitor with clinical potential', *Journal of Antibiotics*, 72(11), pp. 785–792. doi: 10.1038/s41429-019-0228-2.

Hata, M. *et al.* (2005) 'Cloning of a novel gene for quinolone resistance from a transferable plasmid in Shigella flexneri 2b', *Antimicrobial Agents and Chemotherapy*, 49(2), pp. 801–803. doi: 10.1128/AAC.49.2.801-803.2005.

Hearnshaw, S. J. *et al.* (2014) 'A new crystal structure of the bifunctional antibiotic simocyclinone D8 bound to DNA gyrase gives fresh insight into the mechanism of inhibition', *Journal of Molecular Biology*, 426(10), pp. 2023–2033. doi: 10.1016/j.jmb.2014.02.017.

Hearnshaw, S. J. *et al.* (2015) 'The role of monovalent cations in the ATPase reaction of DNA gyrase', *Acta Crystallographica Section D: Biological Crystallography*, 71, pp. 996–1005. doi: 10.1107/S1399004715002916.

Heddle, J. G. *et al.* (2001) 'The antibiotic microcin B17 is a DNA gyrase poison: characterisation of the mode of inhibition.', *Journal of molecular biology*, 307(5), pp. 1223–34. doi: 10.1006/jmbi.2001.4562.

Heddle, J. G. *et al.* (2004) 'Nucleotide Binding to DNA Gyrase Causes Loss of DNA Wrap', *Journal of Molecular Biology*, 337(3), pp. 597–610. doi: 10.1016/j.jmb.2004.01.049.

Heddle, J. and Maxwell, A. (2002) 'Quinolone-binding pocket of DNA gyrase: Role of GyrB', *Antimicrobial Agents and Chemotherapy*, 46(6), pp. 1805–1815. doi: 10.1128/AAC.46.6.1805-1815.2002.

Hegde, S. S. *et al.* (2005) 'A Fluoroquinolone Resistance Protein from Mycobacterium tuberculosis That Mimics DNA', *Science*, 308(5727), pp. 1480–1483. doi: 10.1126/science.1110699.

Hegde, S. S. *et al.* (2011) 'Structural and biochemical analysis of the pentapeptide repeat protein EfsQnr, a potent DNA gyrase inhibitor', *Antimicrobial Agents and Chemotherapy*, 55(1), pp. 110–117. doi: 10.1128/AAC.01158-10.

Herrero, M. and Moreno, F. (1986) 'Microcin B17 blocks DNA replication and induces the SOS system in Escherichia coli', *Journal of General Microbiology*, 132(2), pp. 393–402. doi: 10.1099/00221287-132-2-393.

Hiasa, H., DiGate, R. J. and Marians, K. J. (1994) 'Decatenating activity of Escherichia coli DNA gyrase and topoisomerases I and III during oriC and pBR322 DNA replication in vitro', *Journal of Biological Chemistry*, 269(3), pp. 2093–2099. doi: 10.1016/s0021-9258(17)42140-5.

Higuchi, R., Krummel, B. and Saiki, R. (1988) 'A general method of in vitro preparation and specific mutagenesis of dna fragments: Study of protein and DNA interactions', *Nucleic Acids Research*, 16(15),

pp. 7351–7367. doi: 10.1093/nar/16.15.7351.

Hoff, J. *et al.* (2020) 'Vibrio natriegens: an ultrafast-growing marine bacterium as emerging synthetic biology chassis', *Environmental Microbiology*, 22(10), pp. 4394–4408. doi: 10.1111/1462-2920.15128.

Hong, B. K. *et al.* (2009) 'oqxAB encoding a multidrug efflux pump in human clinical isolates of Enterobacteriaceae', *Antimicrobial Agents and Chemotherapy*, 53(8), pp. 3582–3584. doi: 10.1128/AAC.01574-08.

Hopp, T. P. *et al.* (1988) 'A Short Polypeptide Marker Sequence Useful for Recombinant Protein Identification and Purification', *Bio/Technology*, 6(10), pp. 1204–1210. doi: 10.1038/nbt1088-1204.

Horowitz, D. S. and Wang, J. C. (1987) 'Mapping the active site tyrosine of Escherichia coli DNA gyrase.', *Journal of Biological Chemistry*, 262(11), pp. 5339–5344. doi: 10.1016/s0021-9258(18)61193-7.

Hsieh, T. S. and Plank, J. L. (2006) 'Reverse gyrase functions as a DNA renaturase: Annealing of complementary single-stranded circles and positive supercoiling of a bubble substrate', *Journal of Biological Chemistry*, 281(9), pp. 5640–5647. doi: 10.1074/jbc.M513252200.

Hsieh, T. shih and Brutlag, D. (1980) 'ATP-dependent DNA topoisomerase from D. melanogaster reversibly catenates duplex DNA rings', *Cell*, 21(1), pp. 115–125. doi: 10.1016/0092-8674(80)90119-1.

Hughes, C. S. *et al.* (2014) 'Ultrasensitive proteome analysis using paramagnetic bead technology', *Molecular Systems Biology*, 10(10), p. 757. doi: 10.15252/msb.20145625.

Jacoby, G. A. *et al.* (2006) 'qnrB, another plasmid-mediated gene for quinolone resistance', *Antimicrobial Agents and Chemotherapy*, 50(4), pp. 1178–1182. doi: 10.1128/AAC.50.4.1178-1182.2006.

Jacoby, G. A. *et al.* (2013) 'Mutational analysis of quinolone resistance protein QnrB1', *Antimicrobial Agents and Chemotherapy*, 57(11), pp. 5733–5736. doi: 10.1128/AAC.01533-13.

Jacoby, G. A., Corcoran, M. A. and Hooper, D. C. (2015) 'Protective effect of qnr on agents other than quinolones that target DNA gyrase', *Antimicrobial Agents and Chemotherapy*, 59(11), pp. 6689–6695. doi: 10.1128/AAC.01292-15.

Jacoby, G. A. and Hooper, D. C. (2013) 'Phylogenetic Analysis of Chromosomally Determined Qnr and Related Proteins', *Antimicrobial Agents and Chemotherapy*, 57(4), pp. 1930–1934. doi: 10.1128/aac.02080-12.

Jumper, J. *et al.* (2021) 'Highly accurate protein structure prediction with AlphaFold', *Nature*, 596(7873), pp. 583–589. doi: 10.1038/s41586-021-03819-2.

Kabsch, W. and Sander, C. (1983) 'Dictionary of protein secondary structure: Pattern recognition of hydrogen-bonded and geometrical features', *Biopolymers*, 22(12), pp. 2577–2637. doi: 10.1002/bip.360221211.

Kampranis, S. C., Bates, A. D. and Maxwell, A. (1999) 'A model for the mechanism of strand passage by DNA gyrase', *Proceedings of the National Academy of Sciences of the United States of America*, 96(15), pp. 8414–8419. doi: 10.1073/pnas.96.15.8414.

Kampranis, S. C. and Maxwell, A. (1996) 'Conversion of DNA gyrase into a conventional type II topoisomerase', *Proceedings of the National Academy of Sciences*, 93(25), pp. 14416–14421. doi: 10.1073/pnas.93.25.14416.

Kato, J. ichi *et al.* (1990) 'New topoisomerase essential for chromosome segregation in E. coli', *Cell*, 63(2), pp. 393–404. doi: 10.1016/0092-8674(90)90172-B.

Keeney, S., Giroux, C. N. and Kleckner, N. (1997) 'Meiosis-specific DNA double-strand breaks are catalyzed by Spo11, a member of a widely conserved protein family', *Cell*, 88(3), pp. 375–384. doi: 10.1016/S0092-8674(00)81876-0.

Kerwat, D. *et al.* (2016) 'Synthesis of Albicidin Derivatives: Assessing the Role of N-terminal Acylation on the Antibacterial Activity', *ChemMedChem*, pp. 1899–1903. doi: 10.1002/cmdc.201600231.

Kikuchi, A. and Asai, K. (1984) 'Reverse gyrase—a topoisomerase which introduces positive superhelical turns into DNA', *Nature*, 309(5970), pp. 677–681. doi: 10.1038/309677a0.

Kim, E. S. and Hooper, D. C. (2014) 'Clinical importance and epidemiology of quinolone resistance', *Infection and Chemotherapy*, 46(4), pp. 226–238. doi: 10.3947/ic.2014.46.4.226.

Koster, D. A. *et al.* (2005) 'Friction and torque govern the relaxation of DNA supercoils by eukaryotic topoisomerase IB', *Nature*, 434(7033), pp. 671–674. doi: 10.1038/nature03395.

Kramlinger, V. M. and Hiasa, H. (2006) 'The "GyrA-box" is required for the ability of DNA gyrase to wrap DNA and catalyze the supercoiling reaction', *Journal of Biological Chemistry*, 281(6), pp. 3738–3742. doi: 10.1074/jbc.M511160200.

Kretz, J. *et al.* (2015) 'Total synthesis of albicidin: A lead structure from xanthomonas albilineans for potent antibacterial gyrase inhibitors', *Angewandte Chemie - International Edition*, 54(6), pp. 1969–1973. doi: 10.1002/anie.201409584.

Kreuzer, K. N. (2013) 'DNA Damage Responses in Prokaryotes: Regulating Gene Expression, Modulating Growth Patterns, and Manipulating Replication Forks', *Cold Spring Harbor Perspectives in Biology*, 5(11), pp. a012674–a012674. doi: 10.1101/cshperspect.a012674.

Kreuzer, K. N. and Cozzarelli, N. R. (1979) 'Escherichia coli mutants thermosensitive for deoxyribonucleic acid gyrase subunit A: Effects on deoxyribonucleic acid replication, transcription, and bacteriophage growth', *Journal of Bacteriology*, 140(2), pp. 424–435. doi: 10.1128/jb.140.2.424-435.1979.

Kreuzer, K. N. and Cozzarelli, N. R. (1980) 'Formation and resolution of DNA catenanes by DNA gyrase', *Cell*, 20(1), pp. 245–254. doi: 10.1016/0092-8674(80)90252-4.

Kurepina, N. E. *et al.* (1993) 'Cloning and mapping of the genetic determinants for microcin C51 production and immunity', *MGG Molecular & General Genetics*, 241(5–6), pp. 700–706. doi: 10.1007/BF00279914.

Kwak, Y. G., Jacoby, G. A. and Hooper, D. C. (2015) 'Effect of Qnr on plasmid gyrase toxins CcdB and ParE', *Antimicrobial Agents and Chemotherapy*, 59(8), pp. 5078–5079. doi: 10.1128/AAC.00524-15.

Lahiri, S. D. *et al.* (2015) 'Insights into the mechanism of inhibition of novel bacteria topoisomerase inhibitors from characterization of resistant mutants of Staphylococcus aureus', *Antimicrobial Agents and Chemotherapy*, 59(9), pp. 5278–5287. doi: 10.1128/AAC.00571-15.

Lancia, J. K. *et al.* (2014) 'Sequence context and crosslinking mechanism affect the efficiency of in vivo capture of a protein-protein interaction', *Biopolymers*. Edited by K. J. Breslauer, 101(4), pp. 391–397. doi: 10.1002/bip.22395.

Langford, B. J. *et al.* (2023) 'Antibiotic resistance associated with the COVID-19 pandemic: a systematic review and meta-analysis', *Clinical Microbiology and Infection*, 29(3), pp. 302–309. doi: 10.1016/j.cmi.2022.12.006.

Lanz, M. A. and Klostermeier, D. (2011) 'Guiding strand passage: DNA-induced movement of the gyrase C-terminal domains defines an early step in the supercoiling cycle', *Nucleic Acids Research*, 39(22), pp. 9681–9694. doi: 10.1093/nar/gkr680.

Laponogov, I. *et al.* (2013) 'Structure of an "open" clamp type II topoisomerase-DNA complex provides a mechanism for DNA capture and transport', *Nucleic Acids Research*, 41(21), pp. 9911–9923. doi: 10.1093/nar/gkt749.

Le, T. B. K. *et al.* (2009) 'Coupling of the biosynthesis and export of the DNA gyrase inhibitor simocyclinone in Streptomyces antibioticus', *Molecular Microbiology*, 72(6), pp. 1462–1474. doi: 10.1111/j.1365-2958.2009.06735.x.

Lesher, G. Y. *et al.* (1962) '1,8-Naphthyridine Derivatives. A New Class of Chemotherapeutic Agents', *Journal of Medicinal and Pharmaceutical Chemistry*, 5(5), pp. 1063–1065. doi: 10.1021/jm01240a021.

Liu, L. F., Liu, C. C. and Alberts, B. M. (1980) 'Type II DNA topoisomerases: Enzymes that can unknot a

topologically knotted DNA molecule via a reversible double-strand break', *Cell*, 19(3), pp. 697–707. doi: 10.1016/S0092-8674(80)80046-8.

Liu, L. F. and Wang, J. C. (1987) 'Supercoiling of the DNA template during transcription.', *Proceedings of the National Academy of Sciences of the United States of America*, 84(20), pp. 7024–7027. doi: 10.1073/pnas.84.20.7024.

Madden, K. R., Stewart, L. and Champoux, J. J. (1995) 'Preferential binding of human topoisomerase I to superhelical DNA', *EMBO Journal*, 14(21), pp. 5399–5409. doi: 10.1002/j.1460-2075.1995.tb00224.x.

Marians, K. J. (1987) 'DNA gyrase-catalyzed decatenation of multiply linked DNA dimers.', *Journal of Biological Chemistry*, 262(21), pp. 10362–10368. doi: 10.1016/s0021-9258(18)61121-4.

Martínez-martínez, L., Pascual, A. and Jacoby, G. A. (1998) 'Quinolone resistance from a transferable plasmid', *Lancet*, 351, pp. 797–99. Available at: papers://c5399723-e709-4728-b088-22881cd2bf02/Paper/p99.

Mathers, A. J., Peirano, G. and Pitout, J. D. D. (2015) 'The role of epidemic resistance plasmids and international high- risk clones in the spread of multidrug-resistant Enterobacteriaceae', *Clinical Microbiology Reviews*, 28(3), pp. 565–591. doi: 10.1128/CMR.00116-14.

Maxwell, A. and Howells, A. J. (1999) 'Overexpression and Purification of Bacterial DNA Gyrase', in *DNA Topoisomerase Protocols*. New Jersey: Humana Press, pp. 135–144. doi: 10.1385/1-59259-259-7:135.

Mazurek, Ł. *et al.* (2021) 'Pentapeptide repeat protein QnrB1 requires ATP hydrolysis to rejuvenate poisoned gyrase complexes', *Nucleic Acids Research*, 49(3), pp. 1581–1596. doi: 10.1093/nar/gkaa1266.

Melby, J. O., Nard, N. J. and Mitchell, D. A. (2011) 'Thiazole/oxazole-modified microcins: Complex natural products from ribosomal templates', *Current Opinion in Chemical Biology*, 15(3), pp. 369–378. doi: 10.1016/j.cbpa.2011.02.027.

Meng, E. C. *et al.* (2006) 'Tools for integrated sequence-structure analysis with UCSF Chimera', *BMC Bioinformatics*, 7, pp. 1–10. doi: 10.1186/1471-2105-7-339.

Mérens, A. *et al.* (2009) 'The pentapeptide repeat proteins MfpAMt and QnrB4 exhibit opposite effects on DNA gyrase catalytic reactions and on the Ternary gyrase-DNA-quinolone complex', *Journal of Bacteriology*, 191(5), pp. 1587–1594. doi: 10.1128/JB.01205-08.

Metelev, M. *et al.* (2013) 'Structure of microcin B-like compounds produced by pseudomonas syringae and species specificity of their antibacterial action', *Journal of Bacteriology*, 195(18), pp. 4129–4137. doi: 10.1128/JB.00665-13.

Michalczyk, E. *et al.* (2023) 'Molecular mechanism of topoisomerase poisoning by the peptide antibiotic albicidin', *Nature Catalysis*, 6(1), pp. 52–67. doi: 10.1038/s41929-022-00904-1.

Miki, T. *et al.* (1992) 'Control of segregation of chromosomal DNA by sex factor F in Escherichia coli. Mutants of DNA gyrase subunit A suppress letD (ccdB) product growth inhibition', *Journal of Molecular Biology*, 225(1), pp. 39–52. doi: 10.1016/0022-2836(92)91024-J.

Miki, T., Chang, Z. T. and Horiuchi, T. (1984) 'Control of cell division by sex factor F in Escherichia coli. II. Identification of genes for inhibitor protein and trigger protein on the 42.84-43.6 F segment', *Journal of Molecular Biology*, 174(4), pp. 627–646. doi: 10.1016/0022-2836(84)90087-1.

Mishra, P. K. *et al.* (2020) 'Photo-crosslinking: An Emerging Chemical Tool for Investigating Molecular Networks in Live Cells', *ChemBioChem*, 21(7), pp. 924–932. doi: 10.1002/cbic.201900600.

Mitscher, L. A. (2005) 'Bacterial topoisomerase inhibitors: Quinolone and pyridone antibacterial agents', *Chemical Reviews*, 105(2), pp. 559–592. doi: 10.1021/cr030101q.

Mizuuchi, K. *et al.* (1980) 'DNA gyrase action involves the introduction of transient double-strand breaks into DNA', *Proceedings of the National Academy of Sciences of the United States of America*, 77(4 I), pp. 1847–1851. doi: 10.1073/pnas.77.4.1847.

Mizuuchi, K., O'Dea, M. H. and Gellert, M. (1978) 'DNA gyrase: Subunit structure and ATPase activity of the purified enzyme', *Proceedings of the National Academy of Sciences of the United States of America*, 75(12), pp. 5960–5963. doi: 10.1073/pnas.75.12.5960.

Montero, C. *et al.* (2001) 'Intrinsic resistance of Mycobacterium smegmatis to fluoroquinolones may be influenced by new pentapeptide protein MfpA.', *Antimicrobial Agents and Chemotherapy*, 45(12), pp. 3387–3392. doi: 10.1128/AAC.45.12.3387.

Murray, C. J. *et al.* (2022) 'Global burden of bacterial antimicrobial resistance in 2019: a systematic analysis', *The Lancet*, 399(10325), pp. 629–655. doi: 10.1016/S0140-6736(21)02724-0.

O'riordan, W. *et al.* (2017) 'Efficacy, safety, and tolerability of gepotidacin (GSK2140944) in the treatment of patients with suspected or confirmed gram-positive acute bacterial skin and skin structure infections', *Antimicrobial Agents and Chemotherapy*, 61(6), pp. 1–12. doi: 10.1128/AAC.02095-16.

OneHealthTrust. ResistanceMap: Antibiotic Resistance of Klebsiella pneumoniae in Poland (2021). Available at: https://resistancemap.onehealthtrust.org/AntibioticResistance.php?charttype=trend&organism=Klebsiella pneumoniae&country=Poland&antibiotic[]=Fluoroquinolones&showerrorbars=false.

Oppegard, L. M. *et al.* (2009) 'In vivo and in vitro patterns of the activity of simocyclinone D8, an angucyclinone antibiotic from Streptomyces antibioticus', *Antimicrobial Agents and Chemotherapy*, 53(5), pp. 2110–2119. doi: 10.1128/AAC.01440-08.

Orphanides, G. and Maxwell, A. (1994) 'Evidence for a conformational change in the DNA gyrase-DNA complex from hydroxyl radical footprinting', *Nucleic Acids Research*, 22(9), pp. 1567–1575. doi: 10.1093/nar/22.9.1567.

Osheroff, N. and Zechiedrich, E. L. (1987) 'Calcium-Promoted DNA Cleavage by Eukaryotic Topoisomerase II: Trapping the Covalent Enzyme-DNA Complex in an Active Form', *Biochemistry*, 26(14), pp. 4303–4309. doi: 10.1021/bi00388a018.

Patel J.B., Cockerill R.F., Bradford A.P., Eliopoulos M.G., Hindler A.J., Jenkins G.S., Lewis S.J., Limbago B., Miller A.L., Nicolau P.D., Pwell M., Swenson M.J., Traczewski M.M., Turnidge J.D., W. P. M. Z. L. B. (2015) 'M07-A10: Methods for Dilution Antimicrobial Susceptibility Tests for Bacteria That Grow Aerobically; Approved Standard—Tenth Edition.', *CLSI (Clinical and Laboratory Standards Institute)*, 35(2). doi: 10.1007/s00259-009-1334-3.

Peng, H. and Marians, K. J. (1993) 'Escherichia coli topoisomerase IV. Purification, characterization, subunit structure, and subunit interactions', *Journal of Biological Chemistry*, 268(32), pp. 24481–24490. doi: 10.1016/s0021-9258(20)80551-1.

Peplow, M. (2020) 'Cryo-electron microscopy reaches resolution milestone', *ACS Central Science*, 6(8), pp. 1274–1277. doi: 10.1021/acscentsci.0c01048.

Petrella, S. *et al.* (2019) 'Overall Structures of Mycobacterium tuberculosis DNA Gyrase Reveal the Role of a Corynebacteriales GyrB-Specific Insert in ATPase Activity.', *Structure (London, England : 1993)*, 27(4), pp. 579-589.e5. doi: 10.1016/j.str.2019.01.004.

Pettersen, E. F. *et al.* (2021) 'UCSF ChimeraX: Structure visualization for researchers, educators, and developers', *Protein Science*, 30(1), pp. 70–82. doi: 10.1002/pro.3943.

Pierrat, O. A. and Maxwell, A. (2003) 'The action of the bacterial toxin microcin B17: Insight into the cleavage-religation reaction of DNA gyrase', *Journal of Biological Chemistry*, 278(37), pp. 35016–35023. doi: 10.1074/jbc.M304516200.

Pierrat, O. A. and Maxwell, A. (2005) 'Evidence for the role of DNA strand passage in the mechanism of action of microcin B17 on DNA gyrase', *Biochemistry*, 44(11), pp. 4204–4215. doi: 10.1021/bi0478751.

Poirel, L., Rodriguez-Martinez, J. M., *et al.* (2005) 'Origin of plasmid-mediated quinolone resistance determinant QnrA', *Antimicrobial Agents and Chemotherapy*, 49(8), pp. 3523–3525. doi: 10.1128/AAC.49.8.3523-3525.2005.

Poirel, L., Liard, A., *et al.* (2005) 'Vibrionaceae as a possible source of Qnr-like quinolone resistance determinants', *Journal of Antimicrobial Chemotherapy*, 56(6), pp. 1118–1121. doi: 10.1093/jac/dki371.

Poirel, L., Cattoir, V. and Nordmann, P. (2012) 'Plasmid-mediated quinolone resistance; interactions between human, animal, and environmental ecologies', *Frontiers in Microbiology*, 3(FEB), pp. 1–7. doi: 10.3389/fmicb.2012.00024.

Punjani, A. *et al.* (2017) 'CryoSPARC: Algorithms for rapid unsupervised cryo-EM structure determination', *Nature Methods*, 14(3), pp. 290–296. doi: 10.1038/nmeth.4169.

Redinbo, M. R. *et al.* (1998) 'Crystal structures of human topoisomerase I in covalent and noncovalent complexes with DNA', *Science*, 279(5356), pp. 1504–1513. doi: 10.1126/science.279.5356.1504.

Reece, R. J. and Maxwell, A. (1989) 'Tryptic fragments of the Escherichia coli DNA gyrase A protein', *Journal of Biological Chemistry*, 264(33), pp. 19648–19653. doi: 10.1016/s0021-9258(19)47162-7.

Reece, R. J. and Maxwell, A. (1991) 'Probing the limits of the DNA breakage-reunion domain of the Escherichia coli DNA gyrase A protein', *Journal of Biological Chemistry*, 266(6), pp. 3540–3546.

Reece, Richard J. and Maxwell, A. (1991) 'The C-terminal domain of the Escherichia coli DNA gyrase A subunit is a DNA-binding protein', *Nucleic Acids Research*, 19(7), pp. 1399–1405. doi: 10.1093/nar/19.7.1399.

Renzette, N. (2011) 'Generation of transformation competent E. coli', *Current Protocols in Microbiology*, (SUPPL. 22), pp. 1–5. doi: 10.1002/9780471729259.mca03ls22.

Richter, S. N. *et al.* (2010) 'Simocyclinone D8 turns on against Gram-negative bacteria in a clinical setting', *Bioorganic and Medicinal Chemistry Letters*, 20(3), pp. 1202–1204. doi: 10.1016/j.bmcl.2009.11.135.

Rigaut, G. *et al.* (1999) 'A generic protein purification method for protein complex characterization and proteome exploration', *Nature Biotechnology*, 17(10), pp. 1030–1032. doi: 10.1038/13732.

Robicsek, A. *et al.* (2006) 'Fluoroquinolone-modifying enzyme: A new adaptation of a common aminoglycoside acetyltransferase', *Nature Medicine*, 12(1), pp. 83–88. doi: 10.1038/nm1347.

Roca, J. and Wang, J. C. (1992) 'The capture of a DNA double helix by an ATP-dependent protein clamp: A key step in DNA transport by type II DNA topoisomerases', *Cell*, 71(5), pp. 833–840. doi: 10.1016/0092-8674(92)90558-T.

Rodríguez-Martínez, J. M., Pichardo, C., *et al.* (2008) 'Activity of ciprofloxacin and levofloxacin in experimental pneumonia caused by Klebsiella pneumoniae deficient in porins, expressing active efflux and producing QnrA1', *Clinical Microbiology and Infection*, 14(7), pp. 691–697. doi: 10.1111/j.1469-0691.2008.02020.x.

Rodríguez-Martínez, J. M., Velasco, C., *et al.* (2008) 'Qnr-like pentapeptide repeat proteins in Gram-positive bacteria', *Journal of Antimicrobial Chemotherapy*, 61(6), pp. 1240–1243. doi: 10.1093/jac/dkn115.

Rostock, L. *et al.* (2018) 'Molecular insights into antibiotic resistance - how a binding protein traps albicidin', *Nature Communications*, 9(1), pp. 1–13. doi: 10.1038/s41467-018-05551-4.

Roy, C. and Datta, S. (2018) 'ASBAAC: Automated Salt-Bridge and Aromatic- Aromatic Calculator', *Bioinformation*, 14(04), pp. 164–166. doi: 10.6026/97320630014164.

Roy, R. S. *et al.* (1998) 'Role of the microcin B17 propeptide in substrate recognition: Solution structure and mutational analysis of McbA1-26', *Chemistry and Biology*, 5(4), pp. 217–228. doi: 10.1016/S1074-5521(98)90635-4.

Roy, R. S. *et al.* (1999) 'In vivo processing and antibiotic activity of microcin B17 analogs with varying ring content and altered bisheterocyclic sites', *Chemistry and Biology*, 6(5), pp. 305–318. doi: 10.1016/S1074-5521(99)80076-3.

Roy, R. S., Allen, O. and Walsh, C. T. (1999) 'Expressed protein ligation to probe regiospecificity of

heterocyclization in the peptide antibiotic microcin B17', *Chemistry and Biology*, 6(11), pp. 789–799. doi: 10.1016/S1074-5521(99)80126-4.

Royer, M. *et al.* (2004) 'Albicidin pathotoxin produced by Xanthomonas albilineans is encoded by three large PKS and NRPS genes present in a gene cluster also containing several putative modifying, regulatory, and resistance genes', *Molecular Plant-Microbe Interactions*, 17(4), pp. 414–427. doi: 10.1094/MPMI.2004.17.4.414.

Sadiq, A. A. *et al.* (2010) 'Anti-proliferative effects of simocyclinone D8 (SD8), a novel catalytic inhibitor of topoisomerase II', *Investigational New Drugs*, 28(1), pp. 20–25. doi: 10.1007/s10637-008-9209-1.

Saga, T. *et al.* (2013) 'Characterization of qnrB-like genes in citrobacter species of the american type culture collection', *Antimicrobial Agents and Chemotherapy*, 57(6), pp. 2863–2866. doi: 10.1128/AAC.02396-12.

Sánchez, M. B. *et al.* (2008) 'Predictive analysis of transmissible quinolone resistance indicates Stenotrophomonas maltophilia as a potential source of a novel family of Qnr determinants', *BMC Microbiology*, 8, pp. 1–14. doi: 10.1186/1471-2180-8-148.

Sander, M. and Hsieh, T. (1983) 'Double strand DNA cleavage by type II DNA topoisomerase from Drosophila melanogaster.', *Journal of Biological Chemistry*, 258(13), pp. 8421–8428. doi: 10.1016/s0021-9258(20)82081-x.

Sandri, M. I. *et al.* (1996) 'Differential expression of the topoisomerase IIα and β genes in human breast cancers', *British Journal of Cancer*, 73(12), pp. 1518–1524. doi: 10.1038/bjc.1996.286.

Schacht, P. *et al.* (1988) 'Worldwide clinical data on efficacy and safety of ciprofloxacin', *Infection*, 16(1 Supplement), pp. 29–43. doi: 10.1007/BF01650504.

Schimana, J. *et al.* (2000) 'Simocyclinones, novel cytostatic angucyclinone antibiotics produced by Streptomyces antibioticus Tu 6040. I. Taxonomy, fermentation, isolation and biological activities', *Journal of Antibiotics*, 53(8), pp. 779–787. doi: 10.7164/antibiotics.53.779.

Schimana, J. *et al.* (2001) 'Simocyclinones: Diversity of metabolites is dependent on fermentation conditions', *Journal of Industrial Microbiology and Biotechnology*, 27(3), pp. 144–148. doi: 10.1038/sj.jim.7000024.

Schindelin, J. *et al.* (2012) 'Fiji: an open-source platform for biological-image analysis', *Nature Methods*, 9(7), pp. 676–682. doi: 10.1038/nmeth.2019.

Schoeffler, A. J., May, A. P. and Berger, J. M. (2010) 'A domain insertion in Escherichia coli GyrB adopts a novel fold that plays a critical role in gyrase function', *Nucleic Acids Research*, 38(21), pp. 7830–7844. doi: 10.1093/nar/gkq665.

Sebaugh, J. L. (2011) 'Guidelines for accurate EC50/IC50 estimation', *Pharmaceutical Statistics*, 10(2), pp. 128–134. doi: 10.1002/pst.426.

Segev, S. *et al.* (1999) 'Safety of long-term therapy with ciprofloxacin: Data analysis of controlled clinical trials and review', *Clinical Infectious Diseases*, 28(2), pp. 299–308. doi: 10.1086/515132.

Shah, S. and Heddle, J. G. (2014) 'Squaring up to DNA: pentapeptide repeat proteins and DNA mimicry', *Applied Microbiology and Biotechnology*, 98(23), pp. 9545–9560. doi: 10.1007/s00253-014-6151-3.

Sissi, C. and Palumbo, M. (2009) 'Effects of magnesium and related divalent metal ions in topoisomerase structure and function', *Nucleic Acids Research*, 37(3), pp. 702–711. doi: 10.1093/nar/gkp024.

Slesarev, A. I. *et al.* (1993) 'DNA topoisomerase V is a relative of eukaryotic topoisomerase I from a hyperthermophilic prokaryote', *Nature*, 364(6439), pp. 735–737. doi: 10.1038/364735a0.

Smith, A. B. and Maxwell, A. (2006) 'A strand-passage conformation of DNA gyrase is required to allow the bacterial toxin, CcdB, to access its binding site', *Nucleic Acids Research*, 34(17), pp. 4667–4676. doi: 10.1093/nar/gkl636.

Spencer, A. C. and Panda, S. S. (2023) 'DNA Gyrase as a Target for Quinolones', *Biomedicines*, 11(2).

doi: 10.3390/biomedicines11020371.

Srikannathasan, V. *et al.* (2015) 'Crystallization and initial crystallographic analysis of covalent DNA-cleavage complexes of Staphyloccocus aureus DNA gyrase with QPT-1, moxifloxacin and etoposide', *Acta Crystallographica Section:F Structural Biology Communications*, 71, pp. 1242–1246. doi: 10.1107/S2053230X15015290.

Strahilevitz, J. *et al.* (2009) 'Plasmid-mediated quinolone resistance: A multifaceted threat', *Clinical Microbiology Reviews*, 22(4), pp. 664–689. doi: 10.1128/CMR.00016-09.

Sugimoto-Shirasu, K. *et al.* (2002) 'DNA topoisomerase VI is essential for endoreduplication in Arabidopsis', *Current Biology*, 12(20), pp. 1782–1786. doi: 10.1016/S0960-9822(02)01198-3.

Sugino, A. *et al.* (1977) 'Mechanism of action of nalidixic acid: Purification of Escherichia coli nalA gene product and its relationship to DNA gyrase and a novel nicking-closing enzyme', *Proceedings of the National Academy of Sciences of the United States of America*, 74(11), pp. 4767–4771. doi: 10.1073/pnas.74.11.4767.

Sugino, A. *et al.* (1978) 'Energy coupling in DNA gyrase and the mechanism of action of novobiocin', *Proceedings of the National Academy of Sciences of the United States of America*, 75(10), pp. 4838–4842. doi: 10.1073/pnas.75.10.4838.

Sugino, A. and Cozzarelli, N. R. (1980) 'The intrinsic ATPase of DNA gyrase.', *Journal of Biological Chemistry*, 255(13), pp. 6299–6306. doi: 10.1016/s0021-9258(18)43737-4.

Surivet, J. P. *et al.* (2013) 'Design, synthesis, and characterization of novel tetrahydropyran-based bacterial topoisomerase inhibitors with potent anti-gram-positive activity', *Journal of Medicinal Chemistry*, 56(18), pp. 7396–7415. doi: 10.1021/jm400963y.

Sutormin, D. *et al.* (2019) 'Single-nucleotide-resolution mapping of DNA gyrase cleavage sites across the Escherichia coli genome', *Nucleic Acids Research*, 47(3), pp. 1373–1388. doi: 10.1093/nar/gky1222.

Taneja, B. *et al.* (2006) 'Structure of the N-terminal fragment of topoisomerase V reveals a new family of topoisomerases', *EMBO Journal*, 25(2), pp. 398–408. doi: 10.1038/sj.emboj.7600922.

Taneja, B. *et al.* (2007) 'Topoisomerase V relaxes supercoiled DNA by a constrained swiveling mechanism', *Proceedings of the National Academy of Sciences of the United States of America*, 104(37), pp. 14670–14675. doi: 10.1073/pnas.0701989104.

Taylor, S. N. *et al.* (2018) 'Gepotidacin for the treatment of uncomplicated urogenital gonorrhea: A phase 2, randomized, doseranging, single-oral dose evaluation', *Clinical Infectious Diseases*, 67(4), pp. 504–512. doi: 10.1093/cid/ciy145.

The World Bank (2017) 'DRUG-RESISTANT INFECTIONS A Threat to Our Economic Future', (March).

Theobald, U., Schimana, J. and Fiedler, H. P. (2000) 'Microbial growth and production kinetics of Streptomyces antibioticus Tü 6040', *Antonie van Leeuwenhoek, International Journal of General and Molecular Microbiology*, 78(3–4), pp. 307–313. doi: 10.1023/A:1010282818272.

Tran, J. H. and Jacoby, G. A. (2002) 'Mechanism of plasmid-mediated quinolone resistance', *Proceedings of the National Academy of Sciences*, 99(8), pp. 5638–5642. doi: 10.1073/pnas.082092899.

Tran, J. H., Jacoby, G. A. and Hooper, D. C. (2005a) 'Interaction of the Plasmid-Encoded Quinolone Resistance Protein Qnr with Escherichia coli DNA Gyrase', *Antimicrobial Agents and Chemotherapy*, 49(1), pp. 118–125. doi: 10.1128/AAC.49.1.118-125.2005.

Tran, J. H., Jacoby, G. A. and Hooper, D. C. (2005b) 'Interaction of the Plasmid-Encoded Quinolone Resistance Protein QnrA with Escherichia coli Topoisomerase IV Interaction of the Plasmid-Encoded Quinolone Resistance Protein QnrA with Escherichia coli Topoisomerase IV', *Antimicrobial Agents and Chemotherapy*, 49(7), pp. 4–7. doi: 10.1128/AAC.49.7.3050–3052.2005.

Trefzer, A. *et al.* (2002) 'Biosynthetic gene cluster of simocyclinone, a natural multihybrid antibiotic', *Antimicrobial Agents and Chemotherapy*, 46(5), pp. 1174–1182. doi: 10.1128/AAC.46.5.1174-1182.2002.

Tretter, E. M. and Berger, J. M. (2012a) 'Mechanisms for defining supercoiling set point of DNA gyrase orthologs: I. A nonconserved acidic C-terminal tail modulates escherichia coli gyrase activity', *Journal of Biological Chemistry*, 287(22), pp. 18636–18644. doi: 10.1074/jbc.M112.345678.

Tretter, E. M. and Berger, J. M. (2012b) 'Mechanisms for defining supercoiling set point of DNA gyrase orthologs: II. The shape of the GyrA subunit C-terminal domain (CTD) is not a sole determinant for controlling supercoiling efficiency', *Journal of Biological Chemistry*, 287(22), pp. 18645–18654. doi: 10.1074/jbc.M112.345736.

Tse, Y. C., Kirkegaard, K. and Wang, J. C. (1980) 'Covalent bonds between protein and DNA. Formation of phosphotyrosine linkage between certain DNA topoisomerases and DNA.', *Journal of Biological Chemistry*, 255(12), pp. 5560–5565. doi: 10.1016/s0021-9258(19)70666-8.

Ventola, C. L. (2015) 'The antibiotic resistance crisis: part 1: causes and threats.', *P & T : a peer-reviewed journal for formulary management*, 40(4), pp. 277–283.

Vetting, M. W. *et al.* (2006) 'Pentapeptide Repeat Proteins', *Biochemistry*, 45(1), pp. 1–10. doi: 10.1021/bi052130w.

Vetting, M. W., Hegde, S. S., Zhang, Y., *et al.* (2011) 'Pentapeptide-repeat proteins that act as topoisomerase poison resistance factors have a common dimer interface', *Acta Crystallographica Section F: Structural Biology and Crystallization Communications*, 67(3), pp. 296–302. doi: 10.1107/S1744309110053315.

Vetting, M. W., Hegde, S. S., Wang, M., *et al.* (2011) 'Structure of QnrB1, a Plasmid-mediated Fluoroquinolone Resistance Factor', *Journal of Biological Chemistry*, 286(28), pp. 25265–25273. doi: 10.1074/jbc.M111.226936.

Vieweg, L. *et al.* (2015) 'The Albicidin Resistance Factor AlbD Is a Serine Endopeptidase That Hydrolyzes Unusual Oligoaromatic-Type Peptides', *Journal of the American Chemical Society*, 137(24), pp. 7608–7611. doi: 10.1021/jacs.5b04099.

Vizan, J. L. *et al.* (1991) 'The peptide antibiotic microcin B17 induces double-strand cleavage of DNA mediated by E. coli DNA gyrase', *EMBO Journal*, 10(2), pp. 467–476. doi: 10.1002/j.1460-2075.1991.tb07969.x.

Vobruba, S. *et al.* (2020) 'N-Deacetylation in Lincosamide Biosynthesis Is Catalyzed by a TldD/PmbA Family Protein', *ACS Chemical Biology*, 15(8), pp. 2048–2054. doi: 10.1021/acschembio.0c00224.

Vos, S. M. *et al.* (2011) 'All tangled up: how cells direct, manage and exploit topoisomerase function', *Nature Reviews Molecular Cell Biology*, 12(12), pp. 827–841. doi: 10.1038/nrm3228.

Vos, S. M. *et al.* (2014) 'Direct control of type IIA topoisomerase activity by a chromosomally encoded regulatory protein', *Genes and Development*, 28(13), pp. 1485–1497. doi: 10.1101/gad.241984.114.

Walker, J. E. *et al.* (1982) 'Distantly related sequences in the alpha- and beta-subunits of ATP synthase, myosin, kinases and other ATP-requiring enzymes and a common nucleotide binding fold.', *The EMBO Journal*, 1(8), pp. 945–951. doi: 10.1002/j.1460-2075.1982.tb01276.x.

Wallis, J. W. *et al.* (1989) 'A hyper-recombination mutation in S. cerevisiae identifies a novel eukaryotic topoisomerase', *Cell*, 58(2), pp. 409–419. doi: 10.1016/0092-8674(89)90855-6.

Wang, B. and Sun, D. (2015) 'Detection of NDM-1 carbapenemase-producing Acinetobacter calcoaceticus and Acinetobacter junii in environmental samples from livestock farms', *Journal of Antimicrobial Chemotherapy*, 70(2), pp. 611–613. doi: 10.1093/jac/dku405.

Wang, J. C. (1971) 'Interaction between DNA and an Escherichia coli protein ω', *Journal of Molecular Biology*, 55(3), pp. 523–533. doi: 10.1016/0022-2836(71)90334-2.

Wang, Minghua *et al.* (2009) 'New plasmid-mediated quinolone resistance gene, qnrC, found in a clinical isolate of Proteus mirabilis', *Antimicrobial Agents and Chemotherapy*, 53(5), pp. 1892–1897. doi: 10.1128/AAC.01400-08.

Waterhouse, A. *et al.* (2018) 'SWISS-MODEL: Homology modelling of protein structures and complexes', *Nucleic Acids Research*, 46(W1), pp. W296–W303. doi: 10.1093/nar/gky427.

Weinstock, M. T. *et al.* (2016) 'Vibrio natriegens as a fast-growing host for molecular biology', *Nature Methods*, 13(10), pp. 849–851. doi: 10.1038/nmeth.3970.

Weiss, J. N. (1997) 'The Hill equation revisited: uses and misuses', *The FASEB Journal*, 11(11), pp. 835–841. doi: 10.1096/fasebj.11.11.9285481.

WHO (2017) *Critically Important Antimicrobials for Human Medicine: 5th revision*, *World Health Organization*.

WHO (2021) *2021 antibacterial agents in clinical and preclinical development:*

Wigley, D. B. *et al.* (1991) 'Crystal structure of an N-terminal fragment of the DNA gyrase B protein', *Nature*, 351(6328), pp. 624–629. doi: 10.1038/351624a0.

Williams, C. J. *et al.* (2018) 'MolProbity: More and better reference data for improved all-atom structure validation', *Protein Science*, 27(1), pp. 293–315. doi: 10.1002/pro.3330.

Williams, N. L. and Maxwell, A. (1999) 'Locking the DNA gate of DNA gyrase: Investigating the effects on DNA cleavage and ATP hydrolysis', *Biochemistry*, 38(43), pp. 14157–14164. doi: 10.1021/bi991478m.

Wise, R. (1999) 'A review of the clinical pharmacology of moxifloxacin, a new 8-methoxyquinolone, and its potential relation to therapeutic efficacy', *Clinical Drug Investigation*, 17(5), pp. 365–387. doi: 10.2165/00044011-199917050-00004.

Wise, R., Andrews, J. M. and Edwards, L. J. (1983) 'In vitro activity of Bay 0867, a new quinoline derivative, compared with those of other antimicrobial agents', *Antimicrobial Agents and Chemotherapy*, 23(4), pp. 559–564. doi: 10.1128/AAC.23.4.559.

Witz, G. and Stasiak, A. (2010) 'DNA supercoiling and its role in DNA decatenation and unknotting', *Nucleic Acids Research*, 38(7), pp. 2119–2133. doi: 10.1093/nar/gkp1161.

Wolfson, J. S. and Hooper, D. C. (1988) 'Norfloxacin: A new targeted fluoroquinolone antimicrobial agent', *Annals of Internal Medicine*, 108(2), pp. 238–251. doi: 10.7326/0003-4819-108-2-238.

Yamane, K. *et al.* (2007) 'New plasmid-mediated fluoroquinolone efflux pump, QepA, found in an Escherichia coli clinical isolate', *Antimicrobial Agents and Chemotherapy*, 51(9), pp. 3354–3360. doi: 10.1128/AAC.00339-07.

Yamashiro, K. and Yamagishi, A. (2005) 'Characterization of the DNA gyrase from the thermoacidophilic archaeon Thermoplasma acidophilum', *Journal of Bacteriology*, 187(24), pp. 8531–8536. doi: 10.1128/JB.187.24.8531-8536.2005.

Yorgey, P., Lee, J. and Kördel, J. (1994) 'Posttranslational modifications in microcin B17 define an additional class of DNA gyrase inhibitor', *Proceedings of the National Academy of Sciences of the United States of America*, 91(10), pp. 4519–23. doi: 10.1073/pnas.91.10.4519.

Yoshida, H. *et al.* (1990) 'Quinolone resistance-determining region in the DNA gyrase gyrA gene of Escherichia coli.', *Antimicrobial agents and chemotherapy*, 34(6), pp. 1271–2. doi: 10.1128/AAC.34.6.1271.

Yoshida, H. *et al.* (1991) 'Quinolone resistance-determining region in the DNA gyrase gyrB gene of Escherichia coli', *Antimicrobial Agents and Chemotherapy*, 35(8), pp. 1647–1650. doi: 10.1128/AAC.35.8.1647.

Young, T. S. *et al.* (2010) 'An Enhanced System for Unnatural Amino Acid Mutagenesis in E . coli', *Journal of Molecular Biology*, 395(2), pp. 361–374. doi: 10.1016/j.jmb.2009.10.030.

Yu, X. *et al.* (2017) 'Genome-wide TOP2A DNA cleavage is biased toward translocated and highly transcribed loci', *Genome Research*, 27(7), pp. 1238–1249. doi: 10.1101/gr.211615.116.

Zeghouf, M. *et al.* (2004) 'Sequential Peptide Affinity (SPA) system for the identification of mammalian and bacterial protein complexes', *Journal of Proteome Research*, 3(3), pp. 463–468. doi: 10.1021/pr034084x.

Zhang, R. and Kennedy, M. A. (2021) 'Current understanding of the structure and function of pentapeptide repeat proteins', *Biomolecules*, 11(5), pp. 1–31. doi: 10.3390/biom11050638.

Zhang, R., Ni, S. and Kennedy, M. A. (2019) 'Type I beta turns make a new twist in pentapeptide repeat proteins: Crystal structure of Alr5209 from Nostoc sp. PCC 7120 determined at 1.7 angström resolution', *Journal of Structural Biology: X*, 3(August), p. 100010. doi: 10.1016/j.yjsbx.2019.100010.

Zivanov, J. *et al.* (2018) 'New tools for automated high-resolution cryo-EM structure determination in RELION-3', *eLife*, 7, pp. 1–22. doi: 10.7554/eLife.42166.

9. Supplementary materials

Table S1. List of plasmids used in the study.

Name	Backbone	Source	Purpose
pBAD-*mcbG*	pBAD/His B	this work	Expression of untagged McbG protein
pBAD-*albG*	pBAD/His B	this work	Expression of untagged AlbG protein
pBAD-*albG* Δ91–97	pBAD/His B	this work	Expression of untagged AlbG loop deletion mutant
pBAD-*qnrb1*	pBAD/His B	this work	Expression of untagged QnrB1 protein
pET28a 6xHIS-*mcbG*	pET-28a (+)	this work	Expression of 6xHis-tagged McbG protein
pET28a 6xHIS-*albG*	pET-28a (+)	Gift of Dr. Mikhail Metelev (Uppsala University)	Purification of 6xHis-tagged AlbG protein
pET28a 6xHIS-*qnrb1*	pET-28a (+)	Gift of Dr. Mikhail Metelev (Uppsala University)	Purification of 6xHis-tagged QnrB1 protein
pET28a 6xHIS-*mcbG*	pET-28a (+)	this work	Purification of 6xHis-tagged McbG protein
pBAD 6xHIS-*mcbG*	pBAD/His B	this work	Purification of 6xHis-tagged McbG protein
pET28 STREP-*mcbG*	pET-28a (+)	this work	Purification of STREP-tagged McbG protein
pBAD-*mcbABCDEFG*	pBAD/His B	Gift of Dr. Mikhail Metelev (Uppsala University)	Encodes microcin B17 biosynthetic cluster (microcin B17 production)

pET21-GyrA	pET-21b (+)	this work (Dr. Jonathan Heddle)	Purification of untagged *E. coli* GyrA
pET21-GyrB	pET-21b (+)	this work (Dr. Jonathan Heddle)	Purification of untagged *E. coli* GyrB
pET21-3xFLAG-GyrB	pET-21b (+)	this work	Purification of FLAG-tagged GyrB
pET21-GyrA-FLAG	pET-21b (+)	this work	Purification of FLAG-tagged GyrA
pET28-GyrB47	pET-28a (+)	this work	Purification of 6xHis-GyrB47
pAJR10.18 (GyrB47)	pET-21a (+)	Gift of Anthony. Maxwell, (John Innes Centre)	Purification of GyrB47 (untagged)
pAJ1 (GyrB43)	pET-21a (+)	Gift of Anthony. Maxwell, (John Innes Centre)	Purification of GyrB43 (untagged)
pLIC172-escoGyrBAfus	pLIC	Gift of James Berger, (John Hopkins School of Medicine)	Purification of *E. coli* GyrBA core protein
pET28-HIS_FLAG_*qnrb1*	pET-28a (+)	this work	Purification of FLAG- and 6xHis-tagged QnrB1
pET28-HIS_FLAG_*albG*	pET-28a (+)	this work	Purification of FLAG- and 6xHis-tagged AlbG
pET28-HIS_*qnrb1ΔTTR*	pET-28a (+)	this work	Purification of QnrB1 loop deletion mutant
pEVOL-pBpF	pEVOL	Addgene #31190	Incorporation of *p*Bpa
pBAD-HIS_*qnrb1*_pBpa	pBAD/HisB	this work	Incorporation of *p*Bpa
pBAD-HIS_*albG*_pBpa	pBAD/HisB	this work	Incorporation of *p*Bpa

Table S2. List of primers used in the study

Primer Name	Primer sequence (5'-3')
100For	CGACGCGCTGGGCTACGTC
100Rev	CGCGGGCATCCCGATGCCG
133For	TATCGCCGGCATGGCGGC
133Rev	CAGCATGGCCTGCAACGC
147For	AGGCCATTATCGCCGGCATG
147Rev	GCCTGGACAGCATGGCCTG
220For	CACTGGTCCCGCCACC
220Rev	CGATCCTTGAAGCTGTCC
300For	CGGTATTCGGAATCTTGCAC
300Rev	GCGGTCCAATGATCGAAG
76For	CTACGTCTTGCTGGCGTTCGCGACGCGAGGCTGGATGGCCTTCCCCATTATGATTCTTCTCGCTTCCGGCGGCATC
76Rev	GATGCCGCCGGAAGCGAGAAGAATCATAATGGGGAAGGCCATCCAGCCTCGCGTCGCGAACGCCAGCAAGACGTAG
For_ AlbG_Δ91–97	GTCAACTGGACCAGCGCACAAGCGGGGGCGCTGTCGTTCGAGCGCTG
For_AlbG_D109TAG	TGCATCCTCAACTAGAGCTTGTTCTAC
For_NcoI_6xHis_FLAG_AlbG	ATTACCATGGGCCATCATCATCATCATCATAGCGGCGATTATAAGGACGATGACGATAAGAGCGGCATGCCGGCCAAGACCCTTG
For_NcoI_6xHis_FLAG_QnrB1	ATTACCATGGGCCATCATCATCATCATCATAGCGGCGATTATAAGGACGATGACGATAAGAGCGGCATGGCTCTGGCACTCGTTGGCGAAA
For_NcoI_AlbG	ATCCCATGGGGATGCCGGCCAAGACCCTTGAAAGCAAGG
For_NcoI_McbG	ATCCCATGGGGATGGATATAATAGAAAAAAGAATCACAAAACGA
For_NcoI_McbG-StrepTagII	AATTCCATGGGCTGGAGCCACCCGCAGTTCGAAAAAGGCAGCGGCATGGATATAATAGAAAAAAGAATCACAAAAC
For_NcoI_QnrB1	ATCCCATGGGGATGGCTCTGGCACTCGTTGGCGAAA
For_NdeI_3xFLAG-GyrB	AATACATATGGACTACAAAGACCATGACGGTGATTATAAAGATCATGACATCGATTACAAGGATGACGATGACAAGTCGAATTCTTATGACTCCTC
For_NdeI_GyrA	TTATCATATGAGCGACCTTGCGAGAG
For_NdeI_GyrB47	AATACATATGCGCCGTAAAGGTGCGC
For_NdeI-flag-_McbG	ATA*CATATG*GATTATAAGGACGATGACGATAAGAGCGGCATGGATATAATAGAAAAAAGAATCACAAAACGA

For_Qnrb1_D155TAG	TTCAGTGGTTCATAGCTCTCC
For_Qnrb1_D175TAG	ACACATTGCTAGCTGACCAATTCG
For_Qnrb1_D185TAG	TTGGGTGACTTATAGATTCGGGGC
For_Qnrb1_D95TAG	ACAAGGCGCATAGTTCCGCGGC
For_Qnrb1_E132TAG	GTCGTGTTGTAGAAGTGTGAGCTG
For_Qnrb1_E138TAG	TGTGAGCTGTGGTAGAACCGTTGG
For_Qnrb1_E85TAG	CTGGGCATTTAGATTCGCCAC
For_Qnrb1_F111TAG	CGCACCTGGTAGTGTAGCGCATAT
For_Qnrb1_G83TAG	AGTGCGCTGTAGATTGAAATT
For_Qnrb1_I105TAG	ATGAATATGTAGACCACGCGCACC
For_Qnrb1_I65TAG	CTGAAAGATGCCTAGTTTAAAAGC
For_Qnrb1_L147TAG	GGTGCCCAGGTATAGGGCGCGACGTTC
For_Qnrb1_M73TAG	AGCTGTGATTTATCATAGGCGGATTTT
For_Qnrb1_N120TAG	ACGAATACCTAGCTAAGCTACGCC
For_Qnrb1_N125TAG	AGCTACGCCTAGTTTTCGAAAGTC
For_Qnrb1_N27TAG	ACATTTTTTTAGTGTGATTTTTCA
For_Qnrb1_N78TAG	GCGGATTTTCGCTAGTCCAGTGCGCTG
For_qnrB1_NcoI_6xHis	CATGCCATGGTTCATCATCATCATCATCATGGCAGCGGCATGGCTCTGGCACTC
For_Qnrb1_Q51TAG	GATCGTGAAAGCTAGAAAGGGTGC

For_Qnrb1_R108 TAG	ATGATCACCACGTAGACCTGGTTTTGT
For_Qnrb1_R140 TAG	CTGTGGGAAAACTAGTGGATAGGT
For_Qnrb1_R167 TAG	ACTTTCGACTGGTAGGCAGCAAAC
For_Qnrb1_R187 TAG	GACTTAGATATTTAGGGCGTTGAT
For_Qnrb1_R48T AG	CAGTTCTATGATTAGGAAAGCCAGAAA
For_Qnrb1_R77T AG	GCGGATTTTTAGAATTCCAGTGCG
For_Qnrb1_R90T AG	TGAAATTCGCCACTGCTAGGCACAAGG
For_Qnrb1_S113 TAG	TGGTTTTGTTAGGCATATATCACG
For_Qnrb1_S157 TAG	TTCAGATCTCTAGGGCGGCGA
For_Qnrb1_T106 TAG	AATATGATCTAGACGCGCACCTGG
For_Qnrb1_T107 TAG	AATATGATCACCTAGCGCACCTGGTTT
For_Qnrb1_T109 TAG	ATCACCACGCGCTAGTGGTTTTGTA
For_Qnrb1_T117 TAG	AGCGCATATATCTAGAATACCAATCTA
For_Qnrb1_Y123 TAG	ACCAATCTAAGCTAGGCCAATTTTTCG
Rev_AlbG_D109 TAG	GTAGAACAAGCTCTAGTTGAGGATGCA
Rev_AlbG_Δ91–97	CAGCGCTCGAACGACAGCGCCCCCGCTTGTGCGCTGGTCCAGTTGAC
Rev_GyrB_XhoI	AATACTCGAGTTAAATATCGATATTCGCCGCTTTCAGG
Rev_Qnrb1_D155 TAG	GGAGAGCTATGAACCACTGAA
Rev_Qnrb1_D175 TAG	CGAATTGGTCAGCTAGCAATGTGT
Rev_Qnrb1_D185 TAG	GCCCCGAATCTATAAGTCACCCAA

Rev_Qnrb1_D95TAG	GCCGCGGAACTATGCGCCTTGT
Rev_Qnrb1_E132TAG	CAGCTCACACTTCTACAACACGAC
Rev_Qnrb1_E138TAG	CCAACGGTTCTACCACAGCTCACA
Rev_Qnrb1_E85TAG	GTGGCGAATCTAAATGCCCAG
Rev_Qnrb1_F111TAG	ATATGCGCTACACTACCAGGTGCG
Rev_Qnrb1_G83TAG	AATTTCAATCTACAGCGCACT
Rev_Qnrb1_I105TAG	GGTGCGCGTGGTCTACATATTCAT
Rev_Qnrb1_I65TAG	GCTTTTAAACTAGGCATCTTTCAG
Rev_Qnrb1_L147TAG	GAACGTCGCGCCCTATACCTGGGCACC
Rev_Qnrb1_M73TAG	AAAATCCGCCTATGATAAATCACAGCT
Rev_Qnrb1_N120TAG	GGCGTAGCTTAGCTAGGTATTCGT
Rev_Qnrb1_N125TAG	GACTTTCGAAAACTAGGCGTAGCT
Rev_Qnrb1_N27TAG	TGAAAAATCACACTAAAAAAATGT
Rev_Qnrb1_N78TAG	CAGCGCACTGGACTAGCGAAAATCCGC
Rev_Qnrb1_Q51TAG	GCACCCTTTCTAGCTTTCACGATC
Rev_Qnrb1_R108TAG	ACAAAACCAGGTCTACGTGGTGATCAT
Rev_Qnrb1_R140TAG	ACCTATCCACTAGTTTTCCCACAG
Rev_Qnrb1_R167TAG	GTTTGCTGCCTACCAGTCGAAAGT
Rev_Qnrb1_R187TAG	ATCAACGCCCTAAATATCTAAGTC

Rev_Qnrb1_R48TAG	TTTCTGGCTTTCCTAATCATAGAACTG
Rev_Qnrb1_R77TAG	CGCACTGGAATTCTAAAAATCCGC
Rev_Qnrb1_R90TAG	CCTTGTGCCTAGCAGTGGCGAATTTCA
Rev_Qnrb1_S113TAG	CGTGATATATGCCTAACAAAACCA
Rev_Qnrb1_S157TAG	TCGCCGCCCTAGAGATCTGAA
Rev_Qnrb1_T106TAG	CCAGGTGCGCGTCTAGATCATATT
Rev_Qnrb1_T107TAG	AAACCAGGTGCGCTAGGTGATCATATT
Rev_Qnrb1_T109TAG	TACAAAACCACTAGCGCGTGGTGAT
Rev_Qnrb1_T117TAG	TAGATTGGTATTCTAGATATATGCGCT
Rev_qnrB1_XhoI_TAA	CCGCTCGAGTTAACCAATCACCGCGATGCCAAGTCGCTCCAT
Rev_Qnrb1_Y123TAG	CGAAAAATTGGCCTAGCTTAGATTGGT
Rev_XhoI_Albg	ATCTCTCGAGTCAATCGGACAGCTCGATATCCAGGCT
Rev_XhoI_GyrA_FLAG	TTAACTCGAGTTACTTGTCGTCATCGTCTTTGTAGTCACCGCTACCTTCTTCTTCTGGCTCGTCGTC
Rev_XhoI_McbG	ATCTCTCGAGTCATCCCCCTACAACCACTC
Rev_XhoI_QnrB1	CCGCTCGAGTTAACCAATCACCGCGATGCCAAGTCGCTCCAT

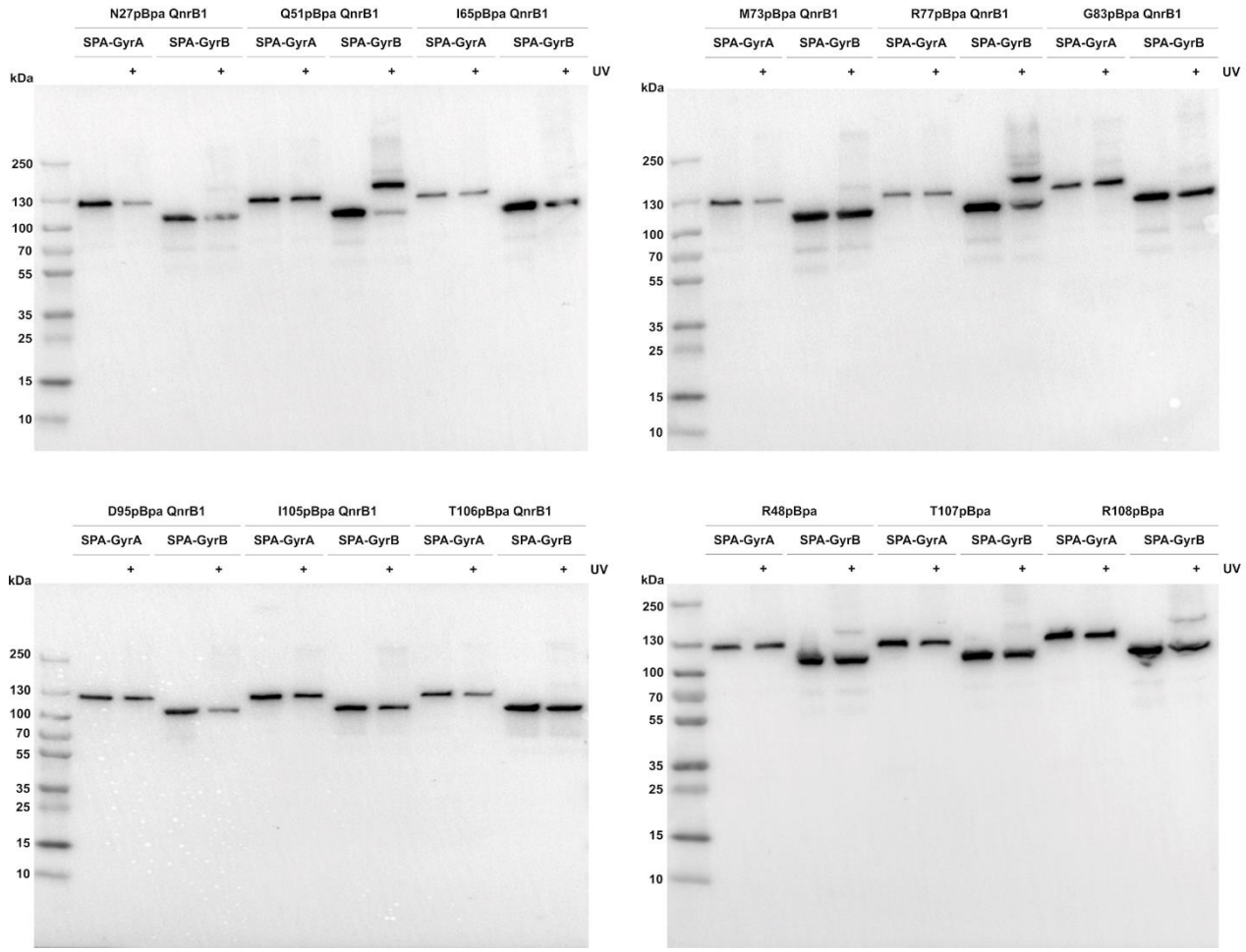

Supplementary Figure S1. Uncropped Western blots for *in vivo* crosslinking of QnrB1 mutants to GyrA-SPA and GyrB-SPA. Residues N27, Q51, I65, M73, R77, G83, D95, I105, T106, R48, T107, R108 are substituted to pBpa. Lanes with UV-treated cells are indicated by (+).

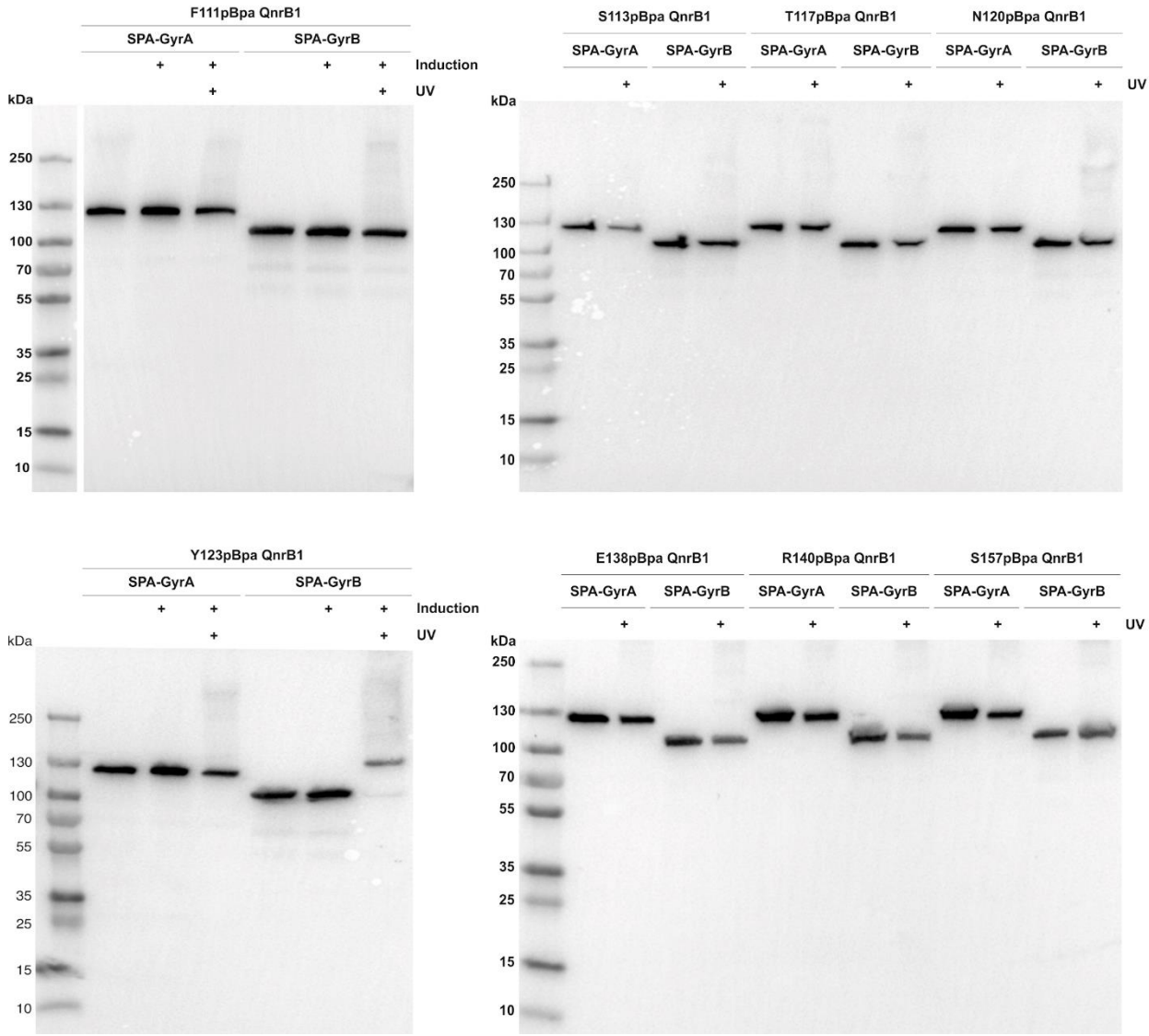

Supplementary Figure S2. Uncropped Western blots for *in vivo* crosslinking of QnrB1 mutants to GyrA-SPA and GyrB-SPA. Residues F111, S113, T117, N120, Y123, E138, R140, S157 are substituted to pBpa. Lanes with UV-treated cells are indicated by (+).

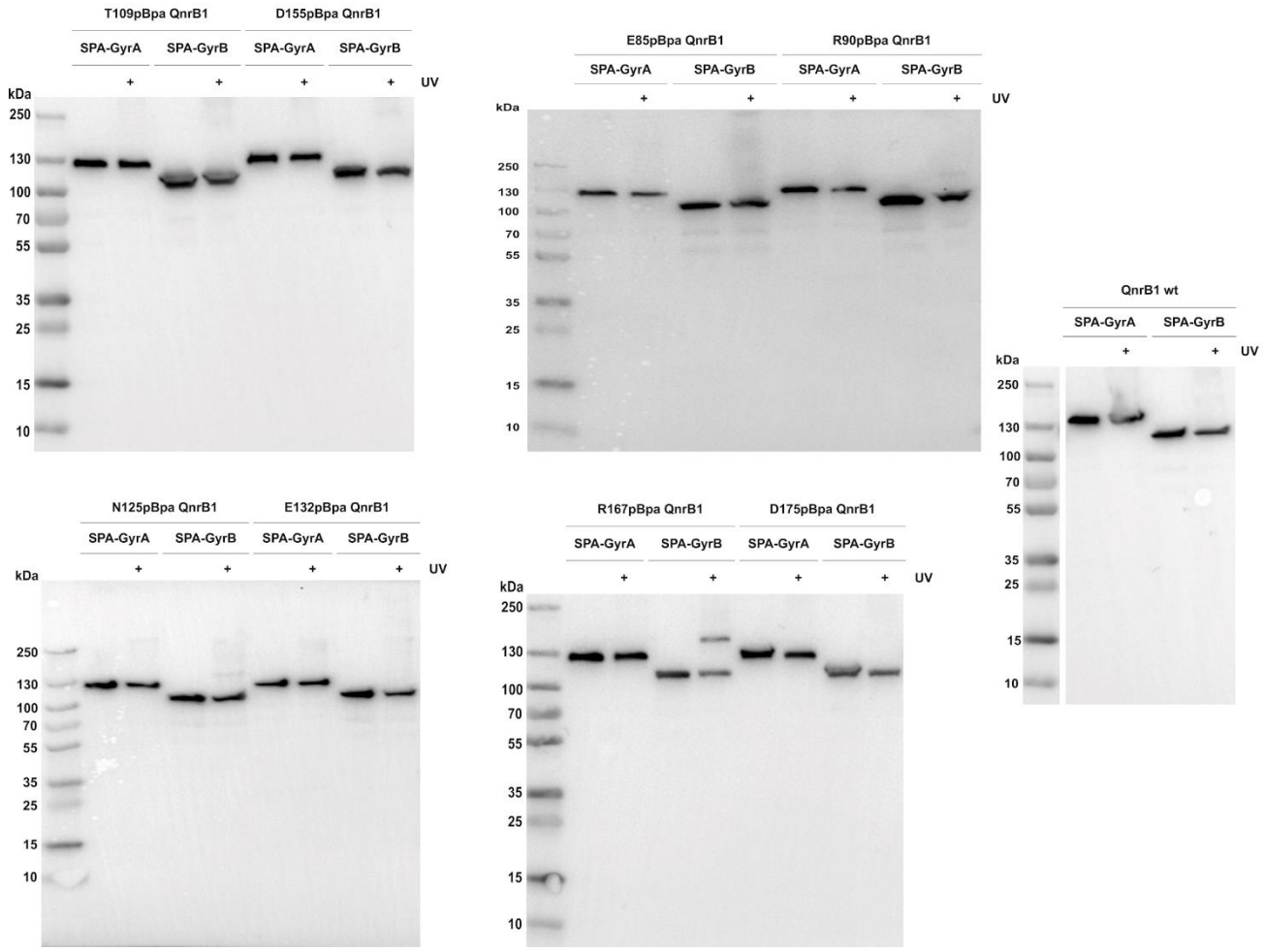

Supplementary Figure S3. Uncropped Western blots for in vivo crosslinking of QnrB1 mutants to GyrA-SPA and GyrB-SPA. Residues T109, D155, E85, R90, N125, E132, R167, D175 substituted to pBpa. Lanes with UV-treated cells are indicated by (+). Also shown is a negative control crosslinking with WT (unlabelled) QnrB1.